Individual and coupled effects of future climate and land use scenarios on water balance components in Australia

Hong Zhang

Thesis submitted in fulfilment of the requirements for the degree of

Doctor of Philosophy

School of Life Sciences, Faculty of Science

University of Technology Sydney

Australia

December 2020

Certificate of Original Authorship

I, Hong Zhang declare that this thesis, is submitted in fulfilment of the requirements for the award of Doctor of Philosophy, in the School of Life Sciences/Faculty of Sciences at the University of Technology Sydney.

This thesis is wholly my own work unless otherwise reference or acknowledged. In addition, I certify that all information sources and literature used are indicated in the thesis.

This document has not been submitted for qualifications at any other academic institution.

Signature of student: *Hong Zhang*

Date: 18 December 2020

Acknowledgements

This four-year Ph.D. journey is an extremely challenging but rewarding experience for me. I would like to thank many people and institutions involved in the completion of this project.

First and foremost, I would like to express my deepest gratitude to my research supervisors at UTS, Professor Qiang Yu, Professor Derek Eamus, Professor Lance M. Leslie, and Professor Alfredo Huete, who have provided me continuous guidance and assistance to accomplish this challenging project. Professor Qiang Yu, my principal supervisor, supported and helped me to apply for CSC-UTS scholarship to pursue Ph.D. at UTS. Professor Yu not only gave me academic advice and guidance, but also gave me confidence in my research. He has always respected my ideas, gave me enough freedom to research my own topics of interest, and encouraged me to publish papers during the whole research period. I would like to show my sincere gratitude to Professor Derek Eamus, who has helped me a lot with the revisions of the HDR stage 1-2 assessments and my first paper. I am also so grateful to Professor Lance M. Leslie, who has always been so conscientious and so helpful, and I have received a lot of encouragement and support talking and working with him. My sincere appreciation goes to Professor Alfredo Huete who welcomed me to the group and expanded my horizons. I am so grateful for the expertise and kindness from all my supervisors.

My special thanks go to the principal research scientist at NSW DPI, Dr. De Li Liu, who provided me with excellent study environment and essential data support. He led me into the research field of hydrological response to climate change, and carefully read through each paper with very professional and beneficial comments. I am so much in debt to his unconditional help and this project could not be achieved without his generous assistance. I also owe my deepest gratitude to Dr. Bin Wang at NSW DPI who guided me through each draft of my writing. He helped me conceptualize the papers, instructed me on how to combine future climate data and hydrological models, how to draw figures using R program, how to write response letters, and so on. Without his responsible step-by-step guidance, it would have been very difficult for me to make enough progress in this project.

I thank my colleagues from UTS, Dr. Puyu Feng, Dr. Song Leng, Lijie Shi, Dr. Jie He, Dr. Rong Gan, Dr. Qinggaozi Zhu, Jianguo Li, Dr. James Cleverly, Dr. Jianxiu Shen, Yuxia Liu, Dr. Qiaoyun Xie, Dr. Wenjie Zhang, and Dr. Cicong Gao, for your kindness and encouragement, and for all the memories and support we share. I am grateful to my friend, Dr. Youbin Hu, for his support with the hydrological model (Xinanjiang model). I would like to thank Dr. Hongtao Xing, Dr. Lei Cheng, and Dr. Jin Teng, for their insightful comments and support on this project.

I am also grateful to staff at UTS and NSW DPI for their continuous assistance, which guaranteed an enjoyable study environment and easy workflow during this Ph.D. journey.

I would like to express my deepest gratitude to my beloved husband Dr. Mingxi Zhang and my parents in China. They have supported and helped me unconditionally during this challenging academic journey, and their encouragement has been a source of motivation for me to keep studying.

Finally, I would like to thank the China Scholarship Council and UTS for providing scholarships, and UTS and NSW DPI for providing nice office environment to conduct this project.

Publications arising from this thesis

Journal papers directly included in this thesis:

Zhang, H., Wang, B., Li Liu, D., Zhang, M., Feng, P., Cheng, L., ... & Eamus, D. (2019). Impacts of future climate change on water resource availability of eastern Australia: A case study of the Manning River basin. Journal of Hydrology, 573, 49-59. (Chapter 4)

Zhang, H., Wang, B., Li Liu, D., Zhang, M., Leslie, L. M., & Yu, Q. (2020). Using an improved SWAT model to simulate hydrological responses to land use change: a case study of a catchment in tropical Australia. Journal of Hydrology, 124822. (Chapter 5)

Zhang, H., Wang, B., Li Liu, D., Leslie, L. M., Shi, L., Zhang, M., & Yu, Q. (2020). Quantifying the impacts of future climate and land use changes on hydrological processes and associated uncertainty in southwestern Australia. (Ready for submission) (Chapter 6)

Peer-reviewed International Conference proceedings:

Zhang, H. (2019). Hydrological responses to land use change in tropical Australia: A case study of the North Johnstone River catchment. The 23rd International Congress on Modelling and Simulation (MODSIM), Canberra, Australia, 3-8 December 2019. (Extended Abstract, Accepted).

Contents

List of Figures

List of Tables

Glossary

AGRL	*agricultural land-generic*
ANOVA	*analysis of variance*
BOM	*Bureau of Meteorology*
CF	*change factor*
CMIP5	*Coupled Model Intercomparison Project phase 5*
CMIP6	*Coupled Model Intercomparison Project phase 6*
CSIRO	*Commonwealth Scientific and Industrial Research Organization*
DEM	*digital elevation model*
ENSO	*El Niño Southern Oscillation*
ET	*evapotranspiration*
FAO	*Food and Agriculture Organization*
FRSD	*forest-deciduous*
FRSE	*forest-evergreen*
FRST	*forest-mixed*
GCM	*global climate model*
GHG	*greenhouse gas*
GWQ	*groundwater*
HRU	*hydrologic response unit*
IPCC	*Intergovernmental Panel on Climate Change*
LAI	*leaf area index*
LAM	*limited-area model*
LATQ	*lateral runoff*
LU	*land use*
LUCC	*land use/cover change*
MK	*Mann-Kendall*
MLRM	*multiple Liner Regression Model*
MODIS	*Moderate Resolution Imaging Spectroradiometer*
NSE	*Nash-Sutcliffe Efficiency*
NSW	*New South Wales*
PBIAS	*percent bias*
PET	*potential evapotranspiration*
R^2	*coefficient of determination*
RC	*runoff coefficient*
RCM	*regional circulation model*
RCP	*Representative Concentration Pathway*
RMSE	*root mean square error*
RNGB	*range-brush*
RNGE	*range-grasses*
SCS CN	*Soil Conservation Service Curve Number*
SILO	*Scientific Information for Land Owners*
SURQ	*surface runoff*
SW	*soil water*

SWA	*south-western Australia*
SWAT	*Soil and Water Assessment Tool*
SWAT-CUP	*SWAT Calibration and Uncertainty Programs*
SWAT-T	*modified SWAT model for tropical areas*
SWWA	*Southwest Western Australia*
T_{max}	*maximum land surface temperature*
T_{min}	*minimum land surface temperature*
UB	*backward trend*
UF	*forward trend*
URBN	*urban*
WETL	*wetlands*
XAJ	*Xinanjiang*

Abstract

The hydrological cycle is influenced by both the climate change and land use change. Assessing the impacts of both climate change and land use change on hydrological variables is crucial for sustainable development of water resources and natural ecosystems. This thesis mainly assessed the effects of land use change and future climate change, both separately and in combination, on water resource availability in Australia. For this evaluation, hydrological models were first calibrated and then forced by an ensemble of global climate models (GCMs) and different land use scenarios. The main findings of this thesis are:

(1) Hydro-meteorological characteristics and climate elasticity. Runoff displayed the greatest correlation with rainfall in most of the four catchments based on correlation analyses. The order of the influencing factors to runoff was: rainfall > parameter n of land use change > net solar radiation > maximum temperature > relative humidity > wind speed ≥ minimum temperature according to climate elasticity for most of the four catchments. As expected, rainfall is the factor that most affects runoff, and an increase of 10% in rainfall caused an increase of 24.4% in runoff according to the average of the four catchments. In addition, the average fractional contributions from climate change and human activity to runoff changes for the four catchments were 55.5% and 44.5%, respectively, based on the climate elasticity analysis method.

(2) Impacts of future climate change on the water cycle. Hydrologic responses to future climate change of a catchment in eastern Australia were evaluated using the XAJ hydrological model and statistically downscaled climate data. Annual rainfall and runoff were projected to decrease slightly in 2021-2060 and increase in 2061-2100 based on the median estimates from the ensemble of GCMs. A slight increase was predicted in annual actual evapotranspiration, while a decrease was projected in annual soil water in the future. The future changes of actual evapotranspiration, runoff, and soil water at seasonal and annual scales are mainly affected by rainfall changes, but less affected by temperature changes. The possible future decrease of water availability in eastern Australia may aggravate due to the trend of decreasing values in future winter runoff and soil water.

(3) Impacts of land use change on the water cycle. Land use change impacts on water balance components in wet tropical eastern Australia were assessed using an improved SWAT model (SWAT-T) with plant growth calibrated using MODIS LAI data. Results indicated that the improved SWAT could simulate MODIS LAI with much better NSE values than the default SWAT model, and to reproduce runoff well with slightly better NSE and R^2 than the default SWAT model. Urbanization increased surface runoff while decreased lateral runoff and

groundwater, but produced no clear change in total runoff, actual evapotranspiration, and soil water using SWAT-T. Additionally, afforestation decreased surface runoff and caused slight changes in other hydrologic variables. Furthermore, SWAT-T simulated larger annual actual evapotranspiration and smaller annual runoff than the default SWAT. These differences can be caused by the difference in seasonal LAI modelled by SWAT-T and default SWAT. It is more reasonable to use SWAT-T in tropical catchments because it can capture seasonal vegetation dynamics.

(4) Coupled impacts of future climate and land use scenarios on the hydrological cycle. Hydrological responses to future climate and land use scenarios in southwestern Australia were studied using the SWAT model forced by statistically downscaled climate data and different land use scenarios. Land use changes have impacts on all hydrologic variables, especially on runoff at the annual scale. Future runoff was projected to decrease in all seasons, especially winter and spring. Multi-GCM ensemble medians suggested annual runoff would decrease by -19.4% in 2020-2060 (RCP4.5), -28.3% in 2020-2060 (RCP8.5), -33.6% in 2060-2100 (RCP4.5), and -55.3% in 2060-2100 (RCP8.5). For the combined impacts of climate and land use changes, the results of different land use change scenarios were only slightly different from the response of the original land use. An uncertainty analysis shows that GCMs had the greatest contribution to hydrologic variables, followed by RCPs and land use scenarios.

Overall, this thesis offers an improved understanding of the individual and coupled impacts of future climate and land use scenarios on water balance components in Australian catchments. It is advisable for impacts analysis to use an ensemble of GCMs under different RCPs, to minimize the uncertainty of projected future hydrologic variables. This thesis can provide crucial information for the development of efficient adaptation strategies and future policy plans for sustainable land and water management in Australia.

Keywords: Climate elasticity; climate change; land use change; GCMs; MODIS LAI; XAJ model; SWAT model; SWAT-T model; Australia; runoff

Chapter 1. Introduction

1.1 Research aim

Global warming is likely to accelerate hydrologic cycle through increasing atmospheric evaporative demand and changing the intensity, frequency and duration of rainfall events (Zeng et al., 2014; Joseph et al., 2018). Hydrologic variables (e.g., runoff, evapotranspiration, and soil water) are highly sensitive to even small changes in rainfall and temperature (Milly et al., 2005; Seneviratne et al., 2010; Joseph et al., 2018). In addition to climate change, the hydrologic cycle also is influenced by land use change, resulting from human activities such as replacing natural forests and wetlands with croplands and built-up land (Sterling et al., 2013). Therefore, research into hydrological responses that may occur in the future needs to consider the combined effects of these two aspects: climate change and land use change.

There is a general recognition that climate change will lead to changes in river flow regimes worldwide (Su et al., 2017). Global climate change will cause changes in precipitation (quantity, distribution, and timing), increase in potential evapotranspiration and changes in other climate variables, which will lead to amplification in runoff (Zhang et al., 2019). Australian climate is the most variable in the world (Stokes and Howden, 2010) and climate change has greatly influenced river and stream flows across Australia. Rainfall and runoff are projected to decline in response to climate change in southern Australia (Pittock, 2003; CSIRO, 2007). Furthermore, average runoff will increase due to the decrease in forested land (Bruijnzeel, 1989). For example, it is estimated through modelling that deforestation has led to an increase in runoff of about 40% in a large catchment in Australia (Siriwardena et al., 2006). The coupling effects of climate and land use changes on runoff are complex and poorly understood. The significance of water resources in nature and society highlights the need to understand the integrated impacts of climate and land use changes on regional streamflow regimes. Therefore, there is an urgent need for hydrological models to synthesize this knowledge and develop explicitly integrated "cause-effect" land use planning and strategies for adaptive land and water management under future climate change at a catchment scale.

This study will use hydrological models to provide a comprehensive understanding of the interactive impacts of climate and land use changes on hydrologic variables in Australia. The hydrological models will be applied to data obtained from the last decades but also into the future (2100). This project will provide answers to the following questions:

(1) How did observed climatic and hydrologic variables change and their relationships?

(2) How will hydrologic variables respond to climate change in the future?

(3) How will hydrologic variables respond to land use change?

(4) What are the integrated impacts of climate and land use changes on hydrologic variables?

The specific aims of this study are to：

(1) Use statistical methods to derive trend, mutation, and cycle characteristics of the climatic and hydrologic variables, and the relationships among them.

(2) Study hydrologic response to future climate change using hydrological models and downscaled GCM projections.

(3) Assess hydrologic response to land use change using hydrological model and defined land use change scenarios.

(4) Evaluate the coupled impacts of climate and land use changes on hydrologic variables using hydrological model, downscaled GCM projections, and defined land use change scenarios.

1.2 Research background

1.2.1 Hydrologic response to climate and land use changes in Australia

Hydrologic cycle is projected to change under the warming climate (IPCC, 2013). Climate variability can notably change the regional hydrologic cycle through changes in the different climatic elements (Su et al., 2017). Rainfall and runoff are projected to decline in response to climate change in southern Australia (Pittock, 2003; CSIRO, 2007). Rainfall decline is amplified in streamflow across southern Australia. In the far southwest, streamflow has decreased by more than 50 percent since mid-1970s. Moreover, in the southeast, since the mid-1990s, streamflow is around half the long-term average (CSIRO, 2016). During the same period, streamflow was 41 percent lower than average in the Murray–Darling basin and streamflow has decreased more than 70 percent in the west and central regions of Victoria such as the Campaspe Basin. A recent study of hydrologic stations with at least 30 years of high-quality records reveals a trend to lower streamflow for southwest and southeast Australia and strong evidence of a trend to higher streamflow in far northern Australia (CSIRO, 2016). These changes in hydrologic variables will influence nearly all aspects of human well-being, such as agricultural productivity, energy use, fish and wildlife management, and municipal and industrial water supply.

The plantation area in Australia has expanded by approximately 700,000 hectares since 1990 (Parsons et al., 2007). The massive land use change in Australia together with the

development of agriculture has led to instability in the hydrological cycle, resulting in the intensification of land and water salinization across extensive regions (Zhang et al., 2001). Forest hydrologic impacts have received much attention in studies of land use change impacts on water cycle, particularly the effects of afforestation and deforestation. It is well acknowledged that surface runoff and groundwater recharge will increase when forests are cut down in favor of agricultural land use (Crosbie et al., 2007). Crosbie et al. (2007) reported that land use change from annual cropping and pasture to tree belts with perennial pasture led to a significant reduction in runoff for a small cultivated catchment in central New South Wales, Australia. Chen and Yu (2015) evaluated the potential effects by using two land use change scenarios in southeast Queensland in Australia and concluded that extreme land use change could influence flooding significantly for rural catchments rather than urbanized catchments. The significance of water resources in nature and society highlights the need to understand how land use change affects regional streamflow regimes. However, General Circulation Models (GCMs) and hydrologic models are widely applied in previous studies to assess future hydrological response without integrating land use change. The impacts of only land use change or only climate change on runoff have been researched in a lot of studies (Lahmer et al., 2001; Tollan, 2002; Bathurst et al., 2011; Reshmidevi et al., 2018). However, not many studies have researched the coupled effects of both climate and land use changes in runoff impact assessment. Therefore, a detailed understanding of the coupling effects of climate and land use changes on runoff can provide valuable scientific reference for water and land use management in a warming climate.

1.2.2 Climate change impacts based on GCMs downscaling data

Climate change can influence the regional water cycle significantly through changes in different climatic variables (Su et al., 2017). GCMs are the primary tools to simulate climate at global and regional scales. GCMs are commonly used for historical climate simulations and future climate projections forced by greenhouse gases and aerosols. They typically separate the ocean and atmosphere into a horizontal grid with the resolution of 2 to 4° latitude and longitude and 10 to 20 layers vertically (Dibike and Coulibaly, 2005). GCMs are the best means for regional and global climatic simulations, especially with the large progress in climatic modelling over the past several decades. Nevertheless, GCMs are usually unreliable to simulate climate variables realistically at local scales (a few kilometers) given their coarse resolutions (175–400 km grid cells). Assessments of future streamflow often require daily data, such as temperature, precipitation at catchment, or even station scales. But archived daily series from GCMs simulation are only available for specific time periods of several decades at present (Liu and Zuo, 2012). Thus, GCMs simulated climate variables are usually too temporally and

spatially coarse to be applied directly in hydrologic modelling. Therefore, it is important to develop downscaling approaches to convert large-scale GCMs outputs into catchment-scale climate variables.

1.2.3 Modelling methods of hydrologic response to climate and land use changes

The impacts of climate and land use changes on water balance in catchments is a priority in current hydrologic research. The combination of climate and hydrologic models is commonly used to evaluate the impact of climate change on hydrologic elements. Usually, climate models (GCMs or RCMs (regional circulation models)) are applied to produce future climate series, and then the simulated sequences from the climate models are downscaled to regional scale for hydrologic simulation using hydrologic models. Land use change will alter hydrological process such as evapotranspiration and surface runoff generation, thereby influence the catchment water balance. Research methods of hydrologic response to land use change mainly contain paired catchment method and hydrologic modelling method. Paired catchment method can provide information of land use change impacts on streamflow directly, but they usually need long periods and only suitable for small catchments. Therefore, hydrologic modelling is becoming a significant method to evaluate land use change effects on water cycle, particularly the distributed hydrologic models with a physical basis (Wang et al., 2008). The spatial distribution of changes in hydrologic variables can be simulated using distributed hydrologic models at a catchment scale. Thus, distributed hydrologic models have become major tools to study the water cycle and can also be adopted as effective means to assess land use change impacts.

Commonly used distributed models include SHE (Abbott et al., 1986), IHDM (Wood, 1996), SWAT (Arnold and Fohrer, 2005), THALES (Adams et al., 2012), USGS (Rose and Peters, 2001), SLURP (Viney et al., 2009), WATFLOOD (Toth et al., 2006), and PRM (CHEN et al., 2009a). SWAT (Soil and Water Assessment Tool) model is a semi-distributed watershed hydrologic model with physical foundation. It can simulate long-term water balance components (e.g., runoff) at daily scale (Brown et al., 2015). This model has been used successfully to model environmental change impacts on hydrologic cycle, which makes SWAT a commonly used hydrologic tool for land use change impacts studies (Zhang et al., 2012; Baker and Miller, 2013; Narsimlu et al., 2013). Nevertheless, cases from tropical or western Australia are scarce with more research focused on the eastern and southeastern areas (Saha and Zeleke, 2015). Generally, plant growth modelling is essential in distributed hydrologic models due to the important role of evapotranspiration in the hydrologic cycle (Abbaspour et al., 2015). SWAT uses a simple plant growth module to simulate the growth and yield of various vegetation types (Abbaspour et al., 2015). This plant growth module was built for temperate

regions and is not applicable for tropical areas (Wagner et al., 2011). Thus, the applicability of the model for simulating plant growth in the tropics has not been critically reflected in most SWAT studies, probably because hydrologic model calibration and validation typically use streamflow or water quality data (Strauch and Volk, 2013). Nevertheless, the successful reproduction of these outputs does not mean the proper simulation of the inner hydrologic process within the catchment (Strauch and Volk, 2013). As a result, several studies including tropical cases have been carried out to modify the plant growth module in the SWAT model (Alemayehu et al., 2017; Ma et al., 2019). For example, Strauch and Volk (2013) proposed an optional method that can generate a new growth season automatically during the dry to wet season transition according to changes of soil moisture in tropics. Nevertheless, as far as we know, SWAT with a modified plant growth module has never been used in tropical Australia before. Hence, the performance of the improved SWAT model (SWAT-T) (Strauch and Volk, 2013) is needed to be explored and assessed in tropical Australia. In addition, as far as we know, coupling SWAT with multiple GCMs and different land use scenarios has not been applied in south-western Australia (SWA) yet. Therefore, the hydrologic responses to climate and land use changes in SWA is needed to be studied with statistically downscaled daily climate data from GCMs and different land use scenarios.

1.3 Significance

As the air temperature rises, climate change is intensifying the water cycle (Huntington, 2006; Oki and Kanae, 2006). Australia has one of the most variable climates in the world (Stokes and Howden, 2010) and river stream flows in Australia have been affected significantly by climate change. Furthermore, land use change in Australia, together with extensive agriculture development, has caused an imbalance in the hydrological cycle, resulting in the intensification of land and water salinization in large regions (Zhang et al., 2001). Thus, it is essential to research the combined impacts of climate and land use changes on water balance components (such as evapotranspiration, runoff, and soil water).

The outcomes of this project can not only improve the evaluation system and method of climate and land use changes impacts on water cycle, but also provide a scientific basis for the sustainable utilization of water resources and comprehensive catchment management in a future changing environment.

1.4 Proposed thesis outline

The proposed outline for this thesis is as listed below:

(1) Introduction

(2) Literature review

(3) Hydro-meteorological characteristics and climate elasticity of catchments under different climatic conditions

(4) Impacts of future climate change on water resource availability of eastern Australia: A case study of the Manning River basin

(5) Using an improved SWAT model to simulate hydrological responses to land use change: a case study of a catchment in tropical Australia

(6) Quantifying the impacts of future climate and land use changes on hydrological processes and associated uncertainty in southwestern Australia

(7) Final conclusions and future research

Chapter 2. Literature review

This chapter will provide a comprehensive review of literature related to the assessment of climate change and land use change impacts on water balance components and related research methods. The objective of this chapter is to provide strong background information for this PhD research in understanding the hydrologic response to climate and land use changes and to provide applicable research methods.

2.1 Climate change and land use change

2.1.1 Climate change

Climate is the atmospheric conditions (e.g. temperature, solar radiation, precipitation, and so on) that prevail in a certain area. Climate change refers to the significant and permanent change of the statistical distribution of weather patterns for any wide range of time scales from decades to millions of years (May, 2008). Evidence shows that global climate is changing. In 2014, IPCC (Intergovernmental Panel on Climate Change) issued the Synthesis Report (IPCC, 2014) which distils and integrates the findings of Working Groups I, II and III contributions to the Fifth Assessment Report (AR5). Among the major conclusions of this report are the following findings:

(1) Many of the changes observed since 1950s have been unprecedented in the past few decades to thousands of years. The atmosphere and oceans have warmed up, the amount of snow and ice has decreased, and sea levels have risen.

(2) Since 1850, each of the Earth's surface temperature of the past three decades has been sequentially higher than any prior decades. In areas where it is possible to make this assessment in the Northern Hemisphere, the period of 1983-2012 may have been the hottest 30-year period in the past 1400 years (medium confidence given in the IPCC report to this conclusion). The global average of the combination of land and sea surface temperature data which was calculated by the linear trend indicates a warming of 0.85 [0.65 to 1.06] °C from 1880 to 2012.

(3) Observations reveal that many extreme weather and climate events have changed since around 1950. Some of these changes are related to human impacts, including an increase in warm temperature extreme events, a decrease in low temperature extreme events, an increase of heavy rainfall events in many regions and a rise of extreme high sea levels. On the global scale, it is highly possible that the number of cold days and cold nights has declined whilst the number of warm days and warm nights has increased. The frequency of heat waves is likely to have increased in most parts of Australia, Europe, and Asia.

Over the 100 years from 1910 to 2009, surface temperature of the Australian continent has risen by just under 1°C, which is more than the global average temperature of 0.7°C for the same period (Cleugh et al., 2011). Average temperature has warmed by about 0.7°C since the middle of the 20th century in Australia (Cleugh et al., 2011). This trend is continuing: the past decade (from 2000 to 2009) was the hottest decade on record in Australia (Cleugh et al., 2011). The precipitation also changes significantly since 1900 and especially since 1950 in four regions: northeast Australia, southeast Australia, northwest Australia, and southwest Australia (Keenan and Cleugh, 2011). During the 'Big Dry' (Sohn, 2009) or Millennium Drought which is in the period from 1995 to 2009, southeast Australia experienced the most severe drought in the last 120 years of instrumental records (Ummenhofer et al., 2009). The temperature over Australia is projected with a 1.0 to 5.0°C rise by the year 2070 (compared to 1990) using CMIP5 models and the climate projections also include a long-term drying in southern regions in winter, particularly in the southwest (IPCC, 2013). Extreme events are predicted to occur more frequently with the continuity of the global warming (Head et al., 2014).

2.1.2 Land use change

Land use change has attracted increasing attention of scholars worldwide since 1990. Recognizing this change is directly associated with human activities, which is the dominant factor in global change (Xiubin, 1996). Land use change contributes greatly in land-atmosphere interaction and biodiversity loss, and is a main factor affecting sustainable development (Turner et al., 1995). Land use change can influence biodiversity, global carbon budgets, and ecosystem function directly (Aide et al., 2013). The increased land surface net energy flux due to deforestation and other types of land use change has been a significant forcing on global climate in the last 200 years (Brovkin et al., 2006). The radiative forcing estimated globally caused by land use change is -0.2 (±0.2) W m^{-2} (IPCC, 2007).

In last decades, many regions of the world have experienced extensive land use change (Schirpke et al., 2012). Although the net reduction of global natural forest area slowed down between 2000 and 2010 (Meyfroidt and Lambin, 2011), deforestation is still one of the main processes of land use change with numerous impacts on global environment change (Lambin and Geist, 2008). During the past two decades, in the process of rapid urbanization, a great number of natural lands such as forests and wetlands have been exploited and developed into farmland or human settlements in China (Song and Ding, 2009; Yu et al., 2011). In the first decade of the 21st century, massive deforestation happened in Caribbean and Latin America, but an increase in >360,000 km^2 of woody vegetation also occurred throughout the area (Aide et al., 2013). Around 30% of the entire forestland is under pressure of rapid land use change in

North-East India, which is recognized as one of the biodiversity hotspots worldwide (Lele and Joshi, 2009).

In Australia, 45% of the indigenous woodland had been cleared in the Comet catchment in the mid-1960s and clearing reduced native woodland cover from 83% to 58% in the Upper Burdekin catchment during the period from 1998 to 2009 (Peña-Arancibia et al., 2012). After the European land use for two centuries, an extensive transformation and disturbance has occurred in the indigenous ecosystems of Australia (Hobbs and Hopkins, 1990; McKeon et al., 2004). About 15% of this continent was cleared or severely transformed, which centered on the intensive land use area in southeastern and southwestern Australia (IPCC, 2007). Massive grazing covers about 43% of this continent and concentrated cropping and improved pastures cover approximately 10% (IPCC, 2007). A large amount of the vastly grazed land has been influenced by periods of pasture and soil degradation followed by fractional recovery, primarily driven by favorable climate conditions (McKeon et al., 2004). Most of the grazed land has experienced a series of increased grazing pressure over favorable climate episodes in the last 200 years, followed by long-term drought episodes with high interference to pasture and soil conditions. Due to the land fragility and a highly variable climate in this continent, land use change and land management practices are extremely important to future vegetation, soil, and water resources in Australia.

2.2 Downscaling methods

2.2.1 Change factors (CFs)

Over recent decades, there has been increasing interest in modelling runoff response studies in various river basins and countries (Chiew et al., 1995; Menzel and Bürger, 2002; Chen et al., 2007; Maurer, 2007; Chen et al., 2012; Gosling et al., 2017). Most research studies focus on runoff and studies on other water balance components such as actual evapotranspiration and soil water are rare. In most of those studies, GCMs have become the main tools available to simulate climate at global and regional scales. Nevertheless, GCMs simulated climate data are usually too coarse and cannot be directly used in hydrologic simulations. Thus, it is necessary to use downscaling methods to convert large-scale GCMs outputs to catchment-scale climate variables.

In the recent decades, a variety of downscaling approaches have been used for converting the large-scale GCMs simulations to catchment-scale climate variables (Gordon and O'Farrell, 1997; Diaz-Nieto and Wilby, 2005; Ahmed et al., 2013). Change factors (CFs) methodology, the most straightforward and simplest method, is often used for strategic-scale evaluations of climate change influences whereby future climate change predicted by GCMs are used in the

baseline climatology (Diaz-Nieto and Wilby, 2005). The differences between the control and future GCMs simulations are used in baseline observations by just scaling or adding the average climatic CFs to each day (Fowler et al., 2007). The production of climate scenarios is made up of two steps in the simple methods. First, estimate mean annual changes in temperature and precipitation with GCMs simulated baseline and future estimates (e.g., $\Delta T = +1, +2$ and $+4°C$ and $\Delta P = 0, \pm10\%, \pm20\%$). Second, adjust the historical temperature and precipitation sequences by adding ΔT and multiplying the values by $(1 + \Delta P/100)$ respectively to obtain the local scaled future values (Xu, 1999). Though CFs can be rapidly used in GCMs to generate a series of climatic scenarios, there are some caveats about this method. For example, CFs assume that GCMs project relative changes more accurately than absolute changes (i.e., assuming a stable bias through time). In addition, this approach only scales the average, maximum, and minimum of climate variables, neglects the variability changes, and assumes that the climatic spatial pattern remains unchanged (Diaz-Nieto and Wilby, 2005). Moreover, there is no change in the temporal sequence of wet days for precipitation, so the method may not be helpful when changes in dry and wet spells are critical to climate change impacts assessments (Anandhi et al., 2011).

2.2.2 Dynamical and statistical downscaling

Another two basic downscaling methods exist to downscale the large-scale GCMs outputs to a more precise spatial resolution: the first one is dynamical downscaling which includes the precise solving of the system's process-based physical dynamics, and the second one is statistical downscaling that employs identified system relationships based on observed data.

2.2.2.1 Dynamical downscaling

RCMs (regional climate models) or LAMs (limited area models) are used in dynamical downscaling to derive finer resolution outputs under GCMs' large-scale and lateral boundary conditions (Fowler et al., 2007). This method can realistically simulate regional climatic features such as daily and seasonal variations of precipitation under different climatic conditions (Zhang et al., 2003), orographic precipitation (Frei et al., 2003), regional scale climatic anomalies and nonlinear effects (Leung et al., 2003), and extreme climatic events (Fowler et al., 2005; Frei et al., 2006). Dynamical downscaling has the ability to produce finer resolution information from GCMs outputs which can resolve atmospheric processes at smaller scales based on physical consistent processes (Fowler et al., 2007).

However, this method is highly computational demanding, is expensive to run as global GCMs (Wilby and Wigley, 1997), and is confined to 'time slices'. For instance, most RCMs are run normally for a 30-year period from 2070 to 2100, which makes climate change impacts

for other time periods hard to evaluate (Fowler et al., 2007). In addition, dynamical downscaling methods tend to inherit systematic biases from GCMs and strongly depend on the presence and strength of forcing at regional scale such as vegetation cover, land-sea contrast, and orography (Fowler et al., 2007).

From previous studies, dynamical downscaling is often more skillful in New Zealand, western U.S. and Europe, where topography impacts on precipitation and temperature are prominent, than in areas such as China, the U.S. and Great Plains where regional forcing is weaker (Wang et al., 2004). Dynamical downscaling generated more realistic estimates of hydrologic impacts in mountainous areas such as the western U.S. derived from an ensemble of climate simulations at regional scale (Leung et al., 2002). This method can also produce improved simulations of higher moment climatic statistics (e.g., extreme climatic variables such as extreme high/low temperatures and intense precipitation) for the control climate, and thus generate more reasonable climate scenarios for climate variability and extreme events at the local scale (Wang et al., 2004). Since human society is more vulnerable to changes of the intensity or frequency in extreme climatic events (such as floods, droughts, and heat waves) rather than moderate climate states, dynamical downscaling will remain as a crucial downscaling method for providing regional climate information to assess climate change impacts.

2.2.2.2 Statistical downscaling

The second method, statistical downscaling method, is less computationally demanding. In this method, regional-scale atmospheric predictor variables (e.g., area mean temperature and precipitation) and circulation characteristics (e.g., average sea-level pressure and vorticity) are linked to station-scale climatic sequences (Kim et al., 1984; Karl et al., 1990; Wigley et al., 1990). Statistical downscaling approaches are commonly categorized into three groups (Wilby and Wigley, 1997), namely: regression approaches (Wigley et al., 1990), weather pattern-based methods (Lamb, 1972; Bardossy and Plate, 1992; Wilby, 1995), and stochastic weather generators (Richardson, 1981; Wilks, 1992; Katz, 1996). A range of methods included in each of the groups all rely on the basic concept that regional climate is primarily a function of large-scale atmospheric condition (Fowler et al., 2007).

The main advantages of statistical downscaling are: (1) it is relatively low-cost and computationally efficient; (2) it can produce point-scale climate variables from GCMs' large-scale outputs; (3) it can be applied to provide variables which are not accessible from RCMs; (4) it is easily transferable to other regions; (5) it can incorporate observations directly into methods; and (6) it is based upon standard and accepted statistical procedures (Fowler et al., 2007). Due to such advantages, statistical downscaling methods have been widely adopted in

regional climate change impacts assessment, particularly in the hydrologic response assessment (Hay and Clark, 2003; Wood et al., 2004; Chen et al., 2012). However, this method also has disadvantages: (1) it requires long and reliable observed sequences for calibration; (2) it depends on the selection of predictors; (3) it has non-stationarity in the predictor-predictand relationship; (4) climate system feedbacks are not included; (5) it is dependent on GCMs boundary forcing and influenced by bias in underlying GCMs; and (7) climatic area, domain sizes, and seasons influence downscaling skill.

Combinations of weather generators and statistical downscaling techniques have been used in improving the realism of the downscaled data. Zhang (2007) downscaled monthly GCMs temperature and precipitation to a specific site using a spatial transfer function and then adopted a Richardson-type weather generator to produce daily climate sequences based upon the spatially downscaled monthly GCMs outputs. Liu and Zuo (2012) used an inverse distance-weighted interpolation approach to downscale monthly GCMs outputs to specific sites, then a bias correction procedure was used for the monthly GCMs values of each site and daily climate projections for each site are produced by using a stochastic weather generator, WGEN. These approaches bridge the spatiotemporal gaps between the coarse resolution of GCMs projections and finer resolution of data requirements of hydrologic models, which can be used for assessments of climate change impacts on water resources using hydrologic models.

2.3 Climate change and land use change impacts on water cycle

One of the key impacts of a warming climate will be on water resources (Gosling et al., 2017). It is widely acknowledged that climate variability will impact streamflow regimes worldwide. In the recent past, hydrological response to global climate change has been widely discussed. Global climate change is intensifying hydrologic processes as the temperature rises (Huntington, 2006; Oki and Kanae, 2006). Changes in mean precipitation of a warmer world are projected to exhibit substantial spatial variation under the RCP8.5 scenario. Average precipitation is predicted to rise in some areas while decrease in other regions, and yet others are projected to have no significant changes at all (IPCC, 2013). The global mean sensitivity of the 20-year return value for the annual maximum daily precipitation varies from 4% $°C^{-1}$ (mean value of CMIP3 models) to 5.3% $°C^{-1}$ of local temperature rise (mean value of CMIP5 models) with regionally wide diversification (IPCC, 2013). Annual surface evaporation will rise as world temperature goes up across most of the ocean and will shift over land following a similar mode as precipitation. By the end of the 21st century under the RCP8.5 scenario, annual runoff is predicted to decline in parts of the Middle East, southern Africa, and southern Europe, while annual runoff is predicted to increase in the high northern latitudes, and in agreement with the great increases in winter and spring precipitation there. By the end of the 21st century, soil

moisture is predicted to decrease in regional to global-scale and the risk of agricultural drought is projected to increase in presently dry areas with medium confidence under the RCP8.5 scenario (IPCC, 2013).

Changes in land use will bring dramatic effects to the structure and function of the earth ecosystems, such as the contamination of the soil surface and groundwater in the hydrological cycle (Honisch et al., 2002). The land use change impacts on water cycle mainly include impacts on water quantity, water quality, and rainfall-runoff relationship. Watershed land use change, such as urbanization, crop cultivation, deforestation, afforestation, and reduction of wetlands and floodplain, have profoundly affected all the processes or links of the water cycle. Runoff can reflect the ecological status of the whole drainage basin and can also be applied to predict the land use change impacts on water resources in the future. Therefore, the research of land use change impacts on hydrologic cycle mainly focuses on the impacts on runoff.

At the regional scale, urbanization is the most dramatic land use change caused by human activities. Study of urbanization impacts on runoff mainly focuses on the following aspects: verify the hydrological theory that urbanization will lead to increase in runoff, the impacts of the ratio, attributes and configuration of the impervious area on runoff, impacts of urbanization on groundwater and so on (Jacobson, 2011).

At the global scale, deforestation and afforestation are the most important drivers of land use change that affect hydrological processes (Calder and Maidment, 1992). In hydrologic response to land use change studies, forest hydrologic impacts have received much attention, particularly the influence of deforestation and afforestation on hydrological cycle. Extensive research has been undertaken to understand the hydrological role of vegetation (Horton, 1919; Penman, 1963; Turner, 1991). It has been established that decreases in forested land area will lead to an increase in average runoff (Bruijnzeel, 1989). Studies in many catchments has shown that conversion of forested land to cultivated land (dry crops) or grassland will lead to an increase in runoff, storm flow, peak discharge, and peak flow velocity, and a decrease in the time at which the flood level reaches its peak (Calder et al., 1995; Fohrer et al., 2001; Roo et al., 2001; Thomas and Megahan, 2001). Deforestation (especially on highland) increases the intensity and frequency of downstream flooding (Richey et al., 1989). From extensive previous studies, infiltration, groundwater recharge, and total annual water yield had a proportional increasing trend to the area of forest removed on small (i.e., <1 km^2), mostly moderate experiment catchments (Bonell and Bruijnzeel, 2005; Brown et al., 2005; Aijm and Keenan, 2007; Peel, 2009). However, there are many arguments about the forest's impacts on hydrological cycle, and it is difficult to draw a consistent conclusion between different catchments, especially between the catchments with large areas (Bruijnzeel, 1990). The main

reason for this may be that the diversified land use types and the great spatial and temporal differences of precipitation in large scale catchments will lead to the non-obvious hydrological response to forest land change (Costa et al., 2003). For example, Wilk et al. (2001) found no variation in average annual streamflow in a big catchment of northeast Thailand after 63% of the original forest cover was removed. But this also occurs in small catchments. For instance, Zhou et al. (2010) found that streamflow did not decrease as would have been concluded based on the experiments of small catchments after 37% afforestation in Guangdong Province in China. Bruijnzeel (1990) analyzed hydrological response to deforestation of moist tropical forests and concluded that selective slight deforestation (< 20% loss of biomass) had very little impacts on runoff and deforestation of natural forest may result in considerable increase in water yield.

Catchment land use change is characterized by the mutual transformation and shifting of different land use types, the expansion or transformation of a certain land use type must be accompanied by the reduction of one or several other land use types. Therefore, land use change impacts on water balance components in a catchment is the comprehensive impacts of change of multiple land use types. The study of Lahmer et al. (2001) showed that when cultivated land was converted into grassland, dry grassland or meadow grassland, the hydrological process did not change significantly in a medium or large scale basin and its sub-basins, and the reason is that the hydrological effects of these land use patterns are similar under mild climate conditions. Land use change impacts on runoff is also related to the proportion of land use change area to the catchment area, the land use change location in the catchment and so on. Eckhardt et al. (2003) found that in the circumstance of a change between pasture and forest and with respect to mean streamflow, the minimum proportion of land use change area to the catchment area to derive significantly obvious model responses amounts to at least 25%. The land use change impacts on runoff are significant, although the conclusions are significantly different because of the differences in climate, vegetation types, and natural geographical features such as catchment areas, river systems, and so on.

2.4 Research methods of hydrologic response to climate and land use changes

2.4.1 Research methods of hydrologic response to climate change

At present, the research methods evaluating climate change impacts on the water cycle fall into three main categories: (1) using statistical methods to detect the relationship between hydrologic factors and climatic variables; (2) using hypothetical climatic scenarios (such as increase temperature or rainfall) to evaluate the sensitivity of hydrologic factors to climate change; and (3) assessing climate change impacts on hydrology using hydrologic models and

future climate projections from GCMs (Fan and Cao, 2008). These methods basically conform to the pattern of 'future climate scenarios production- hydrological simulation - impacts research', in which the build of hydrological models and the generation of future climate scenarios are the most important.

Future climate scenarios are reasonable descriptions of future climate variables at appropriate temporal and spatial scales, which are based on a series of scientific assumptions. At present, there are three common methods to derive future climate scenarios: (1) arbitrary hypothetical scenarios method (Nash and Gleick, 1991); (2) time series analysis method (Jiang, 2011); and (3) GCMs method (Reshmidevi et al., 2018). GCMs are the primary tools usable for regional and global climate simulations. Specific introduction about GCMs and downscaling methods have been discussed in detail in chapter 2.2.

To simulate historical and future runoffs and assess the climate change impacts on runoff, downscaled climatic variables are often used as input data to hydrologic models (Chang and Jung, 2010; Vaze and Teng, 2011; Ruelland et al., 2012). In such hydrologic modelling, hydrologic models are usually first calibrated with historical runoff data, then the hydrologic models are run with downscaled future climate data using the same optimized parameters, and the impacts of climate change on runoff are evaluated with the simulated historical and future runoff (Chiew et al., 2009; Reshmidevi et al., 2018). In this process, according to previous studies, the use of only one GCM has been detected as a main contributor to the whole uncertainty (Wilby and Harris, 2006; Jie et al., 2011). Uncertainties caused by Green House Gas emission scenarios and the structure of hydrological models have been detected to be the least important (Wilby and Harris, 2006; Minville et al., 2008; Jie et al., 2011; Woldemeskel et al., 2012). As a result of the enormous uncertainty caused by the selection of only one GCM, multi-GCMs ensemble has been used in lots of recent studies (Tebaldi and Knutti, 2007; Knutti et al., 2010; Zhang and Huang, 2013) and multi-GCMs mean seems to provide superior simulation for climate variables than only one GCM (Knutti et al., 2010; Zhang and Huang, 2013).

Both the global-scale and local-scale (catchment) models can be adopted to assess hydrological response to climate change. Global-scale models produce comparatively global overviews of hydrological response to climate change which is usually not reliable at the local scales, where the climate change impacts exist and corresponding suitable adaptation strategies should be scheduled and implemented. Consequently, climate variability impacts should be done properly using river-basin models at regional scale (Krysanova and Hattermann, 2017).

2.4.2 Research methods of hydrologic response to land use change

Land use change impacts on the hydrological cycle is mainly reflected in the change of water quantity, water fluxes (e.g., ET and runoff), and water quality. The differences in spatial distribution of evapotranspiration caused by different land uses will have impacts on the hydrological cycle (Mao and Cherkauer, 2005). Compared with the long-term characteristic of climate change, land use change is one of the major driving factors for hydrologic changes in the short term. It impacts the hydrological cycle by influencing canopy interception, infiltration, evapotranspiration, and surface runoff.

Usually, three major approaches are used to analyze land use change impacts on hydrology and water resources quantitatively: (1) "paired-catchment" experiment approach; (2) runoff time series analysis approach; and (3) hydrologic model approach (Guo et al., 2012). Two catchments with similar climate, area, shape, vegetation, and soil will be chosen and observed in the "paired-catchment" experiment approach. Commonly, the first 3-5 years (better if include wet, normal, and dry years) are the correction period without any experiment treatments. Then, the land cover of one of the catchments will be altered artificially with other conditions remain unchanged. The other catchment, referred to as the "reference catchment", will remain its initial state. After a period of observation, land use change impacts on water quantity will be analyzed quantitatively with the comparison of the runoffs in two experiment catchments. The advantage of this method is that it can eliminate the error caused by climate change during the observation period, but its disadvantage is that it can only be studied in the experimental areas with catchment area generally less than $100 \, km^2$. The second statistical analysis of runoff time series method in a single catchment can be applied to examine the changing trend of hydrological and meteorological sequences, but the spatial heterogeneity of the catchment and the mechanism of land use change on hydrological cycle could not be derived. Since 1970s, hydrologic models are more commonly used in land use change impacts on water cycle studies with the development of computer science, Geographic Information System, and Remote Sensing technology. The advantages of hydrologic models are that spatial heterogeneity and hydrological process would be considered, and land use change impacts could be simulated continuously. Therefore, how to build distributed hydrologic models to evaluate land use change impacts on water resources is a question that must be deeply studied.

2.5 Watershed potential evapotranspiration models

Evapotranspiration is one of the principal components in the water balance equation, and its reasonable calculation will directly affect the water balance in a catchment. Catchment evapotranspiration is generally dominated by soil evaporation and plant transpiration.

Catchment evapotranspiration data are mainly obtained from a few evaporation gauge stations, and areal evapotranspiration are derived from point observation data. In this way, the impacts of topography and different land use types on catchment evapotranspiration are not considered, resulting in the error of catchment evapotranspiration data as input into hydrological model. Nowadays, distributed hydrological model, in which the catchment can be divided into different grid elements according to topography, land use, and soil types, has become one of the most important methods in hydrological simulation. Therefore, how to make reasonable estimation of catchment evapotranspiration using meteorological data, land use, and soil data when the observation data is scarce is a hot research issue at present.

The process of watershed actual evapotranspiration is extremely complicated and reasonable estimation relies on the availability of data pertaining to climatic conditions, crop water demand, soil moisture, land use, and soil texture (Morton and Morton, 1983). Evapotranspiration is closely linked with vegetation characteristics. Vegetation is one of the three kinds of natural land surface in the return of rain to the atmosphere, and the other two surfaces are bare or fallow soil and open water (Penman, 1948). The role of vegetation in the hydrological cycle has been researched for several decades (Horton, 1919; Wicht, 1941; Penman, 1963; Bosch and Hewlett, 1982; Turner, 1991). Two categories which are "paired-catchment" experimental techniques and "single-catchment" water balance research were both applied to derive sources of information on water balance related to vegetation change (Zhang et al., 2001). The results of "paired-catchment" experiments (Bosch and Hewlett, 1982) revealed that there were large differences in catchment responses to vegetation cover changes. Nevertheless, one clear conclusion was that the decrease of forest cover would increase water yield through decreasing evapotranspiration. The "single-catchment" water balance research was not designed particularly to assess water yield response to vegetation changes. However, these studies can provide helpful information concerning the hydrologic role of vegetation as they represent catchments with various climates, vegetation, and soils. Based on these studies, some empirical relationships were established correlating evapotranspiration with vegetation types at specific sites (Holmes and Sinclair, 1986; Turner, 1991). However, the suitability of these empirical relationships for other catchments requires evaluation (Zhang et al., 2001). In 2001, Zhang et al. (2001) established a two-parameter model to link average annual evapotranspiration with potential evapotranspiration, rainfall, and plant-available water capacity, this model is scientifically justifiable and has potential application in land use change research.

Potential evapotranspiration is usually first calculated in watershed hydrological models, and then actual evapotranspiration is calculated according to potential evapotranspiration which

is related to parameterization schemes of soil, vegetation, and other factors. Heat balance method and aerodynamic methods are two basic methods to calculate potential evapotranspiration. In 1948, based on energy and aerodynamic basis, Penman (1948) combined the two basic methods and proposed a water surface evaporation formula with definite physical mechanism, that is, the Penman formula. The Penman formula can avoid direct measurement of water surface temperature, and only the conventional meteorological data (such as sunshine hours, temperature, absolute humidity, and wind speed) are needed to calculate evaporation, so this formula is widely used. The disadvantage of this formula is that it does not calculate the water produced by plant transpiration into the atmosphere. In 1965, Monteith (1965) improved Penman formula by adding the concept of leaf stomata opening and water vapor diffusion resistance from leaves and the famous Penman-Monteith formula is obtained by using aerodynamic resistance to describe the turbulent diffusion and using canopy stomatal resistance to describe molecular diffusion. In the early days, the Penman-Monteith formula could only be used for single point evapotranspiration calculations. Since 1960s, the rapid development of computer technology and geographic information technology provide very effective technical means to calculate watershed spatial distribution of evapotranspiration and many researchers began to study the calculation of watershed evapotranspiration (Ma et al., 2012; Ruhoff et al., 2012; Tian and Martinez, 2012). The Penman-Monteith formula is a typical single layer structure formula for evapotranspiration calculation which assumes that all the exchange of energy and substance occurs in a horizontal plane between the canopy of the vegetation and the upper atmosphere. Many scholars have questioned the evapotranspiration model with single layer structure, Tanner and Fuchs (1968) thought that the exchange of energy and substance could occur in any part of the vegetation canopy, and not just focus on a hypothetical plane. Therefore, multilayer evapotranspiration model began to attract the attention of many scholars. The earlier multilayer evapotranspiration models include the Waggoner-Reifsnyder model (Waggoner and Reifsnyder, 1968), however, this model is only suitable for densely and evenly distributed forest areas. After that, Goudriaan and Waggoner (1972) modified the Waggoner-Reifsnyder model by increasing the calculation of soil evaporation to enable the multilayer evapotranspiration model to calculate the soil evaporation under different vegetation coverage. However, the multilayer evapotranspiration model also has some obvious disadvantages, for example, the model contains many calculation equations and requires a large amount of data input which make it more complex and not applicable in engineering applications. Therefore, since 1980s, many researchers have simplified the multilayer evapotranspiration model to derive the simplified model called dual source evapotranspiration model. Shuttleworth and Wallace (2009) established a two-layer evapotranspiration model to calculate sparse vegetation transpiration and soil evaporation, this model can calculate energy balance of vegetation canopy

18

and soil respectively, and the impacts of leaf area index (LAI) and soil water content on evapotranspiration are considered for the first time. Lafleur and Rouse (1988) compared the Penman-Monteith formula with the Shuttleworth-Wallace model and found that the simulation result from two-layer Shuttleworth-Wallace model was better than the single layer Penman-Monteith formula. Based on the Penman-Monteith formula, Choudhury and Monteith (1988) developed a dual source evapotranspiration model and validation indicated that the simulation results were consistent with the observation evapotranspiration. In 2004, MO et al. (2009) improved the dual source evapotranspiration model which based upon the Penman-Monteith formula to enable the model to calculate watershed actual evapotranspiration. Therefore, dual source evapotranspiration model has become widely used in the calculation of watershed evapotranspiration. Remotely sensed data can provide spatially and temporally continuous information of the land surfaces such as leaf area index, vegetation types, and vegetation indices. Thus, there has been considerable effort to estimate the distributed evapotranspiration using such remotely sensed data. In 2008, a simple biophysical model was introduced into surface conductance to modify the Penman-Monteith formula and use remotely sensed leaf area index to estimate daily mean evaporation at kilometer spatial resolution (Leuning et al., 2008). Moreover, downscaled high quality MODIS LAI was integrated into an improved plant growth model in SWAT and high accuracy in streamflow validation in the subtropics was reported by Ma et al. (2019). Therefore, how to integrate remotely sensed leaf area index into evapotranspiration models have become a hot project worthy of study.

2.6 Distributed hydrological models

Hydrological phenomena in nature are complex. Many factors interact in determining the different fluxes in the hydrological cycle. By far, it is impossible to observe all relevant factors of hydrological phenomenon, and unable to describe the causal relationship among each factor in hydrological phenomena using strict physical laws. So, there are still many problems unresolved and strict hydrological rules are still waiting for people to understand and explore. With the gradually increased understanding and researching of the causal relationship among each factor in hydrological phenomena, complex hydrological phenomena are generalized (with minor and stochastic factors ignored) and the main factors and basic laws are retained. Mathematical-physical models with certain physical meanings are then established and called "hydrological simulation". The simulated hydrological phenomena are called prototypes, and simulation is the generalization of the mathematical, physical, and logical aspects of the prototypes. Therefore, the watershed hydrological model is a mathematical structure established to simulate the catchment hydrological process and the first step in hydrological simulation is to develop a hydrological model.

According to the discrete degree of watershed hydrological simulation, watershed hydrological model can be divided into two groups: lumped hydrological model and distributed hydrological model. The lumped hydrological model takes the whole catchment as an entirety to carry out hydrological simulation. Such models do not consider the impacts of factors such as spatial distribution of precipitation and different land surface conditions on hydrological simulation and use the mean values of the entire catchment as the parameters of the hydrological model. Such models require less and simple input data, but the disadvantage is that the impacts of spatial distribution of precipitation and different land surface conditions on runoff production and flow concentration are not considered. However, the simulation results of such models are relatively superior in small-area catchments. Traditional lumped hydrological models include: the Xinanjiang model (Zhao, 1992), Shanbei model, Sacramento model (Burnash et al., 1973), and the tank model (Ismail et al., 1997). In 1969, Freeze and Harlan (1969) published a paper together and proposed physically-based hydrological models with distributed structure for the first time, and it was a prelude for scholars to study distributed hydrologic models. Distributed hydrologic models can capture the spatial distribution of input variables and physical parameters such as precipitation, land use, topography, and soil by dividing the catchment into many smaller computing units. In addition, the distributed hydrological models can simulate the spatial changes of hydrological process, but they need quality and intensive data and require greater simulation and calibration time. In the early 1970s, the development of distributed hydrological model fell behind lumped hydrological model because of the limitation of technical means and data. At that time, the distributed hydrological model could only be sketched as a blueprint or carried out under some experimental catchments. At the end of 1970s and early 80s, with the rapid development of computer and geographic information system, especially with the continuous improvement of the technology of geographic information system, the watershed underlying surface conditions such as topography, soil, and land use can be input accurately into each computing unit in the distributed hydrological model. Therefore, the distributed hydrological model has been developed rapidly and its advantages are also gradually emerging compared with the lumped hydrological model. In 1979, BEVEN and KIRKBY (1979) proposed the TOPMODEL in which the watershed topographic index is calculated using digital elevation model (DEM) and this topographic index can dynamically reflect the influence of different underlying surface conditions on the water cycle in the whole catchment. The advantages of TOPMODEL are that its parameters have clear physical meaning and it can simulate the hydrological process in ungauged areas, but this model is not a strictly distributed hydrological model because the impacts of the spatial distribution of rainfall and evapotranspiration on watershed hydrological cycle are not considered in this model. From the beginning of 1980s, SHE (Abbott et al., 1986), a catchment model produced and improved

together by the British Institute of Hydrology, the Danish Hydraulic Institute, and SOGREAH (France), is regarded as the first distributed hydrological model in the strict sense. This model divides the catchment into many grids to realize the spatial distribution of rainfall and parameters, and this model can be used for water quantity, water quality, and sediment simulation. In the 1990's, Morris built a hydraulics-based distributed hydrological model named IHDM (Wood, 1996). This model calculates overland flow using hydraulic method by some characteristics of watershed hillslope structure. In 1994, Dr. Arnold from the United States department of agriculture worked with the American Agricultural Research Center to develop the SWAT model (Arnold and Fohrer, 2005). This model combines the geographic information system and divides the whole catchment into different hydrological response units, each unit separately calculates water quantity, water quality, and sediment and has its corresponding parameters. Furthermore, THALES model (Adams et al., 2012), USGS model (Rose and Peters, 2001), SLURP model (Viney et al., 2009), WATFLOOD model (Toth et al., 2006), and PRM model (CHEN et al., 2009a) are all distributed hydrological models. To summarize, distributed hydrological models have become one of the hot topics in current hydrological research.

Chapter 3. Hydro-meteorological characteristics and climate elasticity of catchments under different climatic conditions

Abstract

Runoff is affected by underlying surface conditions, climate, and human activities. Driving factors and their impacts on runoff require detailed identification to provide a hydro-climatic foundation for drought-flood control and water resources management. First, the Mann-Kendall trend test, Mann-Kendall abrupt test, and wavelet analysis methods were applied to derive trend, mutation, and periodical characteristics and qualitatively identify relationships between the hydrologic and climatic factors in four Australian catchments (Wooroloo Brook, Murrumbidgee, Manning River, and North Johnstone) with different climatic conditions as case studies. Then linear regression analyses and climate elasticity (Budyko hypothesis) were used to quantitively identified the driving factors (i.e., temperature, precipitation, net radiation, relative humidity, wind, and human activity) and their impacts on runoff. Results showed significant trends of decreasing runoff in the Wooroloo Brook (1977-2017) and Murrumbidgee catchments (1975-2014). Based on a wavelet analysis, almost all climatic and hydrologic variables exhibited similar high frequency cycles (notable but not significant (95% confidence level)) of about 2-4 years. According to correlation analyses between annual hydrologic and climatic factors, runoff displayed the greatest correlation with rainfall in almost all catchments except the Murrumbidgee catchment while FAO56 potential evapotranspiration showed a greatest negative correlation with relative humidity and greatest positive correlations with maximum temperature and solar radiation for all catchments. According to the Budyko hypothesis, the order of influencing factors on runoff was: rainfall > parameter n of land use change > net solar radiation > maximum temperature > relative humidity > wind speed ≥ minimum temperature for Wooroloo Brook, Murrumbidgee, and North Johnstone catchments. For the Manning River catchment, the ranking of the influencing factors was: rainfall > net solar radiation > parameter n of land use change > maximum temperature > relative humidity > wind speed > minimum temperature. As expected, rainfall is the factor that most affects runoff, and an increase of 10% in rainfall generated an increase of 24.4% in runoff according to the average of the four catchments. Furthermore, the fractional contributions from climate change and human activity to runoff change were 55.5% and 44.5%, respectively, across the four catchments in Australia. These outcomes provide significant information for the development of efficient adaptation strategies and effective policy plans for sustainable water management in Australia in the future.

Keywords: Hydro-meteorological characteristics, climate elasticity, Australia

3.1 Introduction

Due mainly to climate change and human activity, water resources are increasingly scarce in most river basins (Vörösmarty et al., 2000; Ye et al., 2013; Brown et al., 2019). Runoff is a significant source of surface and groundwater storage recharge and is as well decreasing in most watersheds (Yang and Tian, 2009). Runoff is affected by underlying surface conditions, climate, and human activities (Zhi and Dongyong, 2015). Thus, recognizing the driving factors and their impacts on runoff has always been the focus in hydrologic studies (Yang and Tian, 2009), and can provide hydro-climatic basis for drought-flood control and water resources management (Teng et al., 2012a; Zhi and Dongyong, 2015).

Australia is the driest inhabited continent with the lowest river flow in comparsion to other continents, and its mean annual precipitation is about 450 mm (Poff et al., 2006). Therefore, water is a valuable resource over the country due to its scarcity (Zhang et al., 2016). Zhang et al. (2016) investigated streamflow variability and trends of 222 high-quality stream gauging stations in Australia and concluded that annual streamflow in New South Wales, Victoria, southeast South Australia, southwest Western Australia (SWWA), and northwest Tasmania displayed significant decreasing trends for most of the gauging stations. Rainfall is the main factor that affects runoff (Chowdhury and Beecham, 2010; Zhang et al., 2018). The variability of rainfall in Australia is greater than in elsewhere of the world with similar climates (Nicholls et al., 1997). This additional variability is largely related to the impacts of the El Niño–Southern Oscillation (ENSO) on Australia (Nicholls et al., 1997; Chowdhury and Beecham, 2010). Since 1970s, rainfall in SWWA has decreased by 15–20%, and the inflows to Perth drinking water reservoirs has declined significantly (Petrone et al., 2010). In addition, many studies have reported a trend of decreasing rainfall in southeast Australia (Hossain et al., 2013). In addition to rainfall, evapotranspiration plays a significant role in water and energy balance of the terrestrial ecosystem, affecting closely connected hydrologic processes such as runoff generation, soil moisture dynamics, and groundwater recharge (Shan et al., 2015). Any changes in climatic variables (e.g., air temperature, solar radiation, relative humidity, and wind speed) will affect evapotranspiration (Shan et al., 2015). Therefore, trend, mutation, and periodicity characteristics of runoff, rainfall, potential evpotranspiration, and other climate variables like air temperature, solar radiation, relative humidity, and wind speed will be detected using statistical analysis methods (e.g., Mann-Kendall trend test method) to help identify the most relevant climatic variables for runoff.

However, the statistical methods described above can only describe qualitatively the impacts of different meteorological variables on runoff. Therefore, climate elasticity of runoff, as a significant indicator to quantify the sensitivity of runoff to meteorological variables, has

been widely applied to assess the impacts of climate change on water cycle (Yang et al., 2014). There are hundreds or even thousands of studies are now available documenting the sensitivity of streamflow to climate for watersheds around the world (Sankarasubramanian et al., 2001; Chiew, 2006). For instance, Yang and Yang (2011) found that the precipitation elasticity of 89 catchments was 1.3-3.9 in Hai River and Yellow River basins in China. Sankarasubramanian and Vogel (2003) used a non-parametric estimator to record the precipitation elasticity of streamflow in 1337 catchments in the United States. Results indicated that 1% change in precipitation led to 1.5–2.5% change in runoff, depending on the degree of buffering by storage processes and further factors. Chiew (2006) estimated rainfall elasticity of streamflow for 219 catchments in Australia and the results indicated that the rainfall elasticity of streamflow was approximately 2.0–3.5 (observed in around 70% of the catchments) across Australia, namely, 1% change in average annual rainfall led to 2.0–3.5% change in average annual streamflow. However, except for precipitation, other factors such as climate variables (e.g., temperature, net radiation, relative humidity, and wind) and human activity also have impacts on streamflow.

The numerous methods to estimate climate elasticity can be divided into five categories (Sankarasubramanian et al., 2001). Within these approaches, an analysis approach for deriving climate elasticity of runoff according to Budyko hypothesis is theoretically clear and does not require a large number of observed climate and streamflow data (Yang et al., 2014). According to the Budyko hypothesis, Yang and Yang (2011) presented an analytical derivation of climate elasticity with parameter n used to describe the influence of the catchment characteristics. Yang et al. (2014) calculated the climate elasticity and assessed the contribution of climate change to runoff for each of the 210 catchments in China after calculating the parameter n. Based on Budyko framework, Huang et al. (2016) estimated the impacts of five climate variables (i.e., temperature, precipitation, net radiation, relative humidity, and wind) on annual streamflow change in 207 catchments in China. Results showed that the main climatic variables affecting annual runoff are precipitation in most regions of China, net radiation primarily in certain catchments in southern China, temperature and wind speed primarily in certain catchments of northern China. However, as far as we know, few studies have applied the Budyko framework to specific Australian catchments to study the effects of climate change and human activity on runoff.

The aim is to identify the driving factors (i.e., precipitation, temperature, net radiation, relative humidity, wind speed, and human activity) and their impact on runoff in four Australian catchments with different climatic conditions as case studies. The specific aims of this study were to: (1) derive trend, mutation, and periodical characteristics of the hydrological and meteorological variables using moving average method, Mann-Kendall trend test method,

Mann-Kendall abrupt test method, and wavelet analysis method; (2) illustrate the relationships between annual hydrological and meteorological variables using regression analysis method; and (3) quantify the sensitivity of runoff to climate variables and human activity using climate elasticity as a significant indicator based on Budyko framework.

3.2 Materials and methods

3.2.1 Study areas
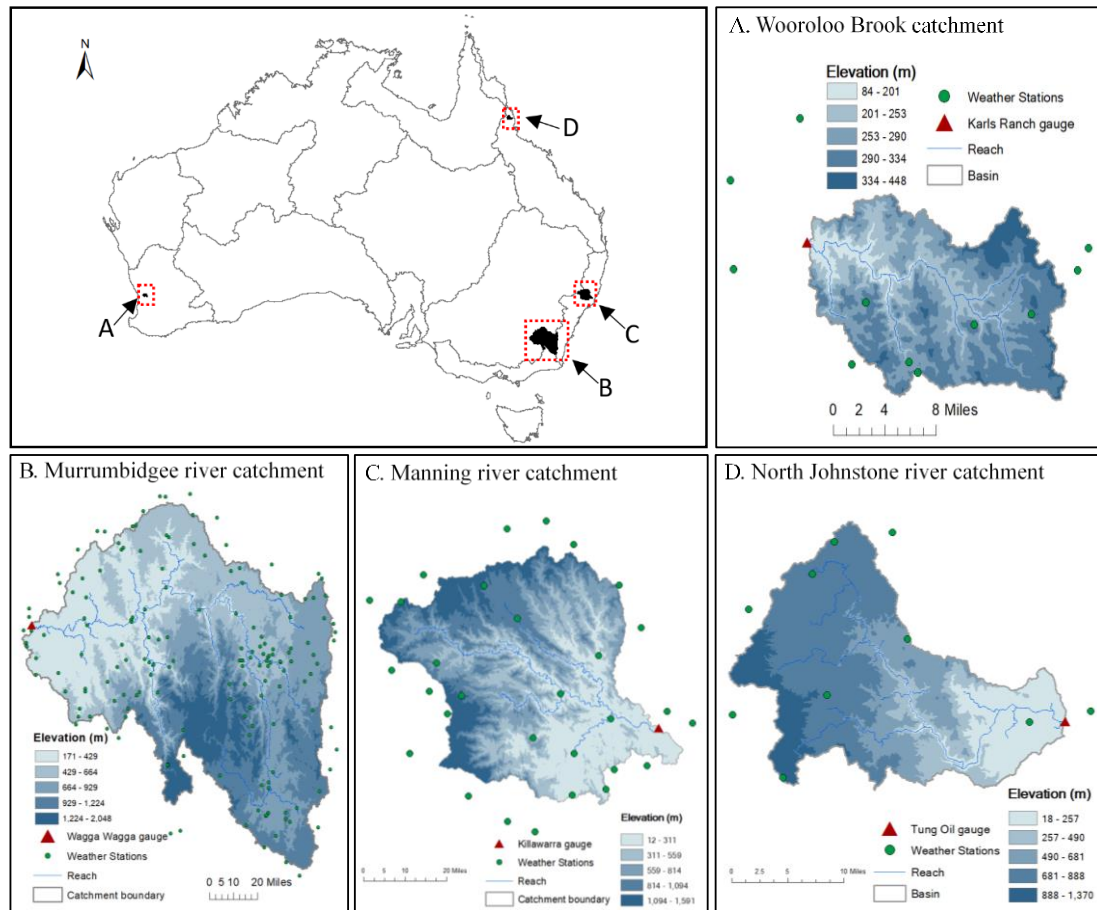
Figure 3-1 The study areas of the 4 catchments and the locations of weather stations and stream gauging stations.

In this study, 4 catchments, which are mainly located in the east coast, Murray-Darling basin, and western Australia (Figure 3-1), have been selected to represent the wide range of climate and streamflow characteristics across Australia.

The Swan-Avon River catchment, covering more than 120 000 km^2, is located in the southwestern Western Australia including parts of the metropolitan area of Perth (Viney and Sivapalan, 2001). Wooroloo Brook is one of the major tributaries of the Swan River in the Swan Coastal basin (CSIRO, 2009). The Wooroloo Brook catchment above Karls Ranch (Figure 3-

1A) was selected as one of the case study areas. The catchment area is around 515 km^2 and the elevation ranges from 84 m to 448 m. The annual average temperature is around 17.4°C, annual average rainfall is about 737.5 mm, and annual average runoff is approximately 75.5 mm (1977-2016) in this catchment.

The Murrumbidgee River basin is situated on New South Wales and the Australian Capital Territory. The Murrumbidgee River, the third longest river in Australia and a crucial river in the Murray-Darling system, flows in a commonly westerly direction before it discharges into the Murray River. Canberra (Australian capital city) and Wagga Wagga (the largest inland city of NSW) are the major cities in this catchment. Around 24% of the precipitation in the Murrumbidgee catchment above Wagga Wagga (27858 km^2, Figure 3-1B) appears as runoff under the mean climate condition, which contributes most of the river flow. The runoff coefficient is less than 2% below Wagga Wagga gauging station (Wen et al., 2011). Thus, the Murrumbidgee River catchment above Wagga Wagga gauging station was chosen as one of the case study areas.

The Manning River catchment, with a temperate climate and summer dominated rainfall, is situated on the mid north coast of New South Wales (Chiew and Mcmahon, 2002). The area of the catchment is around 6630 km^2 and the elevation ranges from 12 m to 1591 m (Figure 3-1C). For this catchment, the annual mean temperature is around 14.9°C, the annual mean potential evaporation is around 1305 mm, the annual average rainfall is about 1052 mm, and the runoff coefficient is about 0.20 (Zhang et al., 2013).

The North Johnstone River catchment (Figure 3-1D) is located on the wet tropics of North Queensland. The catchment area is approximately 924 km^2 and the elevation ranges from 18 m to 1370 m. For this study area, the annual average temperature is around 21.4°C, annual average rainfall is about 2740 mm, and annual average runoff is approximately 1995 mm (1967-2017). Rainfall is highly seasonal and 78% of the whole annual rainfall occurs in the wet season (December to May). Compared to dry tropics, this catchment also receives regular rainfall across the year.

3.2.2 Observed data

Daily maximum and minimum temperature, rainfall, solar radiation, FAO56 potential evapotranspiration, and relative humidity from climate stations (Figure 3-1) within or near the catchments were downloaded from the BOM (Australian Government Bureau of Meteorology) website (http://www.bom.gov.au/climate/data/). Daily observed discharge at stream gauging stations also were downloaded from the BOM website (http://www.bom.gov.au/waterdata/).

Daily wind speed data were collected from the CSIRO data access portal website (https://data.csiro.au/dap/).

3.2.3 Mann-Kendall trend test

The non-parametric Mann-Kendall test is usually applied to detect monotonic trends for a sequence of climate, hydrologic, or environmental data (Pohlert, 2016). It is one of the most commonly used non-parametric test to detect trends and was used in this study to detect trends in hydroclimatic sequences (Barua et al., 2013). The null hypothesis (H_0) refers to the data from a population with independent realizations and are identically distributed. The alternative hypothesis (H_A) refers to the data follow a monotonic trend. The Mann-Kendall test statistic is estimated based on:

$$S = \sum_{k=1}^{n-1}\sum_{j=k+1}^{n} sgn(X_j - X_k) \tag{3-1}$$

with

$$sgn(x) \begin{cases} 1 & if\ x > 0 \\ 0 & if\ x = 0 \\ -1 & if\ x < 0 \end{cases} \tag{3-2}$$

The average of S is $E[S]=0$ and the variance σ^2 is

$$\sigma^2 = \left\{n(n-1)(2n+5) - \sum_{j=1}^{p} t_j(t_j-1)(2t_j+5)\right\}/18 \tag{3-3}$$

where p is the number of the tied groups in the dataset while t_j is the number of data points in the jth tied group. The statistic S is approximately normal distributed given that the following Z-transformation is applied:

$$Z = \begin{cases} \frac{S-1}{\sigma} & if\ S > 0 \\ 0 & if\ S = 0 \\ \frac{S+1}{\sigma} & if\ S < 0 \end{cases} \tag{3-4}$$

The statistic S is closely related to Kendall's τ as follows:

$$\tau = \frac{S}{D} \tag{3-5}$$

where

$$D = \left[\frac{1}{2}n(n-1) - \frac{1}{2}\sum_{j=1}^{p} t_j(t_j-1)\right]^{1/2} \left[\frac{1}{2}n(n-1)\right]^{1/2} \tag{3-6}$$

The null hypothesis (no trend) would be rejected at a certain significance level if $|Z| > Z_{crit}$ (Z_{crit} is the point on the normal distribution which has a probability of exceedance at a certain significance level). For instance, the null hypothesis would be rejected if $|Z| > 1.96$ at the 5% significance level, and the null hypothesis would be rejected if $|Z| > 1.645$ at the 10%

significance level. Statistically, the larger the Z value, the more significant the trend is (Barua et al., 2013).

3.2.4 Mann-Kendall abrupt test

The sequential version of Mann–Kendall test is applied to test the hypothesis about the beginning of a trend in sample $X_1, \ldots, X_n$ from the set of random variable X based upon rank sequences of progressive and retrograde rows of this sample (Yang and Tian, 2009). The magnitudes of X_j (annual average time series, $j = 1, \ldots, n$) are compared with X_k ($k = 1, \ldots, j-1$). The number of cases ($X_k > X_j$) is counted and referred as n_j for each comparison. The test statistic

$$t_j = \sum_1^j n_j \quad (j = 2, 3, \ldots, n) \tag{3-7}$$

is normally distributed with average as follows

$$E(t) = \frac{n(n-1)}{4} \tag{3-8}$$

and variance as follows

$$Var(t_j) = \frac{[j(j-1)(2j+5)]}{72} \tag{3-9}$$

The statistic $U(t)$ is calculated as follows

$$U(t) = \frac{t_j - E(t)}{\sqrt{Var(t_j)}} \tag{3-10}$$

which is the forward sequence, while $U'(t)$ (the backward sequence) is calculated with the same equation only in the reverse data series.

A null hypothesis will be accepted at α significance level in two-sided trend test if $|U(t)| \leq U(t)_{1-\alpha/2}$, where $U(t)_{1-\alpha/2}$ indicates the critical value of standard normal distribution with the probability exceeds $\alpha/2$. A positive $U(t)$ indicates an upward trend while the reverse indicates a downward trend (i.e., $U'(t)$ is similar to $U(t)$). For this study, α will be set at 0.05 and 0.1 significant levels. This Mann–Kendall test can detect the approximate time of trend occurrence from the intersection of the forward and backward curves of test statistics. The critical point of change is at that period if the intersection is significant at $\alpha = 0.05\ or\ 0.1$. Therefore, the sequential Mann–Kendall test is an effective method by which the beginning of a trend is identified.

3.2.5 Wavelet analysis

Wavelet method is a reasonable selection to evaluate periodical phenomena of time series, especially when the potential frequency changes with time. With the increasing interest in the

application of wavelet method, some open-source packages have been brought forth for wavelet analysis in R. This study uses the package named WaveletComp for continuous wavelet analysis of hydrologic and climatic sequences. Detailed introduction of wavelet analysis can be found in the reference (Rösch and Schmidbauer, 2014).

3.2.6 Climate Elasticity

As a crucial indicator to quantify the sensitivity of runoff to climate variables and human activities, climate elasticity has been frequently applied to assess the hydrological responses to climate and land use changes (Zhang et al., 2017). There are lots of approaches to estimate climate elasticity, among which it is theoretically clear to derive climate elasticity of runoff according to the Budyko hypothesis (Yang et al., 2014). Evaporation can be expressed as a function of potential evaporation and precipitation for a catchment in a long-term time scale (Budyko, 1974), which is referred to as the Budyko hypothesis (Yang and Yang, 2011). The Budyko hypothesis has a few formulae which are referred to as the Budyko-type formulae (Yang et al., 2014). Integrating Budyko-type formulae such as M-C-Y equation with Penman Monteith equation, a general partial differential equation was deduced to calculate the fractional contribution of climate variables and land use change to runoff (Liu et al., 2017b).

The M-C-Y equation is as given below:

$$f(P, E_0, n) = R = P - \frac{P \cdot E_0}{(P^n + E_0^n)^{1/n}} \tag{3-11}$$

where E_0 is the long-term annual mean potential evaporation, P is the long-term annual mean precipitation, R is the long-term annual mean runoff, and n is the underlying surface parameter representing the combined effects of the catchment characteristics (e.g., vegetation type or land use, average slope, and climate seasonality) (Yang et al., 2014).

The Penman Monteith equation is as given below:

$$E_0 = \frac{0.408\Delta R_n + \gamma\frac{900}{T+273}U_2(e_s - e_a)}{\Delta + \gamma(1 + 0.34U_2)}, e_s = f(T_{max}, T_{min}), e_a = f(RH) \tag{3-12}$$

where E_0 is the reference evapotranspiration (mm day^{-1}), R_n is the net radiation at the crop surface (MJ m^{-2} day^{-1}), γ is the psychrometric constant (kPa °C^{-1}), T is the daily average air temperature (°C), e_a is the actual vapor pressure (kPa), e_s is the saturation vapor pressure (kPa), Δ is the slope of the vapor pressure (kPa °C^{-1}), U_2 is the wind speed at 2 m height (m s^{-1}), RH is the relative humidity, T_{max} is the daily maximum temperature (°C), and T_{min} is the daily minimum temperature (°C).

The general partial differential equation is as given below:

$$\frac{dR}{R} = \varepsilon_P \frac{dp}{P} + \varepsilon_{R_n} \frac{dR_n}{R_n} + \varepsilon_{T_{max}} \frac{dT_{max}}{T_{max}} + \varepsilon_{T_{min}} \frac{dT_{min}}{T_{min}} + \varepsilon_{U_2} \frac{dU_2}{U_2} + \varepsilon_{RH} \frac{dRH}{RH} + \varepsilon_n \frac{dn}{n} \qquad (3\text{-}13)$$

where ε_P, ε_{R_n}, $\varepsilon_{T_{max}}$, $\varepsilon_{T_{min}}$, ε_{U_2}, ε_{RH}, and ε_n indicate the elasticity of precipitation, net radiation, maximum temperature, minimum temperature, wind speed, relative humidity, and parameter n of land use change to runoff (Liu et al., 2017b).

The fractional contribution of each impact factor to runoff change and the fractional contributions of climate change and human activity to runoff variations can be obtained using the equation in the reference (Liu et al., 2017b) and are as given below:

$$\Delta R_x = \varepsilon_x \frac{R}{x} \Delta x \qquad (3\text{-}14)$$

where R denotes the long-term annual mean runoff, x is the long-term annual mean of each impact factor (e.g., rainfall, maximum air temperature, minimum air temperature, net radiation, land use change, relative humidity, and wind speed. ΔR_x represents the streamflow changes caused by each impact factor. Δx is the change of long-term annual mean for each impact factor.

$$\delta R_{clim} = \frac{\Delta R_{clim}}{\Delta} * 100\%, \ \delta R_{hum} = \frac{\Delta R_{hum}}{\Delta} * 100\% \qquad (3\text{-}15)$$

where δR_{clim} (%) and δR_{hum} (%) are the fractional contributions of climate change and human activity to runoff change. Δ is the sum of climate- and human-induced runoff change.

3.3 Results

3.3.1 Trends in hydroclimatic variables

The lengths of runoff time series are different in each catchment, and the lengths of climate time series (since 1889) are longer than runoff time series. In order to keep consistent with runoff data, the time periods from 1977-2017, 1908-2014, 1991-2016, and 1967-2017 were selected to calculate anomalies and to perform the M-K trend test for hydroclimatic variables in the Wooroloo Brook catchment, Murrumbidgee catchment, Manning River catchment, and North Johnstone River catchment, respectively. For the Manning River catchment, wind speed from 1991-2016 was selected to keep consistent with runoff data. For other catchments, wind speed data available from 1975-2017 were selected.
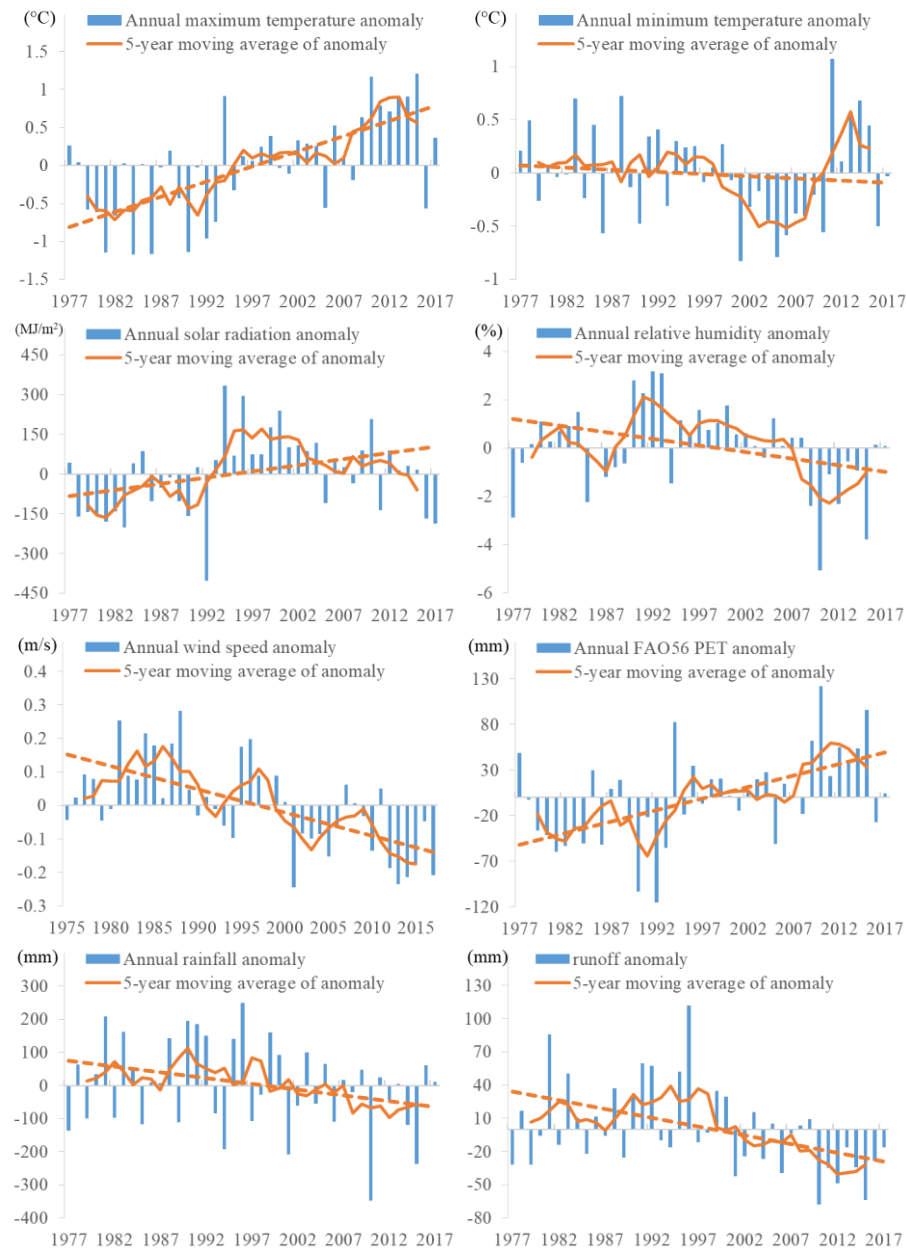
Figure 3-2 The trends and variations of annual hydroclimatic variables anomalies (relative to the average values of 1977-2017) in the Wooroloo Brook catchment from 1977-2017 (1975-2017 for wind). The dashed line shows a linear trend of the 5-year moving average.
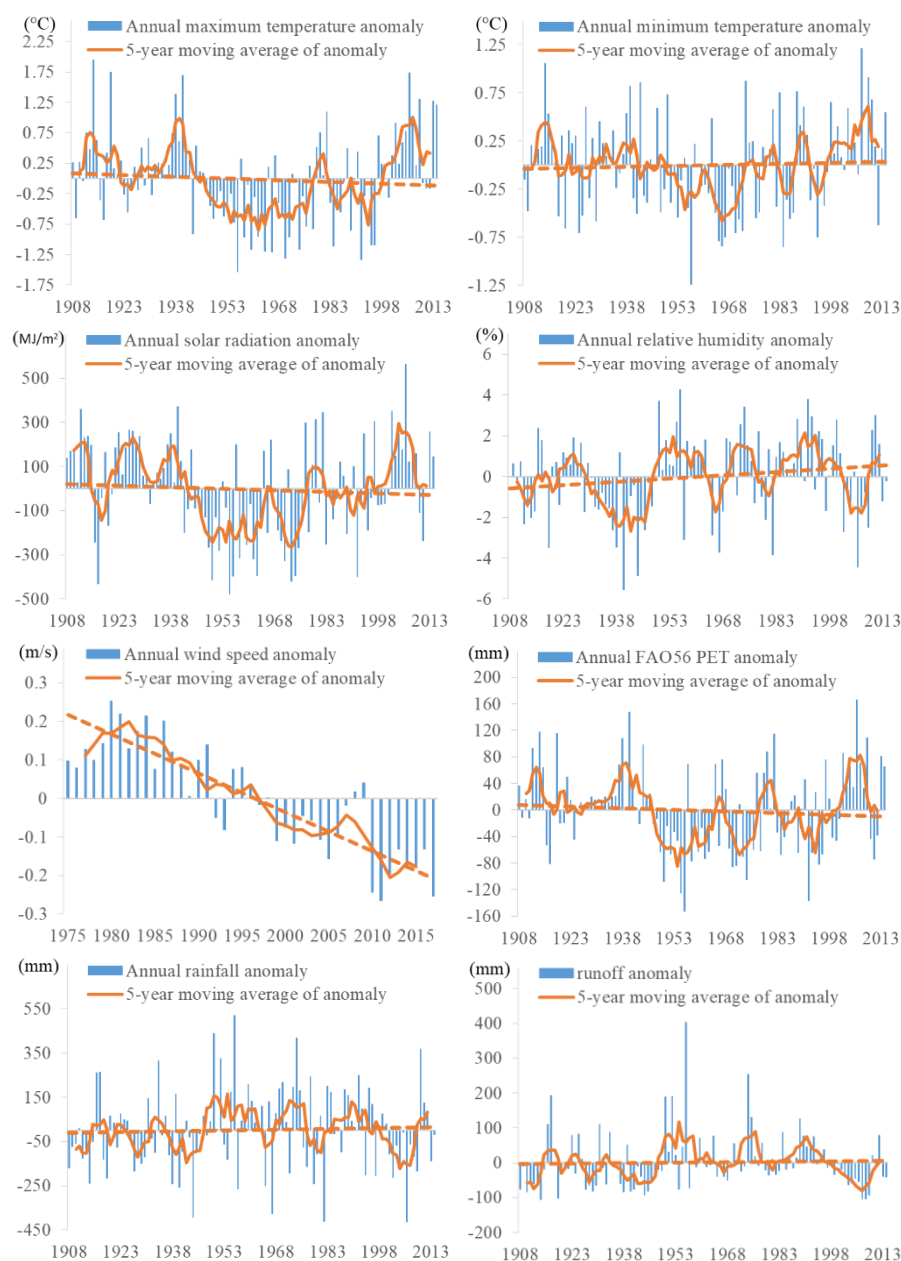
Figure 3-3 The trends and variations of annual hydroclimatic variables anomalies (relative to the average values of 1908-2014) in the Murrumbidgee catchment from 1908-2014 (1975-2017 for wind). The dashed line shows a linear trend of the 5-year moving average.
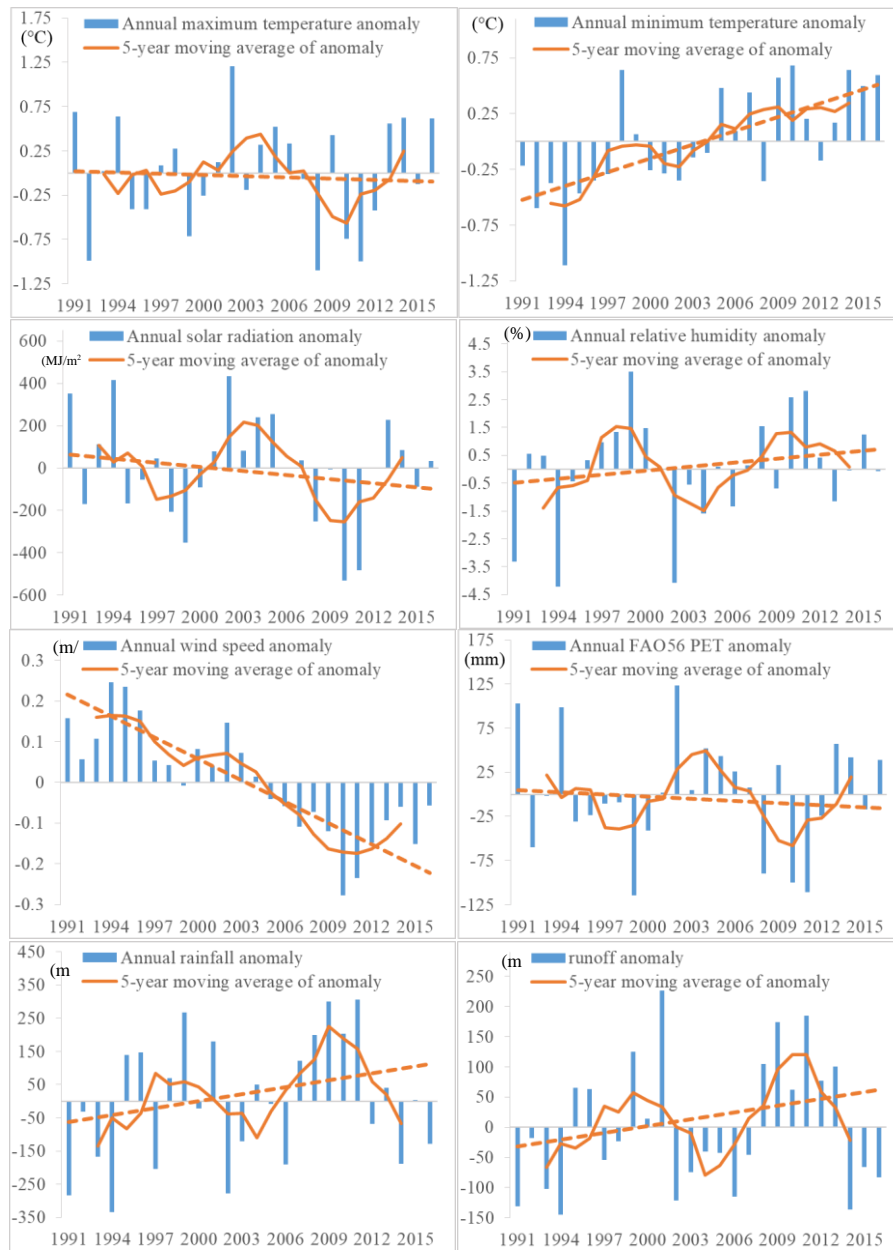
Figure 3-4 The trends and variations of annual hydroclimatic variables anomalies (relative to the average values of 1991-2016) in the Manning River catchment from 1991-2016. The dashed line shows a linear trend of the 5-year moving average.
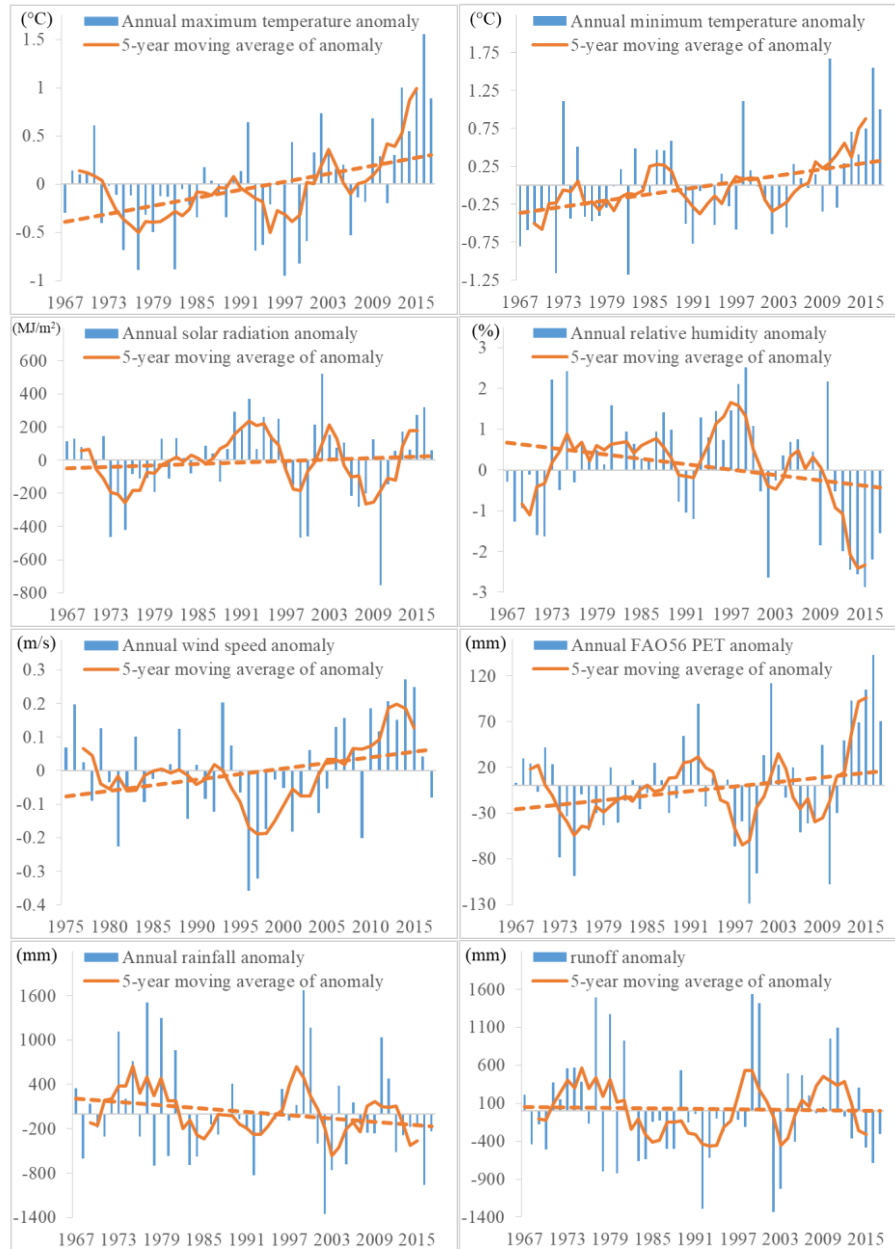
Figure 3-5 The trends and variations of annual hydroclimatic variables anomalies (relative to the average values of 1967-2017) from 1967-2017 (1975-2017 for wind) in the North Johnstone River catchment. The dashed line shows a linear trend of the 5-year moving average.

For the Wooroloo Brook catchment, the trends and variations of annual hydroclimatic variables anomalies from 1977-2017 (1975-2017 for wind) are shown in Figure 3-2. From the slopes of the trend lines, there was an obvious trend of increasing values in annual maximum temperature and FAO56 PET, while there was a distinct trend of decreasing values in annual wind speed and runoff in the recent decades. In addition, according to 5-year moving average of anomaly, annual maximum temperature and FAO56 PET closely replicated temporal variation during 1977-2017, in which the continuous time period of 2009-2015 generally showed the most positive anomaly (high maximum temperature and FAO56 PET). In contrast,

annual rainfall and runoff closely replicated temporal variation during 1977-2017, in which the period of 2009-2015 roughly showed the negative anomaly (low rainfall and runoff). These results indicate qualitatively that potential evapotranspiration (PET) exhibited a positive correlation with maximum temperature, runoff displayed a positive correlation with rainfall and a negative correlation with PET and maximum temperature.

The trends and variations of annual hydroclimatic variables anomalies in the Murrumbidgee catchment from 1908-2014 (1975-2017 for wind) are shown in Figure 3-3. Due to the long-term characteristic of 1908-2014 (107 years), no obvious upward or downward trend can be detected in all hydroclimatic variables except for a remarkable trend of decreasing values in wind speed (1975-2017). Besides, according to 5-year moving average of anomaly, annual maximum temperature, solar radiation, and FAO56 PET closely replicated temporal variation during 1908-2014, in which the continuous period of 2001-2009 generally showed the most positive anomaly (high maximum temperature, solar radiation, and FAO56 PET) for the recent decades, while annual rainfall and runoff showed the negative anomaly (low rainfall and runoff) in the same period.

For the Manning River catchment, observed runoff data in 1983, 1989, and 1990 are largely missing while observed runoff data from 1991-2016 are quite complete and continuous. The trends and variations of annual hydroclimatic variables anomalies in the Manning River catchment from 1991-2016 are shown in Figure 3-4. From the slopes of the trend lines, there was an obvious trend of increasing values in annual minimum temperature while there was a distinct trend of decreasing values in annual wind speed in the period of 1991-2016. In addition, according to 5-year moving average of anomaly, annual maximum temperature, solar radiation, and FAO56 PET closely replicated temporal variation during 1991-2016, in which the continuous period of 2001-2006 generally showed the most positive anomaly (high maximum temperature, solar radiation, and FAO56 PET). In contrast, annual rainfall and runoff closely replicated temporal variation during 1991-2016, in which the continuous period of 2002-2006 roughly showed the negative anomaly (low rainfall and runoff). These results indicate qualitatively that PET exhibited a great correlation with maximum temperature and solar radiation, while runoff displayed a great correlation with rainfall.

Trends and variations of annual hydroclimatic variables anomalies from 1967-2017 (1975-2017 for wind) in the North Johnstone River catchment are presented in Figure 3-5. From the slopes of the trend lines, there was an obvious trend of increasing values in annual maximum temperature and minimum temperature in 1967-2017. In addition, according to 5-year moving average of anomaly, annual maximum temperature and FAO56 PET showed the most positive anomaly (high maximum temperature and FAO56 PET) in the continuous period of 2012-2017.

In contrast, annual rainfall and runoff closely replicated temporal variation during 1967-2017, in which the period of 2012-2017 roughly showed the negative anomaly (low rainfall and runoff).

Table 3-1 Mann-Kendall trend test results for climatic and hydrologic variables at annual time scale in the Wooroloo Brook catchment.

	T_{max}	T_{min}	Mean T	Solar radiation	Relative humidity	Wind speed	FAO56 PET	Rainfall	Runoff
Period (years)	1977-2017	1977-2017	1977-2017	1977-2017	1977-2017	1975-2017	1977-2017	1977-2017	1977-2017
Estimates	0.034	-0.008	0.014	2.759	-0.033	-0.006	2.095	-2.361	-1.194
Statistic	3.92	-1.179	1.853	1.561	-1.584	-3.977	3.066	-1.202	-2.55
p.value	0	0.238	0.064	0.118	0.113	0	0.002	0.229	0.011
Reliability (0.1)	No	Yes	Yes	Yes	Yes	No	No	Yes	No
Reliability (0.05)	No	Yes	Yes	Yes	Yes	No	No	Yes	No

Table 3-2 Mann-Kendall trend test results for climatic and hydrologic variables at annual time scale in the Murrumbidgee catchment.

	T_{max}	T_{min}	Mean T	Solar radiation	Relative humidity	Wind speed	FAO56 PET	Rainfall	Runoff
Period (years)	1975-2014	1975-2014	1975-2014	1975-2014	1975-2014	1975-2014	1975-2014	1975-2014	1975-2014
Estimates	0.03	0.013	0.021	5.319	-0.025	-0.01	1.44	-2.623	-2.174
Statistic	2.482	1.643	2.738	1.806	-0.687	-5.627	1.386	-0.967	-2.924
p.value	0.013	0.1	0.006	0.071	0.492	0	0.166	0.334	0.003
Reliability (0.1)	No	Yes	No	Yes	Yes	No	Yes	Yes	No
Reliability (0.05)	No	Yes	No	Yes	Yes	No	Yes	Yes	No

Table 3-3 Mann-Kendall trend test results for climatic and hydrologic variables at annual time scale in the Manning River catchment.

	T_{max}	T_{min}	Mean T	Solar radiation	Relative humidity	Wind speed	FAO56 PET	Rainfall	Runoff
Period (years)	1991-2016	1991-2016	1991-2016	1991-2016	1991-2016	1991-2016	1991-2016	1991-2016	1991-2016
Estimates	0.013	0.042	0.027	-4.417	0.037	-0.014	0.652	6.063	2.702
Statistics	0.397	3.791	2.292	-0.661	0.617	-4.673	0.264	1.278	0.749
P values	0.692	0	0.022	0.508	0.537	0	0.791	0.201	0.454
Reliability (0.1)	Yes	No	No	Yes	Yes	No	Yes	Yes	Yes
Reliability (0.05)	Yes	No	No	Yes	Yes	No	Yes	Yes	Yes

Table 3-4 Mann-Kendall trend test results for climatic and hydrologic variables at annual time scale in the North Johnstone River catchment.

	T_{max}	T_{min}	Mean T	Solar radiation	Relative humidity	Wind speed	FAO56 PET	Rainfall	Runoff
Period (years)	1967-2017	1967-2017	1967-2017	1967-2017	1967-2017	1975-2017	1967-2017	1967-2017	1967-2017
Estimates	0.015	0.018	0.015	2.267	-0.02	0.003	1.011	-6.548	-1.554
Statistic	2.843	3.184	3.509	1.04	-1.007	1.151	1.641	-1.17	-0.114
p.value	0.004	0.001	0	0.299	0.314	0.25	0.101	0.242	0.909
Reliability (0.1)	No	No	No	Yes	Yes	Yes	Yes	Yes	Yes
Reliability (0.05)	No	No	No	Yes	Yes	Yes	Yes	Yes	Yes

The Mann-Kendall trend test results for climatic and hydrologic variables in the Wooroloo Brook catchment are presented in Table 3-1. Positive values of statistics denote upward trends while negative values show downward trends of the data sequences (Rashid et al., 2015). From the statistics and p values in Table 3-1, it is evident that annual maximum temperature, wind speed, FAO56 PET, and runoff did not pass the MK trend test at two levels of significance (with absolute statistics values of 3.92, -3.98, 3.07 and -2.55 > 1.96), which means there were significant trends of increasing values in annual maximum temperature and FAO56 PET while there was a significant trend of decreasing values in annual wind speed and runoff in the recent decades.

The Mann-Kendall trend test results for climatic and hydrologic variables in the Murrumbidgee catchment are presented in Table 3-2. From the statistics and p values in Table 3-2, annual maximum temperature, mean temperature, wind speed, and runoff clearly did not pass the MK trend test at two levels of significance (with absolute statistics values of 2.48, 2.74, -5.63 and -2.92 > 1.96), which means there were significant trends of increasing values in annual maximum temperature and mean temperature while there was a significant trend of decreasing values in annual wind speed and runoff in the recent decades.

The Mann-Kendall trend test results for climatic and hydrologic variables in the Manning River catchment are presented in Table 3-3. Table 3-3 shows that there are trends of increasing values in all hydroclimatic sequences, except in annual solar radiation and wind speed according to the values of estimates. From the statistics and p values in Table 3-3, annual minimum temperature, mean temperature, and wind speed clearly did not pass the MK trend test at two levels of significance (with absolute statistics values of 3.791, 2.292, and -4.673 > 1.96), which means there were significant trends of increasing values in annual minimum

temperature and mean temperature while there was a significant trend of decreasing values in annual wind speed in the recent decades. The estimates presented in Table 3-3 show that the annual minimum temperature increases 0.042 °C per year while the annual mean temperature increases 0.027 °C per year. In addition, the annual rainfall increases 6.063mm per year while the annual runoff increases 2.702mm per year from 1991 to 2016, although the trends of increasing values in rainfall and runoff are not significant (with statistics values of 1.278 and $0.749 < 1.645$) at two levels of significance.

The Mann-Kendall trend test results for climatic and hydrologic variables in North Johnstone River catchment are presented in Table 3-4. According to the statistics and p values in Table 3-4, annual maximum, minimum, and mean temperatures did not pass the MK trend test at two levels of significance (with absolute statistics values of 2.84, 3.18, and $3.51 > 1.96$), which means there were significant trends of increasing values in annual maximum, minimum, and mean temperatures in the recent decades.

3.3.2 Mann-Kendall abrupt test
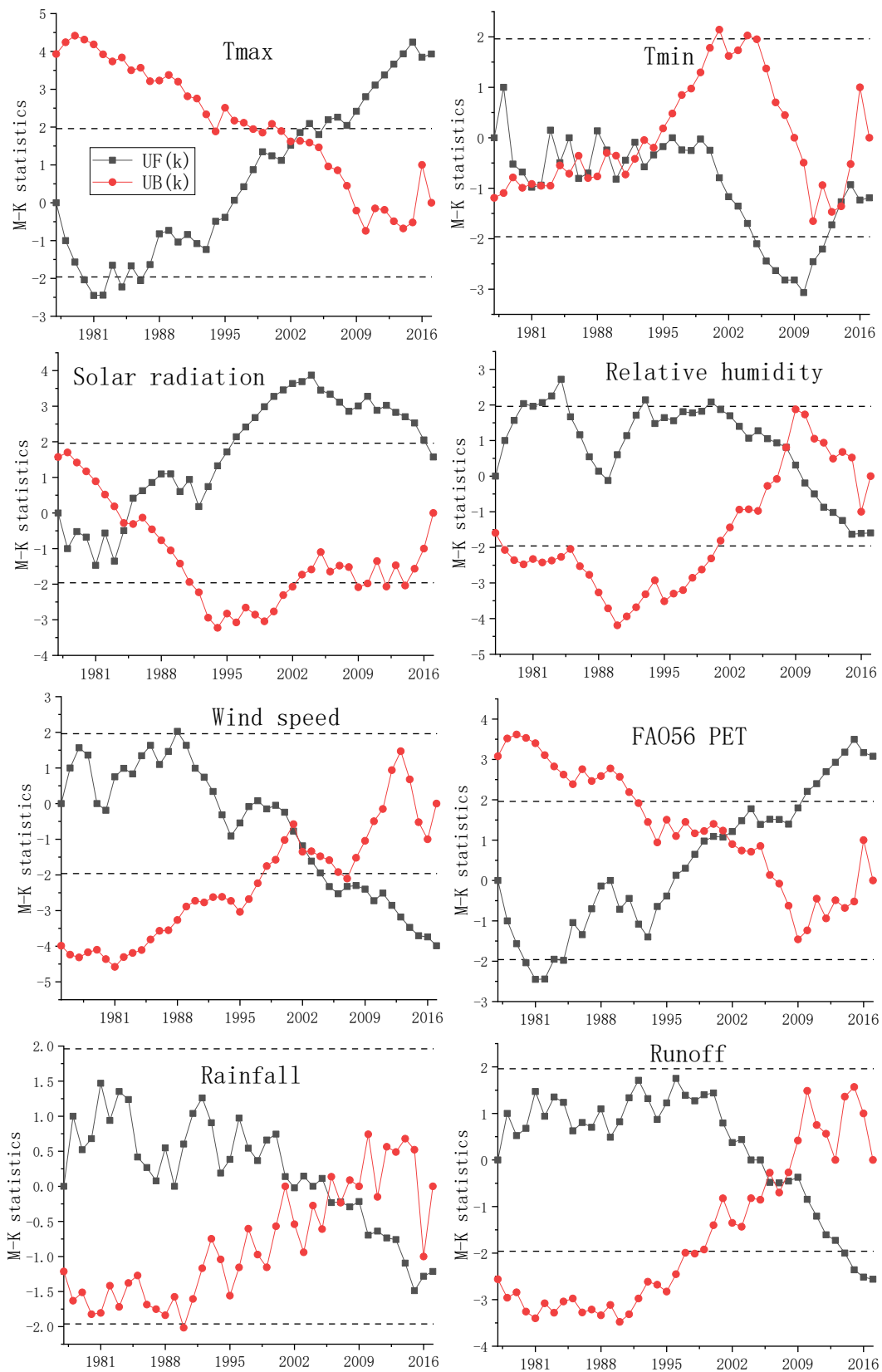
Figure 3-6 Mann-Kendall abrupt test for annual climatic and hydrologic variables in the Wooroloo Brook catchment with forward trend UF (black line) and backward trend UB (red

line). Dotted horizontal lines above (+1.96) and below (-1.96) denote critical values for the 95% confidence interval (Yang and Tian, 2009).
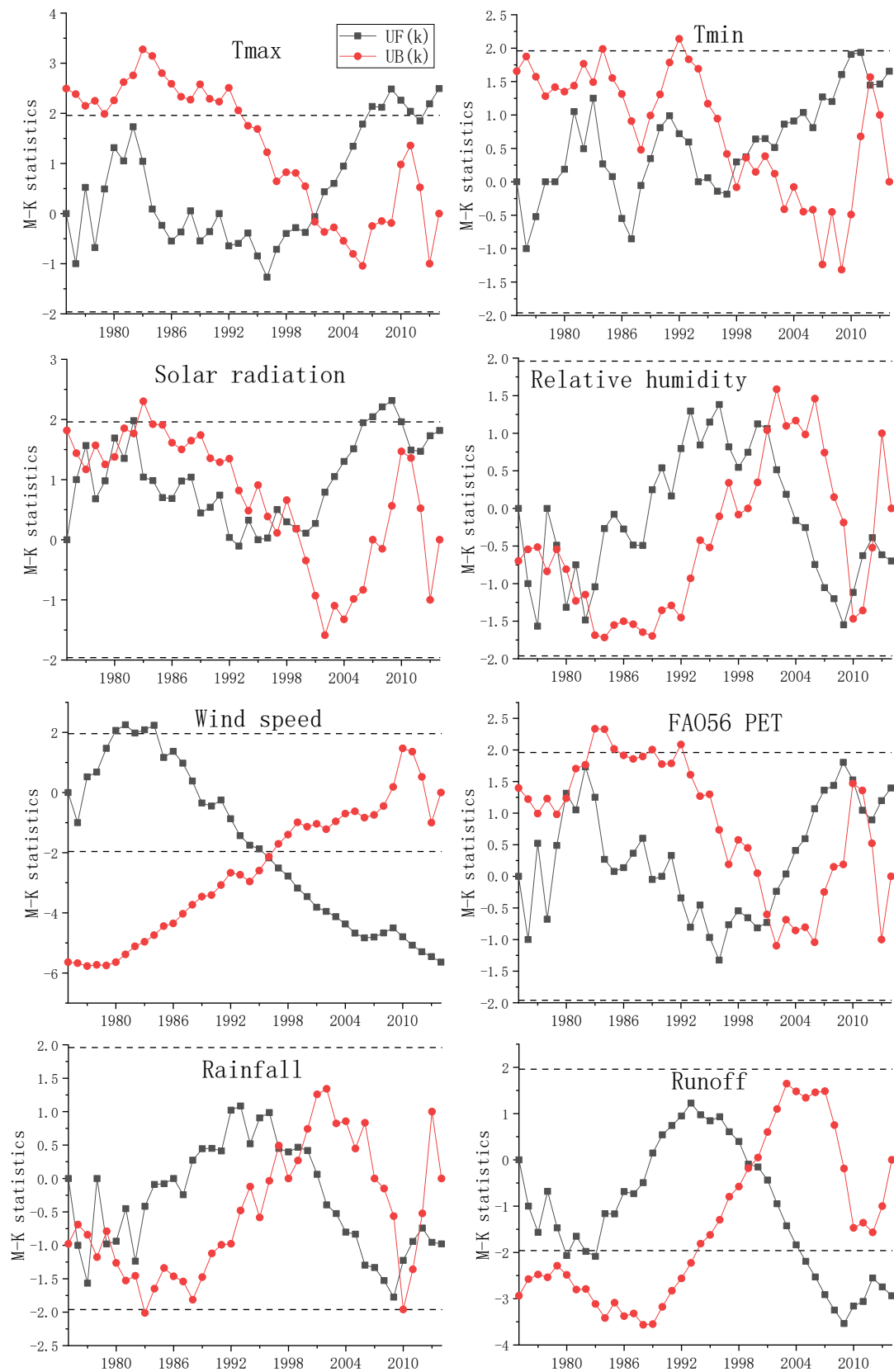
Figure 3-7 Mann-Kendall abrupt test for annual climatic and hydrologic variables in the Murrumbidgee catchment with forward trend UF (black line) and backward trend UB (red line). Dotted horizontal lines above (+1.96) and below (-1.96) denote critical values for the 95% confidence interval (Yang and Tian, 2009).
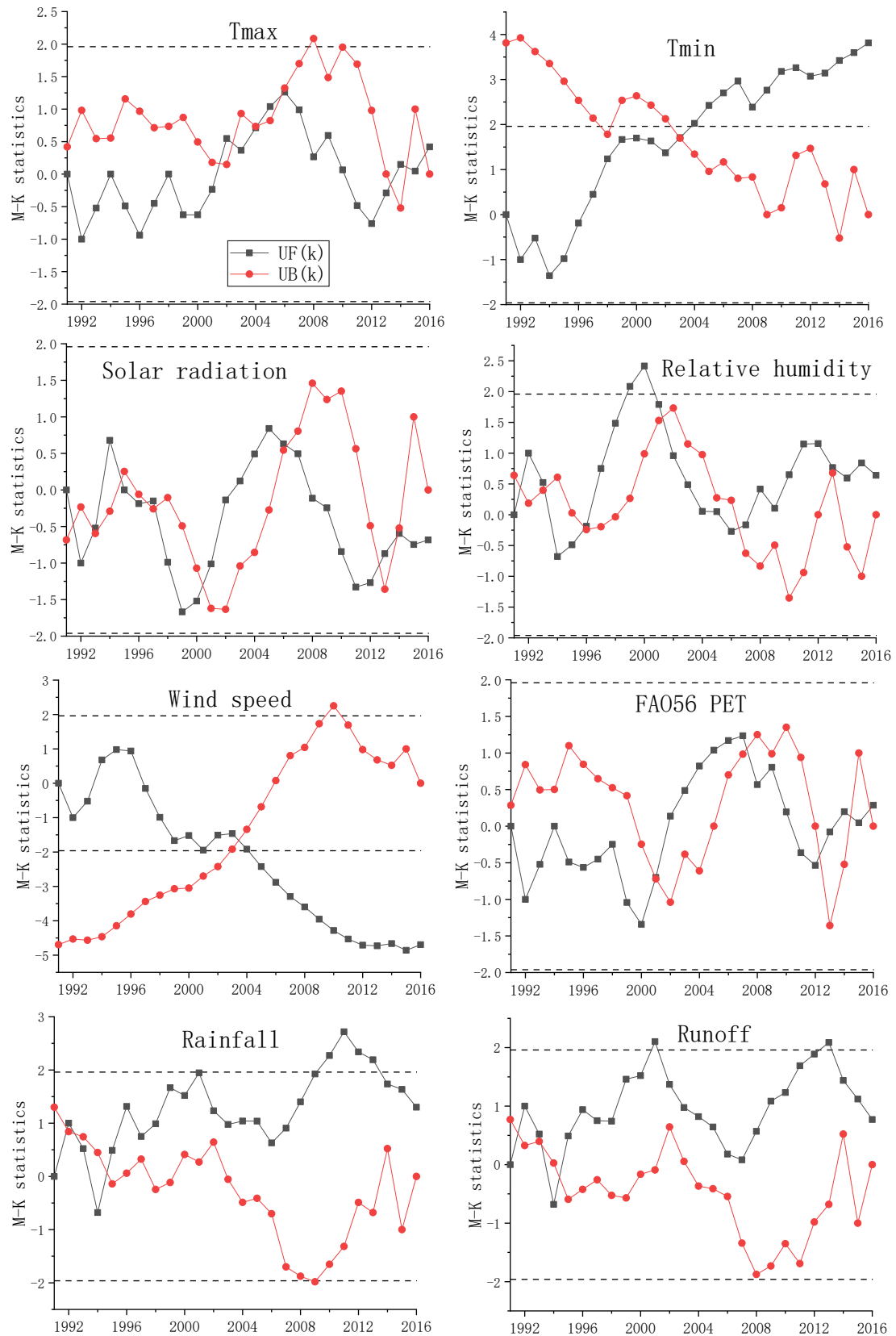
Figure 3-8 Mann-Kendall abrupt test for annual climatic and hydrologic variables in Manning River catchment with forward trend UF (black line) and backward trend UB (red line). Dotted

horizontal lines above (+1.96) and below (-1.96) denote critical values for the 95% confidence interval (Yang and Tian, 2009).
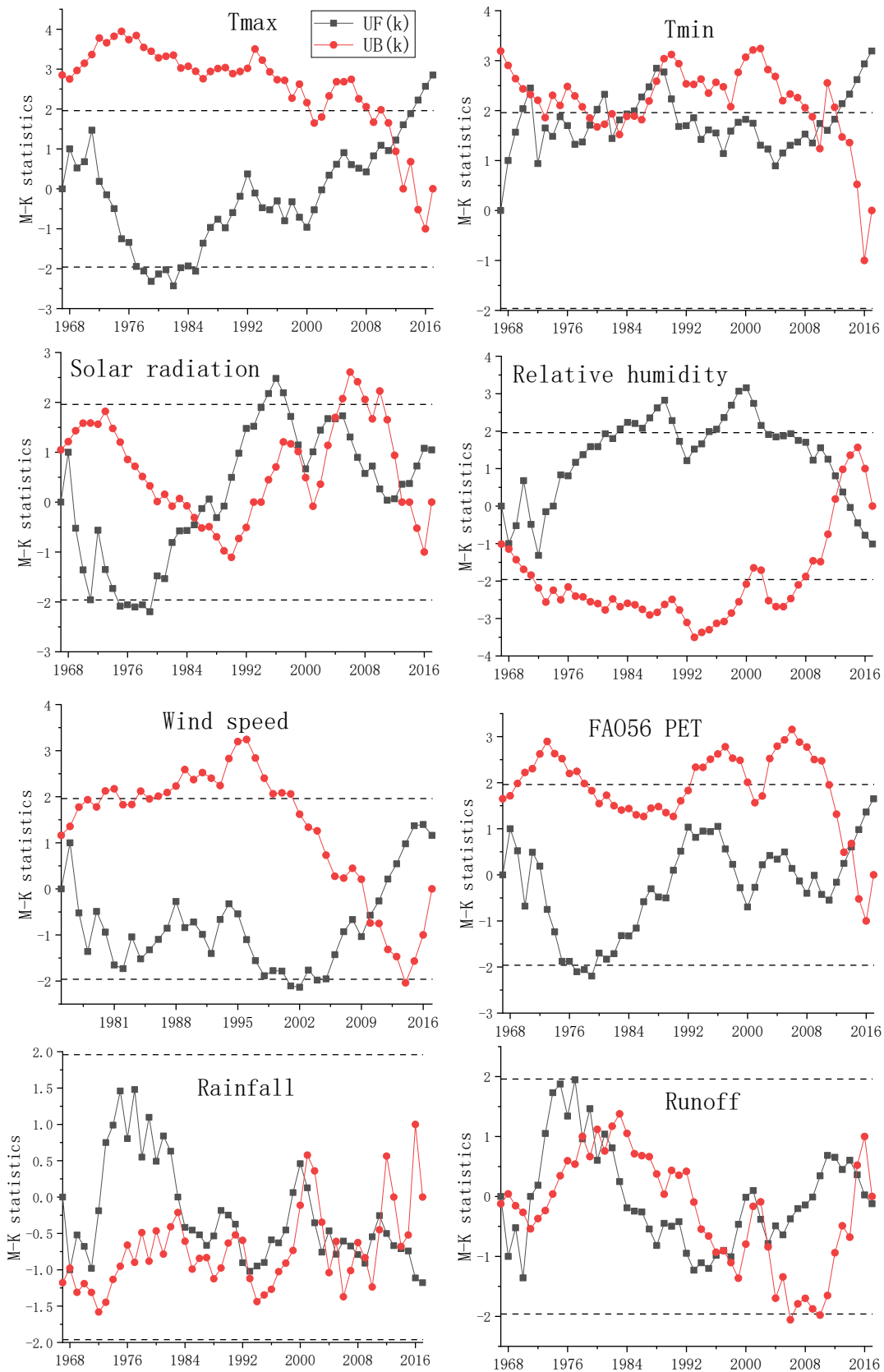
Figure 3-9 Mann-Kendall abrupt test for annual climatic and hydrologic variables in the North Johnstone River catchment with forward trend UF (black line) and backward trend UB (red line). Dotted horizontal lines above (+1.96) and below (-1.96) denote critical values for the 95% confidence interval (Yang and Tian, 2009).

The Mann–Kendall abrupt test was applied to graphically display the forward and backward trends in annual hydroclimatic variables in the Wooroloo Brook catchment for the period 1977-2017 (1975-2017 for wind) (Figure 3-6). Trends in hydroclimatic variables is significant ($p < 0.05$) at the point where the UF curve falls outside the dotted line (Yang and Tian, 2009). Therefore, Figure 3-6 suggests significant upward trends for annual maximum temperature (after 2006) and FAO56 PET (after 2010), and significant downward trends for wind speed (after 2004) and runoff (after 2014). Moreover, the starting point of abrupt hydroclimatic variables change is denoted by the separation point of the upward and downward curves. If the separation point is within the confidence interval, and either the progressive curve or the retrograde curve exceeds a certain limit before or after the intersection point, the trend turning point is deemed significant at the corresponding level (i.e., 1.96 for the 5% significance level) (Rashid et al., 2015). Therefore, an abrupt change was detected for maximum temperature (2002-2003), FAO56 PET (2001-2002), wind speed (around 2002), and runoff (around 2007) using the Mann-Kendall abrupt test, which suggests a more significant trend of increasing values in maximum temperature and FAO56 PET and decreasing values in wind speed and runoff after the intersection point. Moreover, according to UF lines, maximum temperature and FAO56 PET closely replicated temporal variation while rainfall and runoff closely replicated temporal variation in the recent decades. These results indicate qualitatively that potential evapotranspiration exhibited a great correlation with maximum temperature, while runoff displayed a great correlation with rainfall. The result from Mann-Kendall abrupt test in Figure 3-6 is generally consistent with the result from 5-year moving average of anomaly in Figure 3-2.

The Mann–Kendall abrupt test results in the Murrumbidgee catchment for the period 1975-2014 was shown in Figure 3-7. It suggests significant upward trends for annual maximum temperature (after 2007), and significant downward trends for wind speed (after 1996) and runoff (after 2005) (when UF curve generally falls outside the dotted line). Moreover, an abrupt change was detected for maximum temperature (2001) and runoff (1999-2000) using the Mann-Kendall abrupt test, which suggests a more significant trend of increasing values in maximum temperature and decreasing values in runoff after the intersection point. Furthermore, according to UF lines, maximum temperature and FAO56 PET closely replicated temporal variation.

These results indicate qualitatively that potential evapotranspiration exhibited a great correlation with maximum temperature.

The Mann–Kendall abrupt test results in the Manning River catchment for the period 1991-2016 was shown in Figure 3-8. It suggests insignificant upward or downward trends for most hydroclimatic variables except for the minimum temperature and wind speed. According to UF curves and two dotted horizontal lines in Figure 3-8, there is a significant trend of increasing values in minimum temperature and a significant trend of decreasing values in wind speed after 2004 (when UF curve falls outside the dotted line). Moreover, an abrupt change was detected for minimum temperature and wind speed in around 2003-2004 using the Mann-Kendall abrupt test, which suggests a more significant trend of increasing values in minimum temperature and decreasing values in wind speed after 2003-2004. Moreover, according to UF lines, maximum temperature and FAO56 PET closely replicated temporal variation while rainfall and runoff closely replicated temporal variation from 1991 to 2016. These results indicate qualitatively that potential evapotranspiration exhibited a great correlation with maximum temperature, while runoff displayed a great correlation with rainfall. The result from Mann-Kendall abrupt test in Figure 3-8 is generally consistent with the result from 5-year moving average of anomaly in Figure 3-4.

The Mann–Kendall abrupt test results in the North Johnstone River catchment for the period 1967-2017 (1975-2017 for wind) was shown in Figure 3-9. It suggests significant upward trends for annual maximum temperature (after 2014) and minimum temperature (after 2012) (when UF curve generally falls outside the dotted line). Moreover, an abrupt change was detected for maximum temperature (2011-2012) and minimum temperature (2012-2013) using the Mann-Kendall abrupt test, which suggests a more significant trend of increasing values in maximum temperature and minimum temperature after the intersection point. Furthermore, according to UF lines, solar radiation and FAO56 PET closely replicated temporal variation while rainfall and runoff closely replicated temporal variation. These results indicate qualitatively that potential evapotranspiration exhibited a great correlation with solar radiation while runoff displayed a great correlation with rainfall.

3.3.3 Wavelet analysis
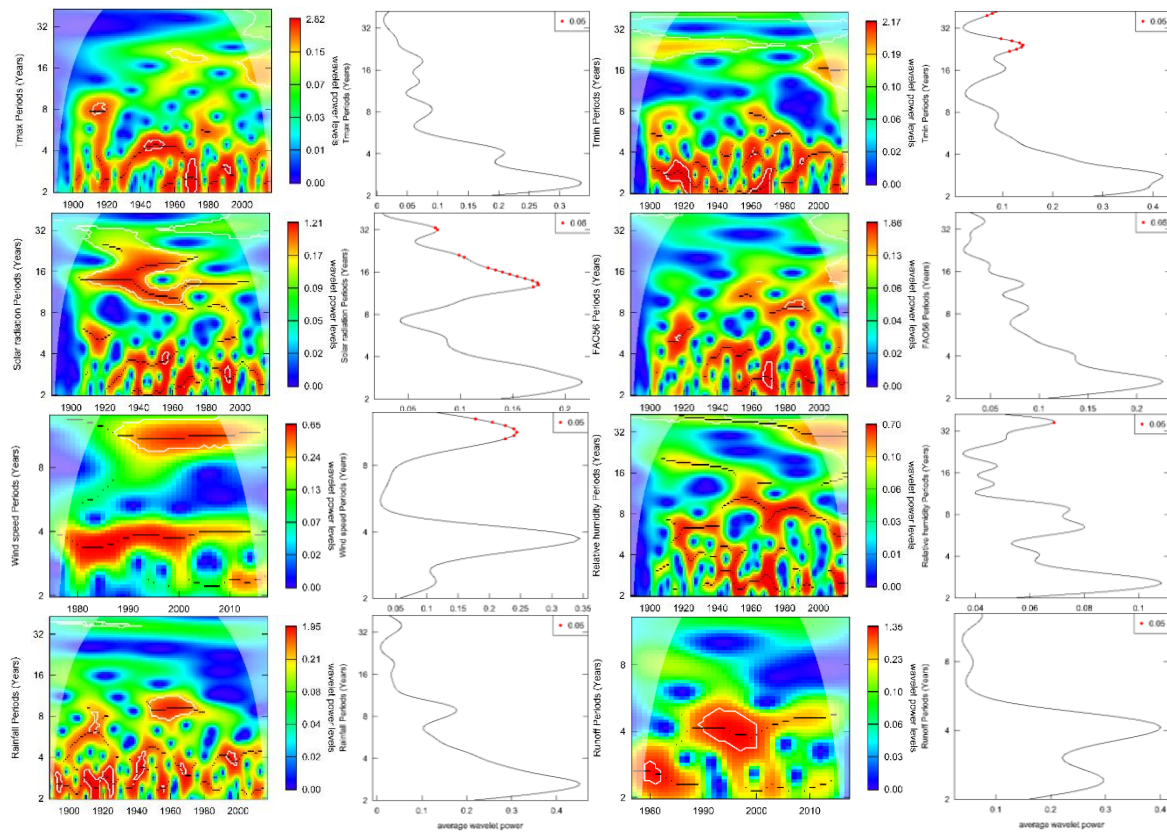
Figure 3-10 Continuous wavelet analysis for annual climatic and hydrologic variables in the Wooroloo Brook catchment. Due to data availability, the period of 1889-2017 (129 years) was used for wavelet analysis, except for wind speed (1975-2017) and runoff (1977-2017). Maximum temperature, minimum temperature, solar radiation, FAO56 PET, relative humidity, and rainfall exhibit similar high frequency cycles (notable but not significant) of about 2-3 years, while wind speed and runoff show similar periodicities of around 4 years (not significant).
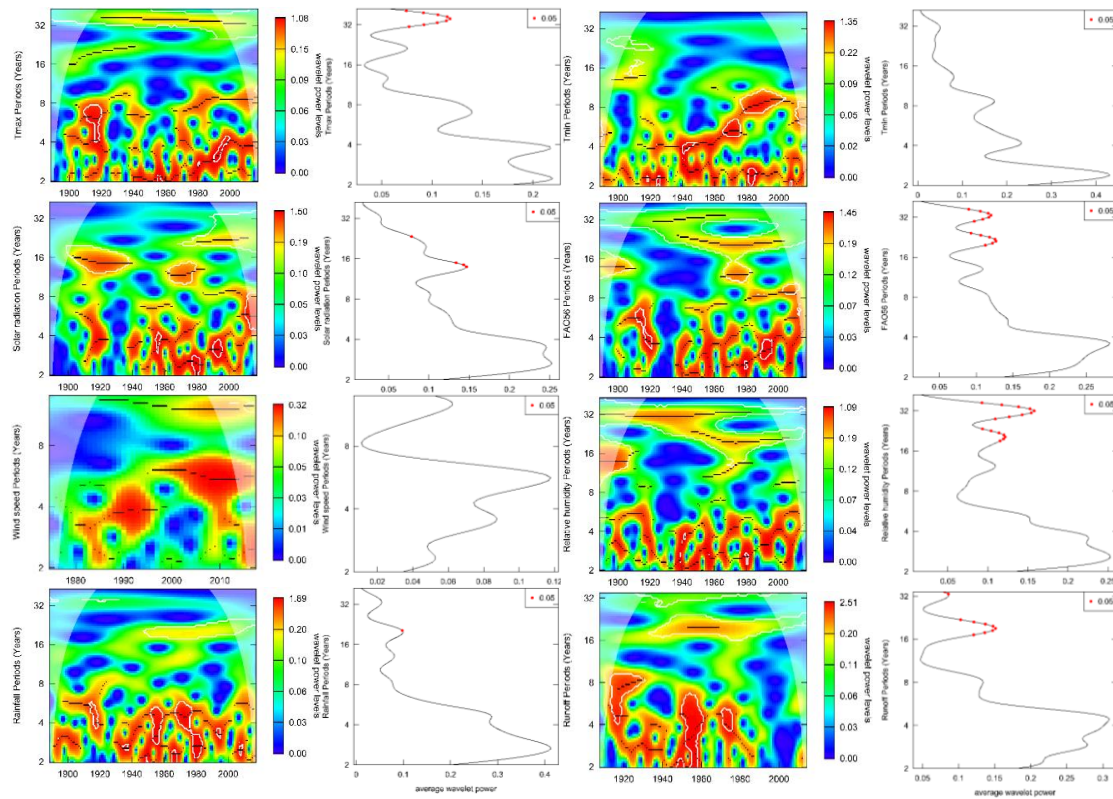
Figure 3-11 Continuous wavelet analysis for annual climatic and hydrologic variables in the Murrumbidgee catchment. Due to data availability, the period of 1889-2017 (129 years) was used for wavelet analysis, except for wind speed (1975-2017) and runoff (1908-2014). Maximum temperature, minimum temperature, solar radiation, relative humidity, and rainfall exhibit similar interannual cycles of about 2-3 years (notable but not significant). Moreover, maximum temperature, solar radiation, FAO56 PET, and runoff show similar periodicities of around 4 years (notable but not significant), while wind speed has periodicity of 6 years (notable but not significant).
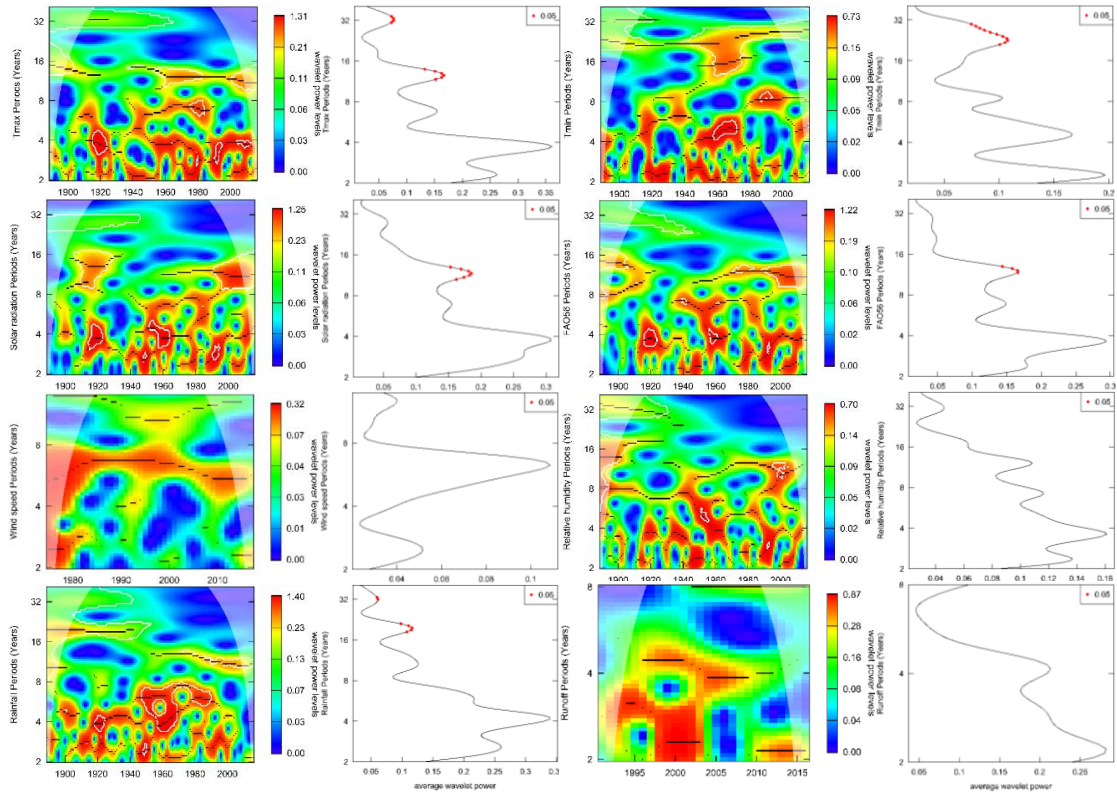
Figure 3-12 Continuous wavelet analysis for annual climatic and hydrologic variables in the Manning River catchment. Due to data availability, the period of 1889-2016 (128 years) was used for wavelet analysis, except for wind speed (1975-2017) and runoff (1991-2016). Maximum temperature, solar radiation, and FAO56 potential evapotranspiration exhibit similar interannual cycles of about 4 years (not significant) and 12 years (significant), while rainfall and runoff show similar periodicities of around 4 years (notable but not significant).
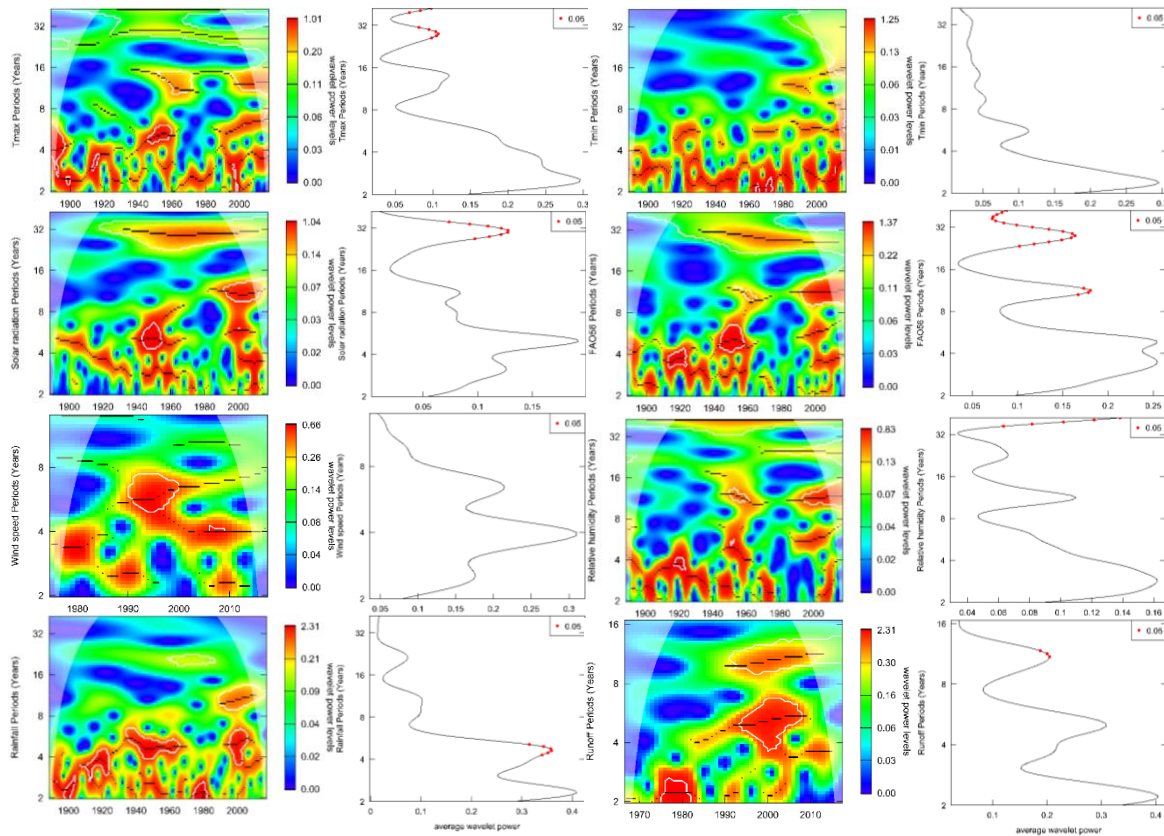
Figure 3-13 Continuous wavelet analysis for annual climatic and hydrologic variables in the North Johnstone River catchment. Due to data availability, the period of 1889-2017 (129 years) was used for wavelet analysis, except for wind speed (1975-2017) and runoff (1967-2017). Maximum temperature, minimum temperature, relative humidity, rainfall, and runoff exhibit similar interannual cycles of about 2-3 years (notable but not significant). In addition, significant cycles of around 28 years (long period/low frequency) were detected for maximum temperature, solar radiation, and FAO56 PET.

Figure 3-10 shows the results of the continuous wavelet analysis for annual climatic and hydrologic variables in the Wooroloo Brook catchment. Maximum temperature, minimum temperature, solar radiation, FAO56 PET, relative humidity, and rainfall exhibit similar high frequency cycles (notable but not significant) of about 2-3 years, while wind speed and runoff show similar periodicities of around 4 years (not significant). In addition, significant cycles of long period (low frequency) were also detected for minimum temperature (24 years), solar radiation (14 years) and wind speed (10 years).

The continuous wavelet analysis was applied to graphically illustrate the periodic characteristics of annual hydroclimatic variables in the Murrumbidgee catchment (Figure 3-11). Maximum temperature, minimum temperature, solar radiation, relative humidity, and rainfall exhibit similar interannual cycles of about 2-3 years (notable but not significant). In addition,

49

maximum temperature, solar radiation, FAO56 PET, and runoff show similar periodicities of around 4 years (notable but not significant), while wind speed has periodicity of 6 years (notable but not significant). Furthermore, significant cycles of around 32 years (long period/low frequency) were detected for maximum temperature, FAO56 PET, and relative humidity, significant cycles of around 20 years were detected for FAO56 PET and runoff, and significant cycles of around 14 years were detected for solar radiation.

Figure 3-12 illustrates the periodicity characteristics of annual hydroclimatic variables in the Manning River catchment using continuous wavelet analysis. Maximum temperature, solar radiation, and FAO56 potential evapotranspiration exhibit similar interannual cycles of about 4 years (not significant) and 12 years (significant), while rainfall and runoff show similar periodicities of around 4 years (notable but not significant). Therefore, potential evapotranspiration exhibited a great correlation with maximum temperature and solar radiation, while runoff displayed a great correlation with rainfall. Thus, the relationships between hydroclimatic variables from continuous wavelet analysis in Figure 3-12 is generally consistent with the results from Mann-Kendall abrupt test in Figure 3-8 and the 5-year moving average of anomaly in Figure 3-4.

The continuous wavelet analysis was applied to graphically illustrate the periodic characteristics of annual hydroclimatic variables in the North Johnstone River catchment (Figure 3-13). Maximum temperature, minimum temperature, relative humidity, rainfall, and runoff exhibit similar interannual cycles of about 2-3 years (notable but not significant). In addition, significant cycles of around 28 years (long period/low frequency) were detected for maximum temperature, solar radiation, and FAO56 PET. Therefore, potential evapotranspiration displayed a close relationship with maximum temperature and solar radiation, while runoff was close related to rainfall with similar cycles according to Figure 3-13.

3.3.4 Linear regression analyses
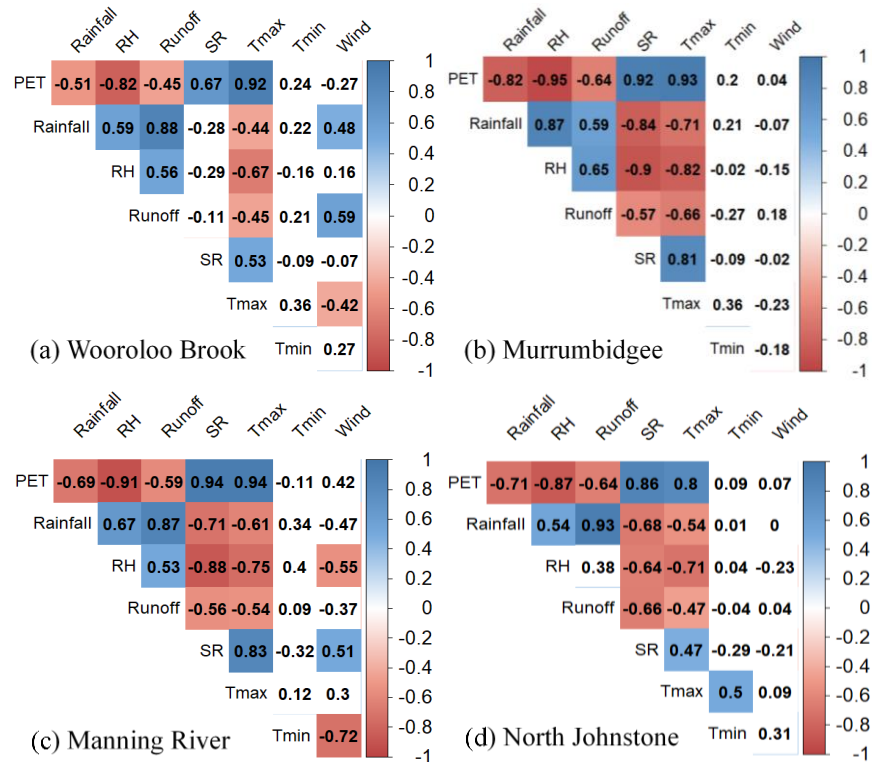
Figure 3-14 Correlation analyses between annual hydrological and climatic variables in the (a) Wooroloo Brook catchment (1977-2017), (b) Murrumbidgee catchment (1975-2014), (c) Manning River catchment (1991-2016), and (d) North Johnstone River catchment (1975-2017). Decimals from -1 to 1 shown in the legend and graph are correlation coefficients "r".

Figure 3-14a shows the correlation analyses between annual hydrological and climatic variables in the Wooroloo Brook catchment from 1977-2017. According to correlation coefficients, runoff displayed the greatest correlation with rainfall (correlation coefficient "r" was 0.88), while FAO56 potential evapotranspiration exhibited a greatest correlation with maximum temperature ("r" was 0.92). Besides, runoff showed significant (absolute r > 0.4) negative correlation with FAO56 potential evapotranspiration and maximum temperature, with the correlation coefficients of -0.45 and -0.45, respectively. In addition, runoff displayed significant positive correlation with rainfall, wind speed, and relative humidity ("r" were 0.88, 0.59 and 0.56 respectively), while showed insignificant negative correlation with solar radiation ("r" was -0.11) and insignificant positive correlation with minimum temperature ("r" was 0.21).

Figure 3-14b indicates the relationships between annual hydroclimatic variables in the Murrumbidgee catchment from 1975-2014. According to correlation coefficients, runoff displayed the greatest positive correlation with relative humidity (r = 0.65), while FAO56 potential evapotranspiration exhibited a greatest positive correlation with maximum temperature ("r" was 0.93) and a greatest negative correlation with relative humidity (r = -0.95).

Besides, runoff displayed significant negative correlation with maximum temperature, FAO56 PET, and solar radiation, with the correlation coefficients of -0.66, -0.64 and -0.57, respectively. In addition, runoff displayed significant positive correlation with relative humidity and rainfall ("r" was 0.65 and 0.59 respectively), while showed insignificant negative correlation with minimum temperature ("r" was -0.27) and insignificant positive correlation with wind speed ("r" was 0.18).

Figure 3-14c illustrates the correlation analyses between annual hydrological and climatic variables in the Manning River catchment from 1991-2016. According to correlation coefficients, runoff displayed the greatest correlation with rainfall ("r" was 0.87), while FAO56 potential evapotranspiration exhibited a greatest correlation with maximum temperature ("r" was 0.94) and solar radiation ("r" was 0.94). Besides, runoff showed significant negative correlation with FAO56 potential evapotranspiration, solar radiation, and maximum temperature, with "r" values of -0.59, -0.56 and -0.54, respectively. In addition, runoff displayed significant positive correlation with rainfall and relative humidity ("r" were 0.87 and 0.53, respectively), while exhibited insignificant negative correlation with wind speed ("r" was -0.37) and insignificant positive correlation with minimum temperature ("r" was 0.09).

Figure 3-14d illustrates the relationships between annual hydroclimatic variables for the North Johnstone River catchment from 1975-2017. Based on correlation coefficients, runoff displayed the greatest correlation with rainfall ("r" was 0.93), while FAO56 potential evapotranspiration showed a greatest positive correlation with solar radiation ("r" was 0.86) and a greatest negative correlation with relative humidity (r = -0.87). Besides, runoff showed significant negative correlation with solar radiation, FAO56 PET, and maximum temperature, with "r" values of -0.66, -0.64, and -0.47, respectively. In addition, runoff displayed insignificant negative correlation with minimum temperature ("r" was -0.04) and insignificant positive correlation with relative humidity and wind speed ("r" was 0.38 and 0.04, respectively).

3.3.5 Climate Elasticity

Table 3-5 Multi-year mean rainfall (P), potential evapotranspiration (E_0), runoff (R), runoff coefficient (RC), and parameter n of land use change in 1991-2014 for the four catchments.

Catchments	P	E_0	R	RC	n
Wooroloo Brook	731.3	1408.1	75.2	0.10	2.09
Murrumbidgee	753.5	1140.5	120.7	0.16	2.04
Manning River	1052.3	1103.9	182.4	0.17	3.25
North Johnstone	2698.3	1323.0	2021.4	0.75	0.71

Table 3-6 Climate elasticity for annual hydroclimatic variables in 1991-2014 for the four catchments. ε_P, ε_{E_0} ε_n, ε_{R_n}, $\varepsilon_{T_{max}}$, $\varepsilon_{T_{min}}$, ε_{U_2}, and ε_{RH} denote the elasticity of rainfall, potential evapotranspiration, parameter n of land use change, net radiation, maximum temperature, minimum temperature, wind speed, and relative humidity to runoff.

Catchments	ε_P	ε_{E_0}	ε_n	ε_{R_n}	$\varepsilon_{T_{max}}$	$\varepsilon_{T_{min}}$	ε_{U_2}	ε_{RH}
Wooroloo Brook	2.77	-1.77	-2.11	-1.32	-1.08	-0.08	-0.42	0.52
Murrumbidgee	2.57	-1.57	-1.57	-1.00	-0.61	-0.05	-0.22	0.33
Manning River	3.20	-2.20	-1.01	-1.49	-0.85	-0.10	-0.26	0.54
North Johnstone	1.21	-0.21	-0.31	-0.19	-0.11	-0.02	-0.02	0.09

Table 3-7 Comparison between observed runoff change and modeled runoff change due to hydroclimatic variables impacts, i.e., $\Delta R_P + \Delta R_n + \Delta R_{Rn} + \Delta R_{Tmax} + \Delta R_{Tmin} + \Delta R_{U2} + \Delta R_{RH}$ in the four catchments, and the fractional contributions (%) of climate change and human activity to runoff changes.

Catchments	Observed runoff change (mm)	Modelled runoff change (mm)	Contribution of climate change to runoff change (%)	Contribution of human activity to runoff change (%)
Wooroloo Brook	-39.5	-38.6	59.0	41.0
Murrumbidgee	-51.7	-55.0	67.3	32.7
Manning River	29.2	38.9	71.2	28.8
North Johnstone	220.6	233.5	24.3	75.7
Average	39.7	44.7	55.5	44.5

Table 3-5 shows multi-year mean rainfall (P), potential evapotranspiration (E_0), runoff (R), runoff coefficient (RC), and parameter n of land use change in 1991-2014 for the four catchments. Generally, the larger the runoff coefficient, the wetter the basin. Compared to other catchments, the North Johnstone catchment has much larger rainfall, runoff, and runoff coefficient. Therefore, the North Johnstone catchment is much more humid than the other three catchments. Furthermore, parameter n in the North Johnstone catchment (n = 0.71) was much smaller than the other catchments (n ≥ 2.09).

Based on annual climatic and hydrologic data in the four catchments, the partial differential equation was used to get the mean contributions of different hydroclimatic factors to runoff, and the results were shown in Table 3-6. According to the absolute values of elasticity coefficients, the order of the affecting factors was: rainfall > parameter n of land use change > net solar radiation > maximum temperature > relative humidity > wind speed ≥ minimum temperature for Wooroloo Brook, Murrumbidgee, and North Johnstone catchments. However, for the Manning River catchment, the order of the affecting factors was: rainfall > net solar

radiation > parameter n of land use change > maximum temperature > relative humidity > wind speed > minimum temperature. Therefore, precipitation is the factor that most affects runoff. In addition, the elasticity coefficients of runoff change to rainfall ranged from 1.21 to 3.20 with an average value of 2.44 in the four catchments, showing that an increase of 10% in rainfall caused an increase of 24.4% in runoff.

According to the results of Mann-Kendall abrupt test in section 3.3.2, the time point of 2002-2003 was accepted as the abrupt change point for runoff sequences for the four catchments and the entire runoff sequences were subdivided into two time periods, i.e., period 1 (1991-2002) and period 2 (2003–2014). Simulated runoff (i.e., $\Delta R_P + \Delta R_n + \Delta R_{Rn} + \Delta R_{Tmax} + \Delta R_{Tmin} + \Delta R_{U2} + \Delta R_{RH}$) and observed runoff are compared in Table 3-7. According to Table 3-7, simulated runoff and observed runoff matched statistically well with the correlation coefficient of 0.99 and the average absolute error of 5.0 mm (44.7-39.7). Therefore, in this study, this hydrothermal coupled balance model based on Budyko hypothesis was applied to differentiate the affecting factors for runoff changes in selected catchments in Australia. To further distinguish the main affecting factors for runoff change, Table 3-7 compares climate-induced runoff change (i.e., $\Delta R_P + \Delta R_{Rn} + \Delta R_{Tmax} + \Delta R_{Tmin} + \Delta R_{U2} + \Delta R_{RH}$) with human-induced runoff change (i.e., ΔR_n). Results indicated that climate change played a major role in changing runoff processes in the Wooroloo Brook, Murrumbidgee, and Manning River catchments. For runoff changes in North Johnstone catchment, human activities had more influence on runoff change than did climate change. Overall, the fractional contributions from climate change and human activity to runoff change were 55.5% and 44.5%, respectively, across the four catchments in Australia.

3.4 Discussion

3.4.1 Trends in hydroclimatic variables

Based on the anomalies in Figures 3-3 and 3-4, positive anomalies (high maximum temperature, solar radiation, and FAO56 PET) are detected in 2001-2009 and 2001-2006 for Murrumbidgee and Manning River catchment (both catchments are in southeast Australia), respectively. In contrast, annual rainfall and runoff showed negative anomalies (low rainfall and runoff) in 2001-2009 and 2002-2006 for the Murrumbidgee and Manning River catchments, respectively. This result is generally consistent with the Millennium Drought in southeast Australia (2001-2009) (one of the worst droughts on record) with ENSO found to be the most important driver (van Dijk et al., 2013). For the Wooroloo Brook catchment (Perth's eastern region in Southwestern Australia), 5-year moving average of anomaly for runoff (Figure 3-2) indicates a negative anomaly (low runoff) in 2010-2017, and Mann-Kendall trend test (Table

3-1) shows that there was a significant trend of decreasing values in annual runoff in the recent decades. Similarly, Liu et al. (2019) found that along with warming (increase in air temperature) and drying (reduction in mean annual precipitation) trends, dramatic declines of streamflow have occurred across the Southwestern Australia. About the trend in wind speed, significant trends of decreasing values in annual wind speed in the recent decades was detected for most of the catchments except for North Johnstone catchment (tropical Australia). Previous studies also reported similar results to ours. For instance, in recent decades, there have been significant trends of decreasing values in near-surface wind speed in mid-latitude areas including Australia, Europe, China, and North America (Shan et al., 2015). Mann-Kendall trend test showed that there was a trend of decreasing values in runoff (at 5% significance level) in two catchments (Wooroloo Brook and Murrumbidgee), while there was no significant trend in rainfall for all catchments. This means that the significant runoff decrease may not be caused by rainfall reduction in the catchments (Yang and Tian, 2009). Zhang et al. (2018) also found that although there was no significant trend of decreasing values in rainfall, there was a significant downward trend in runoff, which could be explained by the nonlinear relationships between rainfall and runoff.

No attempt was made in this study to identify the possible causes for the observed trends. Nevertheless, some previous studies have investigated the drivers of climate variability of Australia (Barua et al., 2013). For example, Australia's climate is affected by large-scale atmospheric circulation, including ENSO (El Niño Southern Oscillation), southern annular mode, and Indian Ocean dipole (Cleverly et al., 2016). Therefore, it is suggested in future studies to further analyze the relationships between changes of observed climatic variables and the changing patterns of atmospheric circulation such as ENSO to find the possible factors influencing changes in climatic variables.

3.4.2 Mann-Kendall abrupt test

According to the Mann-Kendall abrupt test, an abrupt change (generally in 2001–2004) for maximum or minimum temperature is detected for catchments in southern Australia (Wooroloo Brook, Murrumbidgee, and Manning River catchment). Most of southern Australia is affected by the 2000s drought (also called the Millennium drought) which is said by some to be the worst recorded drought since the European settlement. These abrupt changes detected for maximum or minimum temperature in 2001-2004 (sudden increase in temperature) may be related to the strong drought conditions brought on by El Niño from 2001 to 2005 in Australia (https://en.wikipedia.org/wiki/2000s_Australian_drought). Because the extra heat from global warming is expected to speed up the drought, making drying more quick and intense (Trenberth et al., 2014). For instance, through the Mann-Kendall test of the drought index in the last 100

years of China, Qiang (1992) found that the drought process in China had a sudden change and the time of the sudden change was almost the same as the rapid warming in the northern hemisphere. The fact of abrupt climate change has been reported in different areas worldwide, but the reason for this is far from clear (Chen et al., 2014). Solar variability, tropospheric aerosols, volcanicity, carbon dioxide, and other factors, have been invoked to casue changes, however, there are no clear lines of evidence been developed (Berger and Labeyrie, 1987). However, finding out the possible causes of abrupt climate change was not attempted in this research.

3.4.3 Wavelet analysis

Based on a wavelet analysis, almost all climatic and hydrologic variables exhibited similar high frequency cycles (notable but not significant) of about 2-4 years. Australian climate variability is influenced by various large-scale drivers, some of which have a greater impact over specific regions of the continent (Fierro and Leslie, 2014). Over the past few decades, many studies have identified the following atmospheric drivers as playing a major part in Australia's climate: the El Niño Southern Oscillation (ENSO), the Antarctic Oscillation (AAO), the dipole mode index (DMI), the Madden–Julian oscillation (MJO), and atmospheric blocking (Fierro and Leslie, 2014). It was reported by Kestin et al. (1998) that the inter-annual variability of ENSO was contained in a periodicity band of 2 to 10 years. This variability was not equally distributed over time but concentrated in different frequencies at different times. For instance, in their study, they found that two different cycles, 2–5 years and 4–7 years, dominated in 1880–1930 and 1930–1960, respectively (Beecham and Chowdhury, 2010). Additionally, ENSO has been detected as one of the main drivers of winter rainfall in Southern Australia, while spring rainfall is closely related to DMI (Rashid et al., 2015). Recent research also found that these teleconnections are nonstationary and can vary at different time scales (Rashid et al., 2015). Assessing the possible factors influencing observed periodicities was not attempted in this study. Nevertheless, future studies can further investigate the links between the dominant cycles and the large-scale atmospheric drivers.

3.4.4 Linear regression analyses

Based on correlation analyses between annual hydrological and climatic variables, runoff displayed the greatest correlation with rainfall in almost all catchments except the Murrumbidgee catchment. The result that runoff displayed the greatest correlation with rainfall is consistent with earlier studies (Chiew and Mcmahon, 2002). However, in the Murrumbidgee catchment, runoff displayed the greatest correlation with relative humidity ($r = 0.65$) rather than rainfall ($r = 0.59$). In addition, the correlation coefficient between runoff and rainfall in the Murrumbidgee catchment ($r = 0.59$) was much smaller than the other catchments ($r \geq 0.87$).

This might be caused by more human activities in the Murrumbidgee catchment. For instance, the two largest storages which are the Burrinjuck and Blowering Dams were constructed in this catchment. The Burrinjuck Dam was completed in 1928 and then expanded in 1957 to store and regulate irrigation and hydropower generation water, while the Blowering Dam was completed in 1968 to receive water from the Snowy Mountains Scheme to Murrumbidgee (Green et al., 2011). Furthermore, FAO56 potential evapotranspiration showed a greatest negative correlation with relative humidity and greatest positive correlations with maximum temperature and solar radiation for all catchments. Rainfall displayed significant negative correlation with maximum temperature in all catchments. Nicholls (2003) also found a negative correlation between average annual rainfall and maximum temperature in Australia, so the low rainfall years correspond to the mean temperature years (Hossain et al., 2013). In addition, the relationships between hydroclimatic variables from regression analyses in Figure 3-14 were generally consistent with the results from continuous wavelet analysis in Figures 3-10 to 3-13, the Mann-Kendall abrupt test in Figures 3-6 to 3-9, and the 5-year moving average of anomaly in Figure 3-2 to 3-5.

3.4.5 Climate Elasticity

The underlying parameter, n, denotes the characteristics of the underlying surface (e.g., vegetation) and the combined effects of the catchment characteristics (Yang et al., 2014). When n increases, the vegetation coverage area of the catchment increases, and the soil and water conservation function of vegetation increases, resulting in the decrease of runoff (Liu et al., 2016). In addition, larger n values imply the intensification of human activities in these areas, which may reduce the amount of streamflow (Liu et al., 2017b). Therefore, compared to the other catchments, the North Johnstone catchment had much smaller n value and much larger runoff. For the values of n (0.71-3.25 in this study), Yang et al. (2014) calibrated a range of 0.4-3.8 for 210 catchments across China, which showed a large regional variability. Similar ranges of n values have been detected according to another Budyko-based model: the lower bound of n was about 0.6 and, numerically at least, the upper bound appeared to be ~4.0 for catchments in Murray-Darling Basin of Australia (Donohue et al., 2012). The impacts of n (such as the vegetation type and coverage) on runoff are complex and need further study.

The elasticity of runoff refers to the change of runoff depth for a 1% increase of each climate variable. The sensitivity of runoff change to affecting factors can be reflected by the absolute value of elasticity (Liu et al., 2017b). Therefore, according to climate elasticity, rainfall is the main driver of change to runoff, while runoff change was least sensitive to minimum temperature change for all the four catchments. In general, increasing rainfall and relative humidity increased runoff (positive climate elasticity in Table 3-6), but increasing solar

radiation, maximum/minimum temperature, parameter n of land use change, and wind speed tended to decrease runoff (negative climate elasticity), because solar radiation, maximum/minimum temperature, and wind speed tended to increase evapotranspiration. This is in agreement with previous research (Liu et al., 2017b). Furthermore, the North Johnstone catchment (the wettest catchment) showed the smallest rainfall elasticity ($\varepsilon_P = 1.21$). This may be because previous studies reported the phenomenon that the larger values of ε_P exist in more arid areas (Sankarasubramanian et al., 2001; Yang et al., 2014).

3.5 Summary and conclusions

This study identified the driving factors (i.e., temperature, precipitation, net radiation, relative humidity, wind, and human activity) and their impacts on runoff, in four Australian catchments with different climatic conditions as case studies. According to Mann-Kendall trend test, there were significant trends of increasing values in annual mean temperature in the recent decades in the Murrumbidgee, Manning River, and North Johnstone catchments. In addition, results showed significant trends of decreasing runoff in the Wooroloo Brook (1977-2017) and Murrumbidgee catchments (1975-2014), while rainfall displayed no significant trends in all catchments. Based on the Mann-Kendall abrupt test, an abrupt change (generally in 2001–2004) for maximum or minimum temperature was detected for catchments in southern Australia (Wooroloo Brook, Murrumbidgee, and Manning River catchment). Additionally, the time point of 2002-2003 was accepted as the abrupt change point for runoff sequences for the four catchments and the whole runoff sequences was divided into two time periods, i.e., period 1 (1991-2002) and period 2 (2003–2014) for climate elasticity study. Based on wavelet analysis, almost all climatic and hydrologic variables exhibited similar high frequency cycles (notable but not significant) of about 2-4 years. According to correlation analyses between annual hydrological and climatic variables, runoff displayed the greatest correlation with rainfall in almost all catchments except the Murrumbidgee catchment, while FAO56 potential evapotranspiration showed a greatest negative correlation with relative humidity and greatest positive correlations with maximum temperature and solar radiation for all catchments.

According to the Budyko hypothesis, the order of the affecting factors was: rainfall > parameter n of land use change > net solar radiation > maximum temperature > relative humidity > wind speed ≥ minimum temperature for Wooroloo Brook, Murrumbidgee, and North Johnstone catchment. For the Manning River catchment, the order of the affecting factors was: rainfall > net solar radiation > parameter n of land use change > maximum temperature > relative humidity > wind speed > minimum temperature. As expected, rainfall is the factor that most affects runoff, and an increase of 10% in rainfall led to an increase of 24.4% in runoff according to the average of the four catchments. In addition, simulated and observed runoff

matched statistically well with a correlation coefficient of 0.99 and the average absolute error of 5.0 mm. Therefore, this Budyko-based model performed well in selected catchments in Australia and was used to distinguish affecting factors for runoff changes. Furthermore, the fractional contributions from climate change and human activity to runoff changes were 55.5% and 44.5%, respectively, across the four catchments in Australia. These outcomes provide significant information for the development of efficient adaptation strategies and effective policy plans for Australian sustainable water management in the future.

Chapter 4. Impacts of future climate change on water resource availability of eastern Australia: A case study of the Manning River basin

This chapter is based on the following manuscript:

Highlights:

1. Hydrologic impacts of climate change assessed in Manning River basin using XAJ model;

2. XAJ model performs satisfactorily with R^2 and NSE more than 0.94 and 0.92;

3. Runoff is projected to increase in summer and decrease in winter;

4. Projected changes in water availability are largely dominated by change in rainfall.

Abstract

Hydrological responses of catchments to climate change require detailed examination to ensure sustainable management of both water resources and natural ecosystems. This study evaluated the impacts of climate change on water resource availability of a catchment in eastern Australia (i.e. the Manning River catchment) and analyzed climate-hydrology relationships. For this evaluation, the Xinanjiang (XAJ) model was used and validated to simulate monthly rainfall-runoff relationships of the catchment. Statistically downscaled climate data based on 28 global climate models (GCMs) under RCP8.5 scenarios were used to assess the impacts of climate changes on the Manning River catchment. Our results showed that the XAJ model was able to reproduce observed monthly rainfall-runoff relationships with an $R^2 \geq 0.94$ and a Nash-Sutcliffe Efficiency ≥ 0.92. The median estimates from the ensemble of downscaled GCM projections showed a slight decrease in annual rainfall and runoff for the period 2021-2060 and an increase for the period 2061-2100. Annual actual evapotranspiration was projected to increase slightly, while annual soil moisture content was predicted to decrease in the future. Our results also demonstrated that future changes in seasonal and annual runoff, actual evapotranspiration and soil moisture are largely dominated by changes in rainfall, with a smaller influence arising from changes in temperature. An increase in the values of high runoffs and a decrease in the values of low runoffs predicted from the ensemble of the 28 GCMs suggest increased variability of water resources at monthly and seasonal time-scales in the future. A trend of decreasing values in winter runoff and soil moisture content in the future is likely to aggravate possible future reductions in water availability in eastern Australia. These results

contribute to the development of adaptive strategies and future policy options for the sustainable management of water resources in eastern Australia.

Key words: GCMs, Xinanjiang (XAJ) model, climate change, eastern Australia, runoff

4.1 Introduction

Global increases in atmospheric temperature is intensifying hydrological processes (Huntington, 2006; Oki and Kanae, 2006). For example, climate change is associated with changes in rainfall (amount, timing and distribution), increase in rates of evapotranspiration and changes in other climatic variables, and these changes will be amplified in runoff (Chiew et al., 2009; Reshmidevi et al., 2018). As a result, hydrological responses to global climate change have been widely studied in recent years. Thus, Menzel and Bürger (2002) predicted a trend of decreasing mean runoff for a catchment in Germany, while Su et al. (2017) reported that annual average runoff would increase in the 21st century in the upper Yangtze River basin in China. By the end of this century, annual runoff is projected to decrease in parts of southern Africa, the Middle East and southern Europe, while increased annual runoff is projected to occur in high northern latitudes, consistent with large increases in spring and winter rainfall under the RCP8.5 scenario (IPCC, 2013).

Australia has the world's most variable climate (Manolas, 2010; Stokes and Howden, 2010) and climate change has significantly affected Australian regional water availability and ecosystem health (CSIRO, 2016). Eastern Australia, including the majority (*ca* 80%) of the Australian population, is influenced by large-scale drivers of atmospheric circulation, including the El Niño Southern Oscillation, the Indian Ocean dipole and the southern annular mode (Cleverly et al., 2016), leading to high variability and the frequent occurrence of extensive droughts and floods. For instance, eastern Australia has been subject to considerable climate variability, including the Millennium Drought and the two wettest years on record for Australia (2010-2011), the latter as a result of two strong La Niña events. While several studies have assessed the impacts of climate change on the hydrology of eastern Australia (Chiew et al., 2009; Vaze and Teng, 2011) there have been few detailed studies of impacts of climate change on individual catchments in eastern Australia. Consequently, we examined a catchment representative of eastern Australia to provide detailed insight for future options for water management.

In most studies of the impacts of climate change, Global Climate Models (GCMs) have been the primary means used for global and regional climate simulations (Reshmidevi et al., 2018), especially with the large improvements in climate modelling in recent decades (IPCC, 2014). However, climatic variables simulated from GCMs are often too spatially coarse to be

used directly in hydrological models (Jiang et al., 2007). Furthermore, archived daily sequences simulated by GCMs are currently available only for specific periods (time slices) of a few decades (Liu and Zuo, 2012) and for a few GCMs. Therefore, downscaling approaches have to be adopted to transform large-scale GCMs outputs to daily time series at local and regional scales (Liu and Zuo, 2012; Silberstein et al., 2012). Over the last few decades, a series of downscaling methods have been used for this purpose (Gordon and O'Farrell, 1997; Frei et al., 2003; Diaz-Nieto and Wilby, 2005; Hewitson and Crane, 2006; Fowler et al., 2007; Ahmed et al., 2013). Dynamical downscaling and statistical downscaling are the two basic downscaling methods in the one-way coupling of GCMs and hydrological models (Fowler et al., 2007; Chen et al., 2012). Dynamical downscaling models, involving the use of regional numerical models that include full sets of physics (Tang et al., 2016), are highly computationally demanding and restricted to 'time slices', although they have explicit physical meanings (Fowler et al., 2007). In contrast, statistical downscaling models are relatively computationally efficient and have been widely applied in assessments of impacts of regional climate change, particularly in hydrological response assessments (Hay and Clark, 2003; Chen et al., 2012). Thus, in this study, daily rainfall and meteorological variables were downscaled from monthly GCM simulations to specific sites with bias correction procedures using a statistical downscaling approach (Liu and Zuo, 2012) and this represents the first such application.

Downscaled climatic variables are adopted as the input data for hydrological models to simulate historical and future runoff and to estimate impacts of climate change on runoff (Chang and Jung, 2010; Ruelland et al., 2012). In this way, hydrological models are first calibrated using observed runoff data, and then the hydrological models are run using downscaled climatic data with the same calibrated parameters, and impacts of climate change on runoff are estimated using the modelled historical and future runoffs (Chiew et al., 2009; Reshmidevi et al., 2018). However, many uncertainties which depend on climate modelling, downscaling techniques and simulated hydrologic regimes, are incorporated along the entire modeling chain (Prudhomme et al., 2003; Chen et al., 2012). Climatic uncertainty is linked to Green House Gas (GHG) emission scenarios and especially to GCMs (Minville et al., 2008). Previous studies have suggested that choosing a single GCM is the main factor contributing to the overall uncertainty in climate change impact modelling (Wilby and Harris, 2006; Jie et al., 2011). Due to the enormous uncertainty caused by the choice of a single GCM, an ensemble of multiple GCMs has been adopted in many recent analyses (Tebaldi and Knutti, 2007; Zhang and Huang, 2013) and multi-GCMs ensembles appear to provide more comprehensive simulations of climatic variables than a single GCM (Knutti et al., 2010). In addition, using simulations of a multi-GCMs ensemble may balance out non-stationary biases, which is unlikely to be corrected by statistical downscaling approaches (Liu and Zuo, 2012). Therefore,

a diversity of GCMs (28 from CMIP5 under RCP8.5) will be used in the present study to minimize the uncertainty caused by the choice of GCMs.

The Xinanjiang (XAJ) model, a rainfall-runoff basin model, has been successfully and widely used in humid and semi-humid catchments in China as a standard tool for a number of hydrological simulation purposes (Jayawardena and Zhou, 2000; Xu and Singh, 2004; Jiang et al., 2007; Yao et al., 2014). For example, Tian et al. (2013) used the XAJ model to assess impacts of climate change on river high-flows in a basin in China for the near future 2011–2040. It has also been successfully applied in many other countries including the United States, Canada, Germany, Belgium, France, Sweden, Japan and Thailand (Xu and Singh, 2004; Sahoo, 2005). For instance, Seiller and Anctil (2014) examined climate change impacts on the hydrologic regime of a catchment in Canada using the XAJ model and other lumped conceptual models. In addition, the XAJ model has been used across 210 catchments of southeast Australia, including the Murray–Darling basin and the south-east coast drainage basins that cover the most populated and important agricultural regions of Australia, with NSE values in the calibration periods of greater than 0.6 in 80 percent of these catchments (Li et al., 2009a; Zhi et al., 2009). Consequently, this study will apply the XAJ model forced with statistical downscaling of daily climate data based on 28 GCMs to study the hydrological response to climate change in an Australian catchment.

We aimed to evaluate hydrological responses to climate change in eastern Australia. Specifically, using the Manning River catchment as a case study, the objectives of this study were to: (1) test the performance of the XAJ model for simulating rainfall-runoff relationship of the Manning River catchment; (2) project future changes in simulated runoff, actual evapotranspiration and soil moisture content; and (3) identify the importance of different climatic variables in explaining future changes in water availability.

4.2 Materials and methods

4.2.1 Study area

The Manning River catchment is located on the New South Wales (NSW) mid north coast and includes the towns of Taree, Wingham, Gloucester and Walcha, and has a temperate climate with summer dominated rainfall (Chiew and Mcmahon, 2002) (Figure 4-1). The catchment area is approximately 6630 km^2 with elevation ranging from 12 m to 1591 m (see Figure 4-1). Mean annual temperature for the study area is 14.9°C, mean annual rainfall is 1052 mm, mean annual potential evaporation is 1305 mm, and the runoff coefficient is 0.20 (Zhang et al., 2013). The Manning River flows for 250 kilometers, rising in the Great Dividing Range to the east of the basin, and flowing south-east through a coastal floodplain to Taree where it divides in two. The

Manning River catchment does not have large groundwater storages providing base flow to the river and the narrow floodplain pockets are the only source of base flow (Hughes, 2011). In addition, most of the rivers and creeks in the Manning River catchment are unregulated, with no major storages to capture and control flows. As in most unregulated rivers, flows are most affected during relatively dry times and this has been identified as one of the key water management issues in this catchment when water supply is low and consumptive demand high (https://www.industry.nsw.gov.au/water/basins-catchments/snapshots/manning). In addition, significant decreases in river flows, resulting from below average rainfall, affects the stability of the Manning river estuary entrance (Ruprecht and Peirson, 2011). However, very few studies regarding hydrological response to climate change have been carried out in the Manning River catchment. Thus, this study represents an important step toward the assessment of the effects of the changing climate on catchment runoff and can help inform future priorities for regional water management of river basin in the context of global climate change in eastern Australia. The Manning River gauging station at Killawarra receives streamflow from the vast majority of water sources within the Manning EMU (Entitlement Management Unit). Therefore, the Manning River catchment above Killawarra gauging station was selected as the case study area.
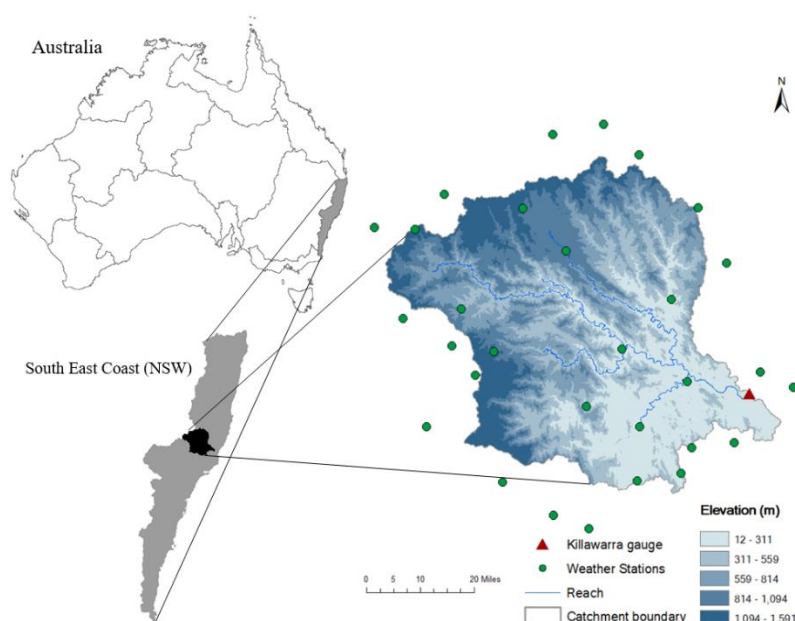
Figure 4-1 The study area of Manning River catchment and location of observation stations including weather stations and gauge station.

4.2.2 Observed data

Daily rainfall and potential evaporation data were used for hydrological simulation. To incorporate the large spatial heterogeneity of rainfall across this catchment, rainfall data from 30 meteorological stations sites within or close to the catchment were sampled (Figure 4-1).

The Thiessen polygon method was selected to estimate the mean area rainfall of this catchment because this is the most common and effective method for calculating spatial distribution of rainfall (Jiang et al., 2007). The method proposed by Abtew (1996) was used to calculate potential evapotranspiration (using solar radiation and maximum daily temperature) (Abtew, 1996). Daily streamflow data of the Killawarra hydrological station were collected from the website of the Australian Government Bureau of Meteorology (http://www.bom.gov.au/waterdata/). Daily observed hydrological and meteorological data in the period from 1991-2016 were used for hydrological model calibration and validation.

4.2.3 Statistical downscaling technique

Monthly gridded rainfall and climate data from GCMs were downscaled to the meteorological observation sites at a daily time step using a statistical downscaling model, NWAI-WG, developed by Liu and Zuo (2012). This rapid and reliable statistical downscaling method consists of two steps to perform spatial and temporal downscaling separately. This approach relies on empirical relationships between observational data and GCM outputs. First, the monthly gridded climate projections from GCMs were spatially interpolated to specific sites of interest (in this case 30 sites within or close to the Manning river catchment, Figure 4-1) using an inverse distance-weighted (IDW) interpolation method, followed by a bias correction procedure to correct site-based monthly GCM simulations. Second, daily climatic variables (e.g. maximum and minimum temperatures and rainfall) were then generated for each site from the spatially downscaled projections by using a modified version of the WGEN stochastic weather generator (Richardson and Wright, 1984) with parameters derived from the bias-corrected monthly data (see Liu and Zuo 2012 for details). The validation carried out by Liu and Zuo (2012) has shown that this downscaling method can reproduce the observed climatic variables at daily, monthly and annual time-scales well. Unlike other statistical downscaling approaches developed in Australia, which have only been applied to either specific time periods (Timbal et al., 2009) or small areas (Mehrotra and Sharma, 2010) due to data availability or time and cost, this approach can be easily applied to any archived monthly GCM data for any site and across multiple time periods as the approach requires only monthly GCM data and daily historical climate records. In this research, we applied a post downscaling treatment to the NWAI-WG downscaled data. When the downscaled site climate data are applied to catchment, the occurrence of inconsistent daily rainfalls between sites can result in a) more rainfall days and b) smaller daily rainfall over the catchment and potentially poor simulation of the peak flows. In the post downscaling treatment, we selected the central station as the reference station and re-downscaled other 29 sites in the catchment to have the same rainfall events with the amounts of GCM projected rainfalls for respective sites. This method is validate based on the hypothesis

that the weather stations are close enough so that the rain days are fairly consistent. The catchment area is approximately 6630 km^2, that is, the radius of the study area is around 40 km. Thus, we considered this catchment downscaling method is validate for this study.

This study was focused on the analyses of three periods of simulations: the first examined the period 1977-2016 (referred to as 'immediate past' or 'baseline'), the second examined the period 2021-2060 (referred to as 'the near future' or '2040s'), and the third the period 2061-2100 (referred to as 'the far future' or '2080s'). In addition, for baseline and future time periods, hydro-meteorological variables were downscaled from 28 GCMs (Wang et al., 2017) of the Coupled Model Intercomparison Project 5 (CMIP5) under the RCP8.5 scenario. RCP 8.5, a scenario that represents comparatively high greenhouse gas emission (Riahi et al., 2011) and matches the current trajectory of GHGs (Fuss et al., 2015; Pagán et al., 2016). To present the range in projected future climate, monthly, seasonal and annual change in maximum and minimum temperatures and rainfall for the 28 GCMs in the near future and the far future compared to baseline were computed for the catchment. In addition, monthly, seasonal and annual changes in runoff, evapotranspiration and soil moisture for the 28 GCMs in the 2040s and 2080s compared to baseline were estimated to show the range in projected future hydrological variables.

4.2.4 The XAJ model

The XAJ model is a lumped conceptual rainfall–runoff model with physical-based parameters (Zhao et al., 1980). The model is widely used in humid and semi-humid basins in China (Hu et al., 2005), and was recently adopted and validated in southeast Australia (Li et al., 2012). Furthermore, the XAJ model consistently performs better than four other conceptual rainfall-runoff models (the Pitman model of South Africa (Hughes, 2013), the Sacramento model of USA (Sorooshian et al., 1993), the NAM model of Denmark (Nielsen and Hansen, 1973) and the SMAR model of Ireland (Kachroo, 1992)) even in relatively dry catchments (Gan et al., 1997). Therefore, the XAJ model was selected for hydrological simulations in the present study. The XAJ model, which uses rainfall and potential evapotranspiration data to simulate runoff, actual evapotranspiration and soil moisture content, is divided into four layers: evapotranspiration, runoff production, separation of runoff components and flow concentration (Zhao, 1992). Its main feature is the concept of runoff formation of repletion of storage, which means that runoff is not produced until the soil moisture content of the aeration zone reaches field capacity, and thereafter runoff equals the rainfall excess without further loss (Zhao, 1992). The flow chart of the XAJ model is shown in Figure 4-2 and the model parameters are listed in Table 4-1. It should be noted that the XAJ model used in this study does not consider vegetation

and its interaction with the atmosphere. However, it has the advantage of fewer input data and simpler application.

It is crucial for water resource managers to be conscious of and prepared for the impacts of climate change on hydrological variables. Therefore, daily hydrological simulations under baseline and future scenarios were obtained using the XAJ model driven by downscaled climatic variables from 28 GCMs to evaluate the changes in catchment hydrological cycle. Runoff, which represents an integrated response to climatic inputs throughout the whole drainage basin, is a very important indicator of the impacts of climate change on water resources. In addition, climate change will lead to changes in other hydrological variables which can also be simulated by the XAJ model. Therefore, changes of actual evapotranspiration and soil moisture content were also included in this study. Soil moisture is defined as the areal mean tension water storage (W) in the XAJ model (Zhao, 1992). The XAJ model was calibrated and validated against river flow data only. We did not calibrate and validate the model simulations in actual evapotranspiration and soil moisture content because of a lack of field data for these variables. The absolute values of soil moisture content should therefore not be used directly. Nevertheless, it is still reasonable and valuable to compare the relative changes in the simulations because the model mimics the actual hydrological processes.
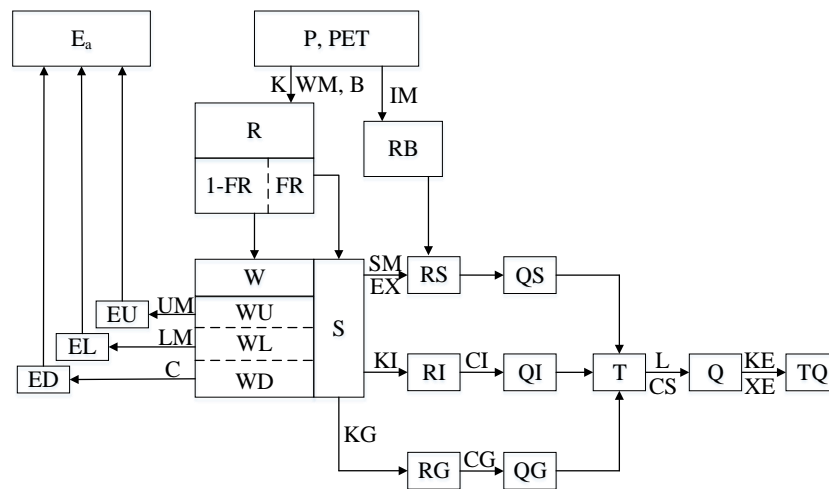
Figure 4-2 Flow chart for the XAJ model. The inputs to the model are P (rainfall) and PET (potential evapotranspiration), the outputs are Ea (the actual evapotranspiration from the whole catchment, which is the sum of the evapotranspiration from the upper soil layer EU, the lower soil layer EL, and the deepest layer ED) and TQ (the outlet discharge from the whole catchment), and W (area mean tension water storage, namely soil moisture, which is the sum of WU, WL and WD in the upper, lower and deepest layer). The meanings for the state variables and parameters appear inside and outside of the blocks in this figure can be found in Table 4-1 and the reference (Zhao, 1992).

4.2.5 Parameter estimation and performance evaluation

There are a lot of missed observed flow data in 1983, 1989 and 1990 at Killawarra gauging station. However, observed flow data from 1991-2016 (26 years) are relatively complete and continuous and were selected for model calibration and validation. The time period for calibration and validation years was determined by the length of the observed data record. For sufficiently long periods of observed data that represent different climate conditions, it is possible to split the available data equally for calibration and validation. However, the observed record (26 years) is not sufficient for an equal split, the length of the data may be different in such a way that the calibration period is sufficiently long since optimized model parameters during calibration are used for model validation without further adjustment (Ayele et al., 2017). Therefore, daily observed and simulated runoff in the period 1991-2008 (18 years) were used for model calibration and data from 2009-2016 (8 years) were used for model validation. A global optimization method, the SCE-UA (shuffled complex evolution method developed at the University of Arizona) (Duan et al., 2015), is an effective and efficient optimization technique for calibration of watershed models and was used to optimize XAJ model parameters. It combines the best features of "multiple complex shuffling" and "competitive evolution" based on the simplex search method (Nelder and Mead, 1965). The XAJ model is calibrated by maximizing the Nash-Sutcliffe Efficiency (NSE) (Nash and Sutcliffe, 1970) of daily flow together with a constraint to ensure that the total modelled flow in the calibration period is within 5% of the total observed flow (Vaze and Teng, 2011). NSE and coefficient of determination (R^2) were used to evaluate the performance of the XAJ model. The NSE is one of the most widely used criteria for comparing hydrologic model performance with observed values (Le and Pricope, 2017). In addition, many studies also used NSE and R^2 to evaluate the performance of hydrological models (Vu et al., 2012; Le and Pricope, 2017). NSE varies from $-\infty$ to 1. A value of 1 means the simulations perfectly match the observations, so the closer the NSE value is to 1, the better the hydrological model is deemed to have performed. In general, when both NSE and R^2 exceed 0.50, the hydrological model is deemed to effectively simulate stream flow for a given catchment (Liu et al., 2017c). The NSE and R^2 were calculated as follows:

$$NSE = 1 - \frac{\sum_{i=1}^{N}(Q_{obs,i} - Q_{sim,i})^2}{\sum_{i=1}^{N}(Q_{obs,i} - \overline{Q}_{obs})^2} \tag{4-1}$$

$$R^2 = \frac{\left[\sum_{i=1}^{N}(Q_{obs,i} - \overline{Q}_{obs})(Q_{sim,i} - \overline{Q}_{sim})\right]^2}{\sum_{i=1}^{N}(Q_{obs,i} - \overline{Q}_{obs})^2 \sum_{i=1}^{N}(Q_{sim,i} - \overline{Q}_{sim})^2} \tag{4-2}$$

where Q_{obs} and Q_{sim} are the observed and simulated daily flow (m^3/s) respectively, $\overline{Q}$ is the mean flow (m^3/s), i is the *ith* sample, and *N* is the number of samples.

4.2.6 Regression analyses

Prior to the analysis of the simulations we applied a bias-correction procedure, called secondary bias correction (Yang et al., 2016) to correct the differences of the simulated outputs forced by GCM projected climate over those forced by observed climate.

A multiple Liner Regression Model (MLRM) was used to quantify the effects of climate variables (maximum and minimum temperatures and rainfall) on hydrologic variables (runoff, evapotranspiration and soil moisture). MLRM is a linear model that describes how y-variable relates to two or more x-variables (Dar, 2017). The general structure of the model is as given below:

$$Y = \beta_0 + \beta_1 X_1 + \beta_2 X_2 + \dots \tag{4-3}$$

Where, y is the dependent (or response) variable, x is independent (or predictor) variable.

In this study, the model is defined as below:

$$\Delta Y = a\Delta T_{max} + b\Delta T_{min} + c\Delta R \tag{4-4}$$

Where ΔY (%) is projected changes in hydrological variables (runoff, actual evapotranspiration or soil moisture), ΔT_{max} (°C), ΔT_{min} (°C) and ΔR (%) are changes in maximum and minimum temperatures and rainfall, respectively. From these regression analyses, the contribution of the change in specific climate factors to changes in hydrologic variables were quantified. In addition, rainfall elasticity (c, defined here as the proportional change in runoff divided by the proportional change in rainfall) can also be derived.

4.3 Results

4.3.1 XAJ model calibration and validation

Calibrated parameters for the XAJ model in the Manning River catchment are shown in Table 4-1. Runoff simulations at daily time scale were aggregated to monthly values, and were compared with the observed data. Monthly observed runoff and the XAJ model simulated runoff for calibration and validation periods in the Manning River catchment were strongly correlated ($R^2 \geq 0.94$ and NSE ≥ 0.92) and closely replicated temporal variation (Figures 4-3 and 4-4), with slopes within 25% of the 1:1 regression. The slope of the regression during the validation period was much closer to the 1:1 line than that in the calibration period, which may be caused by the slight underestimation of the extremely high runoff observed in the calibration period.

Table 4-1 16 calibrated parameters for the XAJ model in Manning River catchment.

Layers	Parameters	Meaning of parameters (units)	Values

Evapotranspiration	UM	Areal mean tension water capacity in the upper layer (mm)	28
	LM	Areal mean tension water capacity in the lower layer (mm)	90
	C	Coefficient of deep evapotranspiration	0.023
Runoff production	WM	Areal mean tension water capacity (mm)	137
	B	Exponent of the tension water capacity curve	0.1
	IM	Ratio of the impervious to the total area of the basin	0.001
Separation of runoff components	SM	Areal mean of the free water capacity of the surface soil layer (mm)	27
	EX	Exponent of the free water capacity curve	0.97
	KG	Outflow coefficient of the free water storage to groundwater	0.52
	KI	Outflow coefficient of the free water storage to interflow	0.26
Flow concentration	CI	Recession constant of the interflow storage	0.78
	CG	Recession constant of groundwater storage	0.996
	CS	Recession constant of surface water storage	0.38
	L	Lag time (day)	0
	KE	Parameters of the Muskingum method (h)	24
	XE	Parameters of the Muskingum method	0.43
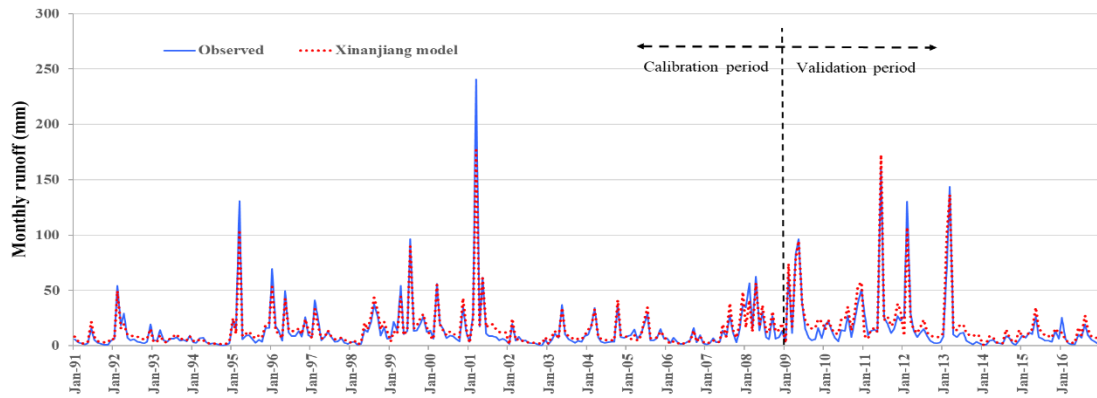
Figure 4-3 The observed and simulated monthly runoff during calibration (1991-2008) and validation periods (2009-2016) in the Manning River catchment.
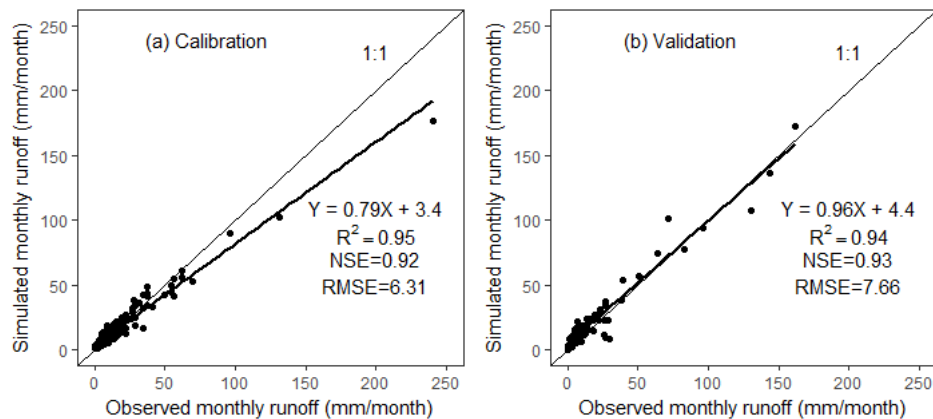
Figure 4-4 Comparison of observed and simulated monthly runoff during (a) calibration and (b) validation periods.

4.3.2 Projected changes in temperature and rainfall

Projected maximum and minimum temperatures and rainfall in the future were aggregated to monthly and seasonal time scales, and compared with baseline values. All 28 GCMs used in this study agree on a future temperature rise, with higher temperature increases in 2080s than 2040s at both monthly and seasonal time-scales (Figures 4-5 and 4-6). For maximum monthly temperatures (Figure 4-5a), the largest median increase was 1.6°C (0.9-1.9°C) in November by 2040s and 3.8°C (3.5-4.2°C) in September by 2080s, while the lowest median increase was 1.1°C (0.9-1.7°C) in March by 2040s and 2.5°C (1.8-3.0°C) in February by 2080s. The range of uncertainty in brackets indicates the 25th and 75th percentiles of the 28 GCMs used herein. At seasonal time-scales (Figure 4-6a), the maximum temperature was projected to increase most in spring in both future periods (the median increase was 1.5°C (1.1-1.8°C) in 2040s and 3.4°C (2.8-3.9°C) in 2080s), while increases were lowest in autumn in 2040s (1.3°C (0.9-1.6°C)) and in summer in 2080s (2.9°C (2.4-3.4°C)). For temperature minima (Figures 4-5b and 4-6b), the median estimate demonstrated the largest increase in May (1.9°C (1.6-2.5°C) in 2040s and 4.9°C (3.7-5.5°C) in 2080s) (autumn (1.7°C (1.4-1.9°C) in 2040s and 4.1°C (3.3-4.7°C) in 2080s) and the smallest increase in temperature minima in February (1.0°C (0.8-1.3°C) in 2040s and 2.5°C (1.8-3.1°C)) in 2080s (summer (1.2°C (0.9-1.3°C) in 2040s and 2.7°C (2.3-3.2°C) in 2080s)) in the future. The median increase for maximum temperature at an annual time-scale was 1.4 °C (1.2-1.5°C) by 2021-2060 and 3.2°C (2.7-3.5°C) by 2061-2100 (Figure 4-6a), while median annual minimum temperatures were predicted to increase by 1.5°C (1.3-1.7°C) in 2040s and 3.5°C (3.1-4.1°C) in 2080s (Figure 4-6b).

Changes to future rainfall differ across the different GCMs and across seasons, with the majority of GCMs simulating increases in November-March rainfall and the majority of GCMs simulating decreases in the period of April to October. The largest ensemble median increase in rainfall occurred in December (4.2% (-7.6~13.4%) in 2040s and 13.4% (-10.9~31.4%) in 2080s), while the largest median decrease occurred in September (-10.6% (-20.7~8.1%) in 2040s and -20.7% (-34.0~9.7%) in 2080s) (Figure 4-5c). Median spring (-1.7% (-13.5~10.0%) in 2040s and 1.4% (-17.4~13.8%) in 2080s) and autumn (-1.1% (-6.0~4.8%) in 2040s and 0.7% (-9.3~7.5%) in 2080s) rainfall was projected to have relatively small changes in the future. In contrast, median rainfall was projected to have a larger increase in summer (4.2% (-3.6~11.7%) in 2040s and 9.1% (-2.9~24.9%) in 2080s) but a decline (-4.0% (-13.1~3.1%) in 2040s and -11.7% (-20.9~3.5%) in 2080s) in winter, with larger changes in 2080s than in 2040s. At annual time-scales, the changes in rainfall, as estimated by the 28, ranged from -5.2% (25th percentile)

to 4.2% (75th percentile) in 2040s and -9.5% (25th percentile) to 10.8% (75th percentile) in 2080s with ensemble median values of -0.3% and 4.6%, respectively.
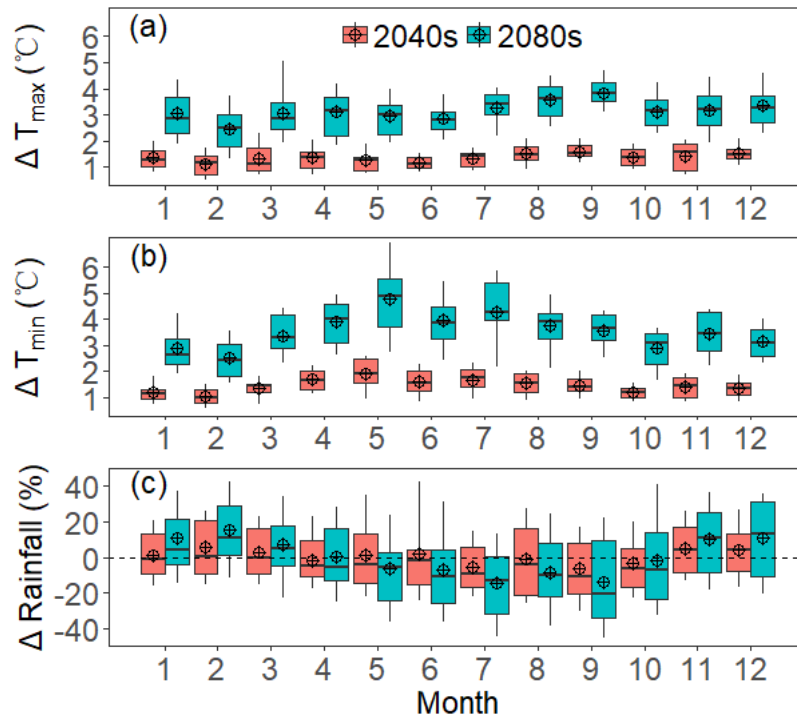
Figure 4-5 Projected changes in maximum temperature (T_{max}) (°C), minimum temperature (T_{min}) (°C) and rainfall (%) in the near future (2021–2060, 2040s) and the far future (2061–2100, 2080s) under RCP8.5 based on 28 GCMs compared with baseline at monthly time scale. Data presented are changes in the 40-year mean values for each of the 28 GCMs. Box boundaries indicate the 25th and 75th percentiles; the black lines and crosshairs within the box mark the median and mean, respectively; the lower and upper whiskers indicate the 10th and 90th percentiles.
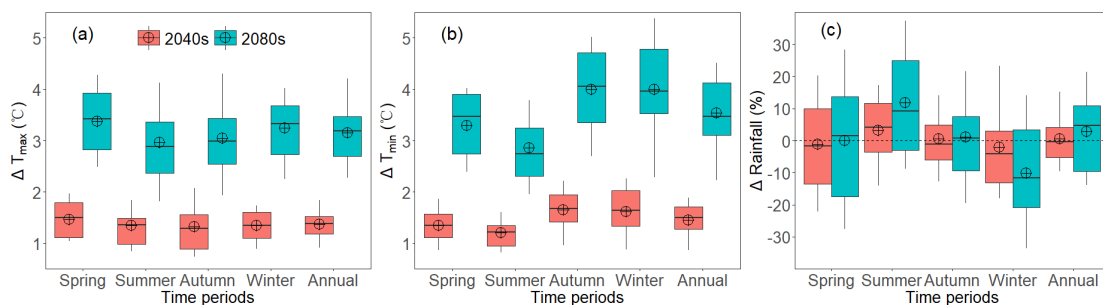
Figure 4-6 Projected changes in maximum temperature (T_{max}) (°C), minimum temperature (T_{min}) (°C) and rainfall (%) in the near future (2021–2060, 2040s) and the far future (2061–2100, 2080s) under RCP8.5 based on 28 GCMs compared with baseline at seasonal and annual time scales. Data presented are changes in the 40-year mean values for each of the 28 GCMs. Box boundaries indicate the 25th and 75th percentiles; the black lines and crosshairs within the

box mark the median and mean, respectively; the lower and upper whiskers indicate the 10th and 90th percentiles.

4.3.3 Changes in simulated runoff, actual evapotranspiration and soil moisture

Projected runoff, evapotranspiration and soil moisture content were aggregated to monthly and seasonal time-scales, and were compared with baseline data. The largest median monthly increase in runoff was 6.9% (-23.2~26.7%) in November by 2040s and 31.1% (-2.6~71.4%) in February by 2080s, while the largest median decrease was -16.7% (-23.9~13.2%) in June by 2040s and -20.5% (-31.1~4.2%) in July by 2080s (Figure 4-7a). Thus, the largest monthly runoff is projected to shift from March (during the baseline period; Table 4-2) to February in the far future. The lowest runoff in September was simulated to decline (-4.3% (-24.2~14.3%) in 2040s and -16.3% (-33.2~3.8%) in 2080s) in the future. The second largest runoff, which occurred in the summer in the baseline period, was projected to increase (11.6% (-12.8~24.9%) in 2040s and 23.8% (-5.3~46.2%) in 2080s) in the future, whereas the second smallest runoff, which currently occurs in winter, was projected to decline (-6.9% (-23.0~4.9%) in 2040s and -14.8% (-28.7~-0.06%) in 2080s) in the future (Table 4-2, Figure 4-8a). Thus, the largest seasonal runoff which currently occurs in the autumn was predicted to change to the summer in 2040s and 2080s. In addition, in 2080s, these monthly and seasonal changes generally became larger than those predicted in the 2040s (Figures 4-7a and 4-8a). There were considerable differences in the runoff projection of different GCMs (Figures 4-7a and 4-8a). Thus, at annual time-scales, runoff change estimated by the 28 GCMs ranged from -10.6% (25th percentile) to 8.9% (75th percentile) in 2040s and -17.2% (25th percentile) to 22.0% (75th percentile) in 2080s with median values of -2.3% and 7.7%, respectively (Figure 4-8a). Furthermore, median values in annual runoff in 2080s showed a slight increase compared to 2040s (Figure 4-8a) and this may be related to the increase in rainfall in 2080s (Figure 4-6c).

There was a wide range in differences among modelled values of actual evapotranspiration responses simulated by the 28 GCMs. Median monthly actual evapotranspiration was projected to decrease only in August (-2.2% (-5.1~5.1%) in 2040s and -4.3% (-13.7~3.7%) in 2080s), September (-4.1% (-11.4~1.3%) in 2040s and -8.9% (-21.1~-1.4%) in 2080s) and October (-5.3% (-11.7~-0.4%) in 2040s and -7.4% (-16.9~3.0%) in 2080s) (winter/spring), while median seasonal actual evapotranspiration only showed a trend of decreasing values (-2.2% (-10.3~2.7%) in 2040s and -3.2% (-15.7~3.7%) in 2080s) in spring in the future (Figures 4-7 and 4-8). At annual time-scales, actual evapotranspiration change estimated by the 28 GCMs ranged from -3.0% (25th percentile) to 3.7% (75th percentile) in 2040s and -4.3% (25th percentile) to 8.6% (75th percentile) in 2080s with median values of 0.6% and 1.8% respectively (Figure 4-8b). However, the differences in actual evapotranspiration changes under different GCMs are

smaller than the modelled changes in runoff (Figures 4-7a, b and Figures. 4-8a, b). Differences in predicted 40-year mean monthly, seasonal and annual soil moisture content resulting from different GCMs were also considerable (Figures 4-7c and 4-8c). Furthermore, the median estimate indicated that monthly soil moisture content was projected to have a trend of decreasing values (except February (1.5% (-8.8~5.3%))) in 2040s and to increase slightly only in December (3.6% (-16.6~14.1%)), January (2.0% (-5.0~9.7%)), February (4.1% (-6.2~14.9%)) and March (0.7% (-7.0~12.9%)) in 2080s, while seasonal soil moisture was predicted to decrease in 2040s and to increase marginally (0.5% (-7.9~10.7%)) only in summer in 2080s. Finally, at annual time-scales, changes in soil moisture content simulated by the 28 GCMs ranged from -8.8% (25th percentile) to 0.2% (75th percentile) in 2040s and -15.5% (25th percentile) to -1.6% (75th percentile) in 2080s with ensemble median values of -4.4% and -5.1% respectively.

Table 4-2 Mean values in climatic and simulated hydrological variables in the baseline period (1977-2016) in Manning River catchment.

Time periods	T_{max} (°C)	T_{min} (°C)	Rainfall (mm)	Runoff (mm)	Actual Evapotranspiration (mm)	Soil moisture content (mm)
January	26.3	14.7	154.7	18.0	100.3	65.7
February	25.6	14.6	144.1	27.0	90.7	79.5
March	24.3	13.0	125.3	28.1	86.5	82.0
April	21.3	9.8	74.4	18.2	60.8	77.7
May	17.4	6.9	77.5	19.2	46.1	79.9
June	14.4	4.6	73.5	19.5	39.4	88.8
July	13.7	3.1	53.9	17.0	43.6	89.4
August	15.3	3.7	55.1	15.6	51.9	80.3
September	18.3	5.8	55.2	11.9	60.1	67.8
October	21.2	8.7	84.8	14.1	74.3	60.9
November	23.5	11.0	91.5	12.7	82.1	58.3
December	25.6	13.2	110.0	13.8	94.9	58.5
Spring	21.0	8.5	231.5	38.6	216.5	62.4
Summer	25.9	14.2	408.8	58.8	286.0	67.9
Autumn	21.0	9.9	277.2	65.5	193.4	79.9
Winter	14.5	3.8	182.5	52.1	135.0	86.2
Annual	20.6	9.1	1100.0	214.9	830.9	74.1
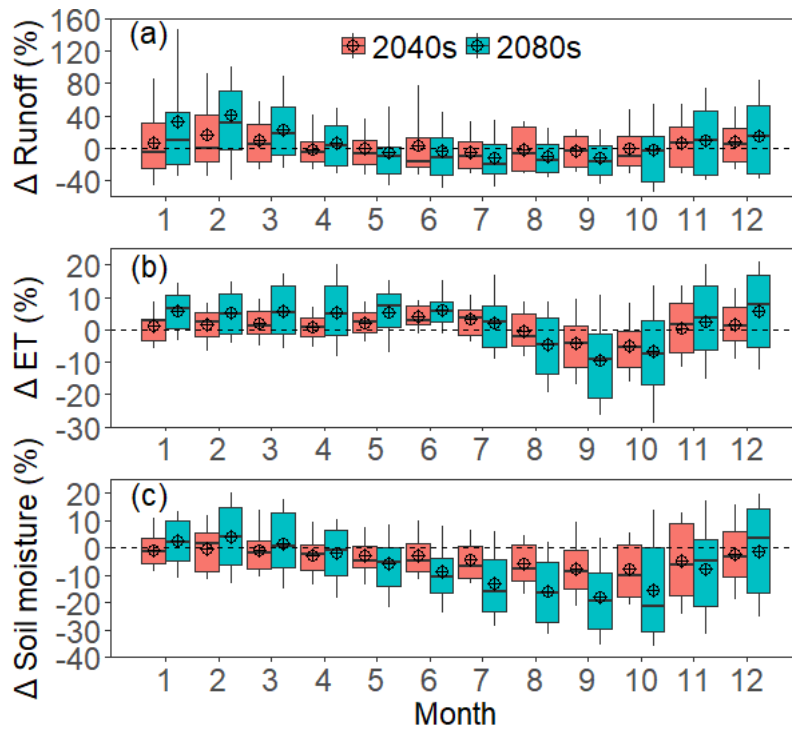
Figure 4-7 Projected changes in runoff (%), actual evapotranspiration (%) and soil moisture (%) in the near future (2021–2060, 2040s) and the far future (2061–2100, 2080s) under RCP8.5 based on 28 GCMs compared with baseline at monthly time scale. Data presented are changes in the 40-year mean values for each of the 28 GCMs. Box boundaries indicate the 25th and 75th percentiles; the black lines and crosshairs within the box mark the median and mean, respectively; the lower and upper whiskers indicate the 10th and 90th percentiles.
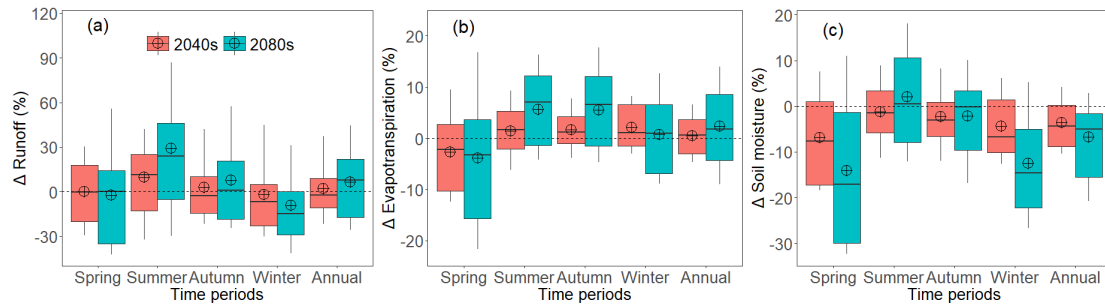
Figure 4-8 Projected changes in runoff (%), actual evapotranspiration (%) and soil moisture (%) in the near future (2021–2060, 2040s) and the far future (2061–2100, 2080s) under RCP8.5 based on 28 GCMs compared with baseline at seasonal and annual time scales. Data presented are changes in the 40-year mean values for each of the 28 GCMs. Box boundaries indicate the 25th and 75th percentiles; the black lines and crosshairs within the box mark the median and mean, respectively; the lower and upper whiskers indicate the 10th and 90th percentiles.

4.3.4 Relationships among hydrological responses and climate variables

Relationships among changes in hydrologic variables (runoff, evapotranspiration and soil moisture content) and changes in daily maximum and minimum temperatures and rainfall are shown in Table 4-3. Runoff, actual evapotranspiration and soil moisture content were all largely dominated by rainfall at annual and seasonal time-scales. At annual time-scales, change in runoff was only significantly correlated with change in rainfall, while change in actual evapotranspiration was significantly correlated with change in rainfall, and daily maximum and minimum temperatures, while soil moisture content was primarily dominated by rainfall and daily maximum temperature. Furthermore, correlations of changes in hydrological variables to changes in climatic variables were estimated using the multiple regression model. For example, runoff could change by 5.1, 7.2, -7.7 and -10.6% in spring, summer, autumn and winter, respectively, with an annual change of -4.9%, as a result of an increase of maximum temperature of 1.0°C. Annual rainfall elasticity of runoff was about 2.1, that is, a 1% change in mean annual rainfall results in a 2.1% change in mean annual runoff in this catchment. Finally, the effect of changes in rainfall on actual evapotranspiration was smaller than its effect on soil moisture content, and much smaller than its impact on runoff at seasonal and annual time-scales. For instance, a 1% change in mean annual rainfall results in a 0.6% and 0.8% change in mean annual actual evapotranspiration and soil moisture content, respectively, in this catchment.

Table 4-3 Regression coefficients of projected changes in hydrological variables (ΔY, %) including runoff, actual evapotranspiration and soil moisture with changes in daily maximum temperature (ΔT_{max}, °C), daily minimum temperature (ΔT_{min}, °C) and rainfall (ΔR, %) in a multiple linear regression model ($\Delta Y = a\Delta T_{max} + b\Delta T_{min} + c\Delta R$); *$p < 0.05$, **$p < 0.01$, ***$p < 0.001$.

Hydrologic variables	Time periods	a	b	c	Adjusted R^2
Δ Runoff	Annual	-4.89	4.50	2.08***	0.85
	Spring	5.10	-5.50	1.46***	0.72
	Summer	7.19*	-8.99*	2.69***	0.89
	Autumn	-7.73***	7.37***	1.84***	0.87
	Winter	-10.62*	10.28**	1.61***	0.77
Δ Actual evapotranspiration	Annual	1.50*	-1.11*	0.55***	0.88
	Spring	-2.98*	1.94	0.58***	0.85
	Summer	1.67*	-1.22	0.37***	0.82
	Autumn	1.06	0.56	0.25***	0.53
	Winter	-0.35	1.61	0.37***	0.64
Δ Soil moisture	Annual	-1.64*	-1.08	0.76***	0.90
	Spring	-3.84*	-0.23	0.68***	0.88
	Summer	-0.05	-1.83*	0.62***	0.88

Autumn	-3.69**	2.11*	0.52***	0.67
Winter	-4.24*	1.82	0.55***	0.80

4.4 Discussion

In this study, hydrological responses to climate change in the Manning River catchment were simulated using an ensemble of 28 GCMs and the XAJ model. The overall calibration and validation results demonstrated that the XAJ model was able to satisfactorily reproduce the observed runoff in this catchment (Figures. 4-3 and 4-4), and the calibrated XAJ model can be further used to evaluate the impacts of climate change on catchment hydrological variables. While the hydrological model was generally able to replicate observed runoff, it might have some difficulties in reproducing the extreme high runoff in the calibration period (Figures 4-3 and 4-4). Similar results in reproducing peak flow also occur in other hydrological models. For example, Tian et al. (2013) used three models (GR4J (Perrin et al., 2003), HBV (Lindström et al., 1997) and XAJ) to simulate daily discharge and their results demonstrated an underestimation of high rates of discharge in all three models. Eum et al. (2016) used the Variable Infiltration Capacity (VIC) hydrologic model to simulate daily runoff and found a poor capacity to simulate both low flows and very high flows. Thus, difficulties in reproducing the highest rates of runoff are common because of the theories of hydrological models and criteria of model calibration. This may be attributed to the theory of runoff production (Hao et al., 2015). For example, the XAJ model assumes that runoff is not generated until soil moisture content of the aeration zone reaches field capacity. This assumption may not be valid during heavy rain events because these can produce runoff when soils are not fully filled with water (unsaturation runoff) due to insufficient infiltration, which is not simulated in the XAJ model (only saturation excess runoff is simulated). Therefore, modification of the model structure by including unsaturation runoff during heavy rainfall events may lead to improved hydrologic simulations during these periods.

Our results indicated that the median annual increase for maximum temperature was 1.4°C (1.2-1.5°C) by 2021-2060 and 3.2°C (2.7-3.5°C) by 2061-2100, while minimum temperature was predicted to increase by 1.5°C (1.3-1.7°C) in 2021-2060 and 3.5°C (3.1-4.1°C) in 2061-2100. The projected trend of increasing temperature agrees with previous studies. For instance, Wang et al. (2017) reported a 3.7°C increase in temperature for RCP8.5 across the wheat belt in NSW by 2061-2100. Moreover, an ensemble of 12 RCM simulations (4 GCMs × 3 RCMs) performed by the NSW and ACT Regional Climate Modelling (NARCliM) project projects a 0.7°C rise in mean temperature by 2020-2039 and a 2.0°C rise by 2060-2079 in the north coast region of NSW (including the Manning River catchment)

(www.ccrc.unsw.edu.au/sites/default/files/NARCliM/index.html). However, it should be noted that future time periods in our research (2021-2060 and 2061-2100) and the NARCliM project (2020-2039 and 2060-2079) are not exactly the same. In addition to temperature, our results also showed that median rainfall is projected to have a significant increase in summer and a decrease in winter in the future, although the largest rainfall is in the summer and the lowest rainfall is in winter in this catchment (Table 4-2). Therefore, the trend of increasing values in high rainfalls and a trend of decreasing values in low rainfalls are likely to generate a larger degree of inter-seasonal variation in the Manning River catchment in the future. This is generally consistent with previous studies. For example, NARCliM also projects an increase in rainfall during summer, autumn and spring and a decrease in winter across the north coast region by 2060-2079. In addition, Liu and Zuo (2012) analyzed the changes in summer and winter rainfall and found an increase in summer rainfall, whilst winter rainfall has a high probability of decreasing in most areas of New South Wales.

Our results showed that multi-GCM ensemble median values exhibit a slight decrease (-2.3% (-10.6~8.9%)) in annual runoff in 2040s, which is similar to the trend of change in previous studies, despite the GCMs, hydrological models, downscaling methods and time periods differing across studies. For instance, Chiew and Mcmahon (2002) concluded that the annual runoff in catchments on the east coast of Australia could change by ±15% by 2030 relative to 1990. Similarly, Chiew et al. (2003) used the SIMHYD model and the CSIRO Mark 2 GCM simulations and found a decrease in mean annual runoff of 6-8% in most of eastern Australia in 2021-2050 relative to 1961-1990. Vaze and Teng (2011) used 15 GCMs and the median estimate indicates that future mean annual runoff in 2030 relative to 1990 will be no change to a slight reduction in the eastern parts of Australia. In addition, median estimates suggest a trend of increasing values in summer runoff (the second largest runoff in the baseline period) and a trend of decreasing values in winter runoff (the second smallest runoff in the baseline period) in the future. Consequently, the trend of increasing values of high runoffs and a trend of decreasing values of low runoffs is likely to generate larger inter-seasonal differences in the future. This seasonal change in runoff is also consistent with previous studies (Chiew et al., 2009; Vaze and Teng, 2011; Eisner et al., 2017). Moreover, median estimates show that seasonal soil moisture content is predicted to decrease significantly in spring and winter. The projected decrease in runoff and soil moisture in winter will threaten surface water supplies and have adverse implications for agriculture (Gardner, 2009), which has significant implication for land and water resource management in the future.

Changes in regional temperature and rainfall expected to occur as a result of future climate change may have significant impacts on different components of a catchment water budget

(Nash and Gleick, 1991). Thus, changes in runoff are largely related to variations in rainfall (Reshmidevi et al., 2018). In addition, changes in temperature are likely to have impacts on runoff production through increasing evapotranspiration from soil and vegetation (Wang et al., 2016). Our results suggested that runoff changes are more sensitive to changes in rainfall than changes to temperature (Table 4-3) and this agrees with previous studies (Chiew et al., 1995). A case in point is that Chiew and Mcmahon (2002) carried out climate change impacts modelling on 28 unimpaired Australian catchments and found that the impact on runoff was much more dependent on rainfall than temperature. Rainfall elasticity is a simple estimate of the sensitivity of runoff to changes in rainfall, and is particularly useful as an initial estimate of climate change impacts on runoff (Chiew, 2006). Thus, it should be noted from Table 4-3 (coefficient "c" for annual runoff is 2.08) that the percentage change in average annual rainfall is generally amplified two fold in average annual runoff change, which is also in commonly observed in previous research (Sankarasubramanian et al., 2001; Chiew, 2006). For example, Jones et al. (2006) estimated the sensitivity of mean annual runoff to climate change using 3 models across 22 Australian catchments and results show mean sensitivities of 2.4%, 2.5% and 2.1% change in mean annual flow for every 1% change in mean annual rainfall, respectively. In addition, Table 4-3 shows that the lowest seasonal rainfall elasticity of runoff was observed in spring, and this may be because of the largest ET/P (Evapotranspiration/Rainfall) ratio occurring in spring (Table 4-2), which means spring is a relatively dry season in this catchment, and the increase in rainfall is mainly used to evaporate and replenish soil moisture content (Table 4-3 shows that the highest value of coefficient "c" for seasonal actual evapotranspiration and soil moisture occurs in spring).

In addition to runoff, variation in modelled actual evapotranspiration and modelled soil moisture content were also both largely dominated by variation in rainfall and have a weaker correlation with changes in temperature at annual and seasonal scales (Table 4-3). Therefore, there was a good correlation between the major components of the water budget and rainfall, reflecting the fact that rainfall is the ultimate source of water for the land surface water budget (Fekete et al., 2004). However, the effect of variation in rainfall on actual evapotranspiration is much smaller than its effect on runoff, in agreement with previous findings (Chiew and Mcmahon, 2002).

Assessments of the impacts of climate change on catchment water budgets are affected by the uncertainties in the GCMs, downscaling methods and GHG emission scenarios, as well as the uncertainty in the hydrologic model itself. This study used an ensemble of 28 GCMs to reduce uncertainties arising from the choice of a single GCM. However, we only used one hydrological model to simulate water resource availability, and therefore this may contribute

some uncertainty because of the choice of model parameters and model structure (Eum et al., 2016). Jiang et al. (2007) applied six, monthly water balance models and found large differences in predicted runoff, actual evapotranspiration and soil moisture content among models. Consequently, using an ensemble of hydrological models, a larger array of climate projections, different downscaling methods and various bias correction algorithms, is recommended to provide a full range and probability of future hydrologic simulations (Teutschbein and Seibert, 2012; Eum et al., 2016). In addition, the present study was focused on the Manning River catchment, which although deemed to be representative of such catchments, lacks replication at the catchment-scale. Consequently, more catchments will be selected in a following study to represent the large range of climate, physical and flow characteristics throughout Australia, and to provide insights for future water management.

4.5 Summary and conclusions

This study analysed the hydrologic sensitivity of the Manning River catchment under projected climate change scenarios using the XAJ hydrological model driven by statistically downscaled climate data from 28 GCMs. For the XAJ model calibration and validation periods, the daily NSE were 0.89 and 0.93, and daily R^2 were 0.93 and 0.93, respectively, with monthly NSE $\geq$ 0.92 and monthly $R^2 \geq$ 0.94. Therefore, the XAJ model performed satisfactorily in this catchment (NSE and R^2 were much larger than 0.50). This study explored the impacts of climate change on the water balance of the Manning River catchment for 2040s and 2080s. Runoff, actual evapotranspiration and soil moisture content were all largely dominated by rainfall at annual and seasonal time-scales. Maximum temperature was predicted to increase 1.4°C (1.2-1.5°C) and 3.2°C (2.7-3.5°C) in 2040s and 2080s, while minimum temperature was predicted to increase 1.5°C (1.3-1.7°C) and 3.5°C (3.1-4.1°C) in 2040s and 2080s, respectively, as estimated from the median of the 28 GCMs. At an annual time-scale, rainfall, runoff, actual evapotranspiration and soil moisture content were projected to change -0.3% (-5.2~4.2%) and 4.6% (-9.5~10.8%), -2.3% (-10.6~8.9%) and 7.7% (-17.2~22.0%), 0.6% (-3.0~3.7%) and 1.8% (-4.3~8.6%), and -4.4% (-8.8~0.2%) and -5.1% (-15.5~-1.6%) in 2040s and 2080s, respectively. Variations at monthly and seasonal time-scales were also analyzed. With the trend of increasing values in high rainfall and runoff, and the trend of decreasing values in low rainfall and runoff estimated from the ensemble of the 28 GCMs, a larger degree of inter-seasonal variation in the Manning River catchment are likely to be generated in the future. In addition, reductions in winter runoff and spring and winter soil moisture content in the future are likely to aggravate future water stress for crop growth and productivity (Elmahdi, 2015). These results can potentially contribute to the development of adaptive strategies and future policy options for the sustainable management of water resources in eastern Australia. The research methods used

in the Manning River catchment of eastern Australia can be further extended to any other catchments and we expect our study provides helpful reference for climate change impact assessments on water resource management in similar areas.

Chapter 5. Using an improved SWAT model to simulate hydrological responses to land use change: a case study of a catchment in tropical Australia

This chapter is based on the following manuscript:

Zhang, H., Wang, B., Li Liu, D., Zhang, M., Leslie, L. M., & Yu, Q. (2020). Using an improved SWAT model to simulate hydrological responses to land use change: a case study of a catchment in tropical Australia. Journal of Hydrology, 124822.

Highlights:

1. Hydrologic impacts of LUCC assessed in tropical Australia using SWAT-T model;

2. SWAT-T performed better for both LAI and streamflow than default SWAT;

3. Urbanization increased surface runoff and decreased lateral runoff and groundwater;

4. Afforestation decreased surface runoff and increased evapotranspiration.

Abstract

Land use change is one of the dominant driving factors of watershed hydrological change. Thus, hydrological responses to land use changes require detailed assessments to ensure sustainable management of both water resources and natural ecosystems. The Soil and Water Assessment Tool (SWAT) model has been widely used to simulate the impacts of land use change on water balance. However, the original SWAT model has poor performance in estimating the leaf area index (LAI) of different vegetation types for tropical areas. The objective of this study was to simulate the impact of different land use change scenarios (deforestation, afforestation and urbanization) on the water balance, using an improved SWAT model with vegetation growth calibrated from MODIS LAI data. The North Johnstone River catchment in wet tropical eastern Australia was selected as the case study area. Results showed that the modified SWAT model was able to reproduce smoothed MODIS LAI with NSE ≥ 0.59 (NSE < 0 for default SWAT), $R^2 \geq 0.70$ ($R^2 \leq 0.66$ for default SWAT), and $|PBIAS| \leq 2.5\%$ ($|PBIAS| \geq 42\%$ for default SWAT), and to predict monthly streamflow well with NSE ≥ 0.92 (NSE ≥ 0.90 for default SWAT), $R^2 \geq 0.94$ ($R^2 \geq 0.90$ for default SWAT). It is noted that SWAT-T had $|PBIAS| \leq 10\%$ while $|PBIAS| \leq 5\%$ for default SWAT. Land use change impacted all hydrological variables, with the impact on surface runoff being the most notable at yearly scale (8.9%, 5.7%, -9.5% and 15.9% for scenario 1, 2, 3 and 4, respectively). Absolute changes of surface runoff under land use change scenarios differed across months, with the most notable absolute change occurring during the wet season (December to May) (1.2 ~

6.6mm, 1.0 ~ 3.5mm, -7.3 ~ -1.1mm and 3.0 ~ 9.0mm for scenario 1, 2, 3 and 4, respectively). Urbanization increased surface runoff (5.7% and 15.9% for scenario 2 and 4, respectively) and decreased lateral runoff (-0.7% and -1.3%) and groundwater (-0.9% and -3.5%), but produced no clear change in total runoff (0.2% and 0.2%), actual evapotranspiration (-0.3% and -0.3%), and soil water (0.5% and 0.7%) at the annual time scale. Furthermore, afforestation could decrease surface runoff (-9.5% for scenario 3) and soil water (-2.0%), increase evapotranspiration (1.7%), and lead to slight changes (absolute values $\leq$ 0.8%) in other hydrological variables at the annual time scale. A strong positive correlation ($r \geq 0.94$) was observed between annual rainfall and total runoff for forest-evergreen, range-grasses, and urban land use. Forest-evergreen generally produced less total runoff than range-grasses and urban land use under conditions of the same rainfall, terrain slope, and soil texture. In addition, urban land use generally produced more surface runoff and less lateral runoff and groundwater than forest-evergreen and range-grasses under the same conditions. These results contribute important information for development of effective adaptation strategies and future policy plans for sustainable water management in tropical eastern Australia.

Key words: MODIS LAI; land use change; SWAT-T model; tropical eastern Australia; runoff

5.1 Introduction

Urbanization, agricultural development, deforestation, and other human activities lead to spatial and temporal changes in land use/land cover, that can affect water flow pathways and the water balance (Welde and Gebremariam, 2017). Land use/cover change (LUCC) plays an important role in earth-atmosphere interactions and biodiversity loss and is a major factor influencing sustainable development (Turner et al., 1995). LUCC can directly affect global carbon budgets, biodiversity, and ecosystem function (Aide et al., 2013). Many regions worldwide have experienced massive LUCC over recent decades (Schirpke et al., 2012). Although the net decrease of natural forest area was slowing down globally in the period from 2000 to 2010 (Meyfroidt and Lambin, 2011), deforestation remains one of the major processes of LUCC, with multiple implications for global environmental change (Lambin and Geist, 2008). For example, a large amount of natural land in China, including wetlands and forests, has been developed into arable land and human settlements due to rapid urbanization over the past two decades (Song and Ding, 2009; Yu et al., 2011). Extensive deforestation occurred in Latin America and the Caribbean during the first decade of the 21st century, but extensive areas also recovered woody vegetation (>360,000 km^2) across the region (Aide et al., 2013). About 30% of total forest land is under pressure from rapid LUCC in Northeast India, which is one of the recognized global biodiversity hotspots (Lele and Joshi, 2009).

Since 1990, Australia's plantation area has increased by around 700,000 hectares (Parsons et al., 2007). The extensive LUCC in Australia along with agricultural development has induced an instability in the water cycle, leading to increased land and water salinization over massive areas (Zhang et al., 2001). In the study of hydrological responses to LUCC, forest hydrological effects have attracted much attention, especially the impacts of afforestation and deforestation. Most results have shown that catchment runoff decreased significantly after afforestation and increased obviously after deforestation (Li et al., 2012). For example, Crosbie et al. (2007) concluded that runoff was significantly reduced in five years after the land use of annual cropping and pastures changed to tree belts with perennial pastures in a small agricultural catchment in central NSW, Australia. Chen and Yu (2015) assessed likely impacts of two LUCC scenarios in southeast Queensland and found that extreme LUCC would significantly affect flooding in rural catchments, but not in urbanized catchments. The importance of water in both nature and society emphasizes the necessity for greater understanding how LUCC could influence regional streamflow regimes.

There are three main methods used to quantitatively analyze the impacts of LUCC on hydrology and water resources: 1) the "paired-catchment" experimental method (Bosch and Hewlett, 1982), 2) the time series analysis method (Li et al., 2012), and 3) the hydrological model method (Mwangi et al., 2016). In the "paired-catchment" experimental method, two catchments with similar areas, shapes, climate, vegetation, and soil are selected and observed. Generally, the first 3-5 years (preferably including a wet year, a normal year, and a dry year) are the control period with no experimental measures. After that, the land use/cover of one of the catchments will be artificially changed, while other conditions remain the same. The other catchment remains in the original state, and is referred to as the "reference catchment". After an observation period, the runoff in the two experimental catchments is compared and analyzed, and the impacts of LUCC on water quantity are quantitatively analyzed. The "paired-catchment" experimental method is generally considered to be the best way to compensate for climate variability in small catchments, but the method is difficult to apply to catchments (other than small ones) as finding two similar medium or large catchments is difficult. Also, even similar catchments may change significantly at different stages (Li et al., 2009b). The second method, the time series analysis method, can be used to analyze the changing trend of hydrologic and climatic data, but the spatial heterogeneity of a catchment and the mechanisms of LUCC and climate change on the water cycle cannot be determined. Since the 1970s, with the development of computer science, geographic information systems and remote sensing technologies, hydrological models have been more widely used to determine LUCC impacts in water cycle studies. Hydrological models provide a framework for conceptualizing and studying the relationships among climate change, land use change, and the water cycle. Among these models,

distributed hydrological models have significant applications because they directly relate model parameters to characteristics of the earth's surface (Legesse et al., 2003). Therefore, determining how to construct a distributed hydrological model to study the hydrological response to LUCC is a question that must be researched in depth.

SWAT (Soil and Water Assessment Tool) is a semi-distributed and physically based watershed-scale hydrological model developed by Arnold et al. (1998) at the USDA-ARS. It simulates long-term hydrological variables (e.g., streamflow) at a daily time scale (Brown et al., 2015). SWAT is considered to be one of the most appropriate models for assessing hydrological responses (water, sediment, and nutrient loss) to land use change in watersheds with different land use, soils, and management conditions (Arnold and Fohrer, 2005). In general, managing vegetation growth is necessary in distributed hydrological models because evapotranspiration is an important component of the water cycle (Abbaspour et al., 2015). A simple plant growth model is used in SWAT to simulate growth and yield of all kinds of vegetation (Abbaspour et al., 2015). The plant growth model in SWAT was developed for temperate areas and is not suitable for monsoon-driven or tropical regions (Wagner et al., 2011). For instance, the day length-driven dormancy used in temperate areas to separate annual plant cycles is not consistent with plant growth in the tropics. Therefore, the model's suitability to simulate plant growth has not been reflected critically in most SWAT research for tropical areas, possibly because model calibration and validation are normally based on streamflow and/or water quality outputs (Strauch and Volk, 2013). However, successfully reproducing these outputs does not imply a correct simulation of the internal hydrological processes in a catchment (Strauch and Volk, 2013). Therefore, a few studies have been conducted to improve the plant growth model in SWAT globally including tropical areas (Strauch and Volk, 2013; Alemayehu et al., 2017; Guo et al., 2019; Ma et al., 2019). For instance, Strauch and Volk (2013) presented an alternative approach to automatically trigger new growing seasons during the transition from dry to wet season based on changes in soil moisture for tropical areas. Meanwhile, a general improvement (independent of whether or not the area is in tropics) has been implemented with the LAI decline rate modified to a logistic function which provides a sigmoidal decrease toward the minimum LAI. Their results showed that the modified plant growth model could reasonably represent seasonal dynamics of the LAI, and the modified model should be useful for large parts of the model community. Alemayehu et al. (2017) modified the SWAT model for the tropics using a straightforward but robust soil moisture index (a quotient of rainfall and reference evapotranspiration) to trigger a new growth cycle within a predefined period, and results indicated that this index was reliable for triggering a new annual growth cycle. In addition, Ma et al. (2019) integrated downscaled high quality MODIS LAI into modified SWAT plant growth model and reported a high accuracy in the validation of

streamflow in the subtropics. However, to the best of our knowledge, the SWAT model with an improved plant growth model has never before been applied to tropical regions of Australia. Consequently, we selected a catchment representative of the tropics in Australia to explore and assess the performance of the modified SWAT (SWAT-T) model, as improved by Strauch and Volk (2013).

The aim is to evaluate the performance of SWAT-T and to assess hydrological responses to land use/cover change in wet tropical Australia. We selected the North Johnstone River catchment as a case study. The specific objectives of this study were to: (1) evaluate the performance of the SWAT-T and default SWAT model for simulating leaf area index (LAI) and streamflow of the North Johnstone River catchment; (2) using both models (SWAT-T and default SWAT) to forecast changes in simulated surface runoff, lateral runoff, groundwater, total runoff, actual evapotranspiration, and soil water under different land use change scenarios; and (3) identify rainfall-runoff relationships of different land covers to explain water availability changes caused by land use/cover change.

5.2 Materials and methods

5.2.1 Study area

The North Johnstone River catchment (Figure 5-1) is situated in the wet tropics of North Queensland. The catchment area is about 924 km^2 with elevation ranging from 18 m to 1370 m. In this catchment, the mean annual temperature is about 21.4°C, mean annual rainfall is approximately 2740 mm and mean annual runoff is about 1995 mm (averaged from 1967 to 2017). Rainfall is affected by monsoons and tropical cyclones/lows/depressions and is strongly seasonal with 78% of the total annual rainfall occurring during the wet season from December to May (Figure 5-2). The catchment also receives regular rainfall throughout the year in contrast to dry tropical areas. The Johnstone River catchment is divided into three distinct regions: the upper (tablelands or hinterland), the central (the Range or World Heritage), and the lower (coastal or floodplain) regions. The two key tributaries that discharge into the Great Barrier Reef lagoon are the North Johnstone and South Johnstone Rivers. The other major streams are the Moresby River, Liverpool Creek, and Maria Creek. These three streams are lowland waterways, whereas the North and South Johnstone Rivers begin in the upland "mixed land use" tablelands. Agriculture, residential, and industrial developments (including roads) can have important impacts on the way water flows through the landscape (https://wetlandinfo.des.qld.gov.au/wetlands/facts-maps/sub-basin-north-johnstone-river/). Thus, understanding how land use/cover changes influence regional streamflow regimes is essential for deciding how best to manage the catchment and to protect its resources.
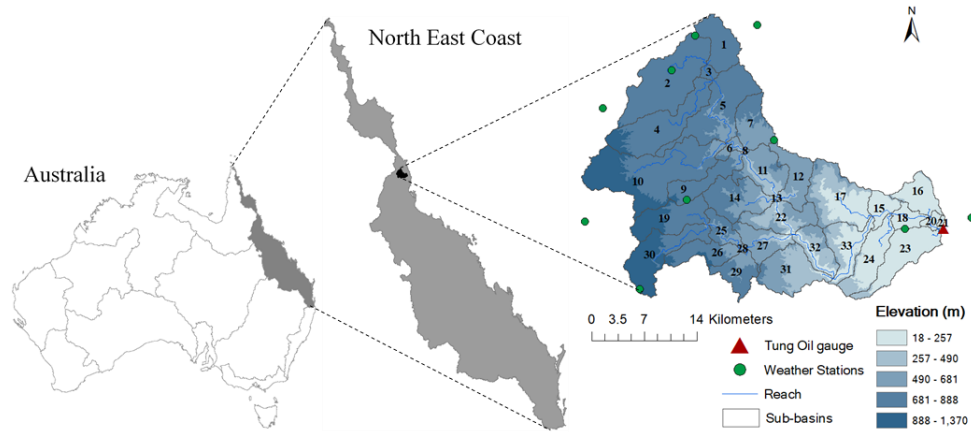
Figure 5-1 The location of the North Johnstone River catchment, Queensland, Australia (divided into 33 sub-basins by the SWAT model), and 11 observation stations (10 weather stations and one hydrologic gauge station (Tung Oil gauge)).
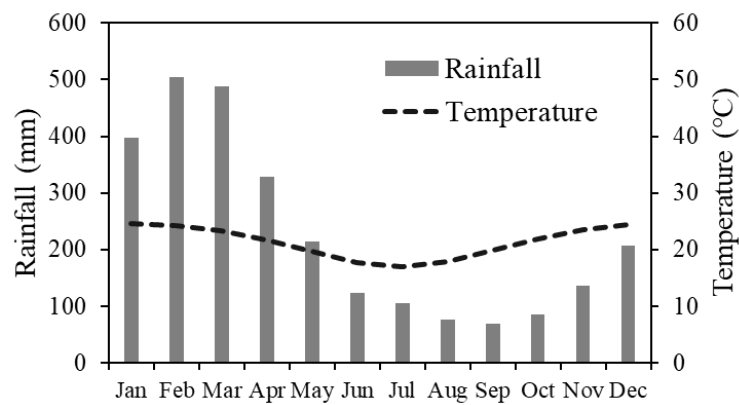
Figure 5-2 Mean monthly rainfall and temperature (1967–2017, average over 10 weather stations shown in Figure 5-1) weighted by catchment area using the Thiessen polygon method.

5.2.2 The SWAT model

The SWAT hydrological model (SWAT 2012) is used to represent the main hydrological processes within the catchment. SWAT is a process-based and semi-distributed hydrological model that simulates the major water balance components continuously at a daily time step (Arnold et al., 1998). SWAT can simulate watershed hydrological characteristics under different land use and climate conditions, making it a widely used hydrology-related tool for land use and climate change research (Li et al., 2011; Shrestha et al., 2017; Reshmidevi et al., 2018). However, examples from tropical Australia are limited with most studies concentrated in the eastern and southeastern part of the country (Saha and Zeleke, 2015). The model was selected based on considerations such as its ability to represent the physical processes related to water movement, support documentation, and additional software (SWAT-CUP, SWAT Calibration and Uncertainty Programs) for model calibration and validation. The Hargreaves

method available in the SWAT interface was used to calculate potential evapotranspiration (Reshmidevi et al., 2018) using air temperature as input data (Brown et al., 2015). In this study, surface runoff and infiltration is computed with daily rainfall using the Soil Conservation Service (SCS) Curve Number (CN) method (USDA, 1972). Further model details can be found in Neitsch et al. (2011).

However, the original SWAT model performs poorly in estimating LAI of different vegetation types for tropical areas, thus, an improved SWAT model (SWAT-T) (Strauch and Volk, 2013) was used in this study. This approach used simulated plant available water in the upper soil layers as a trigger for a new growing cycle. In the SWAT-T model, two new parameters $TRAMO_1$ and $TRAMO_2$ were implemented to define the first and the last month of a region-specific 'transition period' from dry to wet season. In this study, based on the MODIS LAI, the default values of $TRAMO_1$ and $TRAMO_2$ were set to 7 (July) and 8 (August) in the sub-basin input files, respectively. In addition, for this SWAT-T model, a logistic function that provides a sigmoidal decrease towards the minimum LAI was used to modify the LAI decline rate. Further model details can be found in Strauch and Volk (2013). According to the user's manual from Strauch and Volk (2013), no management settings in the operations schedule were defined for the SWAT-T model in this study. Furthermore, the SWAT-T model was calibrated and validated only against streamflow. The model simulations were not calibrated and validated with actual evapotranspiration and soil water content due to a lack of field data for these variables. The absolute values of actual evapotranspiration and soil water content should therefore not be used directly. However, comparing the relative changes in the simulations is still reasonable and valuable because the hydrological model mimics the actual water cycle.

5.2.3 Data preparation

Multiple data sets are required in SWAT as input to develop a semi-distributed model using the ArcSWAT interface. This section describes the processing of the respective data. The data for SWAT model development, data sources, and relevant characteristics are listed in Table 5-1.

Table 5-1 Data used in this study, data sources, and relevant characteristics.

Data	Source	Relevant Characteristics
Digital elevation model (DEM)	Geoscience Australia	1 second SRTM Derived DEM
Land use/land cover map	NASA LP DAAC at the USGS EROS Center	500 m spatial resolution
Soil map	Bureau of rural sciences, Australia	The maps were published at a scale of 1:2,000,000
Observed streamflow	Australian Government Bureau of Meteorology	Average daily discharge (1967–2017)

Observed meteorological data	Bureau of meteorology, Australia	Maximum and minimum daily temperature and rainfall (1967–2017)
Leaf area index	MODIS LAI products MCD15A3H V6	500 m spatial resolution, 4-day composites (2003–2017)

5.2.3.1 Digital elevation model (DEM), land use, and soil data

SWAT primarily relies upon defined hydrologic response units (HRUs) that are based on land use maps, soil maps, and slope characteristics (Pignotti et al., 2017). In this study, five slope classes (i.e., 0-10%, 10-20%, 20-30%, 30-50%, and greater than 50%) were defined for slope discretization and 778 HRUs were produced using a multiple HRU generation method with land use, soil, and slope input (thresholds of 2%-2%-2%) using the SWAT interface. The details of DEM, land use, and soil data used in this study are given below.

DEM data are required in SWAT for watershed and river network delineation, and sub-basin generation. In this study, 33 sub-basins were generated (Figure 5-1). From DEM, sub-basin parameters (e.g., slope gradient and slope length of the terrain) and river network characteristics (e.g., channel length, width, and slope) were obtained. A 1-second resolution Shuttle Rader Topography Mission (SRTM) derived DEM from Geoscience Australia (https://elevation.fsdf.org.au/) was used in this study. DEM was masked for SWAT model development in the North Johnstone River catchment (Figure 5-1).

The land use data developed by NASA LP DAAC at the USGS EROS Center with 500 m spatial resolution (https://lpdaac.usgs.gov/products/mcd12q1v006/) was used and reclassified to match the SWAT land use classes for HRU delineation in the SWAT model (Figure 5-3a). There were eight land use classes in this catchment (Figure 5-3a): forest-evergreen (FRSE), forest-mixed (FRST), forest-deciduous (FRSD), range-brush (RNGB), range-grasses (RNGE), wetlands (WETL), agricultural land-generic (AGRL), and urban (URBN).

A soil map and a database table of soil characteristics (e.g., soil hydrologic group, maximum rooting depth of the soil profile, moist bulk density, etc.) for different soil layers are required by the SWAT model (Saha et al., 2014). We clipped the soil map for the North Johnstone River catchment from the Digital Atlas of Australian Soil (Figure 5-3b). Based on the available references and lookup tables (McKenzie et al., 2000; Western and McKenzie, 2004; Saha et al., 2014), we created a ''usersoil'' database table to delineate HRU in SWAT for the North Johnstone River catchment.
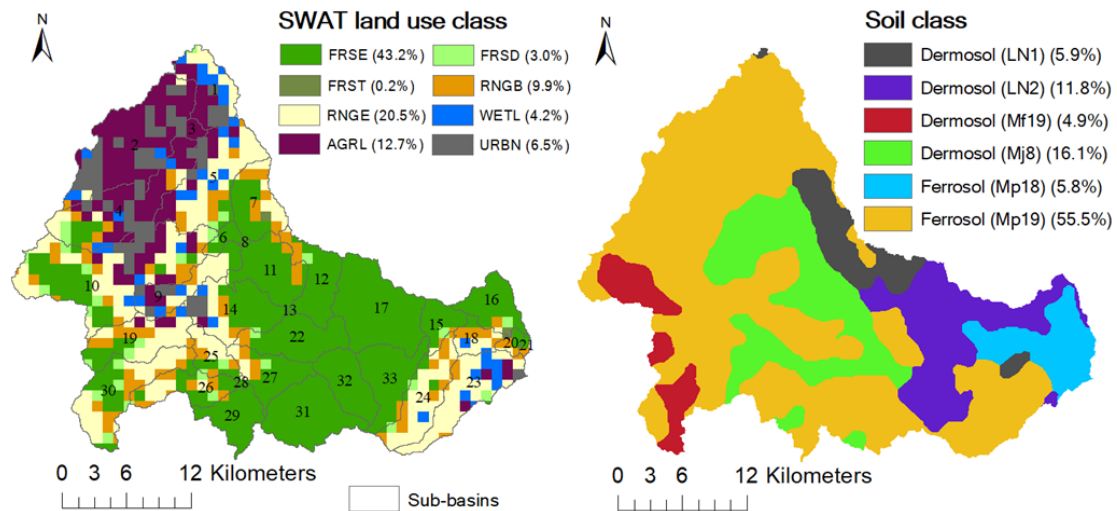
Figure 5-3 The land use classification map (a) and soil map (b) for the North Johnstone River catchment, Queensland, Australia.

5.2.3.2 Climate data and river discharge

Daily maximum temperature, minimum temperature, and rainfall from 1967 to 2017 at 10 climate stations (Figure 5-1) within or near the catchment were collected from the Australian Government Bureau of Meteorology (BOM) website (http://www.bom.gov.au/climate/data/). These climate data were used for driving SWAT model simulations. According to the default setting in SWAT, one climate station was assigned to each sub-basin which was closest to sub-basin's centroid (Sirisena et al., 2018). For streamflow calibration and validation, daily observed discharge at the Tung Oil gauge (Figure 5-1) also were collected from the Australian Government BOM website (http://www.bom.gov.au/waterdata/). For streamflow calibration, a calibration period that includes wet, normal and dry years was selected so that the model parameters were set for a wide range of climate conditions and also for the validation period. Accordingly, daily observed streamflow data for the periods of 2008-2017 (2005-2007 as warm-up) and 2003-2007 (2000-2002 as warm-up) were used for streamflow calibration and validation, respectively, whereas daily observed climatic and hydrological data for the 1967-2017 period were used to assess land use change impacts on water availability with the calibrated SWAT-T model. To be consistent with the calibration and validation periods for streamflow, the same periods were used for LAI calibration and validation.

5.2.3.3 Leaf area index

It was found that the default SWAT model could not well reflect the dynamics of LAI. Therefore, SWAT-simulated LAI was calibrated to MODIS-derived, four-day LAI composites using the SWAT-T model (Strauch and Volk, 2013) for tropical plant growth. This SWAT-T model has been shown to improve the representation of shifts between plant dormancy and

growth in tropics by using soil moisture, rather than day-length, to represent crucial phenological thresholds (Strauch and Volk, 2013). A 4-day composite MCD15A3H V6 LAI dataset with 500 m pixel size was used in this study. For each of the land cover classes, 4-day median LAI time series were extracted from 2003 to 2017 using methods according to previous studies (Strauch and Volk, 2013; Alemayehu et al., 2017). In addition, the BFAST method (Verbesselt et al., 2010) was used to smooth the 4-day raw-median LAI time series for different land use covers (see Figure 5-4) (Hoyos et al., 2019). Since LAI was HRU-related outputs, we derived the area-weighted HRU mean for comparison with the smoothed median MODIS LAI (Strauch and Volk, 2013) and calibrated the LAI parameters manually. Additionally, we aggregated daily simulated LAI to 4-day scale to calibrate LAI parameters using a trial-and-error process such that the SWAT-T simulated 4-day LAI mimicked the MODIS 4-day LAI. According to the smoothed LAI data (Figure 5-4), AGRL and WETL had maximum LAI values (~2.4) in March, and minimum values (1.8 and 1.9) in July and August, respectively. FRSE and FRSD peaked in October (6.0 and 5.3) and February (5.3 and 5.1) and reached minimum values (3.7 and 4.0) in June. RNGB and RNGE had maximum LAI values (3.5 and 2.4) in February and reached minimum values (2.9 and 2.0) in July. The high values of smoothed LAI were generally observed during the wet season (December to May) (Figure 5-4), which indicated consistency in the smoothed LAI time series. Thus, the plant growth module in the SWAT-T model was calibrated and validated using the smoothed LAI time series (Alemayehu et al., 2017).
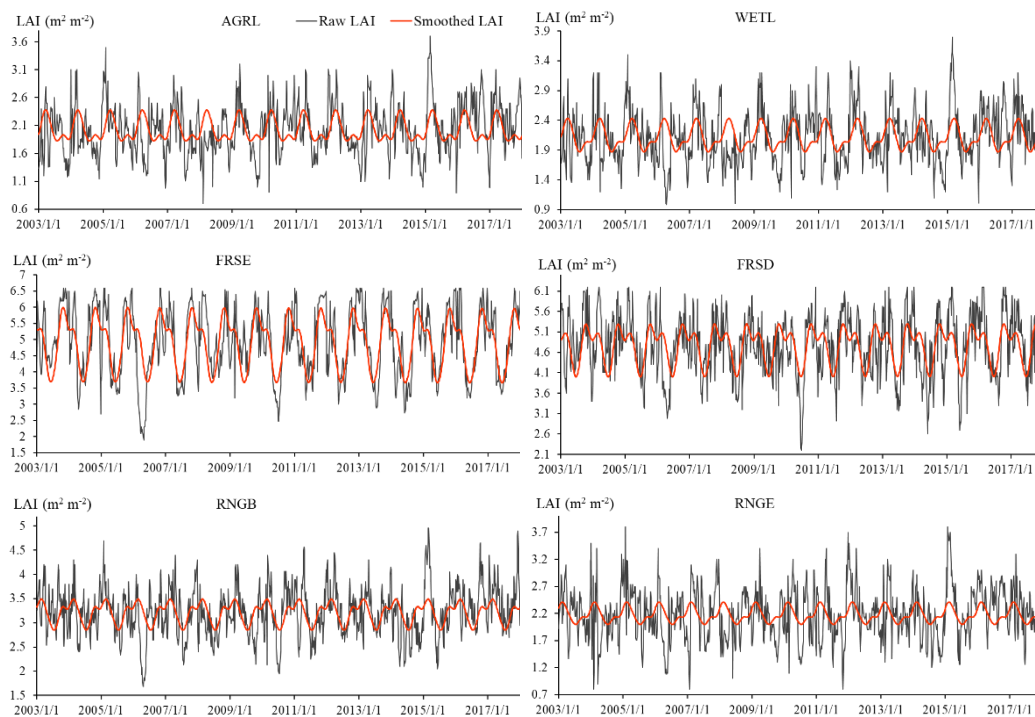
Figure 5-4 The 4-day raw-median LAI and BFAST-smoothed LAI time series for the land use classes of agricultural land-generic (AGRL), wetlands (WETL), forest-evergreen (FRSE), forest-deciduous (FRSD), range-brush (RNGB), and range-grasses (RNGE).

5.2.4 Model calibration and evaluation approach

SWAT Calibration and Uncertainty Programs (SWAT-CUP), a standalone computer program developed for calibration, validation, and uncertainty analysis of SWAT, was used to optimize SWAT model parameters (Abbaspour, 2013). SWAT-CUP links five different calibration procedures, which are Sequential Uncertainty Fitting Ver. 2 (SUFI-2) (Abbaspour et al., 2007), Generalized Likelihood Uncertainty Estimation (GLUE) (Beven and Binley, 1992), Particle Swarm Optimization (PSO) (Zhang et al., 2015), Parameter Solution (ParaSol) (Van Griensven and Bauwens, 2003), and Markov Chain Monte Carlo (MCMC) (Marshall et al., 2004). The program SUFI-2 was selected in this study for SWAT-T calibration, validation, and uncertainty analysis because it was found to be quite efficient for time-consuming large-scale models (Yang et al., 2008). Two types of sensitivity analysis methods are allowed in the SUFI-2 program: global sensitivity method and one-at-a-time sensitivity analysis method (Abbaspour, 2013). The global sensitivity analysis method was used to rank the sensitivity of 22 parameters in SWAT-T. In this sensitivity analysis method, the smaller the p-value and the larger the absolute value of t-stat, the more sensitive the parameter is (Abbaspour, 2013).

Uncertainty in SUFI-2 parameters, conveyed as ranges (uniform distributions), accounts for total sources of uncertainties like uncertainty in driving variables (e.g. rainfall), observed data, conceptual models, and parameters (Abbaspour, 2013). Propagation of the parameter uncertainties results in uncertainties in the SWAT model output variables, which are manifested as the 95% probability distributions (Abbaspour, 2013). These are computed at 2.5% and 97.5% levels of the cumulative distribution of model output variables produced by the propagation of the uncertainties in parameters using Latin hypercube sampling (Abbaspour, 2013). This is called the 95% prediction uncertainty (i.e., 95PPU). Two statistics ''P-factor'' and ''R-factor'' were created to quantify the fit between simulation results (95PPU) and observation data with its error (Abbaspour et al., 2015). The P-factor is the proportion of observed data enveloped by the simulation results, the 95PPU, while the R-factor is the breadth of the 95PPU envelope.

Monthly observed and simulated discharge for the period of 2008-2017 and 2003-2007 were used for SWAT-T calibration and validation, respectively. The results for water balance components all were presented at a monthly or annual time step. Therefore, calibrating discharge at a monthly time step rather than daily time step makes the calculation process faster and more efficient. Monthly streamflow was calibrated with SUFI-2 using 500 simulations per iteration (4 iterations) by maximizing the value of Nash-Sutcliffe Efficiency (NSE) (Nash and

Sutcliffe, 1970). In this study, we followed Shi et al. (2011) by using NSE, percent bias (PBIAS), and coefficient of determination (R^2) as statistical evaluation criteria. NSE is one of the most commonly used standards for comparing simulations of hydrological models with observed data (Le and Pricope, 2017). NSE values vary from $-\infty$ to 1 with a value of 1 indicates that the model-simulated results and observed data are perfectly matched, hence, the closer the NSE is to 1, the better performance the SWAT model will have. PBIAS evaluates the average trend of the model simulations to be greater or less than their observed counterparts. A positive value of PBIAS demonstrates an overestimation bias while a negative value indicates an underestimation (Shi et al., 2011). Therefore, the smaller the absolute value of PBIAS, the better. NSE, PBIAS, and R^2 were calculated as follows:

$$PBIAS = 100(\frac{\sum_{i=1}^{N}(Q_{sim,i} - Q_{obs,i})}{\sum_{i=1}^{N}(Q_{obs,i})}) \tag{1}$$

$$NSE = 1 - \frac{\sum_{i=1}^{N}(Q_{obs,i} - Q_{sim,i})^2}{\sum_{i=1}^{N}(Q_{obs,i} - \bar{Q}_{obs})^2} \tag{2}$$

$$R^2 = \frac{[\sum_{i=1}^{N}(Q_{obs,i} - \bar{Q}_{obs})(Q_{sim,i} - \bar{Q}_{sim})]^2}{\sum_{i=1}^{N}(Q_{obs,i} - \bar{Q}_{obs})^2 \sum_{i=1}^{N}(Q_{sim,i} - \bar{Q}_{sim})^2} \tag{3}$$

where Q_{obs} and Q_{sim} are the observed and SWAT-T model-simulated monthly streamflow (m³/s), respectively; $\bar{Q}_{obs}$ and $\bar{Q}_{sim}$ are the mean observed and SWAT-T model-simulated monthly streamflow (m³/s), respectively; *N* is the number of samples, and *i* is the *ith* sample.

5.2.5 Different land use scenarios

The most common land cover classes of the North Johnstone River catchment were FRSE (forest-evergreen) and RNGE (range-grasses), which accounted for around 63.7% of the total region. To evaluate the hydrological response to land use changes in the catchment, four scenarios (Table 5-2) were considered. These changes were achieved by using the Land Use Update tool in the ArcSWAT interface at the sub-basin scale (Marhaento et al., 2017). For instance, FRSE can be considered to be replaced by RNGE only if both land use types exist in the same sub-basin (Shrestha et al., 2017). Therefore, these partial conversion scenarios mainly occurred in the northwestern part of the catchment where there is less rainfall distribution compared to the downstream part (the forest part) of the catchment (Figure 5-3). Scenario 1 supposes that all current FRSE will be changed to RNGE while the rest of the land covers will remain unchanged. This means an 11.5% increase in RNGE area over the entire catchment. Scenario 2 supposes that all current FRSE will be converted to URBN, representing a 2.3% increase in URBN area over the entire catchment. Scenario 3 supposes that all current RNGE will be changed to FRSE, representing a 14.1% increase in FRSE area over the entire catchment.

Scenario 4 supposes that all current RNGE will be converted to URBN, representing an 8.4% increase in URBN area over the entire catchment. These four land use change scenarios (i.e. deforestation, deforestation/urbanization, afforestation, and urbanization) were on the basis of present land use conditions and potential future land use plans (residential development) in the North Johnstone River catchment (Wang et al., 2008). The land use change scenarios are shown in Table 5-2 and the percentage areas of the four scenarios are shown in Figure 5-5. FRST was classified as FRSD in Figure 5-5 because of its small area proportion shown in Figure 5-3.

Table 5-2 Land use change scenarios in the North Johnstone River catchment, Queensland, Australia.

Scenario 1	Deforestation	Supposes that all present FRSE will be converted to RNGE, and the rest of land uses remain unchanged, i.e. 11.5% increase in RNGE area
Scenario 2	Urbanization /deforestation	Supposes that all present FRSE will be changed to URBN, and the rest of land uses remain unchanged, i.e. 2.3% increase in URBN area
Scenario 3	Afforestation	Supposes that all present RNGE will be converted to FRSE, and the rest of land uses remain unchanged, i.e. 14.1% increase in FRSE area
Scenario 4	Urbanization	Supposes that all present RNGE will be changed to URBN, and the rest of land uses remain unchanged, i.e. 8.4% increase in URBN area
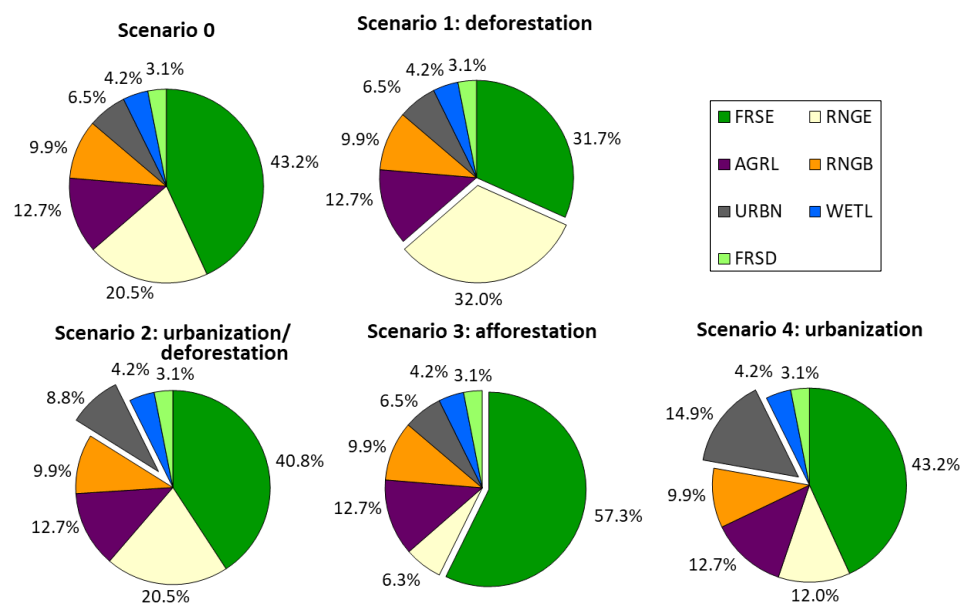
Figure 5-5 Land use proportions for scenario 0 (default land use) and four land use change scenarios in the North Johnstone River catchment, Queensland, Australia. Scenario 1: forest-evergreen (FRSE) to range-grasses (RNGE); scenario 2: forest-evergreen (FRSE) to urban (URBN); scenario 3: range-grasses (RNGE) to forest-evergreen (FRSE); and scenario 4: range-grasses (RNGE) to urban (URBN).

5.3 Results

5.3.1 SWAT-T LAI calibration

Table 5-3 presents the calibrated values for LAI which were adjusted using a manual calibration method. The minimum LAI (ALAI_MIN) for each land use was defined according to long-term MODIS LAI. As suggested by Strauch and Volk (2013), the total number of heat units needed to bring plants to maturity (PHU_PLT) was calculated using the long-term daily mean temperature. The shape coefficients (FRGW1, FRGW2, LAIMX1, LAIMX2, and DLAI) for the LAI curve and the remaining parameters were calibrated by a trial-and-error process to ensure that the LAI simulated by SWAT-T mimicked the smoothed MODIS LAI. The calibrated values and calibration methods for each LAI parameter and each land use are shown in Table 5-3. The LAI parameters of FRST were not calibrated because of the small area proportion in the catchment. Thus, the LAI parameters of FRSD was used for FRST.

Figure 5-6 shows the comparison between 4-day smoothed MODIS LAI with the SWAT-T-simulated LAI using calibrated parameters for the different vegetation types in both the calibration and validation periods. The degree of agreement for MODIS and simulated LAI were assessed both qualitatively (visual comparisons) and quantitatively (statistical evaluations). From a visual comparison, it is clear that the plant growth cycles of the different vegetation types simulated by the SWAT-T model corresponded much better with the MODIS LAI data than the default SWAT results. For instance, the minimum LAI values simulated by the SWAT-T model (1.8, 4.0, 3.7, 2.9, 2.0, and 1.9) were similar to the MODIS LAI (1.8, 4.0, 3.7, 2.9, 2.0, and 1.9) for AGRL, FRSD, FRSE, RNGB, RNGE, and WETL, respectively, while the minimum LAI simulated by the default SWAT was zero for all types of vegetation covers. Figure 5-6 also provides the values of the statistical evaluation indices used to assess the performance of SWAT-T-simulated LAI. For FRSE, which was the dominant land cover in the catchment, the SWAT-T model performed quite well for LAI, with the values of NSE larger than 0.79 during the calibration and validation periods. In contrast, calibration and validation performance for WETL and RNGE was low when the NSE values were larger than 0.59. However, R^2 values were higher than NSE values for all plants types during calibration and validation, ranging from 0.70 to 0.91, and PBIAS values were always within a reasonably small range (±2.5%), indicating overall good model performance.

Table 5-3 Description and calibrated values for LAI parameters of each land use type in the SWAT-T model.

Parameter	Description	Calibrated value[1]					
		AGRL	FRSD	FRSE	RNGB	RNGE	WETL

ALAI_MIN	Minimum leaf area index (m^2/m^2)	1.82*	4.01*	3.68*	2.85*	2.00*	1.87*
BLAI	Maximum potential leaf area index (m^2/m^2)	2.85**	5.30**	6.00**	3.50**	2.45**	2.55**
DLAI	Fraction of PHU when LAI begins to decline	0.72**	0.53**	0.57*	0.75**	0.70**	0.80**
FRGRW1	Fraction of PHU corresponding to the 1st point on the optimal leaf area development curve	0.30**	0.07**	0.10**	0.12**	0.21*	0.28**
FRGRW2	Fraction of PHU corresponding to the 2nd point on the optimal leaf area development curve	0.67**	0.22**	0.29*	0.50**	0.58**	0.70**
LAIMX1	Fraction of BLAI corresponding to the 1st point on the optimal leaf area development curve	0.13*	0.15*	0.14*	0.16*	0.17*	0.20*
LAIMX2	Fraction of BLAI corresponding to the 2nd point on the optimal leaf area development curve	0.88*	0.93*	0.92*	0.94*	0.90*	0.95*
PHU_PLT[2]	Total number of heat units or growing degree days needed to bring plants to maturity	3780	4145	7797	3415	3415	3415
LAI_INIT	Initial leaf area index (m^2/m^2)	1.94	4.90	5.32	3.33	2.30	2.12

[1] *MODIS, **manual adjustment during calibration. [2] Values estimated from local temperature records and default SWAT values for T_BASE (minimum temperature for vegetation growth (°C)).
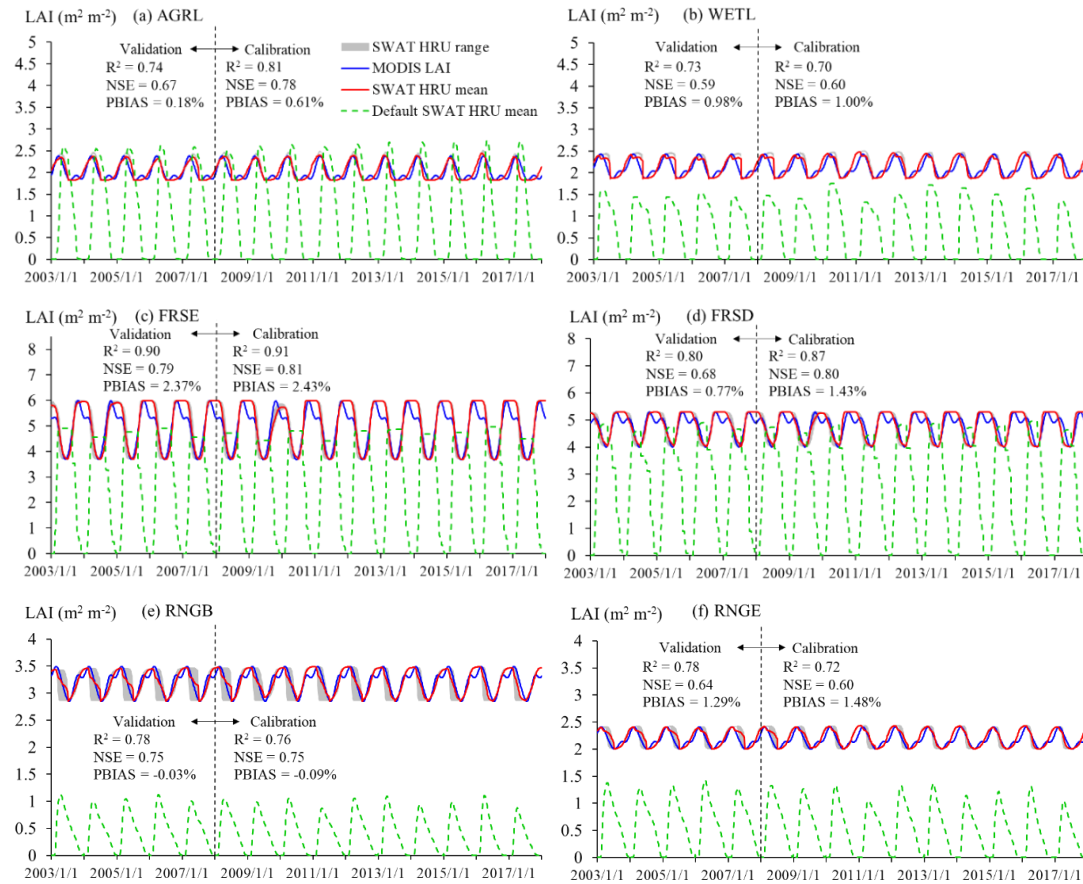
Figure 5-6 SWAT-T HRU mean LAI compared with smoothed MODIS LAI and default SWAT LAI for (a) agricultural land-generic (AGRL), (b) wetlands (WETL), (c) forest-evergreen (FRSE), (d) forest-deciduous (FRSD), (e) range-brush (RNGB), and (f) range-grasses (RNGE) in calibration (1 January 2008 - 31 December 2017) and validation (1 January 2003 - 31 December 2007) periods. Calibrated SWAT results were obtained using the Strauch and Volk (2013) modified plant growth model, while default SWAT LAI values were calculated using the default plant growth algorithm. The gray shadings indicate the boundaries of the 25th and 75th percentages from all HRUs simulated by the SWAT-T model. The vertical dashed lines indicate the termination of the calibration period and the start of the validation period.

5.3.2 Discharge calibration and validation

The 22 parameters were calibrated and ranked for the discharge calibration in the SWAT-T model in the North Johnstone River catchment (Table 5-4). These parameters were ranked according to their sensitivities using the global sensitivity analysis method. The sensitivity analysis in SWAT-CUP suggested that 10 parameters (ranked 1-10, Table 5-4) had significant influence on calibration ($P \leq 0.05$). Groundwater delay (GW_DELAY) was found to be the most sensitive calibration parameter in the North Johnstone River catchment. Figure 5-7 shows

the monthly SWAT-T-simulated streamflow compared with the observed streamflow during calibration and validation periods. Visual comparison showed the simulated hydrograph reproduced the observations reasonably well and closely replicated the temporal variation. Figure 5-8 shows that monthly observed runoff and the SWAT-T-simulated runoff were highly correlated ($R^2 \geq 0.94$, NSE ≥ 0.92, and |PBIAS| $\leq 10\%$) with slopes within 15% of the 1:1 regression during the calibration and validation periods in the North Johnstone River catchment. Furthermore, a comparison of SWAT-T and the default SWAT model was shown in Table 5-5 and results showed that SWAT-T simulated streamflow process better than default SWAT with larger R^2 (0.94 > 0.92 and 0.94 > 0.90) and NSE (0.93 > 0.91 and 0.92 > 0.90) in calibration and validation period, respectively. However, compared to SWAT-T, the default SWAT model produced smaller absolute percent bias (0.9% < 7.3% and 4.9% < 10.0%) in calibration and validation period, respectively.

Table 5-4 The 22 calibrated parameters for the SWAT-T model in the North Johnstone River catchment, Queensland, Australia. The parameters are ranked according to their sensitivities based on global sensitivity analysis.

Ranking	Adjustment and parameter name	Definition	Adjustment range	Calibrated range	Fitted value
1	V__GW_DELAY.gw	Groundwater delay (days)	0 to 300	0 to 100	28.1
2	V__ALPHA_BNK.rte	Baseflow alpha factor for bank storage	0 to 1	0.09 to 0.64	0.28
3	R__HRU_SLP.hru	Average slope steepness	-0.7 to 0.25	-0.61 to -0.19	-0.33
4	R__SOL_AWC(2).sol	Available water capacity of the soil layer	-0.9 to 0.5	-0.8 to -0.4	-0.68
5	R__CN2.mgt	SCS runoff curve number for moisture condition II	-0.25 to 0.25	-0.25 to 0.1	0.05
6	V__RCHRG_DP.gw	Deep aquifer percolation fraction	0 to 0.5	0.01 to 0.06	0.05
7	V__CH_N2.rte	Manning's n value for the main channel	0.014 to 0.15	0.05 to 0.12	0.07
8	V__CH_K2.rte	Effective hydraulic conductivity of main channel	0 to 250	39 to 104	53.9
9	R__SLSUBBSN.hru	Average slope length	-0.5 to 0.25	-0.46 to -0.12	-0.37
10	R__SOL_Z(2).sol	Depth from soil surface to bottom of second soil layer	-0.7 to 0.25	-0.59 to -0.18	-0.33
11	V__GW_REVAP.gw	Groundwater revap coefficient	0.02 to 0.2	0.023 to 0.03	0.023
12	R__CANMX.hru	Maximum canopy storage	-1 to 0.5	-1 to -0.85	-0.93
13	V__GWQMN.gw	Threshold water level in shallow aquifer for base flow (mm)	0 to 2500	61 to 217	206
14	V__ESCO.hru	Soil evaporation compensation factor	0 to 1	0.22 to 0.65	0.48

15	V__CH_N1.sub	Manning's n value for the tributary channels	0.014 to 0.15	0.04 to 0.09	0.05
16	R__SOL_AWC(1).sol	Available water capacity of the soil layer	-0.9 to 0.5	-0.8 to -0.4	-0.77
17	V__EPCO.hru	Plant uptake compensation factor	0 to 1	0.4 to 0.95	0.48
18	V__REVAPMN.gw	Threshold depth of water in the shallow aquifer for revap to occur (mm)	0 to 750	450 to 630	626
19	V__ALPHA_BF.gw	Baseflow alpha factor (days)	0 to 1	0.23 to 0.7	0.54
20	V__SURLAG.bsn	Surface runoff lag time	0.05 to 6	1.5 to 4.5	3.06
21	R__SOL_Z(1).sol	Depth from soil surface to bottom of first soil layer	-0.7 to 0.25	-0.61 to -0.19	-0.22
22	R__OV_N.hru	Manning's n value for overland flow	-0.25 to 0.25	-0.24 to -0.02	-0.23

Table 5-5 Evaluation statistics of monthly streamflow during calibration and validation period. Default SWAT refers to the original SWAT model while SWAT-T refers to the modified SWAT model improved by Strauch and Volk (2013).

Period	Model	NSE	R^2	PBIAS (%)
2008-2017 (calibration)	Default SWAT	0.91	0.92	-0.9
	SWAT-T	0.93	0.94	-7.3
2003-2007 (validation)	Default SWAT	0.90	0.90	-4.9
	SWAT-T	0.92	0.94	-10.0
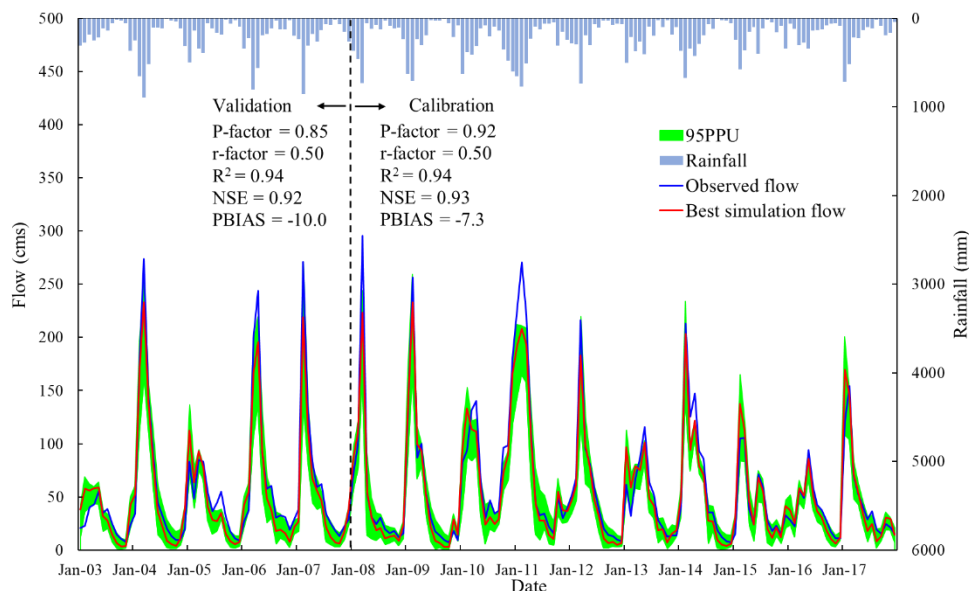
Figure 5-7 The observed and SWAT-T-simulated monthly streamflow for the calibration period (January 2008 to December 2017) and for the validation period (January 2003 to December 2007) in the North Johnstone River catchment, Queensland, Australia.
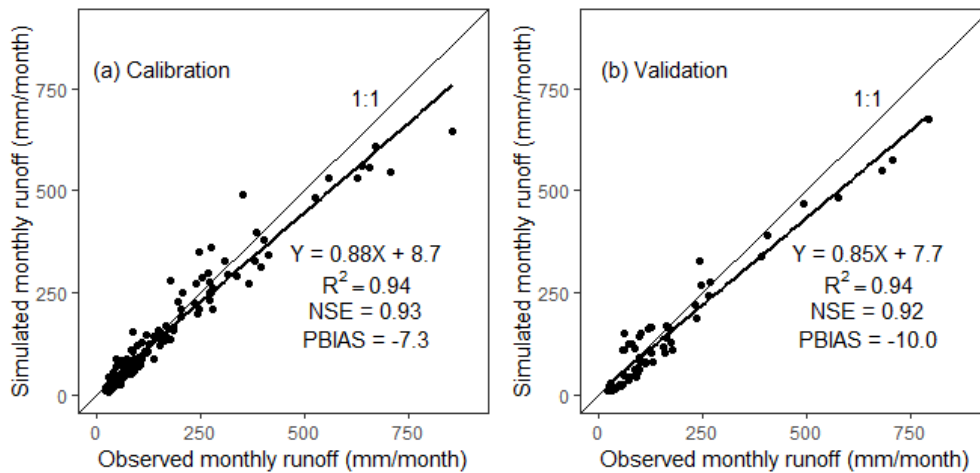
Figure 5-8 Comparison of observed and SWAT-T-modelled monthly runoff in (a) calibration and (b) validation periods in the North Johnstone River catchment, Queensland, Australia.

5.3.3 Hydrological responses to land use change scenarios

The calibrated SWAT-T model was applied to simulate the monthly surface runoff (SURQ), lateral runoff (LATQ), groundwater (GWQ), total runoff, actual evapotranspiration (ET), and soil water (SW) under the four land use change scenarios in 1967-2017 in the North Johnstone River catchment. Figure 5-9 shows monthly SURQ, LATQ, GWQ, total runoff, ET, and SW and their changes under different land-use scenarios, and Table 5-6 summarizes changes in average annual SURQ, LATQ, GWQ, total runoff, ET, and SW under different land-use scenarios. It can be seen from Figure 5-9 that SURQ, LATQ, GWQ, total runoff, ET, and SW had obvious monthly variations, with values generally greater in December-May (summer-autumn) and less in June-November (winter-spring). In addition, Figure 5-9 shows that monthly changes among different land use scenarios of SURQ were more notable than changes of other outputs from SWAT-T. Meanwhile, absolute changes of SURQ under different land-use scenarios differed across months, with the most remarkable changes occurring during the wet season from December to May. Furthermore, Figure 5-9 indicates that monthly SURQ increased under Scenarios 1, 2, and 4 (deforestation or urbanization), and decreased under Scenario 3 (afforestation), and similar results can be found for default SWAT (Figure 5-10).

This result was the same for SURQ at the annual time scale (Table 5-6). Table 5-6 indicates that the mean annual surface runoff increased under deforestation (Scenarios 1 and 2) and urbanization (Scenarios 2 and 4). For example, surface runoff increased 25 mm (8.9%) under Scenario 1 (11.5% decrease in FRSE area), 16 mm (5.7%) under Scenario 2 (2.3% increase in URBN area), and 44 mm (15.9%) under scenario 4 (8.4% increase in URBN area) using SWAT-T. In contrast, the 14.1% increase in FRSE area (Scenario 3) led to a 26 mm (9.5%) decrease in surface runoff. The annual total runoff also increased under deforestation and

urbanization, and decreased under afforestation, but the extent of increase and decrease was much smaller than observed for surface runoff. For instance, Table 5-6 indicates that total runoff increased by just 11 mm (0.6%) under Scenario 1 (11.5% decrease in FRSE area) and decreased 14 mm (0.7%) under Scenario 3 (14.1% increase in FRSE area) using SWAT-T. However, annual changes of LATQ and GWQ to urbanization (Scenarios 2 and 4) were opposite to those of SURQ and total runoff. As shown in Table 5-6, LATQ and GWQ decreased under urbanization. For example, a 2.3% increase in URBN area (Scenario 2) led to 0.7% and 0.9% decreases in LATQ and GWQ, respectively, while an 8.4% increase in URBN area (Scenario 4) contributed to 1.3% and 3.5% decreases in LATQ and GWQ, respectively.

In addition to runoff, Table 5-6 also shows the SWAT-T-simulated changes in average annual actual evapotranspiration and soil water under the four scenarios. Results show that mean annual ET decreased by 11 mm (1.3%) with an 11.5% reduction in forest area (Scenario 1) and increased by 14 mm (1.7%) with a 14.1% increase in FRSE area (Scenario 3) using SWAT-T. That is, under the deforestation scenario (Scenario 1), the mean annual ET declined with decreased forest area, and under the afforestation scenario (Scenario 3), the mean annual ET increased with increased forest area. In addition, Table 5-6 suggests that the change of soil water in different land use scenarios was opposite to ET, with a 1.5% increase under deforestation (Scenario 1) and a 2.0% decrease under afforestation (Scenario 3).

According to Table 5-6, changes in average annual total runoff under Scenarios 1 and 3 were more remarkable than under Scenarios 2 and 4. The spatial distributions of average annual total runoff under land use Scenario 0 and average annual total runoff change under Scenarios 1 and 3 compared with Scenario 0 using SWAT-T and default SWAT in different sub-basins in the North Johnstone River catchment are shown in Figure 5-11. These spatial distributions show that average annual runoff in the eastern sub-basins of the catchment were generally greater than those in the western sub-basins. This was primarily due to the uneven spatial distribution of rainfall, with higher rainfall occurring in the eastern area and lower rainfall in the western area. Compared with Scenario 0, average annual runoff increased in Scenario 1 (under an 11.5% reduction in FRSE area) in some sub-basins (#4-#7, #9, #10, #14, #15, #19, #20, #24-#28 and #30), while it decreased in Scenario 3 (under a 14.1% increase in FRSE area) in the same sub-basins. The reason why changes of average annual runoff occur only in these sub-basins is that the replacement of one land use by another land use can be considered only if both land uses are present in the same sub-basin, as we described in the Materials and Methods section. Furthermore, Figure 5-11 showed that absolute total runoff changes simulated by default SWAT were much smaller than that by SWAT-T in 33 different sub-basins.

To quantify the impacts of land use change on rainfall-runoff relationships, scatter diagrams between annual rainfall and runoff (total runoff, SURQ, LATQ, and GWQ) for FRSE, RNGE, and URBN were plotted (Figure 5-12) using the simulated results from SWAT-T and default SWAT in 1967-2017 from selected HRUs (HRU 30 for FRSE, HRU 41 for RNGE, and HRU 52 for URBN in sub-basin 4). Figure 5-12a-b revealed strong positive correlations ($r \geq 0.94$) between annual rainfall and total runoff for FRSE, RNGE, and URBN. Figure 5-12a-b also showed that the plotted cluster of points for FRSE were generally higher than the RNGE and URBN points, indicating that FRSE generally produced less runoff than RNGE and URBN under the same rainfall amounts. This explains the changes in average annual total runoff in Table 5-6 (Scenarios 1, 2, and 3), and implies that rainfall-runoff relationships could be altered by land use changes. Furthermore, Figure 5-12c-h indicated that URBN generally produced more SURQ and less LATQ and GWQ than FRSE and RNGE under the same rainfall amounts.

Table 5-6 Changes in average annual surface runoff (SURQ), lateral runoff (LATQ), groundwater (GWQ), total runoff, evapotranspiration (ET), and soil water (SW) using SWAT-T and default SWAT (in brackets) under different land use change scenarios in the North Johnstone River catchment, Queensland, Australia in 1967-2017.

Hydrological variables		Scenario 0	Scenario 1	Scenario 2	Scenario 3	Scenario 4
SURQ	Value (mm)	275 (296)	300 (322)	291 (312)	249 (269)	319 (340)
	Absolute change (mm)	0 (0)	25 (25)	16 (16)	-26 (-27)	44 (44)
	Percentage change (%)	**0.0 (0.0)**	**8.9 (8.5)**	**5.7 (5.4)**	**-9.5 (-9.2)**	**15.9 (14.8)**
LATQ	Value (mm)	763 (773)	755 (763)	757 (767)	769 (781)	753 (763)
	Absolute change (mm)	0 (0)	-8 (-10)	-5 (-6)	6 (8)	-10 (-10)
	Percentage change (%)	**0.0 (0.0)**	**-1.1 (-1.3)**	**-0.7 (-0.7)**	**0.8 (1.0)**	**-1.3 (-1.3)**
GWQ	Value (mm)	827 (882)	822 (873)	820 (875)	834 (895)	798 (855)
	Absolute change (mm)	0 (0)	-6 (-10)	-7 (-8)	6 (12)	-29 (-28)
	Percentage change (%)	**0.0 (0.0)**	**-0.7 (-1.1)**	**-0.9 (-0.9)**	**0.8 (1.4)**	**-3.5 (-3.1)**
Total Runoff	Value (mm)	1909 (1998)	1919 (2003)	1912 (2000)	1895 (1992)	1912 (2003)
	Absolute change (mm)	0 (0)	11 (5)	3 (2)	-14 (-6)	3 (5)
	Percentage change (%)	**0.0 (0.0)**	**0.6 (0.2)**	**0.2 (0.1)**	**-0.7 (-0.3)**	**0.2 (0.2)**
ET	Value (mm)	811 (722)	800 (717)	808 (719)	825 (728)	808 (717)
	Absolute change (mm)	0 (0)	-11 (-5)	-3 (-2)	14 (6)	-3 (-5)
	Percentage change (%)	**0.0 (0.0)**	**-1.3 (-0.7)**	**-0.3 (-0.3)**	**1.7 (0.9)**	**-0.3 (-0.7)**
SW	Value (mm)	17.8 (17.6)	18.0 (17.7)	17.8 (17.7)	17.4 (17.4)	17.9 (17.9)
	Absolute change (mm)	0.0 (0.0)	0.3 (0.1)	0.1 (0.1)	-0.4 (-0.2)	0.1 (0.3)
	Percentage change (%)	**0.0 (0.0)**	**1.5 (0.7)**	**0.5 (0.6)**	**-2.0 (-0.9)**	**0.7 (1.7)**
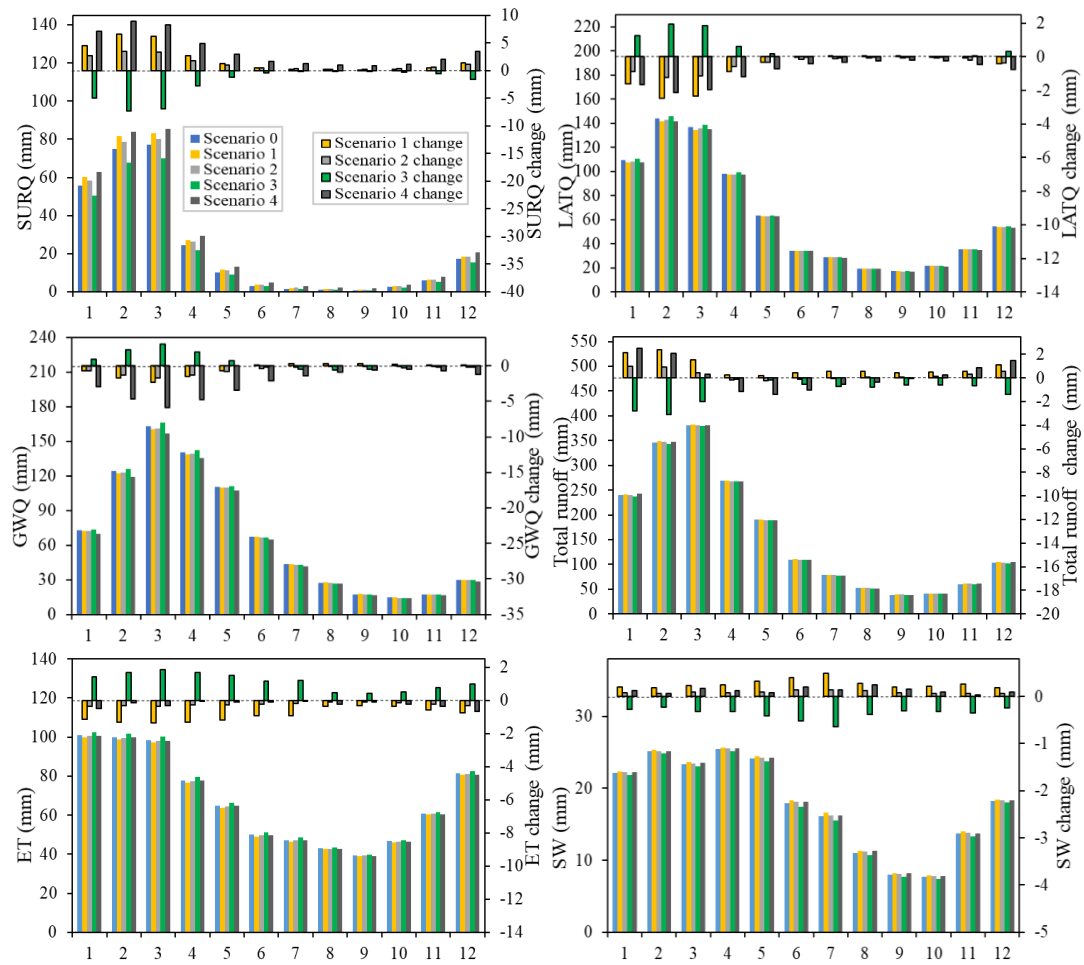
Figure 5-9 Monthly surface runoff (SURQ), lateral runoff (LATQ), groundwater (GWQ), and actual evapotranspiration (ET) and their monthly changes using SWAT-T under different land use change scenarios in the North Johnstone River catchment, Queensland, Australia.
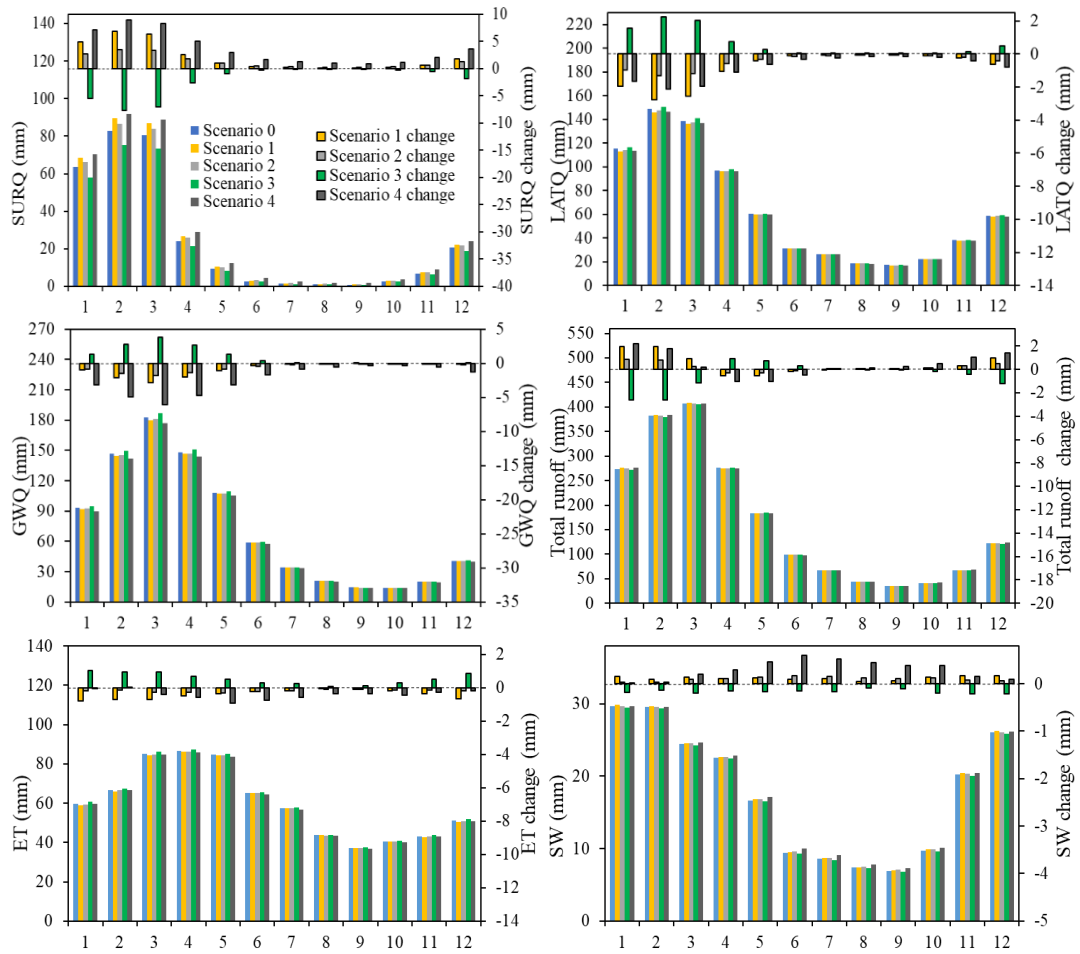
Figure 5-10 Monthly surface runoff (SURQ), lateral runoff (LATQ), groundwater (GWQ), and actual evapotranspiration (ET) and their monthly changes using default SWAT under different land use change scenarios in the North Johnstone River catchment, Queensland, Australia.
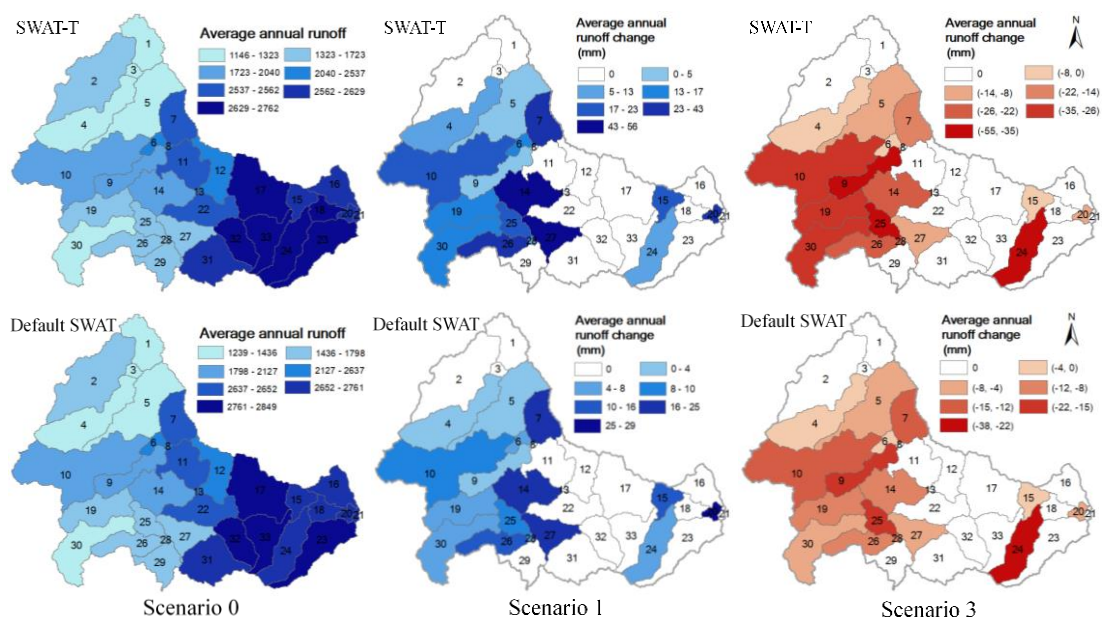
Figure 5-11 Spatial distribution of average annual total runoff (mm) under land use Scenario 0 and average annual total runoff change under Scenarios 1 and 3 compared with Scenario 0 using SWAT-T and default SWAT in 33 different sub-basins in the North Johnstone River catchment, Queensland, Australia.
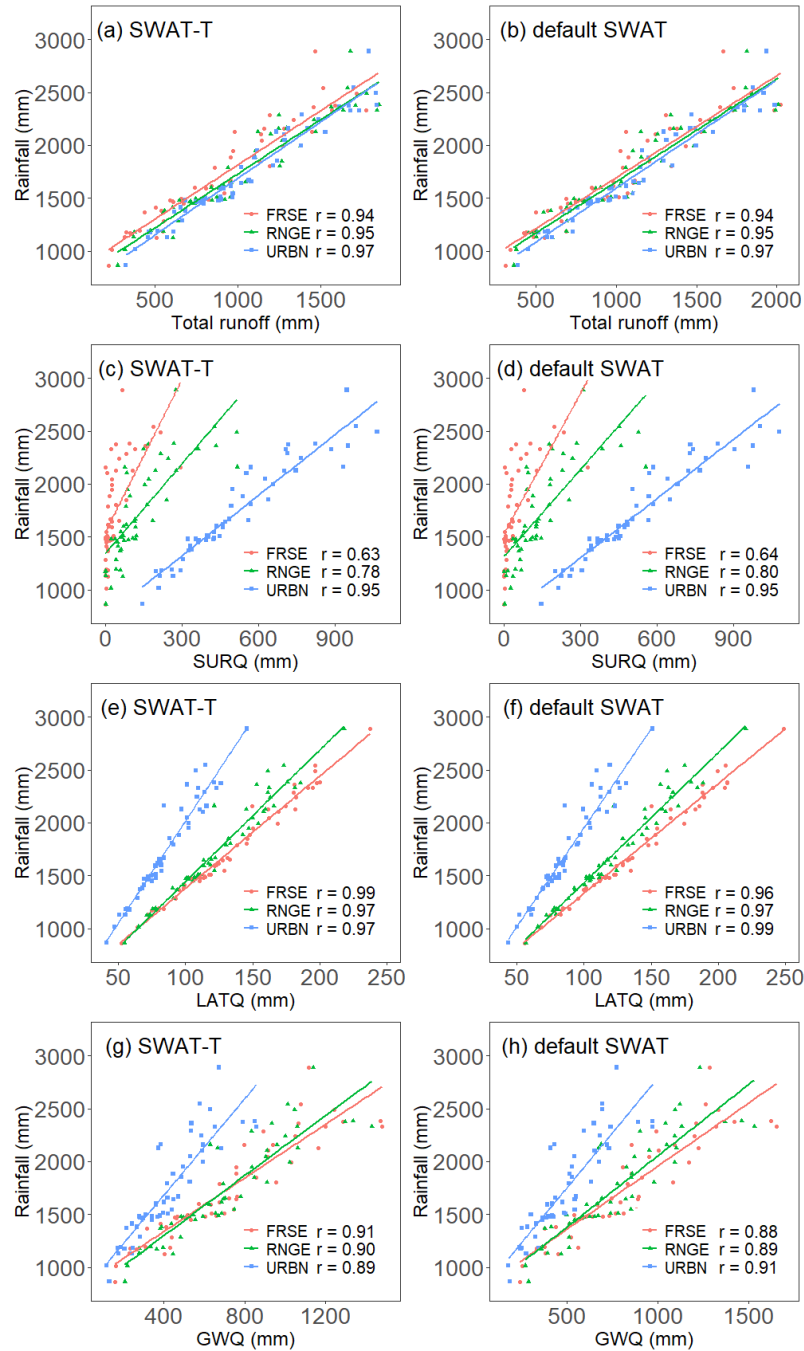
Figure 5-12 The annual rainfall and runoff (total runoff, surface runoff (SURQ), lateral runoff (LATQ), and groundwater (GWQ)) relationships for forest-evergreen (FRSE), range-grasses (RNGE), and urban (URBN) land use by using the simulated results of 1967-2017 from selected hydrologic response units (HRU 30 for FRSE, HRU 41 for RNGE, and HRU 52 for URBN in

sub-basin #4) with the same slope range (0-10°) and soil type (Ferrosol (Mp19)) using SWAT-T and default SWAT in the North Johnstone River catchment, Queensland, Australia. The reason why sub-basin #4 was selected to analyze the rainfall-runoff relationship for FRSE, RNGE, and URBN was that sub-basin #4 ranked third among the 33 sub-basins in area, and the area proportions for FRSE, RNGE, and URBN were relatively uniform for sub-basin #4 compared with the other two larger sub-basins (#5 and #10).

5.4 Discussion

5.4.1 Model comparison and evaluation

It was found that in the default plant growth model of SWAT simulated LAI was zero for all plants at the beginning of each simulation year, which is not true for plants in tropical areas. Previous studies (Mwangi et al., 2016; Alemayehu et al., 2017; Hoyos et al., 2019) reported similar simulations, revealing that the default SWAT has some shortcomings in modelling vegetation growth in tropical regions. While the calibrated SWAT-T model was generally able to replicate BFAST-filtered MODIS LAI values for each land cover type (Figure 5-6), it failed to represent the bimodal seasonality of LAI because the model is capable of simulating only one wet/dry transition within a year (Hoyos et al., 2019). However, the default SWAT LAI mean values failed to correctly represent both LAI seasonality and range for all plants (Figure 5-6). Moreover, the precision of MODIS LAI is also very important because it is directly used to calibrate the parameters of hydrological models. The average LAI of 4.85 (average of maximum LAI 6.0 and minimum LAI 3.7) for FRSE (the dominant land cover in the study area) was approximately equal to values previously reported (4.71±0.37) in the literature (Hill et al., 2006) for tropical rainforests across Australia. Overall, the LAI results simulated by the SWAT-T model were acceptable.

Groundwater delay (GW_DELAY) was found to be the most sensitive calibration parameter in the North Johnstone River catchment (Table 5-4). In addition, half of the parameters identified as sensitive ($P \leq 0.05$) had an impact on either soil moisture or groundwater flow. This may be due to the abundance of groundwater in this area (Figure 5-9 and Table 5-6), so the flow in this catchment was dominated by baseflow. The baseflow ratio was about 0.44 calculated by "GWQ/total runoff" during July 2005 to June 2013 in this study, and it was consistent with previous research (Orr, 2014) in which the mean daily baseflow was 31.579 m^3/s (i.e. baseflow ratio was 0.47) from 1 July 2005 to 1 July 2013. Previous studies (McMahon and Finlayson, 2003; Brown et al., 2015) also reported that Australia's perennial rivers were dominated by baseflow. SWAT parameters associated with baseflow and soil moisture were consistently identified as being highly sensitive to calibration by a review of

SWAT applications (Gassman et al., 2007), supporting the results and suggesting that model operators should focus on these parameters during calibration, to guarantee that the SWAT model is conceptually consistent with regional hydrological conditions. According to the general performance ratings suggested by previous studies (Moriasi et al., 2007; Shi et al., 2011; Wallace et al., 2018), streamflow modelling is deemed reasonable if NSE > 0.50, R^2 > 0.50, and PBIAS within ±25%. Therefore, it was shown that the SWAT-T model simulated monthly streamflow well in the North Johnstone River catchment, with |PBIAS| ≤ 10%, NSE ≥ 0.92, and R^2 ≥ 0.94 during both calibration and validation periods. Furthermore, the uncertainty analysis resulted in a P-factor of 0.92 and an R-factor of 0.50 for SWAT-T calibration after four iterations, while the P-factor was 0.85 and the R-factor was 0.50 for the validation period. Values for P-factor of larger than 0.7 and for R-factor of about 1 (the smaller the better) are suggested for streamflow simulations (Abbaspour, 2013). Therefore, SWAT-T was judged to reasonably simulate streamflow and can be used for further analysis in the North Johnstone River catchment.

Furthermore, results (Table 5-5) showed that SWAT-T simulated streamflow process better than default SWAT with larger R^2 (0.94 > 0.92 and 0.94 > 0.90) and NSE (0.93 > 0.91 and 0.92 > 0.90) in the calibration and validation periods, respectively. Using R^2 and NSE as statistical evaluation criteria to compare SWAT-T and the original SWAT model is consistent with previous studies. For instance, Ma et al. (2019) integrated downscaled high quality MODIS LAI into modified SWAT plant growth model and found that predicted flows with MODIS LAI basically matched the observed flows better than original SWAT supported by an improvement of R^2 and NSE values. However, compared to SWAT-T, the default SWAT model produced smaller absolute percent bias (0.9% < 7.3% and 4.9% < 10.0%) in the calibration and validation periods, respectively. This is most probably because both the default SWAT and the SWAT-T model underestimated streamflow in the North Johnstone River catchment. According to Figure 5-6, LAI values simulated by SWAT-T were much better and larger than the default SWAT, this would lead to greater actual evapotranspiration simulated by SWAT-T than the default SWAT (Table 5-6), leading to lower streamflow simulated by SWAT-T (Table 5-6). Therefore, a larger absolute percent bias was produced by the SWAT-T model. However, achieving good agreement between model simulation and observed streamflow through model calibration does not imply correct description of the underlying processes and parameterizations (Wagner et al., 2011), because good streamflow simulations might be achieved by parameters calibration even with unrealistic underlying premises or without any improvement of the vegetation growth module (Strauch and Volk, 2013). Therefore, it is more reasonable to use the SWAT-T model for land use impacts study as it successfully accounted for seasonal vegetation dynamics (Figure 5-6) which is an important part of the water cycle.

5.4.2 Modelled Hydrological responses to different land use change scenarios

The obvious monthly variations in SURQ, LATQ, GWQ, total runoff, ET, and SW, with values generally greater in December-May (summer-autumn) and less in June-November (winter-spring) (Figure 5-9), were consistent with the inter-annual distribution of rainfall (Figure 5-2). This is because rainfall is the main factor affecting runoff, ET, and soil water content (Fekete et al., 2004), and the catchment that was selected is a summer rainfall dominant region. Meanwhile, changes of SURQ under different land-use scenarios differed across months, with the most remarkable changes occurring during the wet season from December to May. The impacts of vegetation changes on seasonal water yield with the largest volume changes occurred during the wet season and small volume changes during the dry season are consistent with previous studies (Brown et al., 2005). Total runoff is composed of surface runoff (SURQ), lateral runoff (LATQ), and groundwater (GWQ). Surface flow into rivers is mainly controlled by dominant climate conditions and is usually greatest during and shortly after storm or rain events. Groundwater, i.e. baseflow, is the major source of flow during the dry period (Brown et al., 2015). LUCC has been shown to be capable of altering baseflows and river discharges (Costa et al., 2003). Figure 5-9 and Table 5-6 indicated that surface runoff increased under deforestation (Scenarios 1 and 2) and decreased under afforestation (Scenario 3) at monthly and annual time scales, and is similar to previous studies (Foley et al., 2005). This is because forest vegetation increases ET rates, dissipates raindrop energy, slows surface flow velocity, and increases soil organic matter, all of which result in larger infiltration and smaller surface runoff (Alibuyog et al., 2009). Results presented in Table 5-6 also showed that total runoff increased slightly under deforestation (Scenarios 1 and 2) and decreased slightly under afforestation (Scenario 3) at the annual time scale. Similar results for runoff response to LUCC also occurred in other hydrological simulation studies. For example, Weber et al. (2001) found that streamflow simulated by hydrological models increased when forest area decreased and grassland area increased. This is because trees commonly consume more water (extracting water from shallow aquifer storage due to deep root systems and transpiring more due to larger aerodynamic conductance), and, therefore, forest catchments will produce less runoff (Wang et al., 2008; Mwangi et al., 2016). In contrast, data shown in Figure 5-9 and Table 5-6 indicated that LATQ and GWQ decreased while SURQ increased under urbanization (Scenarios 2 and 4) at monthly and annual time scales. This decrease in LATQ and GWQ under urbanization may be attributed to increased surface runoff and decreased infiltration as a result of conversion of vegetation land use to urban land use (Alibuyog et al., 2009). Additionally, the rainfall-runoff relationships in Figure 5-12c-h explain why runoff changes under urbanization generally produced more SURQ and less LATQ and GWQ than FRSE and RNGE with the same rainfall amounts.

In addition to runoff, Figure 5-9 and Table 5-6 indicated that ET decreased under deforestation (Scenarios 1 and 2) and increased under afforestation (Scenario 3) at monthly and annual time scales. This is because forests generally produced more evapotranspiration than other land use types due to higher leaf area and deeper rooting depth (Costa et al., 2003; Li et al., 2009b). Furthermore, it can be seen from Table 5-6 that soil water slightly increased (1.5%) under deforestation (Scenario 1, 11.5% increase in RNGE area), and slightly decreased (2.0%) under afforestation (Scenario 3, 14.1% increase in FRSE area) at the annual time scale using SWAT-T. The greater infiltration for forest may lead to an increase in soil water compared with other vegetation, but the larger evapotranspiration and water use may cause a decrease in soil water, so that the overall change in soil water may be insignificant due to the counterbalancing effects of these two processes under deforestation and afforestation. Chen et al. (2009b) also reported that the effect of greater vegetation cover on soil moisture content was still debatable as it increased transpiration loss and rainfall interception whereas it decreased evaporation loss through shading. Hence, dense vegetation cover reduces soil moisture because of larger transpiration and less rainfall falling on the ground due to greater interception by leaves. In contrast, the soil is shaded more by the greater canopy vegetation, thereby reducing direct radiation absorption, and leading to lower soil temperature and soil evaporation rates, and higher soil moisture (Chen et al., 2009b). Therefore, the relationship between soil water and vegetation is complex, and the positive or negative impacts of vegetation cover on soil moisture likely depend on climate and the length of dry or wet periods (Chen et al., 2009b). Typically, when forest canopy cover exceeds a certain threshold level, the forest would produce less runoff and soil water but more ET than other land cover types (Li et al., 2009b).

Hydrological responses to land use change scenarios using a default (original) SWAT model were shown in Table 5-6, Figures 5-10, 5-11, and 5-12 using calibrated parameters from SWAT-T model. SWAT-T showed greater simulated actual evapotranspiration (ET) and lower streamflow (SURQ, LATQ, GWQ and total runoff) than the default SWAT (Table 5-6) at annual time scale. At monthly time scale, seasonal dynamics of ET and SW simulated by default SWAT (Figure 5-10) were slightly different from those simulated by SWAT-T (Figure 5-9) while seasonal variability of other hydrological factors were similar. In addition, monthly changes of hydrological factors under different land use change scenarios simulated by default SWAT (Figure 5-10) were similar to that simulated by SWAT-T (Figure 5-9), except for ET and SW. Furthermore, Figure 5-11 showed that absolute total runoff changes simulated by default SWAT were much smaller than those from SWAT-T in 33 different sub-basins and may be explained by the smaller difference between annual rainfall and total runoff relationship for default SWAT model (Figure 5-12 b) compared to SWAT-T (Figure 5-12 a). In general, these

differences were probably caused by the difference of seasonal LAI simulated by SWAT-T and default SWAT (Figure 5-6).

5.4.3 Limitations and uncertainties

Even though it met the criteria for satisfactory model performance, similar to other SWAT model applications, calibration and validation hydrograph (Figure 5-7) showed that most of the peak flows (Shrestha et al., 2016) and low flows (Wu and A. Johnston, 2008) were underestimated. In addition, the model overestimated a few peaks during the dry period and underestimated it during the high flow period, which also was the case for other Australian catchments studied by Saha et al. (2014). This was an acceptable result considering the fact that the SWAT model was not calibrated for single-event high streamflow condition (Saha et al., 2014). Furthermore, low capacity to simulate both low flows and peak flows also occur in other hydrological models (Eum et al., 2016). Thus, difficulties in reproducing peak flows and low flows are common due to the theories of hydrological models and standards of model calibration (Zhang et al., 2019). However, if the model has limited capacity to capture peak and low flows, it does affect the extreme value of the surface runoff (Tessema et al., 2014). If we quantify the impacts of different LUCC scenarios on surface runoff with this kind of hydrological model, it may underestimate or overestimate the magnitude of LUCC effect. However, investigating the implications of peak flows and low flows underestimation or overestimation on the LUCC effect analysis on the surface runoff are beyond the scope of our present study and needs to be explored in future studies.

The study also found that land use change had only a small effect on water balance components except surface runoff. This is in line with findings reported in other studies (Shrestha et al., 2017). For instance, Brown et al. (2015) assessed the impact of forestry on streamflow in southeastern Australia using SWAT and found that the modelled introduction of plantation forestry did not significantly change streamflow. Karlsson et al. (2016) also pointed out that land use changes only affected the mean flow by a few percentage points. This result may also be caused by our hypothetical land use scenarios where land use change area in each scenario accounted for less than 15% of the total catchment area. In fact, previous studies (Bosch and Hewlett, 1982; Stednick, 1996) stated that forest land changes of less than 15-20% do not influence the annual water yield. Besides, the small effect found in this study may also be due to the partial conversion scenarios occurring mainly in the northwestern part of the catchment where there is less rainfall distribution compared to the downstream part (the forest part of the catchment), hence the implemented scenarios might not cause remarkable changes in the hydrological processes, particularly at the annual scale. In addition to land use scenarios, a large number of uncertainty sources (hydrological models, calibration periods, objective

function, etc.) may influence the impact analysis. Sources of uncertainty for the hydrological model can be present because of the model structure (e.g. model assumptions and functions) as well as input data (e.g. lack of relevant temporal and spatial variability of data on rainfall, land uses, soils and topography) (Marhaento et al., 2018). Another important issue is the calibration practices, including calibration period and calibration approach (van der Spek and Bakker, 2017; Wallach et al., 2019). Sorooshian et al. (1983) claimed that it is not the length of data used but the information contained in it, and the efficiency with which that information is extracted (i.e. the choice of a stochastically appropriate objective function), that are important. Parameterization of hydrological models is also a well-known source of uncertainty and have been discussed previously a few times as related to impact studies (Karlsson et al., 2016). However, studying these additional sources of uncertainty is beyond the scope of this study, and will be addressed in future research. Furthermore, the current study was focused only on the North Johnstone River catchment. Moreover, even though this catchment was deemed to be representative of all such tropical catchments, this study lacked replication at the catchment scale. Accordingly, additional catchments will need to be chosen in future studies to stand for the large range of climate, physical conditions, and runoff characteristics throughout tropical Australia, and to afford insights for future water management.

5.5 Summary and conclusions

The default (original) SWAT model has poor performance in estimating the LAI of different vegetation types for tropical areas. For the first time, the SWAT-T model (Strauch and Volk, 2013) with an improved vegetation growth module was used to analyze the hydrological sensitivity of a tropical catchment in Australia under different land use change scenarios. Prior to the simulation of land use change scenarios, the SWAT-T model was parameterized, calibrated, and validated with NSE ≥ 0.59 (NSE < 0 for default SWAT), $R^2 \geq 0.70$ ($R^2 \leq 0.66$ for default SWAT), and |PBIAS| $\leq 2.5\%$ (|PBIAS| $\geq 42\%$ for default SWAT) for LAI and NSE ≥ 0.92 (NSE ≥ 0.90 for default SWAT), $R^2 \geq 0.94$ ($R^2 \geq 0.90$ for default SWAT), and |PBIAS| $\leq 10\%$ (|PBIAS| $\leq 5\%$ for default SWAT) for streamflow. Therefore, the SWAT-T model was judged to perform satisfactorily in this catchment according to general performance indices. Overall, the SWAT-T model performed better in predicting monthly streamflow than the default SWAT model, based on our major statistical indicators, in an Australian tropical catchment.

For the first time, we used both models (SWAT-T and default SWAT) to quantify hydrological responses to land use change scenarios in the selected tropical catchment. Results showed that LUCC affected all hydrological variables, of which the impact on surface runoff was the most remarkable at both monthly and annual time scales. Moreover, changes of SURQ

under different land-use scenarios differed across months using SWAT-T, with the most obvious changes occurring during the wet season from December to May, and similar results can be found for default SWAT. The simulations also indicated that urbanization (converting FRSE or RNGE to URBN) resulted in increased surface flow and decreased lateral flow and groundwater, with no notable change in total runoff, ET, and SW using SWAT-T. For instance, surface runoff increased 16 mm (5.7%) with a 2.3% increase in URBN area, and 44 mm (15.9%) with an 8.4% increase in URBN area. The decreases of LATQ and GWQ under urbanization were less than 3.5%, while the impact of urbanization on total runoff, ET, and SW were less than 0.7%. Additionally, afforestation (Scenario 3, 14.1% increase in FRSE area) decreased SURQ by 26 mm (9.5%) and led to slight changes in other hydrological variables (within $\pm 2.0\%$). Annual rainfall and total runoff were strongly positively correlated ($r \geq 0.94$) for FRSE, RNGE, and URBN, and FRSE generally produced less total runoff than RNGE and URBN for the same rainfall amounts. Furthermore, URBN generally produced more SURQ and less LATQ and GWQ than FRSE and RNGE for the same rainfall amounts, as shown in the scatter diagrams of rainfall-runoff relationships (Figure 5-12). Furthermore, we found that SWAT-T showed greater simulated actual evapotranspiration (ET) and lower streamflow (SURQ, LATQ, GWQ and total runoff) than the default SWAT at annual time scale. In contrast, at a monthly scale, seasonal dynamics of ET and SW simulated by default SWAT were slightly different from those simulated by SWAT-T while seasonal variability of other hydrological factors were similar. These differences can be attributed to the diversity of seasonal LAI simulated by SWAT-T and default SWAT. Therefore, we conclude that using SWAT-T is more reasonable in tropical catchments as it captures seasonal vegetation dynamics.

The remarkable increase in surface runoff from deforestation and urbanization can threaten the health of both people and the biosphere. For instance, urbanization has enlarged impermeable surface area, increased runoff coefficient, reduced concentration time, and increased peak flow and frequency of floods in city rivers (Yaa et al., 2012). In addition, increased surface runoff will carry a large amount of sediment and pollutants, degrading river ecosystems and, for this particular catchment, thereby threatening the health of the Great Barrier Reef as the North Johnstone River is a key tributary that discharges into the Great Barrier Reef lagoon. Strategies to ameliorate the effects of land use change include increasing green space in urban areas to reduce runoff (Foley et al., 2005), reducing nutrient and sediment inputs, improving the management of drainage systems, and others. The results of studies such as reported here will provide important information for developing sustainable management of water resources in tropical eastern Australia. The research methods described in this study can be further extended to other tropical catchments for LUCC impact assessments.

Chapter 6. Quantifying the impacts of future climate and land use changes on hydrological processes and associated uncertainty in southwestern Australia

This chapter is based on the following manuscript:

Zhang, H., Wang, B., Li Liu, D., Leslie, L. M., Shi, L., Zhang, M., & Yu, Q. (2020). Quantifying the impacts of future climate and land use changes on hydrological processes and associated uncertainty in southwestern Australia. (Ready for submission).

Highlights:

1. The SWAT model simulated well the observed monthly streamflow in SW Australia;

2. Runoff decreased under afforestation but increased under deforestation/urbanization;

3. Future runoff had a greater decrease in winter and spring than in autumn and summer;

4. GCM contributed to the largest uncertainty in future change of hydrologic variables.

Abstract

Assessing the impacts of both climate and land use changes on hydrologic variables is crucial for sustainable development of water resources and natural ecosystems. We conducted a case study of a catchment in southwestern Australia to assess the impacts of future climate and land use changes, both separately and in combination, on water resource availability. For this evaluation, the Soil and Water Assessment Tool (SWAT) model was first calibrated and then forced by 34 global climate models (GCMs), under two Representative Concentration Pathways (RCP4.5 and RCP8.5) and five land use scenarios (LU0-4). Our results suggested that the SWAT model reproduced well the observed monthly streamflow, with NSE $\geq$ 0.86, R^2 $\geq$ 0.87, and |PBIAS| $\leq$ 8.3%. Land use changes have impacts on all hydrologic variables, especially on runoff at the annual scale (6.0%, 22.8%, -4.3%, and 25.1% for LU1-4, respectively). Future runoff was projected to decrease in all seasons, especially winter and spring. Multi-GCM ensemble medians suggested annual runoff would decrease by -19.4% in 2040s (RCP4.5), -28.3% in 2040s (RCP8.5), -33.6% in 2080s (RCP4.5), and -55.3% in 2080s (RCP8.5). For the combined effects of climate and land use changes, the results of LU1-4 were only slightly different from the response of zero land use. An uncertainty analysis shows that GCMs had the greatest contribution to hydrologic variables, followed by RCPs and land use scenarios. Hence it is advisable for impacts analysis to use an ensemble of GCMs under different RCPs, to minimize the uncertainty of projected future hydrologic variables.

Key words: *climate change; land use change; GCM; southwestern Australia; runoff*

6.1 Introduction

Global warming is likely to accelerate hydrologic cycle through increasing atmospheric evaporative demand and changing the intensity, frequency and duration of rainfall events (Zeng et al., 2014; Joseph et al., 2018). Hydrologic variables (e.g. runoff, evapotranspiration, and soil water) are highly sensitive to even small changes in rainfall and temperature (Milly et al., 2005; Seneviratne et al., 2010; Joseph et al., 2018). Thus, hydrologic sensitivity to climate change has been widely discussed (Jones et al., 2006), due to the importance of water availability for human society and ecosystem processes (Milly et al., 2005), and for the development of appropriate water resources management strategies (Reshmidevi et al., 2018). For instance, the regression between global temperature and runoff shows that a 1°C rise in temperature is associated with a 4% rise in runoff (Labat et al., 2004). However, such global trends should be studied on a regional scale where there are both increasing and decreasing trends. Basin level hydrologic analyses therefore are needed to assess the sensitivity of the basin to climate change scenarios.

In addition to climate change, the hydrologic cycle also is influenced by land use change, resulting from human activities such as replacing natural forests and wetlands with croplands and built-up land (Sterling et al., 2013). According to a recent IPCC report (IPCC, 2019), about 25% of the ice-free land on Earth is being degraded by human activities (medium confidence). Therefore, land use is a key factor in influencing the hydrologic response, primarily due to changes in vegetation cover that alter rainfall interception, infiltration, thereby changing runoff (Mohammady et al., 2018). The impacts of land use change on hydrology have been studied and debated for many years throughout the world (Siriwardena et al., 2006; Li et al., 2013). Several studies reported that forest changes greatly affect water yield, although the magnitude of change varies greatly between catchments (Sun et al., 2006). In contrast, limited effects, no effects, or even positive effects on water yield due to forest changes have been found in other studies, especially in large basins (Zhou et al., 2015). Therefore, a detailed investigation of land use change effects on the hydrologic cycle of a specific catchment is highly valuable for developing catchment management policies.

Since 1910, the mean near-surface temperature in Australia has risen by ~0.9 °C, with the nighttime minimum rising more than daytime maximum (CSIRO, 2015). In addition to climate warming, southwestern Australia (SWA) has experienced a substantial decrease in rainfall over the last century (Heinzeller et al., 2016), and the climate impacts on its water resources have been particularly acute (Silberstein et al., 2012). For instance, rainfall has decreased by 16% since the mid-1970s, resulting in a reduction of more than 50% of stream flows into the main reservoirs in the area which provides water for the state capital, Perth (Petrone et al., 2010). The water shortage is expected to worsen, as climate change projections suggest that rainfall

will decrease further over SWA in the future (Charles SP, 2010; Fraser et al., 2013) and the percentage changes in rainfall will be amplified in decreased runoff (Teng et al., 2012a). In addition, up to 20% more droughts are projected by 2030 in most parts of Australia and up to 80% more droughts by 2070 in SWA (Mpelasoka et al., 2008). Furthermore, catchments in SWA have been subjected to extensive land clearing (Callow, 2007), so the ability to project the possible impacts of land use change on streamflow is seen as a key management tool (Gilfedder et al., 2009). While some studies have assessed the hydrologic response to climate change in SWA (Barron et al., 2012; McFarlane et al., 2012), there have been few detailed studies of the coupling impacts of coincident climate and land use changes on individual catchments in SWA. These coupling effects of climate and land use changes on regional runoff regimes are complex and as yet poorly understood. Consequently, a catchment representative of SWA was examined in this study to provide detailed insights that suggest future options for water management under concurrent climate and land use changes.

In most climate change impacts studies, hydrologic models are first calibrated utilizing historical data. Next, downscaled climatic variables from Global Climate Models (GCMs) are used as input data for hydrologic models to simulate water balance under different climate scenarios (Reshmidevi et al., 2018). In this modelling process, uncertainties stemming from climate models, downscaling methods and modelled hydrologic regimes, are propagated through the entire modeling chain (Bosshard et al., 2013; Chen et al., 2013). Joseph et al. (2018) compared hydrologic impacts from hydrologic parameters and climate models. They found that the uncertainty resulting from hydrologic simulations was quite small when compared to the climate model. This might be due to the fact that the hydrologic cycle is sensitive to changes in precipitation (Crosbie et al., 2010) and GCMs project large variations in rainfall change (Milly et al., 2005). Due to the considerable uncertainty in GCM predictions, the outputs of multiple GCMs typically are used to evaluate hydrologic response to climate change (Zhang and Huang, 2013; Shen et al., 2018).

Both climate and land use changes have strong impacts on water resources. The combined effects of climate and land use changes are not simply the sum of the two effects (Notebaert et al., 2011). Therefore, the study of climate change and land use change impacts on hydrology within a catchment has become a major research topic (Anache et al., 2018). Currently, hydrologic modelling is the most widely used method to quantify and evaluate the impacts of climate change and land use change on the water cycle (Liu et al., 2017a). Soil and Water Assessment Tool (SWAT) is a physically based and semi-distributed watershed hydrologic model developed by Arnold et al. (1998). It can simulate long-term hydrologic variables, such as streamflow, on daily or monthly time scales (Wang et al., 2008), under different climatic and

land-use conditions. The SWAT model has been demonstrated to be effective for quantifying hydrologic response to environmental changes (Arnold and Fohrer, 2005). In recent years, there have been some studies using SWAT for assessment of hydrologic response to future climate and land use changes (Park et al., 2011; Wu et al., 2015; Gabiri et al., 2020), including catchments in Australia (Shrestha et al., 2017). However, to our knowledge, using the SWAT model under multiple GCMs and land use change scenarios has not yet been investigated for southwestern Australia. Consequently, this study is the first to use the SWAT model, run with statistically downscaled daily climate data from 34 GCMs and four land use change scenarios, to assess the hydrologic response to a combination of climate change and land use change of a principal catchment in SWA.

Specifically, our aim is to evaluate the impacts of climate change and land use change on hydrology in SWA, using the Wooroloo Brook catchment as a case study. Hence, the components of this study were to: (1) evaluate the performance of the SWAT model to simulate streamflow in the Wooroloo Brook catchment; (2) project changes in simulated historical hydrologic variables (runoff, actual evapotranspiration, and soil water) under four land use change scenarios; (3) project future changes in simulated hydrologic variables under climate change; (4) project the combined effects of climate change and land use change on hydrology; (5) quantify the contribution of GCM, RCP, and land use scenarios to the overall uncertainty in future changes of hydrologic variables.

6.2 Materials and methods

6.2.1 Study area

The Swan-Avon River catchment is located in SWA, covering an area of more than 120 000 km^2, including parts of Perth's metropolitan area (Degens et al., 2012). About 65% of the Avon River basin has been cleared of its native woodland vegetation for cereal production and sheep grazing, resulting in substantially increased soil erosion (Viney and Sivapalan, 1999). The Swan Coastal Plain also has been extensively cleared for agriculture and urban development (Mulligan, 1996; Garnett et al., 2011). Wooroloo Brook is one of the major tributaries of the Swan River in the Swan Coastal basin (CSIRO, 2009). The Wooroloo Brook catchment above Karls Ranch (Figure 6-1) was chosen as the case study region. This catchment is around 511 km^2 with elevation between 84 - 448 m. According to statistics in 1977-2016, the mean annual temperature was about 17.4 °C, mean annual rainfall was around 737.5 mm and mean annual runoff was approximately 75.5 mm in this catchment. There has been a significant decreasing trend ("p value" ≤ 0.01) in annual runoff resulting from decreasing rainfall in the Wooroloo Brook catchment above Karls Ranch, in recent decades according to the Mann-

Kendall trend test. However, very few studies have been conducted regarding hydrologic response to climate change in the Wooroloo Brook catchment. Consequently, this study is a step towards assessing the combined effects of climate and land use changes on catchment hydrology and can help inform and support regional priotrities for future water management, with respect to both climate and land use changes in SWA.
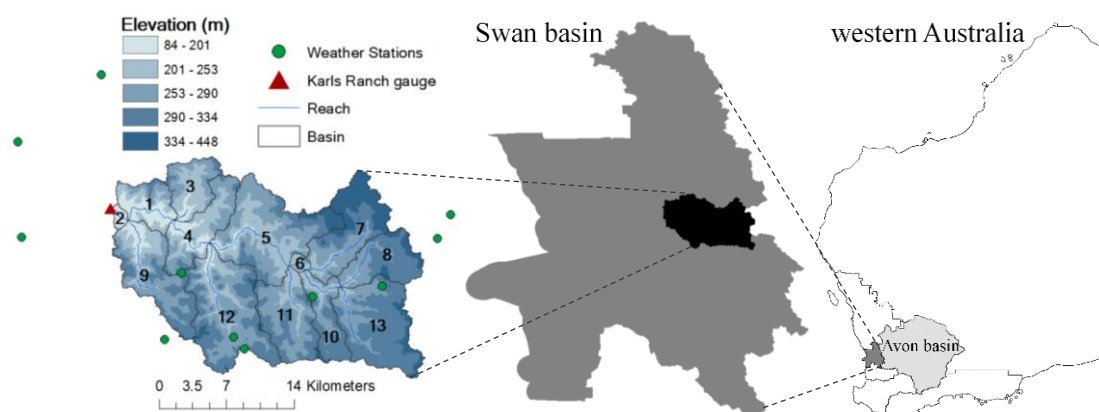
Figure 6-1 Location map of the Wooroloo Brook catchment (consists of 13 sub-basins).

6.2.2 The SWAT model

The SWAT model (Arnold et al., 1998) is a physically based and long term simulation watershed model which runs on a daily time step. It has proved to be an effective means for assessment of water resource over a broad range of scales, globally (Gassman et al., 2007). A modified Soil Conservation Service Curve Number (SCS CN) approach (Bondelid et al., 1982) was used in SWAT to calculate runoff. Using the SCS CN method, SWAT allows the users to evaluate the relative impacts of climate and land cover changes at the sub-basin level (Baker and Miller, 2013). SWAT has been used successfully to model environmental change impacts on hydrology, making it a widely used hydrologic tool in land use change and climate change studies (Zhang et al., 2012; Baker and Miller, 2013; Narsimlu et al., 2013). However, there are limited examples from western Australia, with most research having focused on the far more populous eastern and southeastern Australia (Saha and Zeleke, 2015). Hence, this study will apply the SWAT model to examine the impacts of climate and land use changes on hydrology for a catchment in SWA. The Hargreaves method, using air temperature as input data, was selected to simulate the potential evapotranspiration in the SWAT model (Brown et al., 2015; Reshmidevi et al., 2018). For further model details, see Arnold et al. (1998).

6.2.3 Data preparation

For developing a semi-distributed hydrologic model, various data series are needed as inputs to the SWAT model. Processing of the specific data is described in this section, and the

input data for the SWAT model, sources of the data, and related characteristics of the data are shown in Table 6-1.

Table 6-1 Data input for the SWAT model, data sources, and related characteristics.

Data	Source	Related Characteristics
DEM (Digital elevation model)	Geoscience Australia	1 second resolution SRTM (Shuttle Rader Topography Mission) derived DEM
Land use/land cover map	Australian Bureau of Agricultural and Resource Economics and Sciences (ABARES)	50 m spatial resolution
Soil map	Bureau of rural sciences, Australia	Published at a scale of 1:2,000,000
Observed streamflow	Bureau of Meteorology (BOM)	Mean daily streamflow (1977-2007, 2009-2017)
Observed climate data	BOM	Maximum and minimum daily temperature and rainfall (1974-2017)
Climate data based on 34 GCMs under RCP4.5 and RCP8.5 scenarios	Office of Science, US Department of Energy, downscaled by Liu and Zuo (2012)	Maximum and minimum daily temperature and rainfall (1900-2100)

6.2.3.1 DEM, land use, and soil

DEM, land use, soil, and slope characteristics are basic inputs for HRU (hydrologic response unit) definition in the SWAT model (Roti et al., 2018). The details of data sources adopted in this research are introduced below.

DEM is required by the SWAT model for delineating watershed and generating sub-basins in the Wooroloo Brook catchment (Figure 6-1). In this study, the DEM data were downloaded from Geoscience Australia (https://elevation.fsdf.org.au/) with a resolution of 30 m by 30 m, and 13 sub-basins were generated (Figure 6-1). Sub-basin parameters (e.g. slope gradient and channel length) were obtained from DEM.

Land use is one of the key factors that impacts evapotranspiration and runoff in a basin (Zhang et al., 2014). Land use data with 50 m spatial resolution from ABARES was adopted and reclassified to match the land use classes in the SWAT model (Figure 6-2) in this study. This data was obtained through the integration of fine-scale satellite data, land tenure and other kinds of land use information, and information gathered in the field. There were three land use classes in the study area: FRST (forest-mixed), RNGE (range-grasses), and URBN (urban) (Figure 6-2).

The SWAT model needs a soil map and a soil database which contains multiple soil characteristics such as depth of soil surface to layer bottom, soil bulk density, and saturated hydraulic conductivity for different soil layers (Saha et al., 2014). The soil map was taken from the Digital Atlas of Australian Soil for the Wooroloo Brook catchment (Figure 6-2), and a

"usersoil" database was created according to lookup tables and previous research (McKenzie et al., 2000; Saha et al., 2014).

After DEM, land use, and soil input in the ArcSWAT interface, this study defined 5 slope classes (0-10%, 10-20%, 20-30%, 30-50%, and >50%) for slope discretization. Finally, thresholds of 0%-0%-0% were defined for land use, soil, and slope using a multiple HRU generation approach and 268 HRUs were produced using the ArcSWAT interface.
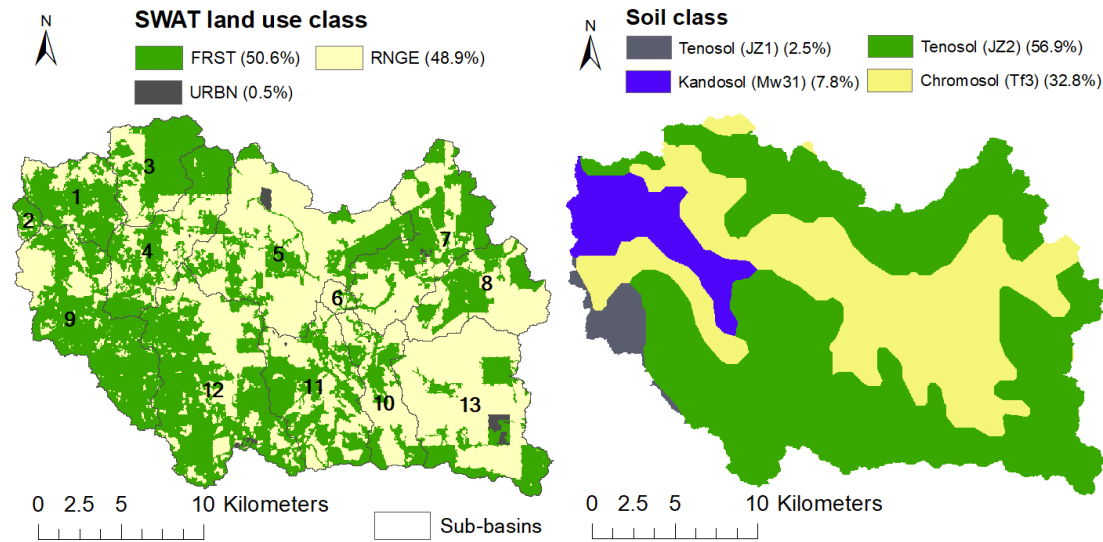
Figure 6-2 The maps of land use classification (left) and soil (right) in the SWAT model for the Wooroloo Brook catchment, SWA.

6.2.3.2 Climate data and streamflow

Daily rainfall and maximum and minimum temperature at 11 weather stations in 1974-2017, used for driving SWAT model simulations, were collected from the Bureau of Meteorology (BOM) (http://www.bom.gov.au/climate/data/). Based on the default settings of SWAT, each sub-basin was assigned a climate station that was nearest to the centroid of the sub-basin (Sirisena et al., 2018). For the calibration and validation of streamflow, daily observed streamflow at the outlet of the catchment was obtained from the BOM (http://www.bom.gov.au/waterdata/). To set model parameters for a great variety of climatic conditions, a period for streamflow calibration including dry, normal, and wet years was chosen in this study. Therefore, the periods of 1992-2017 (1989-1991 as warm-up, streamflow for 2008 was missing) and 1977-1991 (1974-1976 as warm-up) were selected for streamflow calibration and validation, respectively.

6.2.4 Calibration and evaluation methods for the SWAT model

The program Sequential Uncertainty Fitting Ver. 2 (SUFI-2) (Abbaspour et al., 2007) in SWAT Calibration and Uncertainty Programs (SWAT-CUP) was chosen for the SWAT model

parameters calibration, validation, and uncertainty analysis in this study. The sensitivity of 22 parameters in the SWAT model was ranked using the global sensitivity analysis approach available in SUFI-2. The smaller the p-value and the larger the absolute value of t-stat, the more sensitive is the parameter (Abbaspour, 2013).

In this research, the results for climatic and hydrologic variables all were shown at monthly or annual time scales, so the modelling process would be more efficient with streamflow calibrated at a monthly rather than a daily time scale. Thus, monthly simulated and observed streamflow in 1992-2017 (2008 was missing) and 1977-1991 were used for the SWAT model calibration and validation, respectively. By using the SUFI-2 procedure, 4 iterations with 1000 model runs in each iteration were run to maximize Nash-Sutcliffe Efficiency (NSE) (Nash and Sutcliffe, 1970). Percent bias (PBIAS), NSE, and coefficient of determination (R^2) were selected as statistical evaluation criteria (Shi et al., 2011) in this study and were calculated as follows:

$$PBIAS = 100\left(\frac{\sum_{i=1}^{N}(Q_{sim,i}-Q_{obs,i})}{\sum_{i=1}^{N}(Q_{obs,i})}\right) \tag{1}$$

$$NSE = 1 - \frac{\sum_{i=1}^{N}(Q_{obs,i}-Q_{sim,i})^2}{\sum_{i=1}^{N}(Q_{obs,i}-\bar{Q}_{obs})^2} \tag{2}$$

$$R^2 = \frac{\left[\sum_{i=1}^{N}(Q_{obs,i}-\bar{Q}_{obs})(Q_{sim,i}-\bar{Q}_{sim})\right]^2}{\sum_{i=1}^{N}(Q_{obs,i}-\bar{Q}_{obs})^2 \sum_{i=1}^{N}(Q_{sim,i}-\bar{Q}_{sim})^2} \tag{3}$$

where i is the ith sample; N is the number of samples; Q_{sim} and Q_{obs} are simulated and observed monthly streamflow (m³/s), respectively; $\bar{Q}_{sim}$ and $\bar{Q}_{obs}$ are the average simulated and observed monthly streamflow (m³/s), respectively.

6.2.5 Statistical downscaling method

Using the statistical downscaling method NWAI-WG (Liu and Zuo, 2012), gridded climate data from GCMs at monthly time scale were downscaled to the weather stations at daily time scale. First, an inverse distance-weighted interpolation approach was applied to downscale the monthly GCMs climate data to specific sites. A bias correction then was used to correct monthly GCM simulations for each station. Third, a stochastic weather generator was used to generate daily climatic variables for each station. The validation conducted by Liu and Zuo (2012) indicated that this downscaling approach can well reproduce the observed climate data at daily, monthly, and yearly time scales. In this research, a post downscaling treatment was applied to the NWAI-WG model downscaled climate data. When applying downscaled data to a catchment, the existence of inconsistent daily rainfalls among stations could lead to: 1) more rainfall days and 2) less daily rainfall for the catchment and possibly poor modelling of high flows. Therefore, the central station of the catchment was selected as the reference station and

other 10 stations were re-downscaled to have the matching rainfall events with the rainfall quantities for each station. This post downscaling treatment is validated according to the hypothesis that the climate stations are near enough so that the rainfall days are quite uniform. This study area is about 515 km^2, that is, the radius is around 12.8 km. Therefore, this catchment downscaling approach was considered valid for this study.

In this study, 34 GCMs (Wang et al., 2019) from the Coupled Model Inter-comparison Project 5 (CMIP5) were used to minimize the uncertainty created by the selection of GCMs. Two RCPs (representative concentration pathways) were selected to represent the likely future greenhouse gas concentrations with RCP 4.5 and RCP 8.5 represent intermediate and high emission scenarios, respectively (Shrestha et al., 2017). In this research, the period of 1977-2016 was defined as the baseline, 2021-2060 was defined as the near future, or 2040s, and 2061-2100 as the far future, or 2080s. To show the range of future climate projections, changes at seasonal and annual time scales in maximum and minimum temperature and rainfall of 34 GCMs in 2040s and 2080s compared to the baseline period were calculated for this catchment. Furthermore, to provide the range of future hydrologic projection, changes in runoff, actual evapotranspiration (ET), and soil water (SW) at seasonal and annual time scales of 34 GCMs in the 2040s and 2080s compared to the baseline were estimated.

6.2.6 Different land use change scenarios

In this catchment, there were three land use classes (i.e., forest-mixed (50.6%), range-grasses (48.9%) and urban (0.5%)) based on SWAT land use classes reclassification. To assess hydrologic response to land use change in the catchment, four land use change scenarios (Table 6-2) were considered, based on present land use conditions and possible future land use plans. The present land use (Figure 6-2) is hereafter mentioned as LU0 (land use 0) and the four land use change scenarios are mentioned as LU1-4 (land use 1-4). The Land Use Update tool in the SWAT model was used to implement these changes at the sub-basin scale (Marhaento et al., 2017). For example, FRST is expected to be changed to URBN only when the two land use classes occur in the same sub-basin (Shrestha et al., 2017). LU1 assumes that 50% of current FRST will be converted to RNGE with the remaining land uses stay unchanged, representing a 25.3% increase in RNGE area over the whole catchment. The details of other land use change scenarios can be found in Table 6-2, and land use proportions for LU0-4 are shown in Table 6-3.

Table 6-2 The four land use change scenarios based on LU0 (i.e. forest-mixed (50.6%), range-grasses (48.9%) and urban (0.5%)) in the Wooroloo Brook catchment, southwestern Australia.

	LU1	Deforestation	Assumes that 50% of current FRST will be changed to RNGE while the remaining land uses stay unchanged, i.e. 25.3% increase of RNGE area
	LU2	Urbanization /deforestation	Assumes that 100% of current FRST will be converted to URBN while the remaining land uses stay unchanged, i.e. 23.8% increase of URBN area
	LU3	Afforestation	Assumes that 50% of current RNGE will be changed to FRST while the remaining land uses stay unchanged, i.e. 24.4% increase of FRST area
	LU4	Urbanization	Assumes that 100% of current RNGE will be converted to URBN while the remaining land uses stay unchanged, i.e. 29.5% increase of URBN area

Table 6-3 Land use proportions for LU0-4 in the Wooroloo Brook catchment, western Australia.

	LU0	LU1	LU2	LU3	LU4
FRST	50.6%	25.3%	26.8%	75.0%	50.6%
RNGE	48.9%	74.2%	48.9%	24.5%	19.4%
URBN	0.5%	0.5%	24.3%	0.5%	30.0%

6.2.7 Contribution analysis of uncertainty

In uncertainty analysis, the analysis of variance (ANOVA) method has been widely adopted to estimate the contribution of various sources (Aryal et al., 2019; Shi et al., 2020). In this study, a three-way ANOVA (three factors) was used to calculate the contribution of GCM, RCP, and land use scenarios (LU) to the uncertainty in future changes of runoff, ET, and soil water. The three-way ANOVA could be divided into seven parts with three main effects and four interaction effects. Thus, the total sum of squares (SST) was quantified as:

$$SST = SS_{GCM} + SS_{RCP} + SS_{LU} + SS_{GCM:RCP} + SS_{GCM:LU} + SS_{RCP:LU} + SS_{GCM:RCP:LU} \quad (4)$$
$$\underbrace{\qquad\qquad}_{\text{main}} \qquad \underbrace{\qquad\qquad\qquad\qquad}_{\text{interaction terms}}$$

6.3 Results

6.3.1 Streamflow simulation

For streamflow calibration, 22 parameters of the SWAT model were calibrated, validated, and ranked for the Wooroloo Brook catchment (Table 6-4). Global sensitivity analysis in SWAT-CUP was used to rank these parameters based on their sensitivities. The sensitivity analysis indicated that 6 parameters (ranked 1-6, Table 6-4) had significant impacts on calibration of the SWAT model ($P \leq 0.05$). In this catchment, SCS runoff curve number for moisture condition II (CN2) was found to be the most sensitive calibration parameter. The comparison between monthly simulated and observed streamflow during calibration and validation is shown in Figure 6-3. A visual comparison suggests that the simulations reasonably reproduced the observed streamflow and similarly replicated its temporal fluctuation. Figure 6-4 indicates that monthly simulated and observed runoff had a high correlation (NSE $\geq$ 0.86, R^2

≥ 0.87, and |PBIAS| ≤ 8.3%) in model calibration and validation in the Wooroloo Brook catchment.

Table 6-4 The parameters calibrated and ranked in this study for the SWAT model using SWAT-CUP in the Wooroloo Brook catchment, SWA.

Ranking	Adjustment and parameter name	Definition	Adjustment range	Calibrated range	Fitted value
1	R__CN2.mgt	SCS runoff curve number for moisture condition II	-0.25 to 0.35	-0.35 to 0.05	-0.16
2	V__GWQMN.gw	Threshold water level in shallow aquifer for base flow (mm)	0 to 3000	300 to 2500	2035
3	R__SOL_AWC(1).sol	Available water capacity of the soil layer	-0.3 to 0.4	-0.24 to 0.19	-0.19
4	V__ESCO.hru	Soil evaporation compensation factor	0 to 1	0.45 to 1	0.57
5	R__CANMX.hru	Maximum canopy storage	0 to 150	0 to 100	16.4
6	V__RCHRG_DP.gw	Deep aquifer percolation fraction	0 to 0.2	0 to 0.1	0.083
7	R__HRU_SLP.hru	Average slope steepness	-0.3 to 0.3	0.05 to 0.45	0.14
8	R__SLSUBBSN.hru	Average slope length	-0.25 to 0.6	-0.2 to 0.37	0.29
9	V__CH_K2.rte	Effective hydraulic conductivity of main channel	0 to 200	43.54 to 147.9	46.5
10	V__GW_REVAP.gw	Groundwater revap coefficient	0.02 to 0.2	0.025 to 0.11	0.076
11	V__REVAPMN.gw	Threshold depth of water in the shallow aquifer for revap to occur (mm)	0 to 500	0 to 287.4	275.5
12	V__GW_DELAY.gw	Groundwater delay (days)	0 to 150	0 to 31	3.37
13	R__SOL_AWC(2).sol	Available water capacity of the soil layer	-0.3 to 0.4	-0.12 to 0.31	0.19
14	R__OV_N.hru	Manning's n value for overland flow	-0.3 to 0.3	-0.14 to 0.17	0.094
15	V__SURLAG.bsn	Surface runoff lag time	0.05 to 6	2.14 to 5	2.84
16	R__SOL_Z(2).sol	Depth from soil surface to bottom of second soil layer	-0.1 to 0.1	-0.07 to 0.07	0.039
17	R__SOL_Z(1).sol	Depth from soil surface to bottom of first soil layer	-0.1 to 0.1	-0.11 to 0.03	0.006
18	V__CH_N2.rte	Manning's n value for the main channel	0.014 to 0.15	0.01 to 0.083	0.025
19	V__ALPHA_BNK.rte	Baseflow alpha factor for bank storage	0.03 to 0.9	0.15 to 0.7	0.16

20	V__EPCO.hru	Plant uptake compensation factor	0.3 to 1	0.48 to 0.83	0.57
21	V__ALPHA_BF.gw	Baseflow alpha factor (days)	0 to 0.5	0 to 0.7	0.54
22	V__CH_N1.sub	Manning's n value for the tributary channels	0.014 to 0.15	0.028 to 0.11	0.096
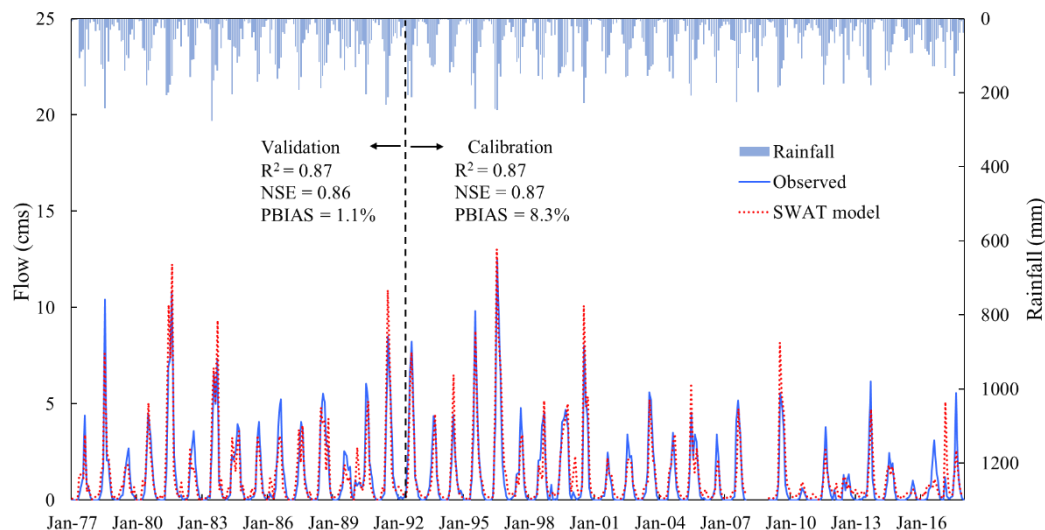
Figure 6-3 The simulated and observed monthly streamflow for calibration (January 1992 to December 2017, data for 2008 are missing) and validation (January 1977 to December 1991) in the Wooroloo Brook catchment, SWA.
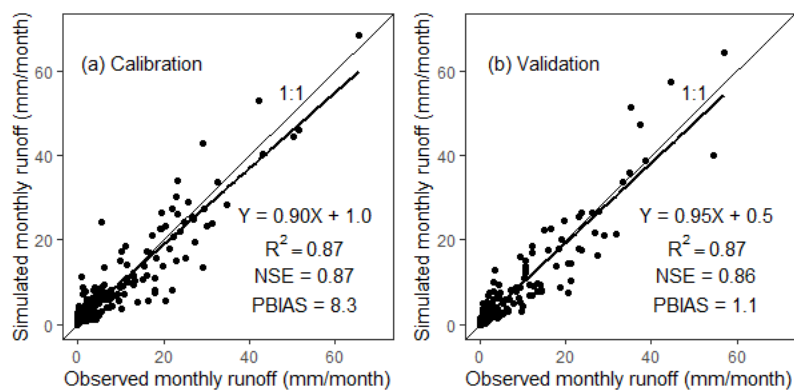
Figure 6-4 Correlation of monthly simulated and observed runoff in model calibration and validation in the Wooroloo Brook catchment, southwestern Australia.

6.3.2 Hydrologic response to land use change

Monthly runoff, actual evapotranspiration, and soil water were simulated using the calibrated SWAT under LU0-4, in 1977-2016, for the Wooroloo Brook catchment. Figure 6-5 displays seasonal runoff, ET, and SW under land use 0-4 while Table 6-5 shows changes in annual runoff, ET, and SW under LU0-4. There were clear seasonal variations for runoff, ET, and SW, with values greatest in winter (wet season) and least in summer (dry season) (Figure

6-5). Moreover, in Figure 6-5, seasonal changes of runoff under LU1-4 were generally more remarkable than changes of ET and SW, especially in winter. In addition, Figure 6-5 suggests that seasonal runoff increased under LU1-2 and LU4 (deforestation or urbanization) while decreased under LU3 (afforestation), and the same result for annual runoff could be found in Table 6-5. For example, runoff increased by 4 mm (6%) under LU1 (25.3% increase in RNGE from FRST), 17 mm (22.8%) under LU2 (23.8% increase in URBN from FRST), and 18 mm (25.1%) under LU4 (29.5% increase in URBN from RNGE) using the SWAT model. In comparison, a 24.4% increase in FRST area from RNGE (LU3) caused a -3 mm (-4.3%) decrease in runoff. In contrast to runoff, Table 6-5 shows that mean annual actual evapotranspiration decreased under LU1-2 and LU4 (deforestation or urbanization), while increased under LU3 (afforestation). In addition, the percentage changes of annual ET were much smaller than that of runoff under LU1-4 (Table 6-5). For instance, average annual ET decreased by -6 mm (-1.0%) with a 25.3% decline in FRST (LU1) and increased by 5 mm (0.9%) with a 24.4% increase in FRST area (LU3) using SWAT. Furthermore, mean annual soil water increased by 4.4% under LU1 (25.3% increase in RNGE from FRST) and very little (≤0.2%) under LU2 (23.8% increase in URBN from FRST), while decreased by -4.2% under LU3 (24.4% increase in FRST from RNGE) and -4.6% under LU4 (29.5% increase in URBN from RNGE) using SWAT.

Table 6-5 Changes in mean annual runoff, actual evapotranspiration, and soil water using the SWAT model under LU0-4 in the Wooroloo Brook catchment, southwestern Australia in 1977-2016.

	Hydrologic variables	LU0	LU1	LU2	LU3	LU4
	Value (mm)	73	77	90	70	91
Runoff	Absolute change (mm)	0	4	17	-3	18
	Percentage change (%)	**0.0**	**6.0**	**22.8**	**-4.3**	**25.1**
	Value (mm)	568	562	558	573	561
ET	Absolute change (mm)	0	-6	-10	5	-7
	Percentage change (%)	**0.0**	**-1.0**	**-1.8**	**0.9**	**-1.3**
	Value (mm)	26.6	27.7	26.6	25.4	25.3
SW	Absolute change (mm)	0.0	1.2	0.0	-1.1	-1.2
	Percentage change (%)	**0.0**	**4.4**	**0.2**	**-4.2**	**-4.6**
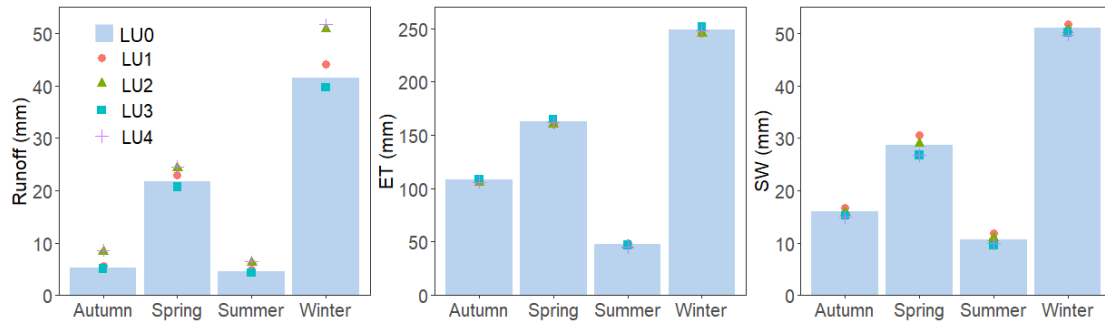
Figure 6-5 Seasonal runoff, ET, and SW in 1977-2016 under land use 0-4 in the Wooroloo Brook catchment, SWA.

6.3.3 Projected changes in climatic variables

Future temperature and rainfall projections were aggregated to seasonal and annual time scales and compared to baseline values (Figure 6-6). In this study, all 34 GCMs were in agreement that the temperature would rise in the future, with greater temperature increases in the 2080s than in the 2040s at both seasonal and annual time scales (Figure 6-6). In addition, higher temperature increases were projected under RCP8.5 than RCP4.5 (Figure 6-6). Figure 6-6a-b shows that seasonal maximum temperature was mainly predicted to increase most in spring in the future (the median increase was 1.3 °C (1.0–1.4 °C) in 2040s (RCP 4.5), 1.6 °C (1.3–1.8 °C) in 2040s (RCP 8.5), 1.9 °C (1.6–2.2 °C) in 2080s (RCP 4.5), and 3.9 °C (3.1–4.4 °C) in 2080s (RCP 8.5)), while increases were mainly lowest in winter (1.0 °C (0.8–1.1 °C) in 2040s (RCP 4.5), 1.2 °C (1.0–1.4 °C) in 2040s (RCP 8.5), 1.5 °C (1.3–1.7 °C) in 2080s (RCP 4.5), and 3.0 °C (2.7–3.6 °C) in 2080s (RCP 8.5)). The uncertainty range, in brackets, shows the 25th and 75th percentage of the 34 GCMs in this study. For temperature minima (Figure 6-6c-d), the median estimate exhibited the largest increase mainly in autumn (1.0 °C (0.8–1.2 °C) in 2040s (RCP 4.5), 1.3 °C (0.9–1.6 °C) in 2040s (RCP 8.5), 1.5 °C (1.3–2.1 °C) in 2080s (RCP 4.5), and 3.4 °C (2.9–4.2 °C) in 2080s (RCP 8.5)), and the smallest increase in minimum temperature in winter (0.9 °C (0.7–1.1 °C) in 2040s (RCP 4.5), 1.1 °C (0.9–1.3 °C) in 2040s (RCP 8.5), 1.4 °C (1.2–1.7 °C) in 2080s (RCP 4.5), and 3.0 °C (2.6–3.4 °C) in 2080s (RCP 8.5)). The ensemble median increase for annual maximum temperature was 1.1 °C (1.0–1.3 °C) in 2040s (RCP 4.5), 1.3 °C (1.2–1.5 °C) in 2040s (RCP 8.5), 1.8 °C (1.5–1.9 °C) in 2080s (RCP 4.5), and 3.4 °C (2.9–3.9°C) in 2080s (RCP 8.5) (Figure 6-6a-b), while the annual minimum temperature was projected to increase by 1.0 °C (0.8–1.1 °C) in 2040s (RCP 4.5), 1.2 °C (1.1–1.5 °C) in 2040s (RCP 8.5), 1.6 °C (1.3–1.9 °C) in 2080s (RCP 4.5), and 3.2 °C (2.9–3.7°C) in 2080s (RCP 8.5) (Figure 6-6c-d).

Future rainfall changes vary across seasons and across GCMs, with most GCMs projecting decreases at both seasonal and annual time scales (Figure 6-6e-f). Future rainfall decreased

more in spring and winter while decreased less in summer and autumn under both RCPs. The largest ensemble median decrease in rainfall occurred in spring (-10.4 % (-17.7 to -6.2 %) in 2040s (RCP 4.5), -16.2 % (-23.0 to -8.1 %) in 2040s (RCP 8.5), -17.1 % (-26.4 to -10.6 %) in 2080s (RCP 4.5), and -35.9 % (-43.2 to -25.8 %) in 2080s (RCP 8.5)), while median summer (-3.9 % (-11.1 to 14.1 %) in 2040s (RCP 4.5), -2.2 % (-13.6 to 11.1 %) in 2040s (RCP 8.5), -0.1 % (-18.5 to 17.9 %) in 2080s (RCP 4.5), and -0.3 % (-18.1 to 25.9 %) in 2080s (RCP 8.5)) rainfall was predicted to have the smallest future changes (Figure 6-6e-f). At annual time scale in 2040s, the decreases in rainfall projected by the 34 GCMs ranged from -12.4 % (25th percentage) to -3.3 % (75th percentage) under RCP 4.5 and -14.6 % (25th percentage) to -6.9 % (75th percentage) under RCP 8.5 with the ensemble median of -8.7 % and -11.0 %, respectively. More decreases were projected for annual rainfall in 2080s with -11.7 % (-15.3 to -7.9 %) under RCP 4.5, and -22.6 % (-32.9 to -16.2 %) under RCP 8.5.
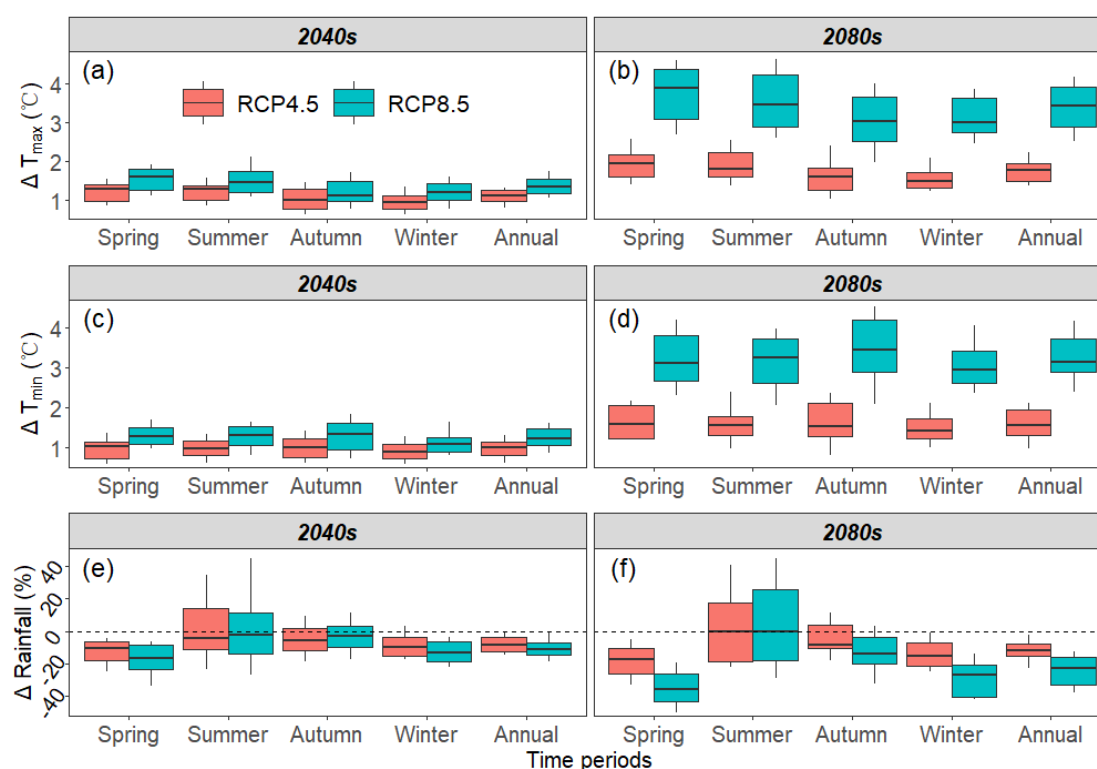
Figure 6-6 Projected seasonal and annual changes in temperature (°C) and rainfall (%) in 2040s and 2080s under both RCPs based on 34 GCMs compared to the baseline period. Data displayed are changes of 40-year averages for each of the 34 GCMs. The lower and upper whiskers show the 10th and 90th percentiles; box boundaries show the 25th and 75th percentiles; the black line within each box marks the median values.

6.3.4 Hydrologic responses to future climate change

Projected runoff, ET, and SW were aggregated into seasonal and annual time scales, and were compared to the baseline values. Similar to rainfall, changes in future runoff differ across

seasons and across GCMs, with most GCMs exhibiting decreases at both seasonal and annual time scales (Figure 6-7-LU0). Future runoff was projected to decrease more in winter and spring but decreasing less in autumn and summer under both RCPs. Also, annual runoff in 2080s decreased more than those predicted in the 2040s, and annual runoff also showed more decreases under RCP8.5 than RCP4.5 (Figure 6-7). The largest runoff, which was in winter in baseline (Figure 6-5), was predicted to decrease most (-20.6 % (-35.3 to 6.4 %) in 2040s (RCP 4.5), -41.2 % (-51.5 to -11.8 %) in 2080s (RCP 4.5), and -62.3 % (-73.2 to -49.6 %) in 2080s (RCP 8.5)) among the four seasons except in 2040s (RCP 8.5) when runoff decreased the most in spring (-34.0 % (-40.6 to -2.5 %)). In addition, runoff was projected to decline least (-12.5 % (-28.9 to 6.2 %) in 2040s (RCP 8.5), -11.1 % (-33.1 to 9.5 %) in 2080s (RCP 4.5), and -31.1 % (-44.1 to -3.6 %) in 2080s (RCP 8.5)) in autumn among the four seasons except in 2040s (RCP4.5) when runoff decreased the least in summer (-3.2 % (-23.8 to 13.9 %)). Annual runoff changes projected by the 34 GCMs in 2040s varied from -31.6% (25th percentage) to 3.2 % (75th percentage) under RCP 4.5 and -39.1 % (25th percentage) to -4.1% (75th percentage) under RCP 8.5 with the median values of -19.4 % and -28.3 %, respectively. More decreases were projected for annual runoff in 2080s with -33.6 % (-45.0 to -14.4 %) under RCP 4.5, and -55.3 % (-68.1 to -41.2 %) under RCP 8.5.

For actual evapotranspiration (ET), the majority of the 34 GCMs simulating decreases at both seasonal and annual time scales except in autumn in 2040s (Figure 6-8-LU0). The changes of ET were smaller than the simulated changes of runoff (Figures 7-8). In autumn in 2040s, ET was projected to increase by 2.2 % (-5.2 to 6.4 %) under RCP 4.5 and 3.0 % (-3.8 to 7.6 %) under RCP 8.5 according to ensemble median of the GCMs. At seasonal time scales (Figure 6-8-LU0), future ET was predicted to decrease most in spring (-11.3 % (-14.4 to -6.8 %) in 2040s (RCP 4.5), -15.1 % (-19.0 to -9.9 %) in 2040s (RCP 8.5), -16.1 % (-21.7 to -11.9 %) in 2080s (RCP 4.5), and -32.8 % (-38.6 to -24.8 %) in 2080s (RCP 8.5)). At annual time scale in 2040s, changes of ET simulated by the 34 GCMs varied from -7.8 % (25th percentage) to -3.5 % (75th percentage) under RCP 4.5 and -10.0 % (25th percentage) to -3.5 % (75th percentage) under RCP 8.5 with the median values of -5.1 % and -6.0 %, respectively (Figure 6-8-LU0). More decreases were projected for annual ET in 2080s with -7.5 % (-10.1 to -4.5 %) under RCP 4.5, and -15.8 % (-23.5 to -9.0 %) under RCP 8.5. In addition, median estimates suggested that there was a trend of decreasing soil water at seasonal and annual time scales in both future periods under both RCPs (Figure 6-9-LU0). Furthermore, ensemble median showed decreases of -15.0 % (-17.9 to -10.1 %) in 2040s (RCP4.5), -16.0 % (-20.1 to -11.3 %) in 2040s (RCP8.5), -17.7 % (-22.3 to -12.2 %) in 2080s (RCP4.5) and -30.0 % (-39.8 to -21.0 %) in 2080s (RCP8.5).
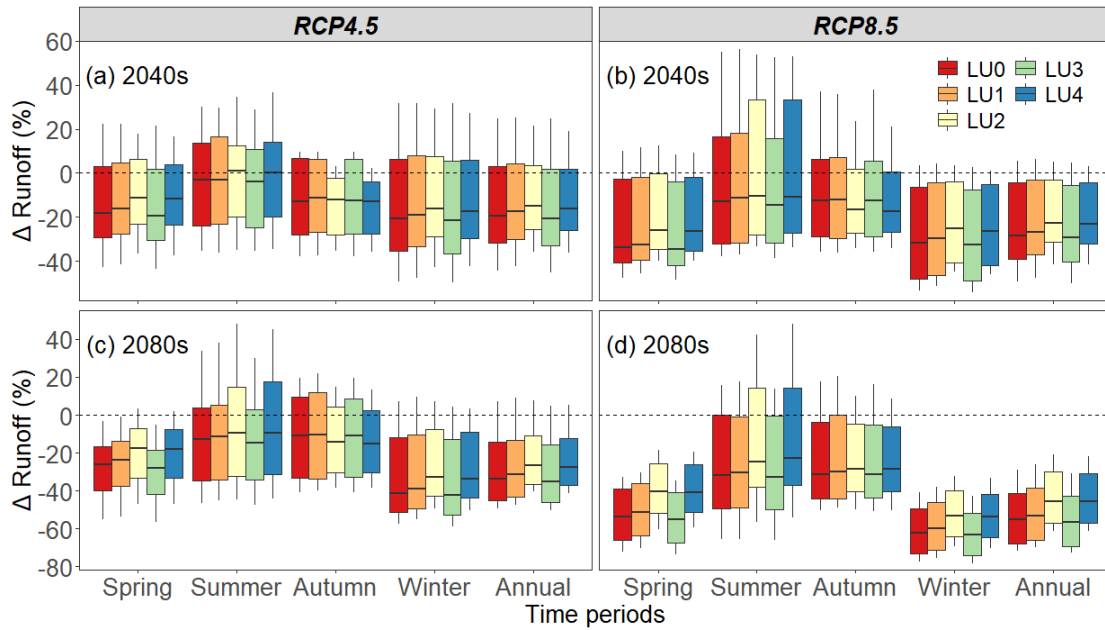
Figure 6-7 Projected seasonal and annual changes in runoff (%) for LU0-LU4 in the 2040s and 2080s under both RCPs estimated from 34 GCMs compared to the baseline period. Data displayed are changes of 40-year averages for each of the 34 GCMs. The lower and upper whiskers show the 10th and 90th percentiles; box boundaries show the 25th and 75th percentiles; the black line within each box marks the median values.
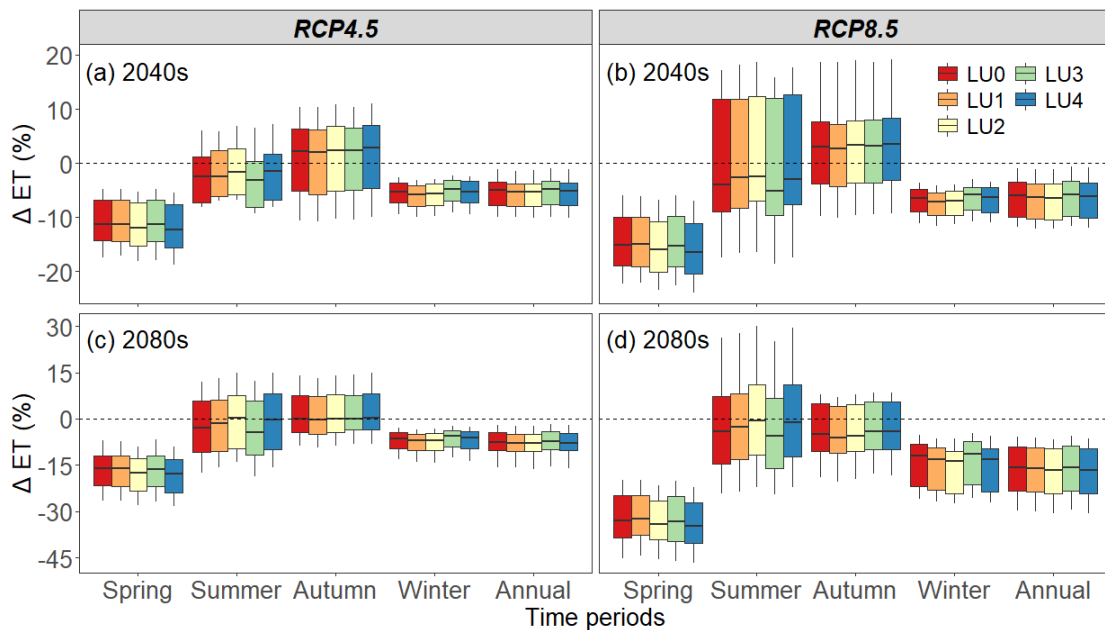
Figure 6-8 Projected seasonal and annual changes in ET (%) for LU0-LU4 in the 2040s and 2080s under both RCPs estimated from 34 GCMs compared to the baseline period. Data displayed are changes of 40-year averages for each of the 34 GCMs. The lower and upper whiskers show the 10th and 90th percentiles; box boundaries show the 25th and 75th percentiles; the black line within each box marks the median values.
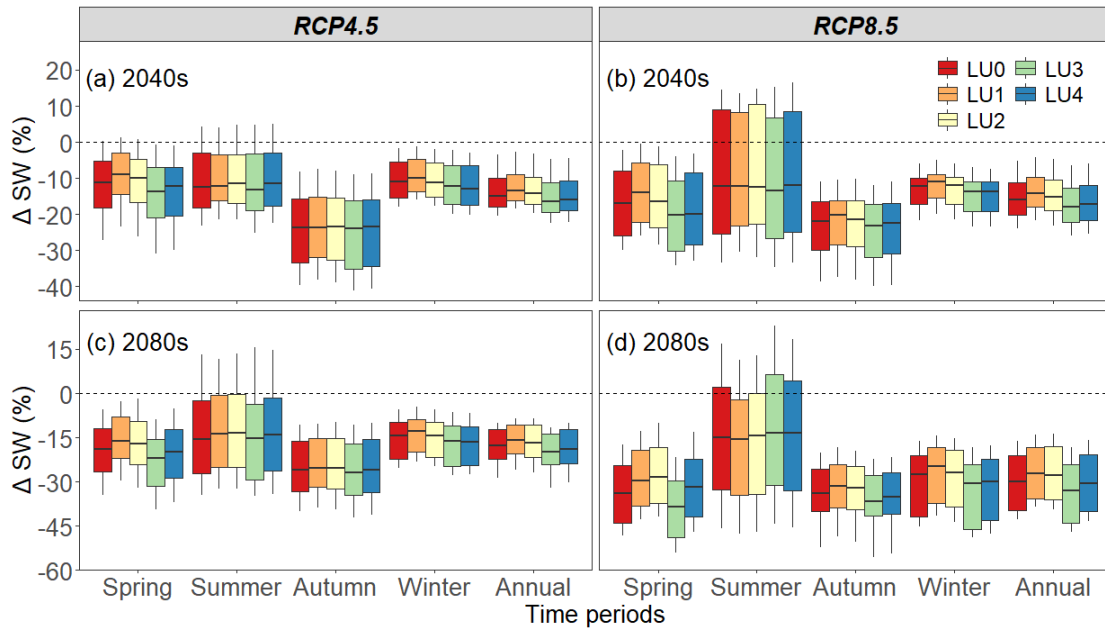
Figure 6-9 Projected seasonal and annual changes in soil water (%) for LU0-LU4 in the 2040s and 2080s under both RCPs estimated from 34 GCMs compared to the baseline period. Data displayed are changes of 40-year averages for each of the 34 GCMs. The lower and upper whiskers show the 10th and 90th percentiles; box boundaries show the 25th and 75th percentiles; the black line within each box marks the median values.

6.3.5 Combined effects of climate and land use changes

Under different land use change scenarios (LU1-4), projected changes in seasonal and annual runoff, ET, and SW in 2040s and 2080s compared with baseline values under both RCPs from the 34 GCMs are shown in Figures 6-7, 6-8, and 6-9. According to the ensemble median of the 34 GCMs, the results of the four land use change scenarios (LU1-4) were only slightly different from the responses to LU0 (Figures 6-7, 6-8, and 6-9). For instance, the ensemble median under LU2 (23.8% increase in URBN from FRST) and LU4 (29.5% increase in URBN from RNGE) showed slightly smaller annual runoff decrease than other land use scenarios (Figure 6-7). In addition, the ensemble median under LU3 (24.4% increase in FRST from RNGE) generally suggested marginally less annual ET decrease than other land use scenarios (Figure 6-8). Furthermore, the annual soil water decrease was slightly less under LU1 (25.3% increase in RNGE from FRST) and slightly larger under LU3 (24.4% increase in FRST from RNGE) than other land use scenarios, according to the ensemble median of the 34 GCMs (Figure 6-9).

Figures 6-10, 6-11, and 6-12 show the projected change in runoff, ET, and SW for each combination of the 34 GCMs under both RCPs and different land use scenarios (LU0-4), in both future time periods compared with baseline at annual time scale. For the same GCM in the

same future period under the same RCP, nearly all the five land use scenarios (LU0-LU4) agreed on the direction of the change signal (Figures 6-10, 6-11, and 6-12). For instance, the climate model MI4 (RCP 4.5) showed a similar negative runoff change under LU0 (-18.9 %), LU1 (-17.0 %), LU2 (-14.6 %), LU3 (-20.4 %), and LU4 (-16.1 %) in 2040s (Figure 6-10a). However, the direction of the change signal might be different for different land use scenarios under the same GCM when runoff changes (mm) were too small. For example, the climate model CE2 (RCP8.5) showed a positive runoff change (3.3 %) under LU1 in 2040s while showing a negative runoff change under LU4 (-1.4 %) (Figure 6-10b). Besides, the directions of the change signal for different GCMs were quite different under the same land use scenario (Figures 6-10, 6-11, and 6-12). For instance, for the same land use (e.g. LU0), 9 GCMs showed a trend of increases for future runoff with the largest increase of 41.3 % (CE2), while 25 GCMs showed decreasing values with the largest decrease of -57.7 % (GF2) in 2040s under RCP 4.5 (Figure 6-10a). In addition, for the same future period (e.g. 2040s), generally more GCMs showed decreasing values for runoff, ET, and SW under RCP 8.5 than that under RCP 4.5 (Figures 6-10, 6-11, and 6-12). Furthermore, almost all GCMs showed decreasing soil water values in the future under both RCPs, and LU3 (24.4% increase in FRST from RNGE) decreased more than other land use scenarios (Figure 6-12).

To quantify the contribution of GCM, RCP, and LU to the uncertainty in future changes of water balance, the ANOVA method was used and the results are presented in Figure 6-13. The ANOVA shows that GCMs have the greatest contribution to uncertainty, followed by RCPs, and the land use scenarios have the least contribution to future changes of runoff, ET, and SW. For instance, ANOVA (Figure 6-13) shows a 48.5 % influence of the GCM, followed by RCP (30.4 %), whereas LU had a negligible impact of 1.08 % on changes of runoff.
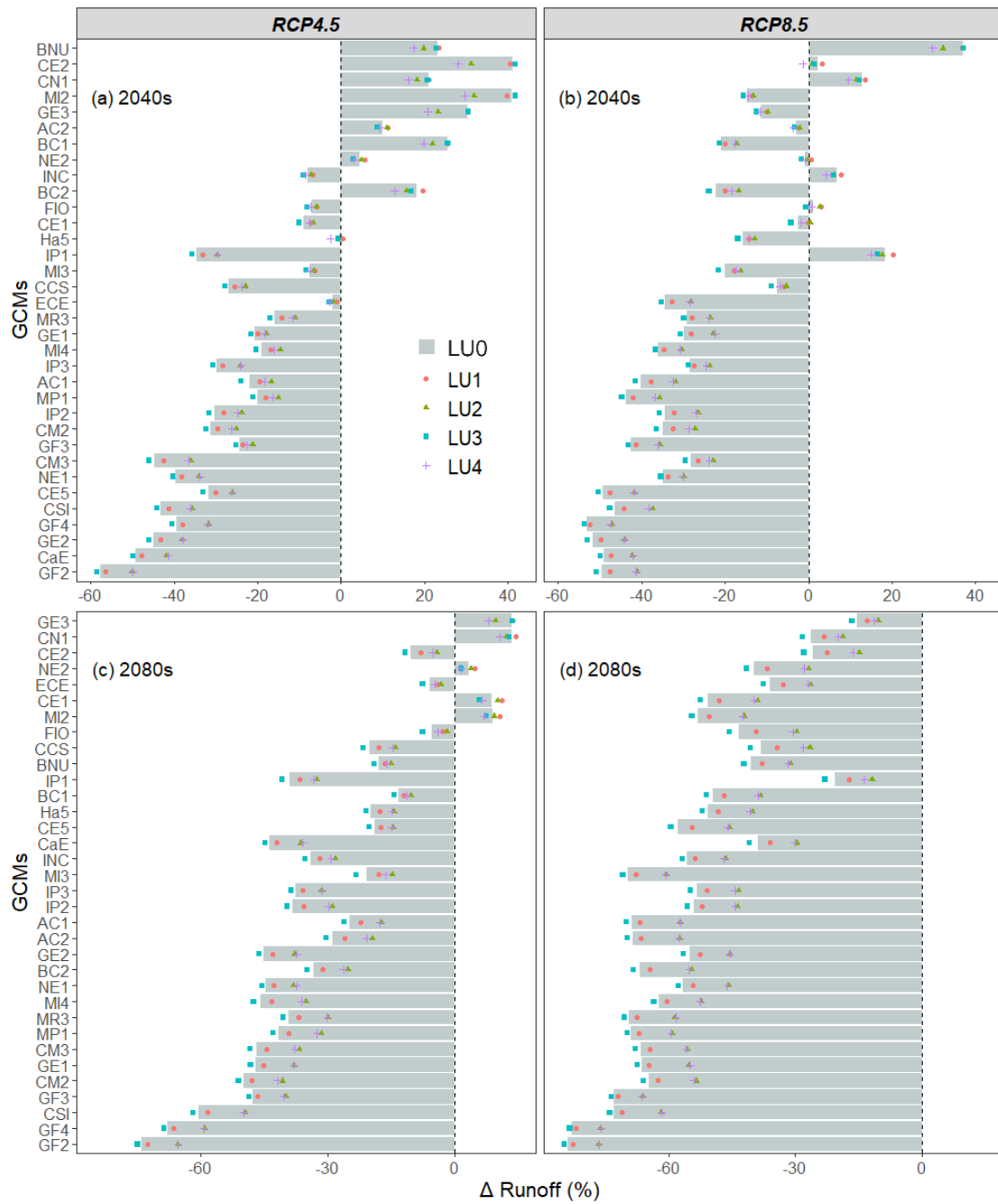
Figure 6-10 Projected changes in runoff (%) for 34 GCMs (RCP4.5 and RCP8.5) and LU0-4 in 2040s and 2080s compared to the baseline values at annual time scale. Data showed are changes in the 40-year average values for each of the 34 GCMs under different land use scenarios.
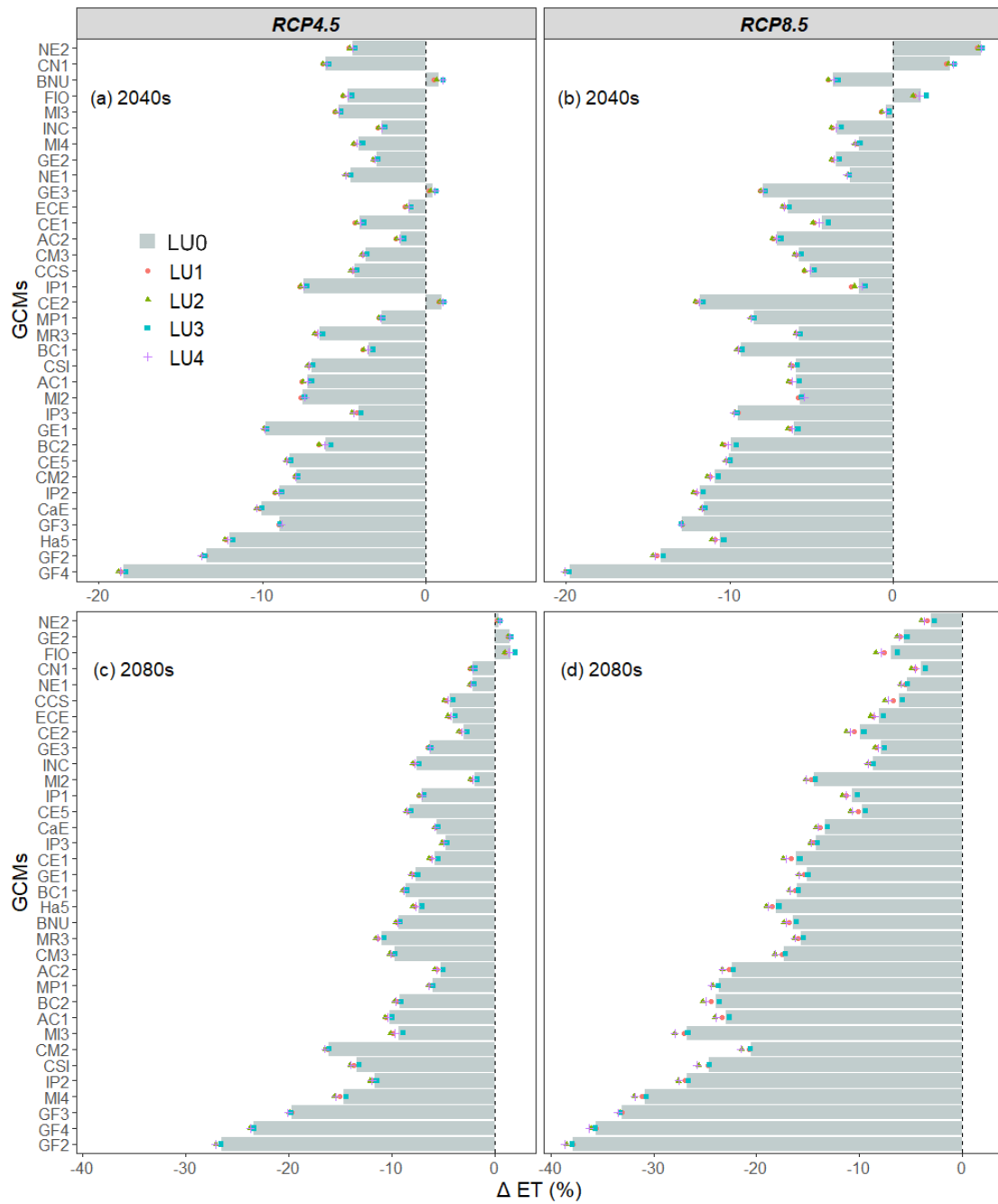
Figure 6-11 Projected changes in actual evapotranspiration (%) for 34 GCMs (RCP4.5 and RCP8.5) and LU0-4 in 2040s and 2080s compared to the baseline values at annual time scale. Data showed are changes in the 40-year average values for each of the 34 GCMs under different land use scenarios.
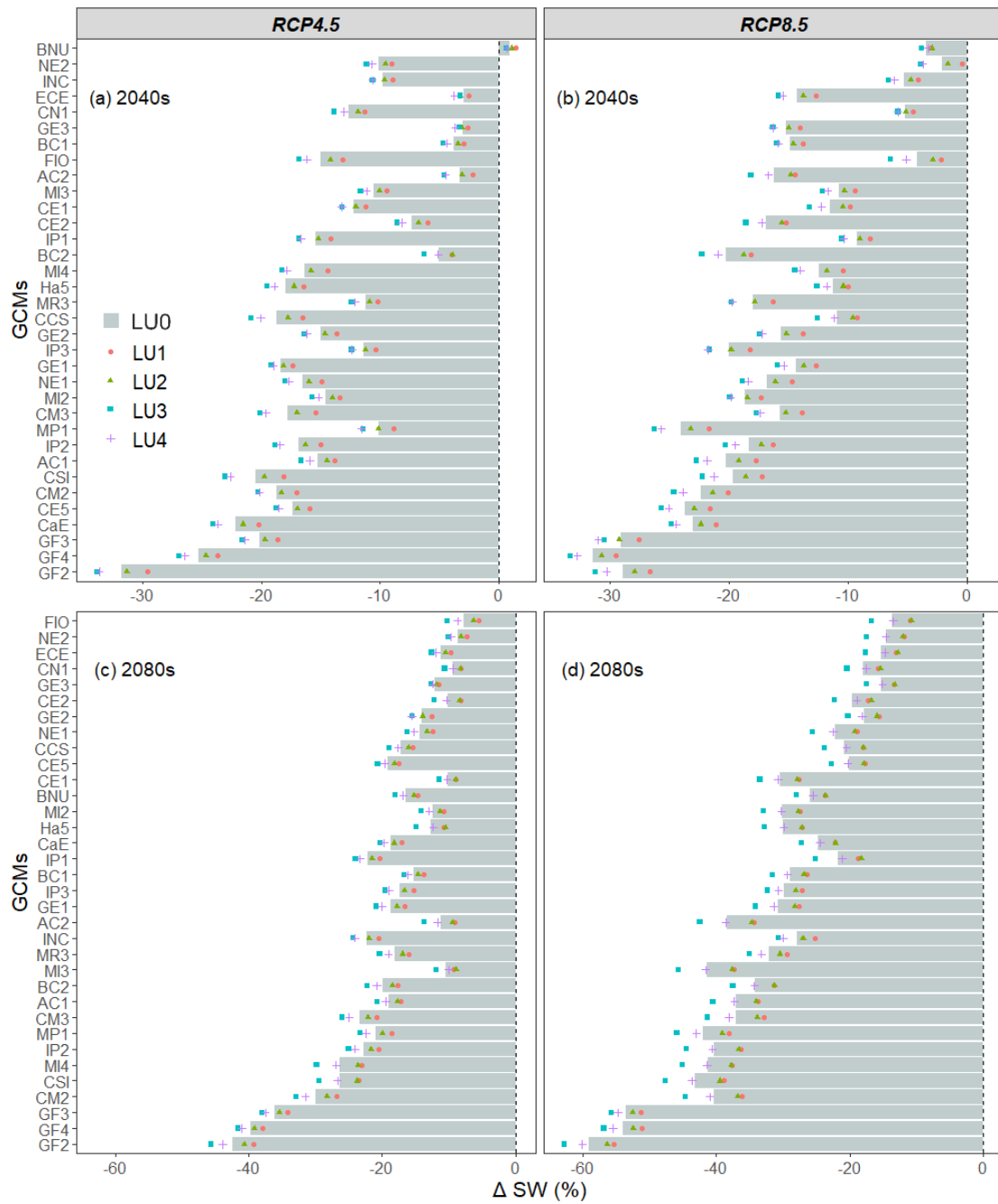
Figure 6-12 Projected changes in soil water (%) for 34 GCMs (RCP4.5 and RCP8.5) and LU0-4 in 2040s and 2080s compared to the baseline values at annual time scale. Data showed are changes in the 40-year average values for each of the 34 GCMs under different land use scenarios.
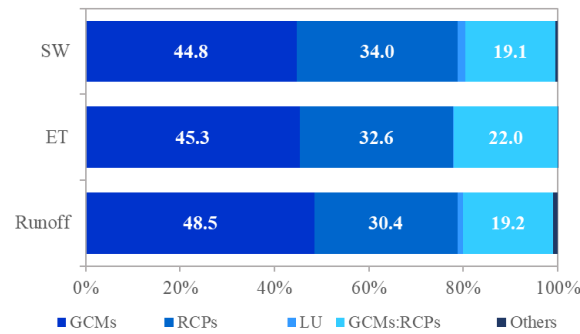
Figure 6-13 The contribution of uncertainty sources to the percentage change of annual runoff, ET, and SW using ANOVA.

6.4 Discussion

6.4.1 SWAT modelling assessment

CN2 was ranked as the most sensitive calibration parameter, implying that the generation of surface runoff is important for streamflow (Guo and Su, 2019) in the Wooroloo Brook catchment. This parameter traditionally is one of the most important parameters in the SWAT model (Feyereisen et al., 2007; Nossent et al., 2011; Abbas et al., 2017; Das et al., 2019). For instance, Saha et al. (2014) studied streamflow modelling using SWAT in southeastern Australia and also found that CN2 was the most sensitive parameter at daily and monthly time scales. Based on the model evaluation performance ratings proposed by earlier research (Moriasi et al., 2007; Wallace et al., 2018), a streamflow simulation is considered acceptable when $|PBIAS| \leq 25\%$, $NSE > 0.5$, and $R^2 > 0.5$. Consequently, SWAT has performed well for monthly streamflow simulation when applied to the Wooroloo Brook catchment, with $|PBIAS| \leq 8.3\%$, $NSE \geq 0.86$, and $R^2 \geq 0.87$ in calibration and validation. While SWAT was able to reproduce observed streamflow, there might be some difficulties in replicating peak flows (Figure 6-3). Earlier research (Fukunaga et al., 2015; Shrestha et al., 2016) also have concluded that SWAT provided better results for low or average flows than for peak flows. A possible reason is that the routing techniques used in SWAT sometimes are inappropriate (Kim and Lee, 2010). For instance, the curve number approach in the SWAT model uses mean daily rainfall without considering the intensity and duration of the rainfall (Shrestha et al., 2016), which may lead to difficulties in reproducing peak flows. Nevertheless, SWAT was judged to simulate the observed runoff very satisfactorily with NSE and R^2 well above the satisfactory criteria, and the calibrated SWAT could be further applied to assess the hydrologic response to climate and land use change in this catchment.

6.4.2 Modelled hydrologic response to land use change scenarios

The clear seasonal distributions in runoff, ET, and soil water, with values greatest in winter and least in summer (Figure 6-5), were consistent with the seasonal variation in rainfall which also was greatest in winter (383.9 mm) and least in summer (43.6 mm). Reason for this is that rainfall is the major element influencing runoff, ET, and SW (Fekete et al., 2004), and this study catchment is a winter rainfall dominant area (Chiew and Mcmahon, 2002). In addition, changes in runoff under different land use change scenarios varied across seasons, with the most notable changes appearing in winter (wet season). The seasonal runoff response to land use changes with the largest absolute changes (mm) happened in the rainy season and the smallest absolute changes (mm) in the dry period were in line with findings in other research (Brown et al., 2005; Zhang et al., 2020). However, it is noted that although the absolute change (mm) of runoff in the dry season (summer) was much smaller compared with the wet season (winter), the percentage changes (%) in runoff were noticeable during all seasons. Results indicated that mean annual actual evapotranspiration would decrease under deforestation or urbanization, while increasing under afforestation, and these responses are in general agreement to research literatures (Wattenbach et al., 2007; Lin et al., 2015). In contrast, annual runoff increased under deforestation or urbanization while declined under afforestation. Previous hydrologic simulations also found similar results for runoff responses to such land use changes. For instance, Siriwardena et al. (2006) reported that the impact of clearing forest in an Australian catchment from 83 to 38% was to increase the runoff by approximately 40%. This is due to the higher evapotranspiration (Hundecha and Bárdossy, 2004) and water consumption (deep root system extracting water from shallow aquifer storage) (Mwangi et al., 2016) in forests, which leads to a reduction in runoff. Furthermore, mean annual soil water decreased under afforestation while increased under deforestation using SWAT. Previous studies have found that both shallow and deep soils became very dry following tree planting (Jia et al., 2017). Consequently, afforestation efforts in the future should consider include growing tree types with low water consumption to help sustainable conservation of soil, without compromising water needs, in dry areas.

6.4.3 Modelled hydrologic response to future climate change

The ensemble median of GCMs indicated that annual maximum temperature and minimum temperature would rise by 1.0-1.3 °C in 2040s and 1.6-3.4 °C in 2080s, regardless of emission scenarios. The temperature changes projected in this study are generally within the ranges given in previous research literature. For instance, climate projections for Southern and South-Western Flatlands showed that temperature would increase by 0.5-1.1 °C (10th to 90th percentile) by 2030 with only minor difference between the scenarios, and by 1.2-2.0 °C and

2.6-4.0 °C by 2090 under RCP4.5 and RCP8.5, respectively (Hope et al., 2015). In addition to temperature, median values of the 34 GCMs showed that rainfall was projected to decrease in all seasons and decrease greatest in spring (season of the second largest rainfall) and winter (season of the largest rainfall), in the future. For instance, rainfall was projected to decline by -35.9 % in spring and -26.9 % in winter by 2061-2100, under RCP 8.5. This is in agreement with earlier research. For example, Hope et al. (2015) reported that there was high confidence that spring, winter, and annual rainfall would decline in the Southern and South-Western Flatlands in Australia, and rainfall declines were greatest during spring and winter, at 36% and 29%, respectively, by 2090 for RCP 8.5.

The multi-GCM ensemble median for annual runoff showed considerable decreases by -19.4 % in 2040s (RCP4.5), -28.3 % in 2040s (RCP8.5), -33.6 % in 2080s (RCP4.5), and -55.3 % in 2080s (RCP8.5), which is consistent with the trend of changes in previous research, despite the study area, time periods, GCMs, downscaling techniques, and modelled hydrologic regimes differing across research. For example, the median forecast of 15 GCMs for an 8% decline in rainfall across SWA by 2030 was projected to reduce runoff by 25% (Silberstein et al., 2012). In addition, Hope et al. (2015) projected that runoff in SWA would decline by about 45% (median values) under RCP 4.5 and 64% under RCP 8.5 by 2090 (Sudmeyer, 2016). Besides, annual rainfall change was amplified in annual runoff change. For instance, a 2.5 % change in annual runoff for 1% change in annual rainfall can be inferred from Figures 6-6 and 6-7, which is also broadly supported by previous research (Silberstein et al., 2012). Moreover, annual actual evapotranspiration was also predicted to decrease (at a smaller extent compared to runoff) by -5.1 % in the 2040s (RCP4.5), -6.0 % in 2040s (RCP8.5), -7.5 % in the 2080s (RCP4.5) and -15.8 % in 2080s (RCP8.5). It is noted that the decrease in actual evapotranspiration may be related to the decreasing rainfall, although the potential evapotranspiration increases with higher temperature. This is because the study area has a small runoff coefficient (about 0.10) which means this area is relatively dry, so rainfall and soil water can also highly affect actual evapotranspiration, in addition to temperature. Furthermore, median estimates indicate that annual soil water was also projected to decline by -15.0 % in 2040s (RCP4.5), -16.0 % in 2040s (RCP8.5), -17.7 % in 2080s (RCP4.5), and -30.0 % in 2080s (RCP8.5), with the extent of decrease less than runoff and more than actual evapotranspiration. Hope et al. (2015) also reported projected decrease (high confidence) in soil moisture in SWA, and with extremely low soil moisture there was likely to be an increase of up to 80% more drought months in SWA by 2070 (Sudmeyer, 2016).

6.4.4 Modelled hydrologic responses to combined effects and uncertainties

According to the ensemble median of the 34 GCMs, the results from the four land use scenarios (LU1-4) differ only slightly from the response to LU0 (Figures 6-7, 6-8, and 6-9). Besides, for the same GCM in the same future period under the same RCP, almost all five land use scenarios (LU0-LU4) showed a similar direction and magnitude of changes, while the directions or magnitude of changes for different GCMs were quite different under the same land use scenario (Figures 6-10, 6-11, and 6-12). Therefore, according to Figures 6-7, 6-8, 6-9, 6-10, 6-11, and 6-12, GCMs were expected to have much more impacts on changes of hydrologic variables than land use scenarios. Other studies found similar trends, where changes in runoff were primarily affected by climate change whereas the role of land use change was limited compared with climate change (Phung et al., 2019). In addition, although land use scenarios had a much smaller effect on changes of hydrologic variables compared to GCMs and RCPs, it is noteworthy that the combined impacts of land use and climate changes could further increase or decrease the future changes of hydrologic variables. For instance, annual soil water under LU3 (24.4% increase in FRST from RNGE) tended to decrease more than other land use scenarios (Figure 6-9 and Figure 6-12). This highlights the need for reforestation programs to be carefully targeted to maximizing ecological benefits while also minimizing soil water losses.

Previous research has shown that the selection of GCM is the major contributor to the total uncertainty (Chen et al., 2011b; Teng et al., 2012b), which is consistent with our results from the ANOVA analysis. For instance, Nasonova et al. (2018) studied streamflow response to climate change in large-scale watersheds and found that the contribution of GCMs to the runoff projection uncertainty was almost twice higher than that of the RCPs. Karlsson et al. (2016) projected the combined effects of land use and climate changes on hydrology and found that the selection of climate models remained dominant while the contribution of land use scenarios to the average streamflow was only 1%. Therefore, caution is recommended when selecting climate models for hydrologic impacts assessment, and an ensemble of GCMs should be used to minimize the uncertainty resulting from the selection of GCMs.

6.4.5 Caveats and limitations

This research concentrates on the impacts of uncertainties caused by GCMs, RCPs, and land use scenarios. However, hydrologic model structures, model parameterization, and downscaling procedures also generate uncertainties. For instance, Chen et al. (2011a) compared six downscaling techniques to study the uncertainties in quantifying climate change impacts and their results indicated that regression-based statistical downscaling techniques had a significant contribution to the uncertainty envelope. Karlsson et al. (2016) applied three

hydrologic models to study combined effects of climate models and land use scenarios and found that the hydrologic model structure also significantly affected the impact analysis results, particularly for extreme events. However, an investigation of these supplementary sources is outside the context of this research.

6.5 Conclusions

This study assessed the hydrologic response to climate change and land use change, both separately and when combined, in the important Wooroloo Brook catchment, located in southwestern Australia. The SWAT model was calibrated and validated before simulating climate change and land use change impacts, and performed well in this study area with NSE and R^2 values far larger than 0.5. Historical simulation under land use change showed that seasonal and annual runoff increased under deforestation or urbanization, while declining under afforestation. Future runoff was projected to decrease more in winter and spring, but decrease less in autumn and summer. Annual ET was predicted to decrease to a smaller extent compared to runoff, whereas annual SW was projected to decrease less than runoff and more than ET. The calibrated SWAT then was applied to study hydrologic response to combined climate and land use changes on water balance in the 2040s and 2080s periods. The results of four land use change scenarios (LU1-4) were only slightly different from the response of zero land use (LU0), according to the ensemble median of the 34 GCMs. ANOVA showed that GCM has the greatest contribution to uncertainty, followed by RCP, and the land use scenario contributes least to future changes of runoff, ET, and SW. Although the land use scenario had limited effects on water balance compared with GCM and RCP, the joint impacts of climate and land use changes could further increase or decrease the future changes of hydrologic variables. For instance, annual soil water under LU3 (24.4% increase in FRST from RNGE) was projected to decrease more than other land use scenarios. Therefore, soils could become drier after planting trees, suggesting that afforestation in the future shall consider tree types with less water consumption, to help sustainable conservation of soil without compromising water needs in dry areas. In addition, this study focused upon the Wooroloo Brook catchment, which though selected as representative of such catchments (similar climatic and hydrologic conditions), lacks repetition at the catchment-scale. Moreover, current newest GCMs from CMIP6 (Coupled Model Inter-comparison Project 6) are expected to improve and enhance climate change projections for Australia (Grose et al., 2020). Therefore, more catchments, hydrologic models, different downscaling methods, and CMIP6 models will be chosen in future research to make a comprehensive range and probability of projections on future hydrology.

Chapter 7. Final conclusions and future research

7.1 Final conclusions

This study mainly investigated the individual and coupled effects of future climate change and land use change on water balance components in Australia. The outcomes of this project can provide crucial information for the development of sustainable land and water management under future climate change at a catchment scale in Australia. The research approaches presented in this study can be further applied to other catchments with similar climatic and hydrologic conditions for climate and land use changes impact assessments.

To identify the driving factors (i.e., precipitation, temperature, net radiation, relative humidity, wind, and human activity) and their impacts on runoff, statistical methods were used to derive trend, mutation, and cycle characteristics of the climatic and hydrologic variables, and the relationships among them in four Australian catchments with different climatic conditions (Chapter 3). According to correlation analyses between annual hydrologic and climatic factors, runoff displayed the greatest correlation with rainfall in most of the four catchments while FAO56 potential evapotranspiration showed a greatest negative correlation with relative humidity and greatest positive correlations with maximum temperature and solar radiation for all catchments. Based on the climate elasticity, the order of the affecting factors to runoff was: rainfall > parameter n of land use change > net solar radiation > maximum temperature > relative humidity > wind speed ≥ minimum temperature for most of the four catchments. As expected, rainfall is the factor that most affects runoff, and an increase of 10% in rainfall led to an increase of 24.4% in runoff according to the average of the four catchments. In addition, the fractional contributions from climate change and human activity to runoff change were 55.5% and 44.5%, respectively, across the four catchments in Australia.

To evaluate the impacts of future climate change on water balance components, the XAJ hydrological model and downscaled GCM projections were applied to a catchment in eastern Australia (Chapter 4). Annual rainfall and runoff were projected to decrease slightly in 2021-2060 and increase in 2061-2100 based on the median estimates from the ensemble of GCMs. A slight increase was predicted in annual actual evapotranspiration, while a decrease was projected in annual soil water in the future. The future changes of actual evapotranspiration, runoff, and soil water at seasonal and annual scales are mainly affected by rainfall changes, but less affected by temperature changes. The increase of high runoff values and decrease of low runoff values projected from the ensemble of GCMs indicate that the variability of future water resources will increase at monthly and seasonal scales. The possible future decrease of water

availability in eastern Australia may aggravate due to the trend of decreasing values in future winter runoff and soil water.

To assess the impacts of land use change on water balance components, the SWAT model with plant growth calibrated using MODIS LAI data was applied in wet tropical eastern Australia (Chapter 5). The improved SWAT could reproduce MODIS LAI with much better NSE values than the original SWAT, and to simulate runoff well with slightly better NSE and R^2 than the original SWAT. Land use change has an influence on all hydrologic variables, and the influence on surface runoff is the most remarkable at annual scale. Urbanization increased surface runoff while decreased lateral runoff and groundwater, but produced no clear change in total runoff, actual evapotranspiration, and soil water at yearly scale. In addition, afforestation was able to increase evapotranspiration, reduce surface runoff and soil moisture, and result in slight changes in other hydrologic variables at yearly scale. The total runoff for urban, range-grasses, and forest-evergreen land uses were strongly correlated ($r \geq 0.94$) with rainfall at yearly scale. Under the same rainfall, soil texture, and terrain slope, the total runoff produced by forest-evergreen was usually less than that by range-grasses and urban land uses. Furthermore, under the same condition, more surface runoff and less lateral runoff and groundwater were usually generated by urban land use than that by forest-evergreen and range-grasses.

To study the impacts of both climate change and land use change on hydrologic variables, a case study of a catchment in southwestern Australia was conducted using the SWAT model, 34 GCMs under two RCPs, and five land use scenarios. For the combined impacts of climate and land use changes, the results of the four land use change scenarios were only slightly different from the response of the original land use. An uncertainty analysis shows that GCMs had the greatest contribution to hydrologic variables, followed by RCPs and land use scenarios. Hence it is advisable for impacts analysis to use an ensemble of GCMs under different RCPs, to minimize the uncertainty of projected future hydrologic variables. Although the land use scenario had limited effects on water balance compared with GCM and RCP, the joint impacts of climate and land use changes could further increase or decrease the future changes of hydrologic variables.

7.2 Future research

The aims of future research are to: (1) study hydrologic responses to climate and land use changes using large-scale hydrological models in larger areas to provide insights for future water management; (2) study land use change impacts on hydrology using projected future land use maps in Australia; (3) make a comprehensive range and probability of projections on future hydrological cycle by choosing more hydrologic models and downscaling methods; (4)

consider the influence of increasing atmospheric CO_2 on stomatal conductance in the SWAT model, which may offset the magnitude of the potential evapotranspiration caused by the warming climate; (5) provide further insights into impacts on future hydrological variables by using the up-to-date CMIP6 (Coupled Model Intercomparison Project phase 6), which is expected to improve and enhance climate change projections for Australia.

Reference

Abbas, N., Wasimi, S.A., Bhattarai, S., Al-Ansari, N., 2017. The Impacts of Climate Change on Fitzroy River Basin, Queensland, Australia: The Impacts of Climate Change on Fitzroy River Basin, Queensland, Australia. Journal of Civil Engineering and Architecture, 11(1): 38-47.

Abbaspour, K.C., 2013. SWAT-CUP 2012: SWAT calibration and uncertainty programs–a user manual. Eawag: Dübendorf, Switzerland, 103.

Abbaspour, K.C. et al., 2015. A continental-scale hydrology and water quality model for Europe: Calibration and uncertainty of a high-resolution large-scale SWAT model. Journal of Hydrology, 524: 733-752.

Abbaspour, K.C. et al., 2007. Modelling hydrology and water quality in the pre-alpine/alpine Thur watershed using SWAT. Journal of hydrology, 333(2-4): 413-430.

Abbott, M.B., Bathurst, J.C., Cunge, J.A., O'Connell, P.E., Rasmussen, J., 1986. An introduction to the European Hydrological System — Systeme Hydrologique Europeen, "SHE", 1: History and philosophy of a physically-based, distributed modelling system. Journal of Hydrology, 87(1–2): 45-59.

Abtew, W., 1996. EVAPOTRANSPIRATION MEASUREMENTS AND MODELING FOR THREE WETLAND SYSTEMS IN SOUTH FLORIDA. Jawra Journal of the American Water Resources Association, 32(3): 465-473.

Adams, R., Western, A.W., Seed, A.W., 2012. An analysis of the impact of spatial variability in rainfall on runoff and sediment predictions from a distributed model. Hydrological Processes, 26(21): 3263–3280.

Ahmed, K.F. et al., 2013. Statistical downscaling and bias correction of climate model outputs for climate change impact assessment in the US northeast. Global and Planetary Change, 100: 320-332.

Aide, T.M. et al., 2013. Deforestation and reforestation of Latin America and the Caribbean (2001–2010). Biotropica, 45(2): 262-271.

Aijm, V.D., Keenan, R.J., 2007. Planted forests and water in perspective. Forest Ecology & Management, 251(1–2): 1-9.

Alemayehu, T., Griensven, A.v., Woldegiorgis, B.T., Bauwens, W., 2017. An improved SWAT vegetation growth module and its evaluation for four tropical ecosystems. Hydrology and Earth System Sciences, 21(9): 4449-4467.

Alibuyog, N. et al., 2009. Predicting the effects of land use change on runoff and sediment yield in Manupali River subwatersheds using the SWAT model. International Agricultural Engineering Journal, 18(1): 15.

Anache, J.A., Flanagan, D.C., Srivastava, A., Wendland, E.C., 2018. Land use and climate change impacts on runoff and soil erosion at the hillslope scale in the Brazilian Cerrado. Science of The Total Environment, 622: 140-151.

Anandhi, A. et al., 2011. Examination of change factor methodologies for climate change impact assessment. Water Resources Research, 47(3): 341-351.

Arnold, J.G., Fohrer, N., 2005. SWAT2000: current capabilities and research opportunities in applied watershed modelling. Hydrological Processes, 19(3): 563-572.

Arnold, J.G., Srinivasan, R., Muttiah, R.S., Williams, J.R., 1998. Large area hydrologic modeling and assessment part I: model development 1. JAWRA Journal of the American Water Resources Association, 34(1): 73-89.

Aryal, A., Shrestha, S., Babel, M.S., 2019. Quantifying the sources of uncertainty in an ensemble of hydrological climate-impact projections. Theor Appl Climatol, 135(1-2): 193-209.

Ayele, G.T., Teshale, E.Z., Yu, B., Rutherfurd, I.D., Jeong, J., 2017. Streamflow and sediment yield prediction for watershed prioritization in the Upper Blue Nile River Basin, Ethiopia. Water, 9(10): 782.

Baker, T.J., Miller, S.N., 2013. Using the Soil and Water Assessment Tool (SWAT) to assess land use impact on water resources in an East African watershed. Journal of hydrology, 486: 100-111.

Bardossy, A., Plate, E.J., 1992. Space-time model for daily rainfall using atmospheric circulation patterns. Water Resources Research, 28(5): 1247-1259.

Barron, O. et al., 2012. Climate change effects on water-dependent ecosystems in south-western Australia. Journal of Hydrology, 434: 95-109.

Barua, S., Muttil, N., Ng, A., Perera, B., 2013. Rainfall trend and its implications for water resource management within the Yarra River catchment, Australia. Hydrological Processes, 27(12): 1727-1738.

Bathurst, J.C. et al., 2011. Forest impact on floods due to extreme rainfall and snowmelt in four Latin American environments 1: Field data analysis. Journal of Hydrology, 400(3): 281-291.

Beecham, S., Chowdhury, R.K., 2010. Temporal characteristics and variability of point rainfall: a statistical and wavelet analysis. International Journal of Climatology: A Journal of the Royal Meteorological Society, 30(3): 458-473.

Berger, W.H., Labeyrie, L.D., 1987. Abrupt climatic change: evidence and implications, 216. Springer Science & Business Media.

Beven, K., Binley, A., 1992. The future of distributed models: model calibration and uncertainty prediction. Hydrological processes, 6(3): 279-298.

BEVEN, K.J., KIRKBY, M.J., 1979. A physically based, variable contributing area model of basin hydrology / Un modèle à base physique de zone d'appel variable de l'hydrologie du bassin versant. Hydrological Sciences Bulletin, 24(1): 43--69.

Bondelid, T.R., McCuen, R.H., Jackson, T.J., 1982. Sensitivity of SCS Models to Curve Number Variation 1. JAWRA Journal of the American Water Resources Association, 18(1): 111-116.

Bonell, M., Bruijnzeel, L.A., 2005. Forests, water, and people in the humid tropics. Cambridge University Press, 158-193 pp.

Bosch, J.M., Hewlett, J., 1982. A review of catchment experiments to determine the effect of vegetation changes on water yield and evapotranspiration. Journal of hydrology, 55(1-4): 3-23.

Bosshard, T. et al., 2013. Quantifying uncertainty sources in an ensemble of hydrological climate-impact

projections. Water Resources Research, 49(3): 1523-1536.

Brovkin, V. et al., 2006. Biogeophysical effects of historical land cover changes simulated by six Earth system models of intermediate complexity. Climate Dynamics, 26(6): 587-600.

Brown, A.E., Zhang, L., Mcmahon, T.A., Western, A.W., Vertessy, R.A., 2005. A review of paired catchment studies for determining changes in water yield resulting from alterations in vegetation. Journal of Hydrology, 310(1): 28-61.

Brown, S.C., Versace, V.L., Lester, R.E., Walter, M.T., 2015. Assessing the impact of drought and forestry on streamflows in south-eastern Australia using a physically based hydrological model. Environmental earth sciences, 74(7): 6047-6063.

Brown, T.C., Mahat, V., Ramirez, J.A., 2019. Adaptation to future water shortages in the United States caused by population growth and climate change. Earth's Future, 7(3): 219-234.

Bruijnzeel, L.A., 1989. (De)forestation and dry season flow in the tropics: A closer look. Journal of Tropical Forest Science, 1(3): 229-243.

Bruijnzeel, L.A., 1990. Hydrology of moist tropical forests and effects of conversion: a state of knowledge review. Journal of Hydrology, 129(1–4): 397-399.

Budyko, M., 1974. Climate and Life, 508 pp. Academic Press, New York.

Burnash, R.J., Ferral, R.L., McGuire, R.A., 1973. A generalized streamflow simulation system, conceptual modeling for digital computers.

Calder, I.R. et al., 1995. The impact of land use change on water resources in sub-Saharan Africa: a modelling study of Lake Malawi. Journal of Hydrology, 170(1–4): 123-135.

Calder, I.R., Maidment, D.R., 1992. Hydrologic effects of land-use change. J.am.water Works Assoc.

Callow, J.N., 2007. River response to land clearing and landscape salinisation in southwestern Australia. University of Western Australia Perth, Western Australia.

Chang, H.J., Jung, I.W., 2010. Spatial and temporal changes in runoff caused by climate change in a complex large river basin in Oregon. Journal of Hydrology, 388(3): 186-207.

Charles SP, S.R., Teng J, Fu G, Hodgson G, Gabrovsek C, Crute J, Chiew FHS, Smith IN, Kirono DGC, Bathols JM, Li LT, Yang A, Donohue RJ, Marvanek SP, McVicar TR, Van Niel TG and Cai W, 2010. Climate analyses for south-west Western Australia. A report to the Australian Government from the CSIRO South-West Western Australia Sustainable Yields Project, CSIRO, Australia. 83 pp.

Chen, H., Guo, S., Xu, C.-y., Singh, V.P., 2007. Historical temporal trends of hydro-climatic variables and runoff response to climate variability and their relevance in water resource management in the Hanjiang basin. Journal of hydrology, 344(3): 171-184.

Chen, H., Xu, C.-Y., Guo, S., 2012. Comparison and evaluation of multiple GCMs, statistical downscaling and hydrological models in the study of climate change impacts on runoff. Journal of hydrology, 434: 36-45.

Chen, J., Brissette, F.P., Chaumont, D., Braun, M., 2013. Performance and uncertainty evaluation of empirical downscaling methods in quantifying the climate change impacts on hydrology over

two North American river basins. Journal of Hydrology, 479: 200-214.

Chen, J., Brissette, F.P., Leconte, R., 2011a. Uncertainty of downscaling method in quantifying the impact of climate change on hydrology. Journal of hydrology, 401(3-4): 190-202.

Chen, J., Brissette, F.P., Poulin, A., Leconte, R., 2011b. Overall uncertainty study of the hydrological impacts of climate change for a Canadian watershed. Water Resources Research, 47(12).

CHEN, S., LOVELL, B.C., SHAN, T., 2009a. ROBUST ADAPTED PRINCIPAL COMPONENT ANALYSIS FOR FACE RECOGNITION. International Journal of Pattern Recognition & Artificial Intelligence, 23(03): 491-520.

Chen, X., Zhang, Z., Chen, X., Shi, P., 2009b. The impact of land use and land cover changes on soil moisture and hydraulic conductivity along the karst hillslopes of southwest China. Environmental Earth Sciences, 59(4): 811-820.

Chen, Y., Deng, H., Li, B., Li, Z., Xu, C., 2014. Abrupt change of temperature and precipitation extremes in the arid region of Northwest China. Quaternary International, 336: 35-43.

Chen, Y.R., Yu, B., 2015. Impact assessment of climatic and land-use changes on flood runoff in southeast Queensland. Hydrological Sciences Journal, 60(10): 1759-1769.

Chiew, F., Whetton, P.H., Mcmahon, T.A., Pittock, A.B., 1995. Simulation of the impacts of climate change on runoff and soil moisture in Australian catchments. Journal of Hydrology, 167(1): 121-147.

Chiew, F.H.S., 2006. Estimation of rainfall elasticity of streamflow in Australia. Hydrological Sciences Journal, 51(4): 613-625.

Chiew, F.H.S., Harrold, T.I., Siriwardena, L., Jones, R.N., Srikanthan, R., 2003. Simulation of Climate Change Impact on Runoff Using Rainfall Scenarios that Consider Daily Patterns of Change from GCMs, MODSIM 2003: International Congress on Modelling and Simulation: Proceedings, Modelling and Simulation Society of Australia and New Zealand, Canberra ACT, Townsville, pp. 154-159.

Chiew, F.H.S., Mcmahon, T.A., 2002. Modelling the impacts of climate change on Australian streamflow. Hydrological Processes, 16(6): 1235–1245.

Chiew, F.H.S. et al., 2009. Estimating climate change impact on runoff across southeast Australia: method, results, and implications of the modeling method. Water Resources Research, 45(10): 82-90.

Choudhury, B.J., Monteith, J.L., 1988. A 4-layer model for the heat budget of homogenous land surfaces. Quarterly Journal of the Royal Meteorological Society, 114(480): 373–398.

Chowdhury, R., Beecham, S., 2010. Australian rainfall trends and their relation to the southern oscillation index. Hydrological Processes: An International Journal, 24(4): 504-514.

Cleugh, H. et al., 2011. Climate change: science and solutions for Australia. Climate Change Science & Solutions for Australia, 179(10): 154-155.

Cleverly, J. et al., 2016. The importance of interacting climate modes on Australia's contribution to global carbon cycle extremes. Scientific reports, 6: 23113.

Costa, M.H., Botta, A., Cardille, J.A., 2003. Effects of large-scale changes in land cover on the discharge of the Tocantins River, Southeastern Amazonia. Journal of Hydrology, 283(1–4): 206-217.

Crosbie, R.S., Hughes, J.D., Friend, J., Baldwin, B.J., 2007. Monitoring the hydrological impact of land use change in a small agricultural catchment affected by dryland salinity in central NSW, Australia. Agricultural Water Management, 88(1–3): 43-53.

Crosbie, R.S., McCallum, J.L., Walker, G.R., Chiew, F.H., 2010. Modelling climate-change impacts on groundwater recharge in the Murray-Darling Basin, Australia. Hydrogeology Journal, 18(7): 1639-1656.

CSIRO, 2007. Climate Change in Australia: technical report 2007. Environment.

CSIRO, 2009. Surface water yields in south-west Western Australia. A report to the Australian Government from the CSIRO South-West Western Australia Sustainable Yields Project, CSIRO Water for a Healthy Country Flagship, Australia.

CSIRO, 2016. State of the climate report 2016, CSIRO and The Bureau of Meteorology, Canberra.

CSIRO, B.o.M., 2015. Climate Change in Australia Information for Australia's Natural Resource Management Regions: Technical Report, CSIRO and Bureau of Meteorology, Australia.

Dar, L.A., 2017. Rainfall-Runoff Modeling using Multiple Linear Regression Technique. International Journal for Research in Applied Science & Engineering Technology 5(VII): 214-218.

Das, B., Jain, S., Singh, S., Thakur, P., 2019. Evaluation of multisite performance of SWAT model in the Gomti River Basin, India. Applied Water Science, 9(5): 134.

Degens, B., Muirden, P., Kelly, B., Allen, M., 2012. Acidification of salinised waterways by saline groundwater discharge in south-western Australia. Journal of Hydrology, 470: 111-123.

Diaz-Nieto, J., Wilby, R.L., 2005. A comparison of statistical downscaling and climate change factor methods: impacts on low flows in the River Thames, United Kingdom. Climatic Change, 69(2): 245-268.

Dibike, Y.B., Coulibaly, P., 2005. Hydrologic impact of climate change in the Saguenay watershed: comparison of downscaling methods and hydrologic models. Journal of hydrology, 307(1): 145-163.

Donohue, R.J., Roderick, M.L., McVicar, T.R., 2012. Roots, storms and soil pores: Incorporating key ecohydrological processes into Budyko's hydrological model. Journal of Hydrology, 436: 35-50.

Duan, Q., Sorooshian, S., Gupta, V.K., 2015. Optimal use of the SCE-UA global optimization method for calibrating watershed models. Journal of Hydrology, 158(3-4): 265-284.

Eckhardt, K., Breuer, L., Frede, H.G., 2003. Parameter uncertainty and the significance of simulated land use change effects. Journal of Hydrology, 273(1–4): 164-176.

Eisner, S. et al., 2017. An ensemble analysis of climate change impacts on streamflow seasonality across 11 large river basins. Climatic Change, 141(3): 1-17.

Elmahdi, A., 2015. Water in Australia 2013 - 14/ Bureau of Meteorology, Melbourne.

Eum, H.I., Dibike, Y., Prowse, T., 2016. Climate-induced alteration of hydrologic indicators in the Athabasca River Basin, Alberta, Canada. Journal of Hydrology, 544: 327-342.

Fan, Y.U., Cao, Y., 2008. Research progress summarization for the impacts of global climate change to the regional water resources. Journal of Water Resources & Water Engineering.

Fekete, B.M., Vörösmarty, C.J., Roads, J.O., Willmott, C.J., 2004. Uncertainties in Precipitation and Their Impacts on Runoff Estimates. Journal of Climate, 17(2): 294-304.

Feyereisen, G., Strickland, T., Bosch, D., Sullivan, D., 2007. Evaluation of SWAT manual calibration and input parameter sensitivity in the Little River watershed. Transactions of the ASABE, 50(3): 843-855.

Fierro, A.O., Leslie, L.M., 2014. Relationships between southeast Australian temperature anomalies and large-scale climate drivers. Journal of Climate, 27(4): 1395-1412.

Fohrer, N., Haverkamp, S., Eckhardt, K., Frede, H.G., 2001. Hydrologic Response to land use changes on the catchment scale. Physics & Chemistry of the Earth Part B Hydrology Oceans & Atmosphere, 26(7–8): 577-582.

Foley, J.A. et al., 2005. Global consequences of land use. science, 309(5734): 570-574.

Fowler, H., Ekström, M., Kilsby, C., Jones, P., 2005. New estimates of future changes in extreme rainfall across the UK using regional climate model integrations. 1. Assessment of control climate. Journal of Hydrology, 300(1): 212-233.

Fowler, H.J., Blenkinsop, S., Tebaldi, C., 2007. Linking climate change modelling to impacts studies: recent advances in downscaling techniques for hydrological modelling. International journal of climatology, 27(12): 1547-1578.

Fraser, E.D., Simelton, E., Termansen, M., Gosling, S.N., South, A., 2013. "Vulnerability hotspots": Integrating socio-economic and hydrological models to identify where cereal production may decline in the future due to climate change induced drought. Agricultural and Forest Meteorology, 170: 195-205.

Freeze, R.A., Harlan, R.L., 1969. Blueprint for a physically-based, digitally-simulated hydrologic response model. Journal of Hydrology, 9(3): 237-258.

Frei, C. et al., 2003. Daily precipitation statistics in regional climate models: Evaluation and intercomparison for the European Alps. Journal of Geophysical Research: Atmospheres, 108(D3).

Frei, C., Schöll, R., Fukutome, S., Schmidli, J., Vidale, P.L., 2006. Future change of precipitation extremes in Europe: Intercomparison of scenarios from regional climate models. Journal of Geophysical Research: Atmospheres, 111(D6).

Fukunaga, D.C., Cecílio, R.A., Zanetti, S.S., Oliveira, L.T., Caiado, M.A.C., 2015. Application of the SWAT hydrologic model to a tropical watershed at Brazil. Catena, 125: 206-213.

Fuss, S. et al., 2015. Betting on negative emissions. Nature Climate Change, 4(10): 850-853.

Gabiri, G. et al., 2020. Impact of Climate and Land Use/Land Cover Change on the Water Resources of a Tropical Inland Valley Catchment in Uganda, East Africa. Climate, 8(7): 83.

Gan, T.Y., Dlamini, E.M., Biftu, G.F., 1997. Effects of model complexity and structure, data quality, and objective functions on hydrologic modeling. Journal of Hydrology, 192(s 1–4): 81–103.

Gardner, L.R., 2009. Assessing the effect of climate change on mean annual runoff. Journal of Hydrology, 379(3–4): 351-359.

Garnett, S., Szabo, J., Dutson, G., 2011. The action plan for Australian birds 2010. CSIRO publishing.

Gassman, P.W., Reyes, M.R., Green, C.H., Arnold, J.G., 2007. The soil and water assessment tool: historical development, applications, and future research directions. Transactions of the ASABE, 50(4): 1211-1250.

Gilfedder, M., Walker, G.R., Dawes, W.R., Stenson, M.P., 2009. Prioritisation approach for estimating the biophysical impacts of land-use change on stream flow and salt export at a catchment scale. Environmental Modelling & Software, 24(2): 262-269.

Gordon, H.B., O'Farrell, S.P., 1997. Transient climate change in the CSIRO coupled model with dynamic sea ice. Monthly Weather Review, 125(5): 875-908.

Gosling, S.N. et al., 2017. A comparison of changes in river runoff from multiple global and catchment-scale hydrological models under global warming scenarios of 1 °C, 2 °C and 3 °C. Climatic Change, 141(3): 577-595.

Goudriaan, J., Waggoner, P.E., 1972. Simulating both aerial microclimate and soil temperature from observations above the foliar canopy. Neth J Agr Sci, 20: 104-124.

Green, D., Petrovic, J., Moss, P., Burrell, M., 2011. Water resources and management overview: Murrumbidgee catchment. NSW Office of Water, Sydney.

Grose, M.R. et al., 2020. Insights from CMIP6 for Australia's future climate. Earth's Future, 8(5): e2019EF001469.

Guo, J., Su, X., 2019. Parameter sensitivity analysis of SWAT model for streamflow simulation with multisource precipitation datasets. Hydrology Research, 50(3): 861-877.

Guo, J., Zhang, Z., Wang, S., Yao, A., Ma, S., 2012. Effects of climate and land use changes on stream flow and sediment yield in Chaohe river basin. Transactions of the Chinese Society of Agricultural Engineering, 28(14): 236-243.

Guo, T. et al., 2019. Development and improvement of the simulation of woody bioenergy crops in the Soil and Water Assessment Tool (SWAT). Environmental Modelling & Software, 122: 104295.

Hao, F., Sun, M., Geng, X., Huang, W., Ouyang, W., 2015. Coupling the Xinanjiang model with geomorphologic instantaneous unit hydrograph for flood forecasting in northeast China. International Soil & Water Conservation Research, 3(1): 66-76.

Hay, L.E., Clark, M.P., 2003. Use of statistically and dynamically downscaled atmospheric model output for hydrologic simulations in three mountainous basins in the western United States. Journal of Hydrology, 282(1–4): 56-75.

Head, L., Adams, M., Mcgregor, H.V., Toole, S., 2014. Climate change and Australia. Wiley Interdisciplinary Reviews Climate Change, 5(2): 175-197.

Heinzeller, D., Junkermann, W., Kunstmann, H., 2016. Anthropogenic aerosol emissions and rainfall

decline in Southwestern Australia: coincidence or causality? Journal of Climate, 29(23): 8471-8493.

Hewitson, B., Crane, R., 2006. Consensus between GCM climate change projections with empirical downscaling: precipitation downscaling over South Africa. International Journal of Climatology, 26(10): 1315-1337.

Hill, M.J. et al., 2006. Assessment of the MODIS LAI product for Australian ecosystems. Remote Sensing of Environment, 101(4): 495-518.

Hobbs, R., Hopkins, A., 1990. From frontier to fragments: European impact on Australia's vegetation [degradation; rehabilitation].[Symposium paper], Proceedings of the Ecological Society of Australia (Australia). Ecological Society of Australia.

Holmes, J., Sinclair, J., 1986. Water yield from some afforested catchments in Victoria, Hydrology and Water Resources Symposium 1986: River Basin Management; Preprints of Papers. Institution of Engineers, Australia, pp. 214.

Honisch, M., Hellmeier, C., Weiss, K., 2002. Response of surface and subsurface water quality to land use changes. Geoderma, 105(3–4): 277-298.

Hope, P. et al., 2015. Southern and South-Western Flatlands cluster report, climate change in Australia: projections for Australia's natural resource management regions.', Cluster Reports. CSIRO and Bureau of Meteorology. Australia.

Horton, R.E., 1919. Rainfall interception. Monthly weather review, 47(9): 603-623.

Hossain, M., Rahman, A., Haddad, K., Ishak, E.H., 2013. Trend analysis of flood data in Australia: A case study for Victoria, Adapting to Change: the Multiple Roles of Modelling: Proceedings of the 20th International Congress on Modelling and Simulation (MODSIM2013), 1-6 December 2013, Adelaide, South Australia, pp. 2318-2324.

Hoyos, N. et al., 2019. Modeling Streamflow Response to Persistent Drought in a Coastal Tropical Mountainous Watershed, Sierra Nevada De Santa Marta, Colombia. Water, 11(1): 94.

Hu, C., Guo, S., Xiong, L., Peng, D., 2005. A Modified Xinanjiang Model and Its Application in Northern China. Hydrology Research, 36(2): 175-192.

Huang, Z., Yang, H., Yang, D., 2016. Dominant climatic factors driving annual runoff changes at the catchment scale across China. Hydrology & Earth System Sciences, 20(7).

Hughes, D.A., 2013. A review of 40 years of hydrological science and practice in southern Africa using the Pitman rainfall-runoff model. Journal of Hydrology, 501(20): 111-124.

Hughes, K., Watkins, G., Hughes, K., Kaliska, A., Andersons, L., Boyling, M., 2011. Working With Our Catchment: Manning River Catchment Management Program, Taree, NSW.

Hundecha, Y., Bárdossy, A., 2004. Modeling of the effect of land use changes on the runoff generation of a river basin through parameter regionalization of a watershed model. Journal of hydrology, 292(1-4): 281-295.

Huntington, T.G., 2006. Evidence for intensification of the global water cycle: Review and synthesis. Journal of Hydrology, 319(1–4): 83-95.

IPCC, 2007. IPCC, 2007: Climate Change 2007: The Physical Science Basis. Contribution of Working Group I to the Fourth Assessment. Report of the Intergovernmental Panel on Climate Change [Solomon, S., D. Qin, M. Manning, Z. Chen, M. Marquis, K.B. Averyt, M. Tignor and H.L. Miller (eds.)]. Cambridge University Press, Cambridge, United Kingdom and New York, NY, USA, 996 pp. Cambridge University Press.

IPCC, 2013. IPCC, 2013: Climate Change 2013: The Physical Science Basis. Contribution of Working Group I to the Fifth Assessment Report of the Intergovernmental Panel on Climate Change [Stocker, T.F., D. Qin, G.-K. Plattner, M. Tignor, S.K. Allen, J. Boschung, A. Nauels, Y. Xia, V. Bex and P.M. Midgley (eds.)]. Cambridge University Press, Cambridge, United Kingdom and New York, NY, USA, 1535 pp., of the Intergovernmental Panel on Climate Change, pp. 710-719.

IPCC, 2014. IPCC, 2014: Climate Change 2014: Synthesis Report. Contribution of Working Groups I, II and III to the Fifth Assessment Report of the Intergovernmental Panel on Climate Change [Core Writing Team, R.K. Pachauri and L.A. Meyer (eds.)]. IPCC, Geneva, Switzerland, 151 pp.

IPCC, 2019. Climate Change and Land: An IPCC Special Report on climate change, desertifcation, land degradation, sustainable land management, food security, and greenhouse gas fluxes in terrestrial ecosystems., Intergovernmental Panel on Climate Change, pp. 1-41.

Ismail, K.A.R., Leal, J.F.B., Zanardi, M.A., 1997. Models of liquid storage tanks. Energy, 22(8): 805-815.

Jacobson, C.R., 2011. Identification and quantification of the hydrological impacts of imperviousness in urban catchments: a review. Journal of Environmental Management, 92(6): 1438.

Jayawardena, A.W., Zhou, M.C., 2000. A modified spatial soil moisture storage capacity distribution curve for the Xinanjiang model. Journal of Hydrology, 227(1-4): 93-113.

Jia, X., Zhu, Y., Luo, Y., 2017. Soil moisture decline due to afforestation across the Loess Plateau, China. Journal of Hydrology, 546: 113-122.

Jiang, T. et al., 2007. Comparison of hydrological impacts of climate change simulated by six hydrological models in the Dongjiang Basin, South China. Journal of Hydrology, 336(3-4): 316-333.

Jiang, Y., 2011. VARIATIONS OF TANGNAIHAI RUNOFF AND PRECIPITATION AND TEMPERATURE IN THE UPPER REACH OF THE YELLOW RIVER. Meteorology & Disaster Reduction Research.

Jie, C., Brissette, F.P., Annie, P., Robert, L., 2011. Overall uncertainty study of the hydrological impacts of climate change for a Canadian watershed. Water Resources Research, 47(12): 1-16.

Jones, R.N., Chiew, F.H.S., Boughton, W.C., Zhang, L., 2006. Estimating the sensitivity of mean annual runoff to climate change using selected hydrological models. Advances in Water Resources, 29(10): 1419-1429.

Joseph, J., Ghosh, S., Pathak, A., Sahai, A., 2018. Hydrologic impacts of climate change: Comparisons between hydrological parameter uncertainty and climate model uncertainty. Journal of

hydrology, 566: 1-22.

Kachroo, R.K., 1992. River flow forecasting. Part 5. Applications of a conceptual model. Journal of Hydrology, 133(1-2): 141-178.

Karl, T.R., Wang, W.C., Schlesinger, M.E., Knight, R.W., Portman, D., 1990. A Method of Relating General Circulation Model Simulated Climate to the Observed Local Climate. Part I: Seasonal Statistics. Journal of Climate, 3(10): 1053-1079.

Karlsson, I.B. et al., 2016. Combined effects of climate models, hydrological model structures and land use scenarios on hydrological impacts of climate change. Journal of Hydrology, 535: 301-317.

Katz, R.W., 1996. Use of conditional stochastic models to generate climate change scenarios. Climatic Change, 32(3): 237-255.

Keenan, T., Cleugh, H., 2011. Climate Science Update: A Report to the 2011 Garnaut Review.

Kestin, T.S., Karoly, D.J., Yano, J.-I., Rayner, N.A., 1998. Time–frequency variability of ENSO and stochastic simulations. Journal of Climate, 11(9): 2258-2272.

Kim, J.W., Chang, J.T., Baker, N.L., Wilks, D.S., Gates, W.L., 1984. The Statistical Problem of Climate Inversion: Determination of the Relationship between Local and Large-Scale Climate. Monthly Weather Review, 112(112).

Kim, N.W., Lee, J., 2010. Enhancement of the channel routing module in SWAT. Hydrological Processes: An International Journal, 24(1): 96-107.

Knutti, R., Furrer, R., Tebaldi, C., Cermak, J., Meehl, G.A., 2010. Challenges in Combining Projections from Multiple Climate Models. Journal of Climate, 23(10): 2739-2758.

Krysanova, V., Hattermann, F.F., 2017. Intercomparison of climate change impacts in 12 large river basins: overview of methods and summary of results. Climatic Change, 141(3): 363-379. DOI:10.1007/s10584-017-1919-y

Labat, D., Goddéris, Y., Probst, J.L., Guyot, J.L., 2004. Evidence for global runoff increase related to climate warming. Advances in Water Resources, 27(6): 631-642.

Lafleur, P.M., Rouse, W.R., 1988. The influence of surface cover and climate on energy partitioning and evaporation in a subarctic wetland. Boundary-Layer Meteorology, 44(4): 327-347.

Lahmer, W., Pfützner, B., Becker, A., 2001. Assessment of land use and climate change impacts on the mesoscale. Physics & Chemistry of the Earth Part B Hydrology Oceans & Atmosphere, 26(7): 565-575.

Lamb, H.H., 1972. British Isles weather types and a register of the daily sequence of circulation patterns. H.m.stationery Off.

Lambin, E.F., Geist, H.J., 2008. Land-use and land-cover change: local processes and global impacts. Springer Science & Business Media.

Le, A.M., Pricope, N.G., 2017. Increasing the Accuracy of Runoff and Streamflow Simulation in the Nzoia Basin, Western Kenya, through the Incorporation of Satellite-Derived CHIRPS Data. Water, 9(2): 114.

Legesse, D., Vallet-Coulomb, C., Gasse, F., 2003. Hydrological response of a catchment to climate and land use changes in Tropical Africa: case study South Central Ethiopia. Journal of Hydrology, 275(1-2): 67-85.

Lele, N., Joshi, P., 2009. Analyzing deforestation rates, spatial forest cover changes and identifying critical areas of forest cover changes in North-East India during 1972–1999. Environmental monitoring and assessment, 156(1): 159-170.

Leung, L.R., Mearns, L.O., Giorgi, F., Wilby, R.L., 2003. Regional climate research: needs and opportunities. Bulletin of the American Meteorological Society, 84(1): 89-95.

Leung, L.R., Qian, Y., Bian, X., Hunt, A., 2002. Hydroclimate of the Western United States Based on Observations and Regional Climate Simulation of 1981-2000. Part II: Mesoscale ENSO Anomalies. Journal of Climate, 16(12): 1892-1911.

Leuning, R., Zhang, Y.Q., Rajaud, A., Cleugh, H., Tu, K., 2008. A simple surface conductance model to estimate regional evaporation using MODIS leaf area index and the Penman-Monteith equation. Water Resources Research, 44(10): 652-655.

Li, H., Zhang, Y., Chiew, F.H.S., Xu, S., 2009a. Predicting runoff in ungauged catchments by using Xinanjiang model with MODIS leaf area index. Journal of Hydrology, 370(370): 155-162.

Li, H., Zhang, Y., Vaze, J., Wang, B., 2012. Separating effects of vegetation change and climate variability using hydrological modelling and sensitivity-based approaches. Journal of Hydrology, 420(7): 403-418.

Li, Q. et al., 2011. Investigation into the impacts of land-use change on runoff generation characteristics in the upper Huaihe River Basin, China. Journal of Hydrologic Engineering, 18(11): 1464-1470.

Li, Q. et al., 2013. Investigation into the impacts of land-use change on runoff generation characteristics in the upper Huaihe River Basin, China. Journal of Hydrologic Engineering, 18(11): 1464-1470.

Li, Z., Liu, W.-z., Zhang, X.-c., Zheng, F.-l., 2009b. Impacts of land use change and climate variability on hydrology in an agricultural catchment on the Loess Plateau of China. Journal of hydrology, 377(1-2): 35-42.

Lin, B. et al., 2015. Analyses of landuse change impacts on catchment runoff using different time indicators based on SWAT model. Ecological Indicators, 58: 55-63.

Lindström, G., Johansson, B., Persson, M., Gardelin, M., Bergström, S., 1997. Development and test of the distributed HBV-96 hydrological model. Journal of Hydrology, 201(1–4): 272-288.

Liu, D.L., Zuo, H., 2012. Statistical downscaling of daily climate variables for climate change impact assessment over New South Wales, Australia. Climatic Change, 115(3-4): 629-666.

Liu, J., Zhang, C., Kou, L., Zhou, Q., 2017a. Effects of climate and land use changes on water resources in the Taoer river. Advances in Meteorology, 2017.

Liu, J., Zhang, Q., Chen, X., Gu, X., 2016. Quantitative evaluations of human-and climate-induced impacts on hydrological processes of China. Acta. Geogr. Sin, 11: 1875-1885.

Liu, J., Zhang, Q., Singh, V.P., Shi, P., 2017b. Contribution of multiple climatic variables and human activities to streamflow changes across China. Journal of hydrology, 545: 145-162.

Liu, L., Xu, H., Wang, Y., Jiang, T., 2017c. Impacts of 1.5 and 2 °C global warming on water availability and extreme hydrological events in Yiluo and Beijiang River catchments in China. Climatic Change(10): 1-14.

Liu, N., Harper, R., Smettem, K., Dell, B., Liu, S., 2019. Responses of streamflow to vegetation and climate change in southwestern Australia. Journal of Hydrology, 572: 761-770.

Ma, T., Duan, Z., Li, R., Song, X., 2019. Enhancing SWAT with remotely sensed LAI for improved modelling of ecohydrological process in subtropics. Journal of hydrology, 570: 802-815.

Ma, W., Hafeez, M., Rabbani, U., Ishikawa, H., Ma, Y., 2012. Retrieved actual ET using SEBS model from Landsat-5 TM data for irrigation area of Australia. Atmospheric Environment, 59(59): 408-414.

Manolas, E., 2010. Adapting agriculture to climate change: preparing Australian agriculture, forestry and fisheries for the future. International Journal of Climate Change Strategies and Management, 2(3): 362 -377.

Mao, D., Cherkauer, K.A., 2005. Effects of Land Use Change on Evapotranspiration and Water Yield in the Great Lakes Region, AGU Fall Meeting.

Marhaento, H., Booij, M.J., Hoekstra, A.Y., 2018. Hydrological response to future land-use change and climate change in a tropical catchment. Hydrological sciences journal, 63(9): 1368-1385.

Marhaento, H., Booij, M.J., Rientjes, T., Hoekstra, A.Y., 2017. Attribution of changes in the water balance of a tropical catchment to land use change using the SWAT model. Hydrological processes, 31(11): 2029-2040.

Marshall, L., Nott, D., Sharma, A., 2004. A comparative study of Markov chain Monte Carlo methods for conceptual rainfall-runoff modeling. Water Resources Research, 40(2).

Maurer, E.P., 2007. Uncertainty in hydrologic impacts of climate change in the Sierra Nevada, California, under two emissions scenarios. Climatic Change, 82(3-4): 309-325.

May, R.M., 2008. Britannica guide to climate change. Robinson.

McFarlane, D. et al., 2012. Climate change impacts on water yields and demands in south-western Australia. Journal of Hydrology, 475: 488-498.

McKenzie, N., Jacquier, D., Ashton, L., Cresswell, H., 2000. Estimation of soil properties using the Atlas of Australian Soils. CSIRO Land and Water Technical Report, 11(00): 1-12.

McKeon, G., Hall, W., Henry, B., Stone, G., Watson, I., 2004. Pasture degradation and recovery in Australia's rangelands: learning from history. NRSc Publishing.

McMahon, T., Finlayson, B., 2003. Droughts and anti-droughts: the low flow hydrology of Australian rivers. Freshwater biology, 48(7): 1147-1160.

Mehrotra, R., Sharma, A., 2010. Development and Application of a Multisite Rainfall Stochastic Downscaling Framework for Climate Change Impact Assessment. Water Resources Research, 46(7): 759-768.

Menzel, L., Bürger, G., 2002. Climate change scenarios and runoff response in the Mulde catchment (Southern Elbe, Germany). Journal of hydrology, 267(1): 53-64.

Meyfroidt, P., Lambin, E.F., 2011. Global forest transition: prospects for an end to deforestation. Annual review of environment and resources, 36.

Milly, P.C., Dunne, K.A., Vecchia, A.V., 2005. Global pattern of trends in streamflow and water availability in a changing climate. Nature, 438(7066): 347-350.

Minville, M., Brissette, F., Leconte, R., 2008. Uncertainty of the impact of climate change on the hydrology of a nordic watershed. Journal of Hydrology, 358(1–2): 70-83.

MO, X. et al., 2009. Grid-size effects on estimation of evapotranspiration and gross primary production over a large Loess Plateau basin, China. Hydrological Sciences Journal, 54(1): 160-173.

Mohammady, M. et al., 2018. Modeling and assessing the effects of land use changes on runoff generation with the CLUE-s and WetSpa models. Theor Appl Climatol, 133(1-2): 459-471.

Monteith, J.L., 1965. Evaporation and environment. Symposia of the Society for Experimental Biology, 19(19): 205.

Moriasi, D.N. et al., 2007. Model evaluation guidelines for systematic quantification of accuracy in watershed simulations. Transactions of the ASABE, 50(3): 885-900.

Morton, F.I., Morton, F.I., 1983. Operational estimates of areal evapotranspiration and their significance to the science and practice of hydrology. Journal of Hydrology, 66(1): 1-76.

Mpelasoka, F., Hennessy, K., Jones, R., Bates, B., 2008. Comparison of suitable drought indices for climate change impacts assessment over Australia towards resource management. International Journal of Climatology: A Journal of the Royal Meteorological Society, 28(10): 1283-1292.

Mulligan, D.R., 1996. Environmental management in the Australian minerals and energy industries: principles and practices. UNSW Press.

Mwangi, H.M., Julich, S., Patil, S.D., McDonald, M.A., Feger, K.H., 2016. Modelling the impact of agroforestry on hydrology of Mara River Basin in East Africa. Hydrological Processes, 30(18): 3139-3155.

Narsimlu, B., Gosain, A.K., Chahar, B.R., 2013. Assessment of future climate change impacts on water resources of Upper Sind River Basin, India using SWAT model. Water resources management, 27(10): 3647-3662.

Nash, J.E., Sutcliffe, J.V., 1970. River flow forecasting through conceptual models part I — A discussion of principles. Journal of Hydrology, 10(3): 282-290.

Nash, L.L., Gleick, P.H., 1991. Sensitivity of streamflow in the Colorado Basin to climatic changes. Journal of Hydrology, 125(125): 221-241.

Nasonova, O.N., Gusev, Y.M., Kovalev, E.E., Ayzel, G.V., 2018. Climate change impact on streamflow in large-scale river basins: projections and their uncertainties sourced from GCMs and RCP scenarios. Proceedings of the International Association of Hydrological Sciences, 379: 139.

Neitsch, S.L., Arnold, J.G., Kiniry, J.R., Williams, J.R., 2011. Soil and water assessment tool theoretical documentation version 2009, Texas Water Resources Institute.

Nelder, J.A., Mead, R., 1965. A simplex method for function minimization. The computer journal, 7(4): 308-313.

Nicholls, N., 2003. Continued anomalous warming in Australia. Geophysical Research Letters, 30(7).

Nicholls, N., Drosdowsky, W., Lavery, B., 1997. Australian rainfall variability and change. Weather, 52(3): 66-72.

Nielsen, S.A., Hansen, E., 1973. Numerical simulation of the rainfall runoff process on a daily basis. Hydrology Research, 4(3): 171-190.

Nossent, J., Elsen, P., Bauwens, W., 2011. Sobol'sensitivity analysis of a complex environmental model. Environmental Modelling & Software, 26(12): 1515-1525.

Notebaert, B., Verstraeten, G., Ward, P., Renssen, H., Van Rompaey, A., 2011. Modeling the sensitivity of sediment and water runoff dynamics to Holocene climate and land use changes at the catchment scale. Geomorphology, 126(1-2): 18-31.

Oki, T., Kanae, S., 2006. Global hydrological cycles and world water resources. science, 313(5790): 1068-1072.

Orr, D., Turner, R.D.R., Huggins, R., Vardy, S., Warne. M. St. J., 2014. Wet Tropics water quality statistics for high and base flow conditions, Department of Science, Information Technology, Innovation and the Arts, Brisbane.

Pagán, B.R. et al., 2016. Extreme hydrological changes in the southwestern US drive reductions in water supply to Southern California by mid century. Environmental Research Letters, 11(9): 094026.

Park, J.-Y. et al., 2011. Assessment of MIROC3. 2 HiRes climate and CLUE-s land use change impacts on watershed hydrology using SWAT. Transactions of the ASABE, 54(5): 1713-1724.

Parsons, M., Frakes, I., Gerrand, A., 2007. Plantations and water use. Australian Government, Bureau of Rural Sciences.

Peel, M.C., 2009. Hydrology: catchment vegetation and runoff. Progress in Physical Geography, 33(6): 837-844.

Peña-Arancibia, J.L. et al., 2012. Detecting changes in streamflow after partial woodland clearing in two large catchments in the seasonal tropics. Journal of Hydrology, s 416–417(2): 60-71.

Penman, H.L., 1948. Natural Evaporation from Open Water, Bare Soil and Grass. Proceedings of the Royal Society of London, 193(1032): 120.

Penman, H.L., 1963. Vegetation and hydrology. Soil Science, 96(5): 357.

Perrin, C., Michel, C., Andréassian, V., 2003. Improvement of a parsimonious model for streamflow simulation. Journal of Hydrology, 279(1): 275-289.

Petrone, K.C., Hughes, J.D., Van Niel, T.G., Silberstein, R.P., 2010. Streamflow decline in southwestern Australia, 1950–2008. Geophysical Research Letters, 37(11).

Phung, Q.A. et al., 2019. Climate and Land Use Effects on Hydrologic Processes in a Primarily Rain-Fed, Agricultural Watershed. JAWRA Journal of the American Water Resources Association, 55(5): 1196-1215.

Pignotti, G., Rathjens, H., Cibin, R., Chaubey, I., Crawford, M., 2017. Comparative analysis of HRU and grid-based SWAT models. Water, 9(4): 272.

Pittock, B., 2003. Climate Change: An Australian Guide to the Science and Potential Impacts. Australian Greenhouse Office.

Poff, N.L., Olden, J.D., Pepin, D.M., Bledsoe, B.P., 2006. Placing global stream flow variability in geographic and geomorphic contexts. River Research and Applications, 22(2): 149-166.

Pohlert, T., 2016. Non-parametric trend tests and change-point detection. CC BY-ND, 4.

Prudhomme, C., Jakob, D., Svensson, C., 2003. Uncertainty and climate change impact on the flood regime of small UK catchments. Journal of Hydrology, 277(1): 1-23.

Qiang, F.C.W., 1992. The Definition and Detection of the Abrupt Climatic Change [J]. Chinese Journal of Atmospheric Sciences, 4.

Rashid, M.M., Beecham, S., Chowdhury, R.K., 2015. Assessment of trends in point rainfall using Continuous Wavelet Transforms. Advances in water resources, 82: 1-15.

Reshmidevi, T., Kumar, D.N., Mehrotra, R., Sharma, A., 2018. Estimation of the climate change impact on a catchment water balance using an ensemble of GCMs. Journal of Hydrology, 556: 1192-1204.

Riahi, K. et al., 2011. RCP 8.5—A scenario of comparatively high greenhouse gas emissions. Climatic Change, 109(1-2): 33.

Richardson, C.W., 1981. Stochastic simulation of daily precipitation, temperature, and solar radiation. Water Resources Research, 17(1): 182–190.

Richardson, C.W., Wright, D.A., 1984. WGEN: a model for generating daily weather variables, ARS-8. U.S. Department of Agriculture, Agricultural Research Service, 83 pp.

Richey, J.E., Nobre, C., Deser, C., 1989. Amazon river discharge and climate variability: 1903-1985. Science, 246(4926): 101.

Roo, A.D., Odijk, M., Schmuck, G., Koster, E., Lucieer, A., 2001. Assessing the effects of land use changes on floods in the meuse and oder catchment. Physics & Chemistry of the Earth Part B Hydrology Oceans & Atmosphere, 26(7): 593-599.

Rösch, A., Schmidbauer, H., 2014. WaveletComp 1.1: A guided tour through the R package.

Rose, S., Peters, N.E., 2001. Effects of urbanization on streamflow in the Atlanta area (Georgia, USA): a comparative hydrological approach. Hydrological Processes, 15(8): 1441-1457.

Roti, V., Kashyap, P., Anilkumar, S.R., Srivastava, R., Harish, C., 2018. Runoff and sediment yield estimation by SWAT model: review and outlook. Int. J. Curr. Microbiol. Appl. Sci., 7(10): 879-886.

Ruelland, D., Ardoin-Bardin, S., Collet, L., Roucou, P., 2012. Simulating future trends in hydrological regime of a large Sudano-Sahelian catchment under climate change. Journal of Hydrology, s 424–425(6): 207-216.

Ruhoff, A.L. et al., 2012. A MODIS-Based Energy Balance to Estimate Evapotranspiration for Clear-Sky Days in Brazilian Tropical?Savannas. Remote Sensing, 4(3): 703-725.

Ruprecht, J.E., Peirson, W.L., 2011. Stability of the Manning River entrances, Coasts and Ports 2011 :

Diverse and Developing: Proceedings of the 20th Australasian Coastal and Ocean Engineering Conference and the 13th Australasian Port and Harbour Conference, Barton, A.C.T., pp. 641 - 646.

Saha, P.P., Zeleke, K., 2015. Rainfall-Runoff modelling for sustainable water resources management: SWAT model review in Australia, Sustainability of Integrated Water Resources Management. Springer, pp. 563-578.

Saha, P.P., Zeleke, K., Hafeez, M., 2014. Streamflow modeling in a fluctuant climate using SWAT: Yass River catchment in south eastern Australia. Environmental earth sciences, 71(12): 5241-5254.

Sahoo, B., 2005. The Xinanjiang model and its derivatives for modeling soil moisture variability in the land-surface schemes of the climate change models: an overview, Hydrological Perspectives for Sustainable Development, pp. 518-532.

Sankarasubramanian, A., Vogel, R.M., 2003. Hydroclimatology of the continental United States. Geophysical Research Letters, 30(7).

Sankarasubramanian, A., Vogel, R.M., Limbrunner, J.F., 2001. Climate elasticity of streamflow in the United States. Water Resources Research, 37(6): 1771-1781.

Schirpke, U., Leitinger, G., Tappeiner, U., Tasser, E., 2012. SPA-LUCC: Developing land-use/cover scenarios in mountain landscapes. Ecological Informatics, 12(11): 68-76.

Seiller, G., Anctil, F., 2014. Climate change impacts on the hydrologic regime of a Canadian river: comparing uncertainties arising from climate natural variability and lumped hydrological model structures. Hydrology and Earth System Sciences, 18(6): 2033.

Seneviratne, S.I. et al., 2010. Investigating soil moisture–climate interactions in a changing climate: A review. Earth-Science Reviews, 99(3-4): 125-161.

Shan, N., Shi, Z., Yang, X., Gao, J., Cai, D., 2015. Spatiotemporal trends of reference evapotranspiration and its driving factors in the Beijing–Tianjin Sand Source Control Project Region, China. Agricultural and forest meteorology, 200: 322-333.

Shen, M. et al., 2018. Estimating uncertainty and its temporal variation related to global climate models in quantifying climate change impacts on hydrology. Journal of Hydrology, 556: 10-24.

Shi, L. et al., 2020. Projecting potential evapotranspiration change and quantifying its uncertainty under future climate scenarios: A case study in southeastern Australia. Journal of Hydrology, 584: 124756.

Shi, P. et al., 2011. Evaluating the SWAT model for hydrological modeling in the Xixian watershed and a comparison with the XAJ model. Water resources management, 25(10): 2595-2612.

Shrestha, M.K., Recknagel, F., Frizenschaf, J., Meyer, W., 2016. Assessing SWAT models based on single and multi-site calibration for the simulation of flow and nutrient loads in the semi-arid Onkaparinga catchment in South Australia. Agricultural Water Management, 175: 61-71.

Shrestha, M.K., Recknagel, F., Frizenschaf, J., Meyer, W., 2017. Future climate and land uses effects on flow and nutrient loads of a Mediterranean catchment in South Australia. Science of the Total Environment, 590: 186-193.

Shuttleworth, W.J., Wallace, J.S., 2009. Calculating the water requirements of irrigated crops in Australia using the Matt-Shuttleworth approach. Transactions of the Asabe, 52(6): 1895-1906.

Silberstein, R.P. et al., 2012. Climate change and runoff in south-western Australia. Journal of Hydrology, 475(12): 441-455.

Sirisena, T., Maskey, S., Ranasinghe, R., Babel, M.S., 2018. Effects of different precipitation inputs on streamflow simulation in the Irrawaddy River Basin, Myanmar. Journal of Hydrology: Regional Studies, 19: 265-278.

Siriwardena, L., Finlayson, B.L., McMahon, T.A., 2006. The impact of land use change on catchment hydrology in large catchments: The Comet River, Central Queensland, Australia. Journal of Hydrology, 326(1): 199-214.

Sohn, E., 2009. The big dry: Prolonged drought threatens Australia's people, wildlife, and economy. Science News, 172(17): 266-268.

Song, Y., Ding, C., 2009. Smart urban growth for China. Lincoln Institute of Land Policy Cambridge.

Sorooshian, S., Duan, Q., Gupta, V.K., 1993. Calibration of rainfall-runoff models: Application of global optimization to the Sacramento Soil Moisture Accounting Model. Water Resources Research, 29(4): 1185–1194.

Sorooshian, S., Gupta, V.K., Fulton, J.L., 1983. Evaluation of maximum likelihood parameter estimation techniques for conceptual rainfall-runoff models: Influence of calibration data variability and length on model credibility. Water Resources Research, 19(1): 251-259.

Stednick, J.D., 1996. Monitoring the effects of timber harvest on annual water yield. Journal of hydrology, 176(1-4): 79-95.

Sterling, S.M., Ducharne, A., Polcher, J., 2013. The impact of global land-cover change on the terrestrial water cycle. Nature Climate Change, 3(4): 385-390.

Stokes, C., Howden, S.M., 2010. Adapting agriculture to climate change : preparing Australian agriculture, forestry and fisheries for the future. CSIRO Pub.

Strauch, M., Volk, M., 2013. SWAT plant growth modification for improved modeling of perennial vegetation in the tropics. Ecological Modelling, 269: 98-112.

Su, B.D., Huang, J.L., Zeng, X.F., Gao, C., Jiang, T., 2017. Impacts of climate change on streamflow in the upper Yangtze River basin. Climatic Change, 141(3): 533-546.

Sudmeyer, R., Edward, A, Fazakerley, V, Simpkin, L & Foster, 2016. 'Climate change: impacts and adaptation for agriculture in Western Australia', Bulletin 4870, Department of Agriculture and Food, Western Australia, Perth.

Sun, G. et al., 2006. Potential water yield reduction due to forestation across China. Journal of Hydrology, 328(3-4): 548-558.

Tang, J. et al., 2016. Statistical downscaling and dynamical downscaling of regional climate in China: Present climate evaluations and future climate projections. Journal of Geophysical Research Atmospheres, 121(5): 2110-2129.

Tanner, C.B., Fuchs, M., 1968. Evaporation from unsaturated surfaces: A generalized combination

method. Journal of Geophysical Research, 73(4): 1299–1304.

Tebaldi, C., Knutti, R., 2007. The use of the multi-model ensemble in probabilistic climate projections. Philos Trans A Math Phys Eng Sci, 365(1857): 2053-2075.

Teng, J., Chiew, F., Vaze, J., Marvanek, S., Kirono, D., 2012a. Estimation of climate change impact on mean annual runoff across continental Australia using Budyko and Fu equations and hydrological models. Journal of Hydrometeorology, 13(3): 1094-1106.

Teng, J., Vaze, J., Chiew, F.H., Wang, B., Perraud, J.-M., 2012b. Estimating the relative uncertainties sourced from GCMs and hydrological models in modeling climate change impact on runoff. Journal of Hydrometeorology, 13(1): 122-139.

Tessema, S.M., Lyon, S.W., Setegn, S.G., Mörtberg, U., 2014. Effects of different retention parameter estimation methods on the prediction of surface runoff using the SCS curve number method. Water resources management, 28(10): 3241-3254.

Teutschbein, C., Seibert, J., 2012. Bias correction of regional climate model simulations for hydrological climate-change impact studies: Review and evaluation of different methods. Journal of Hydrology, 456: 12-29.

Thomas, R.B., Megahan, W.F., 2001. Peak flow responses to clear-cutting and roads in small and large basins, Western Cascades, Oregon: A second opinion. Water Resources Research, 34(4): 959-974.

Tian, D., Martinez, C.J., 2012. Comparison of two analog-based downscaling methods for regional reference evapotranspiration forecasts. Journal of Hydrology, 475(475): 350-364.

Tian, Y., Xu, Y.P., Zhang, X.J., 2013. Assessment of Climate Change Impacts on River High Flows through Comparative Use of GR4J, HBV and Xinanjiang Models. Water Resources Management, 27(8): 2871-2888.

Timbal, B., Fernandez, E., Li, Z., 2009. Generalization of a statistical downscaling model to provide local climate change projections for Australia. Environmental Modelling & Software, 24(3): 341-358.

Tollan, A., 2002. Land-use change and floods: what do we need most, research or management? Water Science & Technology A Journal of the International Association on Water Pollution Research, 45(8): 183.

Toth, B., Pietroniro, A., Conly, F.M., Kouwen, N., 2006. Modelling climate change impacts in the Peace and Athabasca catchment and delta: I—hydrological model application. Hydrological Processes, 20(19): 4197-4214.

Trenberth, K.E. et al., 2014. Global warming and changes in drought. Nature Climate Change, 4(1): 17-22.

Turner, B.L., Skole, D., Sanderson, S., 1995. Land Use and Land Cover Change. Ambio, 21(1): 122-122.

Turner, K.M., 1991. ANNUAL EVAPOTRANSPIRATION OF NATWE VEGETATION IN A MEDITERRANEAN-TYPE CLIMATE. JAWRA Journal of the American Water Resources Association, 27(1): 1-6.

Ummenhofer, C.C. et al., 2009. What causes southeast Australia's worst droughts? Geophysical Research Letters, 36(4): 1-5.

USDA, S., 1972. National engineering handbook, section 4: Hydrology. Washington, DC.

van der Spek, J.E., Bakker, M., 2017. The influence of the length of the calibration period and observation frequency on predictive uncertainty in time series modeling of groundwater dynamics. Water Resources Research, 53(3): 2294-2311.

van Dijk, A.I. et al., 2013. The Millennium Drought in southeast Australia (2001–2009): Natural and human causes and implications for water resources, ecosystems, economy, and society. Water Resources Research, 49(2): 1040-1057.

Van Griensven, A., Bauwens, W., 2003. Multiobjective autocalibration for semidistributed water quality models. Water Resources Research, 39(12).

Vaze, J., Teng, J., 2011. Future climate and runoff projections across New South Wales, Australia: results and practical applications. Hydrological Processes, 25(1): 18–35.

Verbesselt, J., Hyndman, R., Newnham, G., Culvenor, D., 2010. Detecting trend and seasonal changes in satellite image time series. Remote sensing of Environment, 114(1): 106-115.

Viney, N.R. et al., 2009. Assessing the impact of land use change on hydrology by ensemble modelling (LUCHEM) II: Ensemble combinations and predictions. Advances in Water Resources, 32(2): 147-158.

Viney, N.R., Sivapalan, M., 1999. A conceptual model of sediment transport: application to the Avon River Basin in Western Australia. Hydrological Processes, 13(5): 727-743.

Viney, N.R., Sivapalan, M., 2001. Modelling catchment processes in the Swan–Avon river basin. Hydrological Processes, 15(13): 2671-2685.

Vörösmarty, C.J., Green, P., Salisbury, J., Lammers, R.B., 2000. Global water resources: vulnerability from climate change and population growth. science, 289(5477): 284-288.

Vu, M., Raghavan, S.V., Liong, S.Y., 2012. SWAT use of gridded observations for simulating runoff–a Vietnam river basin study. Hydrology and Earth System Sciences, 16(8): 2801-2811.

Waggoner, P.E., Reifsnyder, W.E., 1968. Simulation of the Temperature, Humidity and Evaporation Profiles in a Leaf Canopy. Journal of Applied Meteorology, 7(3): 400-409.

Wagner, P., Kumar, S., Fiener, P., Schneider, K., 2011. Hydrological modeling with SWAT in a monsoon-driven environment: experience from the Western Ghats, India. Transactions of the ASABE, 54(5): 1783-1790.

Wallace, C.W., Flanagan, D.C., Engel, B.A., 2018. Evaluating the effects of watershed size on SWAT calibration. Water, 10(7): 898.

Wallach, D. et al., 2019. How well do crop models predict phenology, with emphasis on the effect of calibration? bioRxiv: 708578.

Wang, B. et al., 2019. Future climate change likely to reduce the Australian plague locust (Chortoicetes terminifera) seasonal outbreaks. Science of the total environment, 668: 947-957.

Wang, B. et al., 2017. Spatiotemporal changes in wheat phenology, yield and water use efficiency under the CMIP5 multimodel ensemble projections in eastern Australia. Climate Research, 72(2): 83-99.

Wang, G. et al., 2016. Simulating the hydrological responses to climate change of the Xiang River basin, China. Theoretical & Applied Climatology, 124(3-4): 769-779.

Wang, S., Kang, S., Zhang, L., Li, F., 2008. Modelling hydrological response to different land-use and climate change scenarios in the Zamu River basin of northwest China. Hydrological Processes, 22(14): 2502-2510.

Wang, Y. et al., 2004. Regional Climate Modeling: Progress, Challenges, and Prospects. Journal of the Meteorological Society of Japan, 82(6): 1599-1628.

Wattenbach, M. et al., 2007. Hydrological impact assessment of afforestation and change in tree-species composition–a regional case study for the Federal State of Brandenburg (Germany). Journal of Hydrology, 346(1-2): 1-17.

Weber, A., Fohrer, N., Möller, D., 2001. Long-term land use changes in a mesoscale watershed due to socio-economic factors—effects on landscape structures and functions. Ecological modelling, 140(1-2): 125-140.

Welde, K., Gebremariam, B., 2017. Effect of land use land cover dynamics on hydrological response of watershed: Case study of Tekeze Dam watershed, northern Ethiopia. International Soil and Water Conservation Research, 5(1): 1-16.

Wen, L., Rogers, K., Ling, J., Saintilan, N., 2011. The impacts of river regulation and water diversion on the hydrological drought characteristics in the Lower Murrumbidgee River, Australia. Journal of Hydrology, 405(3-4): 382-391.

Western, A., McKenzie, N., 2004. Soil hydrological properties of Australia. Melbourne: CRC for Catchment Hydrology.

Wicht, C., 1941. Diurnal fluctuations in Jonkershoek streams due to evaporation and transpiration. Journal of the South African Forestry Association, 7(1): 34-49.

Wigley, T.M.L., Jones, P.D., Briffa, K.R., Smith, G., 1990. Obtaining sub-grid-scale information from coarse-resolution general circulation model output. Journal of Geophysical Research Atmospheres, 95(D2): 1943–1953.

Wilby, R., 1995. Simulation of precipitation by weather pattern and frontal analysis. Journal of Hydrology, 173(1-4): 91-109.

Wilby, R.L., Harris, I., 2006. A framework for assessing uncertainties in climate change impacts: Low-flow scenarios for the River Thames, UK. Water Resources Research, 420(2): 563-575.

Wilby, R.L., Wigley, T.M.L., 1997. Downscaling general circulation model output: a review of methods and limitations. Progress in Physical Geography, 21(4): 530-548.

Wilk, J., Andersson, L., Plermkamon, V., 2001. Hydrological impacts of forest conversion to agriculture in a large river basin in northeast Thailand. Hydrological Processes, 15(14): 2729–2748.

Wilks, D.S., 1992. Adapting stochastic weather generation algorithms for climate change studies.

Climatic Change, 22(1): 67-84.

Woldemeskel, F.M., Sharma, A., Sivakumar, B., Mehrotra, R., 2012. An error estimation method for precipitation and temperature projections for future climates. Journal of Geophysical Research Atmospheres, 117(D22): 279-87.

Wood, A.W., Leung, L.R., Sridhar, V., Lettenmaier, D.P., 2004. Hydrologic Implications of Dynamical and Statistical Approaches to Downscaling Climate Model Outputs. Climatic Change, 62(1-3): 189-216.

Wood, W.L., 1996. A note on how to avoid spurious oscillation in the finite-element solution of the unsaturated flow equation. Journal of Hydrology, 176(1): 205-218.

Wu, F., Zhan, J., Su, H., Yan, H., Ma, E., 2015. Scenario-based impact assessment of land use/cover and climate changes on watershed hydrology in Heihe River Basin of northwest China. Advances in Meteorology, 2015.

Wu, K., A. Johnston, C., 2008. Hydrologic comparison between a forested and a wetland/lake dominated watershed using SWAT. Hydrological Processes: An International Journal, 22(10): 1431-1442.

Xiubin, L., 1996. A review of the international researches on land use/land cover change [J]. Acta Geographica Sinica, 6.

Xu, C.Y., 1999. From GCMs to river flow: A review of downscaling methods and hydrologic modelling approaches. Progress in Physical Geography, 23(2): 229--249.

Xu, C.Y., Singh, V.P., 2004. Review on Regional Water Resources Assessment Models under Stationary and Changing Climate. Water Resources Management, 18(6): 591-612.

Yaa, L., Youpeng, X., Yi, S., 2012. Hydrological Effects of Urbanization in the Qinhuai River Basin, China. Procedia Engineering, 28: 767-771.

Yang, H., Qi, J., Xu, X., Yang, D., Lv, H., 2014. The regional variation in climate elasticity and climate contribution to runoff across China. Journal of hydrology, 517: 607-616.

Yang, H., Yang, D., 2011. Derivation of climate elasticity of runoff to assess the effects of climate change on annual runoff. Water Resources Research, 47(7).

Yang, J., Reichert, P., Abbaspour, K.C., Xia, J., Yang, H., 2008. Comparing uncertainty analysis techniques for a SWAT application to the Chaohe Basin in China. Journal of Hydrology, 358(1-2): 1-23.

Yang, Y. et al., 2016. Water use efficiency and crop water balance of rainfed wheat in a semi-arid environment: sensitivity of future changes to projected climate changes and soil type. Theoretical and applied climatology, 123(3-4): 565-579.

Yang, Y., Tian, F., 2009. Abrupt change of runoff and its major driving factors in Haihe River Catchment, China. Journal of Hydrology, 374(3-4): 373-383.

Yao, C., Zhang, K., Yu, Z., Li, Z., Li, Q., 2014. Improving the flood prediction capability of the Xinanjiang model in ungauged nested catchments by coupling it with the geomorphologic instantaneous unit hydrograph. Journal of Hydrology, 517(2): 1035-1048.

Ye, X., Zhang, Q., Liu, J., Li, X., Xu, C.-y., 2013. Distinguishing the relative impacts of climate change

and human activities on variation of streamflow in the Poyang Lake catchment, China. Journal of Hydrology, 494: 83-95.

Yu, W., Zang, S., Wu, C., Liu, W., Na, X., 2011. Analyzing and modeling land use land cover change (LUCC) in the Daqing City, China. Applied Geography, 31(2): 600-608.

Zeng, Z. et al., 2014. A worldwide analysis of spatiotemporal changes in water balance-based evapotranspiration from 1982 to 2009. Journal of Geophysical Research: Atmospheres, 119(3): 1186-1202.

Zhang, A. et al., 2012. Assessments of impacts of climate change and human activities on runoff with SWAT for the Huifa River Basin, Northeast China. Water resources management, 26(8): 2199-2217.

Zhang, D.L., Zheng, W.Z., Xue, Y.K., 2003. A Numerical Study of Early Summer Regional Climate and Weather over LSA-East. Part I: Model Implementation and Verification. Monthly Weather Review, 131(8): 1895.

Zhang, H., Huang, G.H., 2013. Development of climate change projections for small watersheds using multi-model ensemble simulation and stochastic weather generation. Climate Dynamics, 40(3-4): 805-821.

Zhang, H. et al., 2019. Impacts of future climate change on water resource availability of eastern Australia: A case study of the Manning River basin. Journal of Hydrology, 573: 49-59.

Zhang, H. et al., 2020. Using an improved SWAT model to simulate hydrological responses to land use change: a case study of a catchment in tropical Australia. Journal of Hydrology, 585: 124822.

Zhang, J., Li, Q., Guo, B., Gong, H., 2015. The comparative study of multi-site uncertainty evaluation method based on SWAT model. Hydrological Processes, 29(13): 2994-3009.

Zhang, L., Dawes, W., Walker, G., 2001. Response of mean annual evapotranspiration to vegetation changes at catchment scale. Water resources research, 37(3): 701-708.

Zhang, Q., Liu, J., Singh, V.P., Shi, P., Sun, P., 2017. Hydrological responses to climatic changes in the Yellow River basin, China: Climatic elasticity and streamflow prediction. Journal of Hydrology, 554: 635-645.

Zhang, T., Wang, Y., Wang, B., Feng, P., 2018. Understanding the Main Causes of Runoff Change by Hydrological Modeling: A Case Study in Luanhe River Basin, North China. Water, 10(8): 1028.

Zhang, X., Xu, Y.-P., Fu, G., 2014. Uncertainties in SWAT extreme flow simulation under climate change. Journal of Hydrology, 515: 205-222.

Zhang, X.C., 2007. A comparison of explicit and implicit spatial downscaling of GCM output for soil erosion and crop production assessments. Climatic Change, 84(3-4): 337-363.

Zhang, X.S. et al., 2016. How streamflow has changed across Australia since the 1950s: evidence from the network of hydrologic reference stations. Hydrology and Earth System Sciences, 20(9): 3947-3965.

Zhang, Y. et al., 2013. Collation of Australian modeller's streamflow dataset for 780 unregulated Australian catchments. Water for a Healthy Country National Research Flagship, 115pp.

Catchment Management.

Zhao, R., Yilin, Z., Lerun, F., Xinren, L.I.U., Quan, Z., 1980. The Xinanjiang model, In Proceedings of the Oxford Symposium. IAHS Publ, pp. 351-356.

Zhao, R.J., 1992. The Xinanjiang model applied in China. Journal of Hydrology, 135(1–4): 371-381.

Zhi, L., Dongyong, S., 2015. Trend and abrupt analysis of rainfall change during last 50 years in the Weihe Basin. Earth Sciences, 4(6): 228.

Zhi, L., Liu, W.Z., Zhang, X.C., Zheng, F.L., 2009. Impacts of land use change and climate variability on hydrology in an agricultural catchment on the Loess Plateau of China. Journal of Hydrology, 377(1–2): 35-42.

Zhou, G. et al., 2015. Global pattern for the effect of climate and land cover on water yield. Nature communications, 6: 5918.

Zhou, G.Y. et al., 2010. Forest recovery and river discharge at the regional scale of Guangdong Province, China. Water Resources Research, 46(9): 5109-5115.